Combination of Chemical Reaction and Analysis

Catalyst Screening by On-Column Reaction Chromatography

E_i^{mob} P_i^{mob}

$K_{i, phys}^{\circ}$ $K_{i, phys}^{\circ}$ mobile phase

stationary phase

E_i^{diss} P_i^{diss} *dissolved state*

$K_{i, chem}^{\circ}$ $K_{i, chem}^{\circ}$

$E_i^{cat} \xrightarrow[k_{-1}^{cat}]{k_1^{cat}} P_i^{cat}$ *catalysis*

The Reactor
selective stationary phase & catalytic activity

fused-silica capillary

DISSERTATION

SVEN K. WEBER

2009

INAUGURAL-DISSERTATION

zur

Erlangung der Doktorwürde

der

Naturwissenschaftlich-Mathematischen

Gesamtfakultät

der

Ruprecht-Karls-Universität

Heidelberg

vorgelegt von

Diplom-Chemiker Sven Karsten Weber

aus Bonn

Tag der mündlichen Prüfung: 12.06.2009

Combination of Chemical Reaction and Analysis

Catalyst Screening by On-Column Reaction Chromatography

Dekan: Prof. Dr. Heinz Friedrich Schöler

Gutachter: Prof. Dr. Oliver Trapp

Prof. Dr. A. Stephen K. Hashmi

Für meine Familie

Freude, schöner Götterfunken
Tochter aus Elysium,
Wir betreten feuertrunken,
Himmlische, dein Heiligthum!
Deine Zauber binden wieder
Was die Mode streng getheilt;
Alle Menschen werden Brüder,
Wo dein sanfter Flügel weilt.

Friedrich Schiller

Acknowledgement

Abstract

The combination of catalysis and analysis in a single chromatographic reactor is an efficient method for the comprehensive kinetic characterization of catalysts and materials. This concept, called on-column reaction chromatography, incorporates catalytic activity and separation selectivity in the polymeric stationary phase of a chromatographic separation capillary. This thesis aims to study mechanistic details of (enantioselective) catalytic processes by applying this strategy.

After an introduction about general aspects of on-column reaction chromatography in chapter **1**, the combination of enantioselective hydrogenations of α-keto esters over quinine-modified Pt and Pd nanoparticles and the consecutive separation of the obtained enantiomers in microcapillaries is reported in chapter **3**. This combination makes it possible to simultaneously determine enantiomeric excesses and reaction kinetics for entire substrate libraries by injecting a broad variety of different substrates at the same time. Chirally modified Pt and Pd nanoparticles, embedded in a stabilizing polysiloxane matrix, serve as catalysts and selective chromatographic stationary phases for these multiphase (gas-liquid-solid) reactions. These polymer embedded catalysts are coated as a thin film onto the inner surface of fused-silica capillaries. A systematic kinetic study for the Pt-catalyzed enantioselective hydrogenation of ethyl pyruvate **(1)** is presented. Furthermore, the high-throughput screening of a substrate library consisting of different α-keto esters over chirally modified Pt- and Pd-catalysts was investigated (Scheme 1).
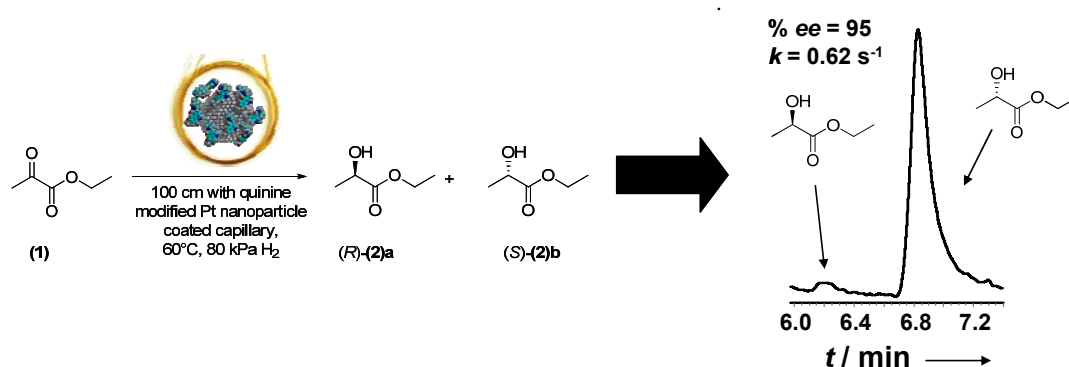
Scheme 1. Enantioselective on-column hydrogenation of ethylpyruvate over quinine modified Pt nanoparticles stabilized in a polysiloxane matrix and coated on micro capillary, which was used as the reactor.

A study about the activity of different ruthenium olefin metathesis catalysts in ring-closing metathesis (RCM) reactions is described in chapter **4**. The Grubbs-type catalysts 1st **(22)** and 2nd generation **(23)** as well as Hoveyda-Grubbs-type catalysts 1st generation **(24)** were dissolved in polysiloxanes and coated onto the inner surface of microcapillaries. Temperature- and flow-dependent conversion measurements with Grubbs-type catalysts for RCM allowed the determination of reaction rate constants k and activation parameters ($\Delta G^{\neq}$, $\Delta H^{\neq}$ and $\Delta S^{\neq}$). The obtained comprehensive experimental kinetic data are a prerequisite for a better understanding of catalytic mechanisms (Scheme 2).
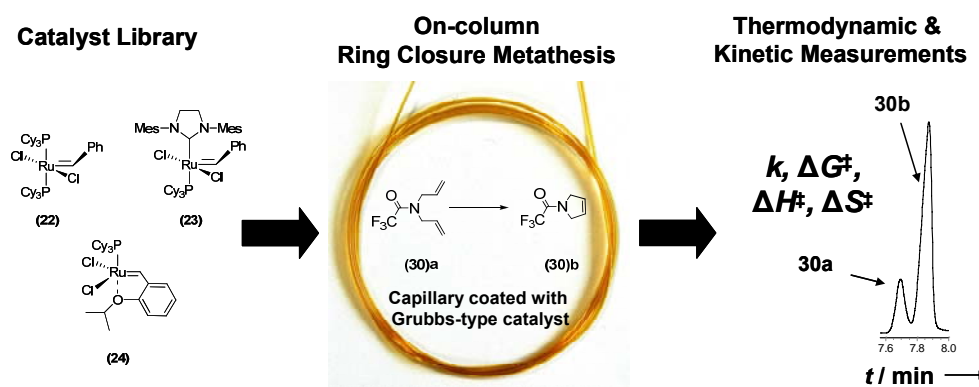
Scheme 2. On-column ring-closing metathesis of *N,N*-diallyltrifluoroacetamide (30)a over a Grubbs-type catalyst library.

In chapter **5**, the concept of on-column reaction gas chromatography was used to combine separation selectivity of ionic liquids (ILs) and catalysis by Grubbs-type catalyst 1st generation **(22)** in RCM reactions. This combination allows the investigation of catalyst stability and recyclability, which are important aspects for future catalyst applications. With this combination, it is possible to investigate the catalyst stability and recyclability. Reaction rate constants k that are hardly accessible by other techniques can be efficiently determined for various substrates with this approach (Scheme 3).
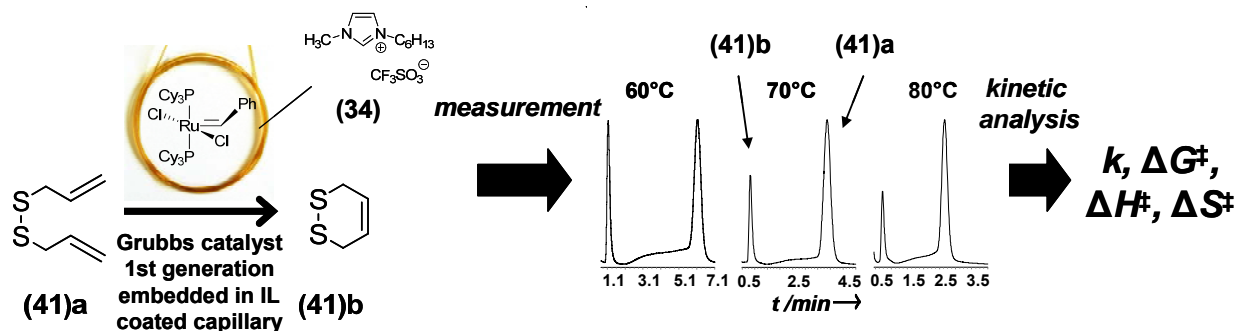
Scheme 3. On-column ring-closing metathesis of diallyl disulfide (41)a over Grubbs 1st generation catalyst (22) dissolved in a room temperature ionic liquid (34).

Chapter **6** describes the synthesis and application of polysiloxane-immobilized chiral camphor-based transition metal catalysts. The enantioselective separation efficiency and catalytic activity of these novel stationary phases are investigated (Scheme 4a).
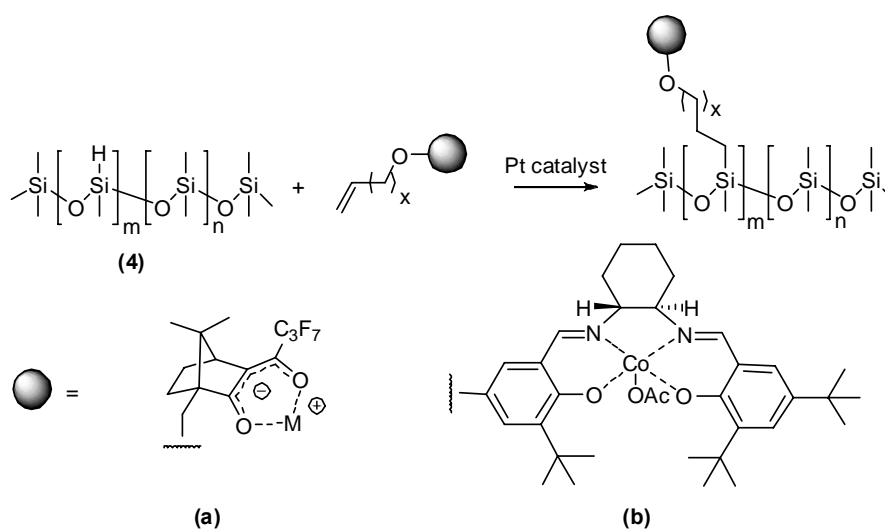
Scheme 4. A flexible and versatile strategy for the covalent immobilization of homogeneous chiral catalysts on modified polysiloxanes.

The synthetic applicability of polysiloxane-supported chiral Co-salen-complexes is described in chapter **7**. A modular, covalent immobilization method for monofunctionalized enantiopure unsymmetrical salen ligands by an ether linkage has been elaborated (Scheme 4a).

Zusammenfassung

Die Kombination von Katalyse und Analyse in einem chromatographischen Reaktor ist eine effiziente Methode zur umfassenden kinetischen Charakterisierung von Katalysatoren und Materialien. Dieses Konzept wird On-Column Reaktionschromatographie genannt und verbindet katalytische Aktivität und Trennungsselektivität in einer polymeren stationären Phase einer chromatographischen Trennkapillare. Das Ziel der vorliegenden Arbeit ist die Untersuchung mechanistischer Details von (enantioselektiven) katalytischen Prozessen mit Hilfe dieser Strategie.
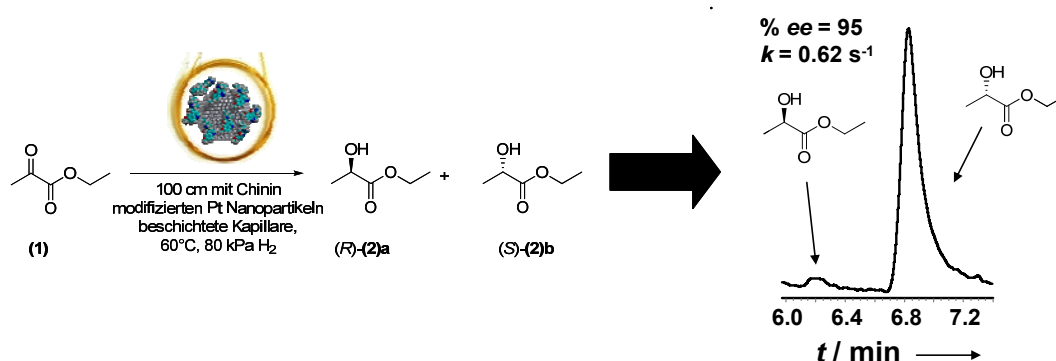

Abbildung 1. Enantioselektive on-column Hydrierung von Ethylpyruvat über Chinin-modifizierten und Polysiloxan-stabilisierten Pt Nanopartikeln, die auf der Innenwand einer fused-silica Kapillare immobilisiert sind, welche als Reaktor dient.

Nach einer Einleitung über generelle Aspekte der On-Column Reaktionschromatographie in Kapitel **1** wird in Kapitel **3** die Kombination von enantioselektiven Hydrierungen von α-Ketoestern über Chinin-modifizierten Platin- und Palladium-Nanopartikeln und die anschließende Trennung der erhaltenen Enantiomere in Mikrokapillaren beschrieben (Abbildung 1). Diese Kombination ermöglicht die simultane Ermittlung von Enantiomerenüberschüssen und Reaktionskinetiken für komplette Substratbibliotheken durch die gleichzeitige Injektion von verschiedenen Edukten. Chinin-modifizierte Platin- und Palladium-Nanopartikel, die in einer stabilisierenden Polysiloxan-Matrix eingebettet sind, agieren zugleich als Katalysator und selektive chromatographische Stationärphase in diesen Mehrphasenreaktionen (gasförmig-flüssig-fest). Mit dem im Polymer eingebetteten Katalysator werden die Innenwände einer fused-silica Kapillare beschichtet. Eine systematische kinetische Studie für die enantioselektive Hydrierung von Ethylpyruvat mit

Chinin-modifizierten Pt-Katalysatoren wird vorgestellt. Des Weiteren wird in diesem Kapitel ein Hochdurchsatz-Screening einer Reaktandenbibliothek über mit Chinin-modifizierten Pt- und Pd-Katalysatoren beschrieben, die aus verschiedenen α-Ketoestern besteht.

Eine Studie zur Aktivität von verschiedenen Olefinmetathese-Rutheniumkatalysatoren für Ringschlussmetathesen ist in Kapitel **4** beschrieben. Grubbs-Katalysatoren der ersten und zweiten Generation sowie der Hoveyda-Grubbs-Katalysator der ersten Generation wurden in Polysiloxanen gelöst und auf der Innenwand einer Quarzglaskapillare immobilisiert. Temperatur- und druckabhängige Umsatzmessungen mit Grubbs-Katalysatoren in Ringschlussmetathesen für verschiedene Substrate führen zu Reaktionsgeschwindigkeits-konstanten k und Aktivierungsparametern ($\Delta G^{\neq}$, $\Delta H^{\neq}$ und $\Delta S^{\neq}$). Die Ermittlung von experimentellen, kinetischen Daten ist die Voraussetzung für ein besseres Verständnis des Katalysemechanismus.
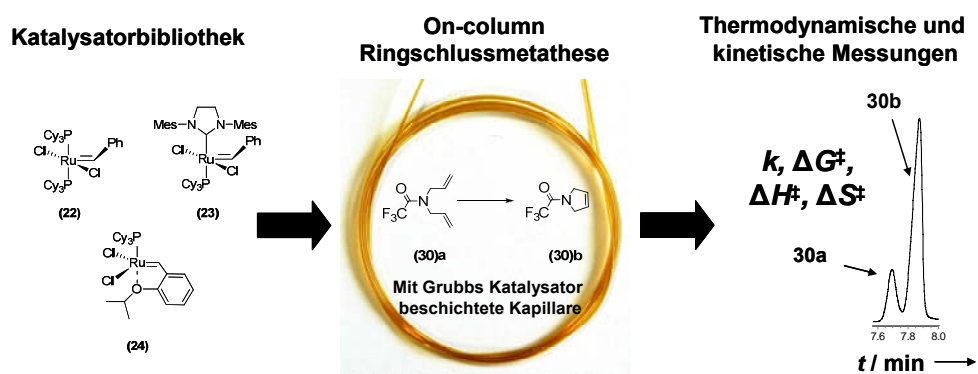
Abbildung 2. On-column Ringschlussmetathese von *N,N*-diallyltrifluoracetamid (30)a über einer Grubbs-Katalysatorbibliothek in einer Mikrokapillare als Reaktor.

Kapitel **5** beschreibt die Nutzung des Konzeptes der „On-Column" Reaktions-chromatographie zur Kombination von Trennungsselektivitäten ionischer Flüssigkeiten und Katalyse durch den Grubbs-Katalysator der ersten Generation in Ringschlussmetathesen. Diese Kombination ermöglicht die Ermittlung der Katalysatorstabilität und des Katalysatorrecyclings, die wichtige Aspekte für zukünftige katalytische Anwendungen darstellen. Mit dieser Technik können Reaktionsgeschwindigkeitskonstanten, die mit anderen Techniken nur schwer erschließbar sind, für eine Vielzahl von Substraten effizient ermittelt werden (Abbildung 3).
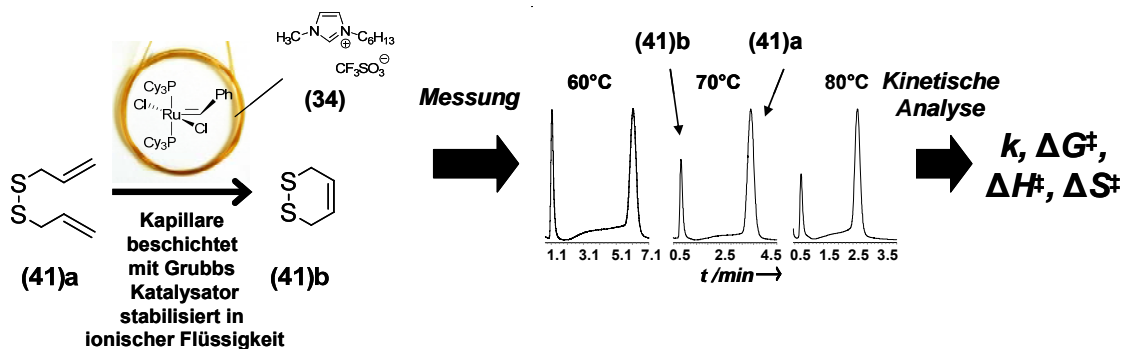
Abbildung 3. On-column Ringschlussmetathese von Diallyldisulfid (41)a katalysiert durch den in der ionischen Flüssigkeit (34) stabilsierten Grubbs Katalysator der 1. Generation (22).

In Kapitel **6** wird die Synthese und Anwendung von Polysiloxan-immobilisierten, chiralen Campher-Übergangsmetall-Katalysatoren beschrieben. Die enantioselektive Trennungs-effizient und die katalytische Aktivität dieser stationären Phasen wurden untersucht (Abbildung 4a).
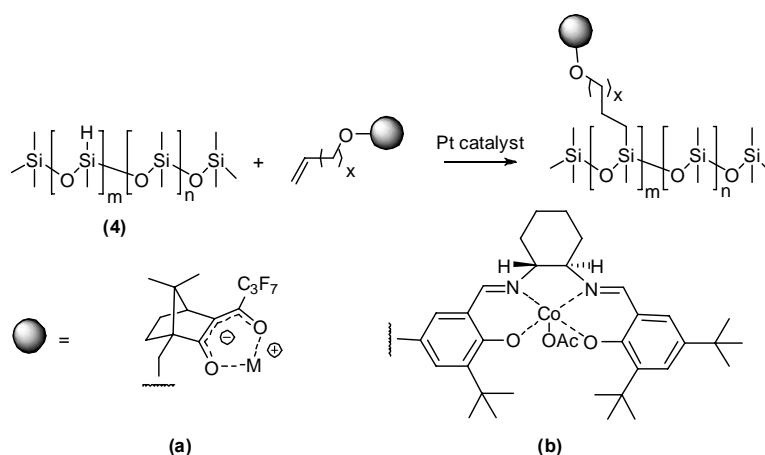
Abbildung 4. Eine flexible Strategie für die kovalente Anbindung von homogenen chiralen Katalysatoren an modifizierten Polysiloxanen.

Die synthetische Anwendbarkeit von chiralen, auf Polysiloxan-immobilisierten Cobalt-Salen Komplexen ist in Kapitel **7** beschrieben. Eine flexible, kovalente Immobilisierungsmethode von monofunktionalen, enantiomerenreinen und unsymmetrischen Salen-Liganden durch eine Etherfunktionalität wird vorgestellt (Abbildung 4b).

Publications

Refereed Publications

S. K. Weber, O. Trapp, **2009**, *submitted for publication.* Integration of Enantioselective Catalysis and Separation – Kinetic Investigations by Enantioselective On-Column Reaction Chromatography.

S. K. Weber, S. Bremer, M. Spallek, O. Trapp, **2009**, *manuscript in preparation*. Kinetic Study of Olefin Metathesis Catalysts by On-Column Reaction Chromatography.

S. K. Weber, O. Trapp, **2009**, *manuscript in preparation*. Direct Access to Reaction Kinetics of Catalytic Processes in Ionic Liquids by Integration of Catalysis and Separation.

O. Trapp, S. K. Weber, S. Bauch, T. Bäcker, W. Hofstadt, B. Spliethoff, *Chem. Eur. J.* **2008**, *14*, 4657–4666. High-throughput kinetic study of hydrogenations over palladium nanoparticles – Combination of reaction and analysis.

O. Trapp, S. K. Weber, S. Bauch, W. Hofstadt, *Angew. Chem. Int. Ed.* **2007**, *46*, 7307–7310. High-throughput screening of catalysts by combining chemical reaction and analysis. *Angew. Chem.* **2007**, *119*, 7447–7451. Hochdurchsatzscreening von Katalysatoren durch Integration von Reaktion und Analyse.

Poster Presentations

S. K. Weber, O. Trapp; European Conference on Combinatorial Catalysis Research and High-Throughput Technologies **2009**, Gandia, Spain, High-throughput reaction monitoring of ring-closing metathesis by on-column reaction chromatography.

S. K. Weber, S. Bremer, O. Trapp; Ruperto-Carola-Symposium **2008**: Small Molecule Activation and Bioenergy Conversion, Heidelberg, Germany, High-throughput reaction monitoring of enantioselective hydrogenations with on-column reaction chromatography.

S. K. Weber, O. Trapp; 20th International Symposium on Chirality **2008**, Geneva, Switzerland, High-throughput reaction monitoring of enantioselective hydrogenations with on-column reaction chromatography.

S. K. Weber, O. Trapp, 41. Jahrestreffen Deutscher Katalytiker **2008**, Weimar, Germany, Hochdurchsatz-Screening von Grubbs-Katalysatoren durch Integration von Reaktion und Analyse.

S. K. Weber, S. Bauch, O. Trapp; 19th International Symposium on Chirality **2007**, San Diego, USA, Combination of chemical reaction and analysis with chiral camphor-based transition metal catalysts in one chromatographic reactor.

S. K. Weber, O. Trapp; 40. Jahrestreffen Deutscher Katalytiker **2007**, Weimar, Germany Synthese von polymer-gebundenen chiralen Übergangsmetall-Katalysatoren und deren Untersuchung mittels on-column Reaktionschromatographie.

Conference Talks

S. K. Weber, S. Bauch, O. Trapp, 10th Young Scientist Conference on Chemistry **2008**, Rostock, Germany**.** Lab-in-a-capillary: Integrated reactor for high-throughput screening of catalysts and for synthesis.

Table of Contents

List of Abbreviations

$[\alpha]$	specific angle of rotation
Δ	chemical shift
$\Delta G^{\neq}$	Gibbs activation energy
$\Delta H^{\neq}$	activation enthalpy
$\Delta S^{\neq}$	activation entropy
acac	acetylacetonate
bmim	1-butyl-3-methylimidazolium
bdmim	1-butyl-2,3-dimethylimidazolium
Chirasil-ß-Dex	octamethylen-permethyl-ß-cyclodextrin-poly(dimethylsiloxane)
Chira-Ni(II)	nickel(II)-bis[3-(heptafluorobutanoyl)-(1R)-camphorate] dissolved in poly(dimethylsiloxane)
Chirasil-Ni(II)	nickel(II)-bis[3-(heptafluorobutanoyl)-(1S)-10-methylene-camphorate]-poly(dimethylsiloxane)
Chirasil-Eu(III)	europium(III)-tris[3-(heptafluorbutanoyl-(1S)-10-methylene-camphorate]-poly(dimethylsiloxane)
Chirasil-Ni(II)-Propoxy-Camphor	nickel(II)-bis [3-(heptafluorbutanoyl-(1S)-10-propoxy-camphorate]-poly(dimethylsiloxane)
Chirasil-Eu(III)-Propoxy-Camphor	europium(III)-tris [3-(heptafluorbutanoyl-(1S)-10-propoxy-camphorate]-poly(dimethylsiloxane)
Chirasil-Co(II)-Propoxy-Salen	cobalt(II)-[2,4-di-*tert*-butyl-6-((E)-((1R,2R)-2-((E)-3-*tert*-butyl-2-hydroxy-5-propoxy-benzylideneamino)cyclohexylimino)methyl)phenol]- poly(dimethylsiloxane)
Chirasil-Co(II)-Hexyloxy-Salen	cobalt(II)-[2,4-di-*tert*-butyl-6-((E)-((1R,2R)-2-((E)-3-*tert*-butyl-2-hydroxy-5-heyyloxy-benzylideneamino)cyclohexylimino)-methyl)phenol]-poly(dimethylsiloxane)
Chirasil-Co(II)-Octyloxy-Salen	cobalt(II)-[2,4-di-*tert*-butyl-6-((E)-((1R,2R)-2-((E)-3-*tert*-butyl-2-hydroxy-5-octyloxy-benzylideneamino)cyclohexylimino)-methyl)phenol]-poly(dimethylsiloxane)
Chirasil-Quinine	[(1R)-(8-ethylquinuclidin-2-yl)(6-methoxyquinolin-4-yl)methanol]-poly(dimethylsiloxane)
CM	cross metathesis
CSP	chiral stationary phase
D	doublet
DCM	dichloromethane
DME	dimethoxyethane (ethylene glycol)
DMF	dimethyl formamide
ESI	electrospray ionization
Ee	enantiomeric excess

EI	electron ionization
eq.	equivalent(s)
etlac	ethyl lactate
etpy	ethyl pyruvate
FID	flame ionization detector
GC	gas chromatography
GC-MS	gas chromatography-mass spectrometry
H	hour(s)
HFB-	heptafluorobutanoyl-
H_2IMes	*N,N*-bis(*mesityl*)-4,5-dihydroimidazol-2-ylidene
HMIM	1-hexyl-3-methylimidazolium
HMPS	hydridomethylsiloxane-dimethylsiloxane copolymer
HPLC	high performance liquid chromatography
HRMS	high resolution mass spectrometry
ht	high-throughput
i.d.	inner diameter
IL	ionic liquid
IR	infrared spectroscopy
LC	liquid chromatography
LDA	lithium diisopropylamide
m	multiplett
min	minute(s)
mol%	mol percent
MS	mass spectrometry
MVPS	methylvinylsiloxane-dimethylsiloxane copolymer
NHC	*N*-heterocyclic carbene
NMR	nuclear magnetic resonance
PDMS	poly(dimethylsiloxane)
PMPS	poly(methylphenylsiloxane)
ppm	parts per million
PS	polysiloxane
RCM	ring closing metathesis
R_f	retention factor
ROMP	ring opening metathesis polymerization
t	time
t	triplett
t_R	retention time
TEM	transmission electron microscope
THF	tetrahydrofurane

Chapter 1

Introduction

1. Introduction

1.1. Catalysis

Catalysis is a key technology for chemical transformations that allows us to convert raw materials into valuable chemicals in an efficient, economical, and environmentally friendly manner. Already in antiquity, catalytic transformations with enzymes were used by mankind in fermentations of sugar to ethanol. After Berzelius introduced the term "catalysis" in 1838 to explain various decomposition and transformation reactions, it was Ostwald in 1895, who defined that "a catalyst accelerates a chemical reaction without affecting the position of the equilibrium". Although this conclusion of Ostwald is still valid today, the definition of a catalyst was subject of numerous discussions.[1] In general, a catalyst is defined as a material that converts reactants into products through a series of elementary steps. In a catalytic cycle, the catalyst participates in the transition state, while regenerating to its initial state at the end of each cycle during its lifetime. In fact, about 75% of all chemicals in industry are produced with the aid of catalysts.[2, 3] The discovery of new active, selective, and stable catalysts is of particular importance to sustainable chemical processes in industry, as well as to expand the capacity of synthetic methodologies and techniques in chemistry. In particular, asymmetric catalytic transformations are in the focus of attention,[4] because of the growing demand for enantiopure compounds in pharmaceutical industry.

Although catalysts can be classified by numerous criteria, they are mainly divided according to the state of aggregation: heterogeneous catalysts[5, 6] (solid-state catalysts) and homogeneous catalysts.[7] In heterogeneous catalysis, phase boundaries are always present between the catalyst and the reactants, whereas in homogeneous catalysts, starting materials and products are present in the same phase. In industrial processes, heterogeneous catalysts play a major role, as they are used in about 90% of all chemical processes. The catalytically active substance[8] is often applied to a support material with a large surface area that can be removed after reaction and also allows a continuous operation mode. On the other hand, homogeneous catalysts exhibit a higher activity per unit mass of metal than heterogeneous catalysts due to their high degree of dispersion in solution. In homogeneous catalysis, well-defined reaction sites often result in higher selectivities, lower catalyst concentrations, and milder reaction conditions.

1.2. Immobilization of Homogeneous Catalysts

Despite the advantages of homogeneous catalysis, the separation of homogeneous catalysts from the reaction product and from any reaction solvent is often more difficult compared to heterogeneous procedures. Whereas heterogeneous catalysts are automatically removed by filtration or centrifugation, more complicated processes such as liquid-liquid extraction or distillation must often be used for homogeneous catalysts. Many homogeneous catalytic systems have not been commercialized, because of high-priced and air-sensitive catalysts and ligands. Further difficulties might appear, when the catalysts, the ligands and their degradation by-products, as well as residual metals, have to be removed during the work-up procedure. Within an efficient (industrial) process, expensive ligands and catalysts have to be recovered and re-used.

To overcome the separation problems, chemists and engineers investigated a wide range of strategies. One successful approach to combine the advantages of homogeneous and heterogeneous catalysis, such as high activity and selectivity on the one hand, and separation and recycling on the other, is the immobilization of homogeneous catalysts on a suitable support.[9-20] Immobilized homogeneous catalysts are easily separated and recycled, and product contamination with metal traces can be minimized. Different immobilization strategies and the role of the support will be briefly addressed in the following section.

1.2.1. Immobilization Strategies

The success of the solid-phase peptide synthesis developed by Merrifield in the 1960s,[21] who was later awarded with the Nobel Prize in Chemistry "for his development of methodology for chemical synthesis on a solid matrix", has resulted in the development of covalently attached (chiral) ligands and catalysts. This new concept of (chiral) catalyst immobilization has provided to be a promising approach to bridge the gap between homogeneous and heterogeneous catalysis.

Different immobilization strategies are discussed: The chiral ligand or the preassembled metal complex can be immobilized by covalent or noncovalent attachment (adsorption, electrostatic interactions, entrapping) on the support (Scheme 5).[18, 19] Alternatively, the ligand can be

synthesized on the support, which also opens the possibility of an efficient ligand screening. Comparing the different immobilization strategies, each method has its assets and drawbacks. In contrast to transition-metal catalysts, which are covalently immobilized (Scheme 5a), leaching is a major problem of entrapped catalysts (Scheme 5d), where metal complexes are incorporated (or intentionally "assembled") inside the porous network of crystalline inorganic supports such as zeolites, or entrapped between the layers of lamellar materials such as natural smectite clays or synthetic zirconium phosphates. On the other hand, entrapped catalysts have the advantage that they are easily prepared, because known catalysts can be used without further modification. Depending on the counter ion, catalyst anchoring via electrostatic interactions (Scheme 5c) might change the catalytic performance. The covalent heterogenization of chiral homogeneous ligands or its metal complexes is known as a classical immobilization method, despite the sometimes costly synthesis of new ligand systems that is required for the anchoring on a suitable support. Among other things, the immobilization of a metal complex is influenced by the modification of the chiral ligand, the length and flexibility of the linker, the catalyst loading, the accessibility of the active catalyst center, and the choice of the solvent.
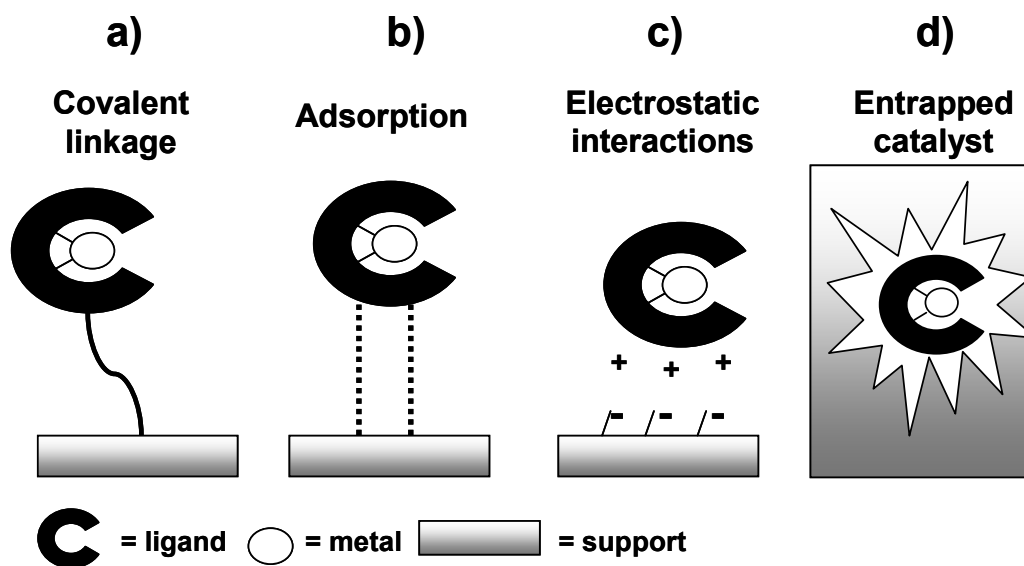
Scheme 5. Different immobilization strategies for homogeneous transition metal catalysts.

Two conflictive strategies are pursued for the interactions between the support and the catalyst: (i) the usage of long and flexible linker systems to avoid interactions that might

influence the catalytic performance; (ii) the close attachment of the catalyst to the support, which sometimes leads to an improved catalytic performance.

1.2.2. Supports for Catalyst Immobilization

The different types of catalyst supports can be classified into solid or liquid organic (such as organic polymers,[22-24] carbon nanotubes,[25] and ILs[26]) and inorganic materials[27] (such as inorganic polymers, ordered mesoporous materials, alumina, silica, and inorganic oxides). A suitable support for the immobilization of transition metal complex catalysts highly depends on the catalytic system and has to be chosen carefully in the case of air-sensitive catalysts. Various supports show different properties concerning mechanical strength, thermal stability, solubility, and swelling properties. Numerous problems[18, 19] can occur during the immobilization of a homogeneous catalyst and diminish its performance: (i) undesired interactions between the support and the metal-ligand complex, (ii) blockage of the optimal catalyst geometry (crucial for high enantioinduction) by the support, (iii) unsatisfactory stability of the linkage between the catalyst and support or the catalyst itself which results in leaching, (iv) limited accessibility of the active site, (v) undesired isolation of catalyst centers that need to cooperate during the reaction.

Surprisingly, linear polysiloxanes, being widely used as fluids, surfactants, release agents, and lubricants,[28] possessing good thermal, oxidative, chemical, and biological stability have been rarely used as catalyst supports,[29, 30] although hydrosilylation reactions allow to immobilize tailor-made homogeneous catalysts onto polysiloxanes in a very efficient way.

1.3. Integration of Chemical Reaction and Analysis

1.3.1. Microfluidic Devices

Depending on the support, the immobilized catalysts can be applied as a stationary phase in a continuous flow reactor.[31] So far, flow-through processes are limited to production processes, although they assure automation, safety, and reproducibility. Only recently, chemists have begun to broaden their toolkit by focusing on the development of flow-through devices for laboratory use and industrial applications.[32-43] Microfluidic devices represent a promising approach for parallelized high-throughput (ht) screening of catalysts and materials
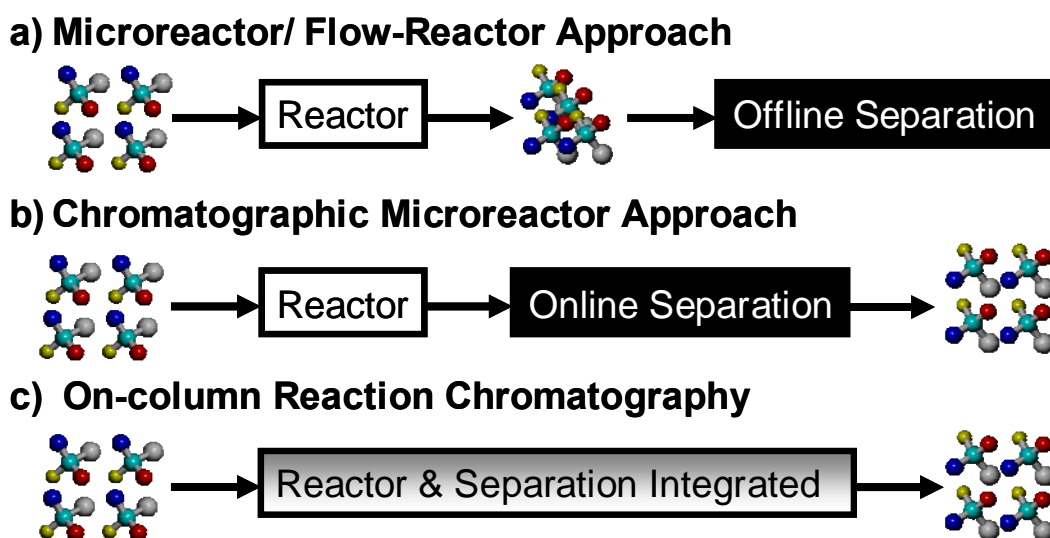
with reduced reagent costs and amount of chemical waste.[44-50] The development of microfluidics started with microanalytical methods,[46, 51] e.g. in chromatography, where capillary formats were used to separate molecules from mixtures. Interestingly, initial theoretical work on scaling down devices in chromatography was published as early as in the 1950s.[52, 53] Using very small amounts of sample, today these techniques achieve a high sensitivity and resolution analysis: On the other side, these applications are facing major challenges like sample preparation and detection.[50] Most recently, new types of organic synthesis in small-channel systems for the generation of compound-libraries has been developed.[47] Although non-catalytic liquid phase applications play a major role, the high surface-to-volume ratio of a microfluidic reactor is suitable for heterogeneous catalysis.[48] A further development was achieved with systems that integrate synthesis and analysis on the same chip (so-called lab-on-a-chip[54]). In these systems, real-time product identification and quantitation is achieved by the combination of microfluidic reactors with analytical devices. With this combination, the control of reaction parameters such as temperature, reagent concentration, and pH, but also real-time identification of the small-molecule products can be achieved. Despite the rapid development in this area, there are still many challenges,[50] which need to be solved, among these is the control of mixing, because diffusion rates contribute to apparent reaction rates and incompatibility with standard analytical instruments.

1.3.2. High-Throughput Gas Chromatographic Analysis

Chromatographic techniques allow separating complex product mixtures that are often obtained in ht screenings, usually being the time limiting step in the whole workflow. Concerning gas chromatography (GC), ht screening techniques[55] use (a) offline GC analysis, (b) online GC analysis and (c) the integration of chemical transformation and analysis (on-column reaction chromatography) (Scheme 6).

Offline GC analysis, where the sample is first collected and then injected into an external GC, is widely used to analyze reaction mixtures from catalytic studies in a sequential or parallelized fashion by detecting conversions at defined points of time. This technique is not perfectly suited for kinetic measurements, because samples have to be taken out of the reactor in pre-defined time intervals and have to be quenched[56, 57] to avoid further conversion. This often leads to irreproducible or imprecise kinetic data.

In contrast, systems with a GC directly coupled to the chemical reactor offer the possibility of real-time analysis.[58-60] The measured reaction mixtures are always analyzed under comparable conditions and reaction times are precisely controlled. Furthermore, online GC analysis is ideal to study fast reaction processes ($k > 10^{-2}$ s^{-1}) of substrate libraries in an ht mode.

a) Microreactor/ Flow-Reactor Approach

b) Chromatographic Microreactor Approach

c) On-column Reaction Chromatography

Scheme 6. Schematic representation of a) microreactor / flow-reactor approach with offline GC analysis, b) chromatographic microreactor approach with online GC analysis and c) on-column reaction chromatography with integration of chemical transformation and analysis.

Although GC is generally considered as a slow analysis method, cycling times in the range of several minutes can be achieved to analyze high-throughput experiments[61] with optimized temperature programs, with fast GC methods using decreased column diameters, high heating rates and decreased column lengths, with multidimensional techniques, or with multi-capillary columns consisting of multiple single liquid phase coated capillaries that are bundled in one monolithic glass tube in a regular geometric structure.[62-64] In so-called micro-GC systems the column is miniaturized, which results substantially decreased analysis times. A drawback of these systems is the limited range of compounds which can routinely be analyzed with micro-GCs due to the restricted choice with respect to the columns. Two-dimensional chromatographic methods allow shortening of analysis times, since those sections of the chromatogram that are difficult to resolve and thus would need longer run times are injected into a second column, which allows efficient separation of these compounds.[65]

A significant shortening of analysis time can be achieved with multiplexing techniques. Trapp has implemented a multiplexing approach to GC.[66-69] Specifically, a distinct binary injection sequence was assigned to each sample. Multiple samples were injected continuously onto a separation column in according to their assigned bar-code sequence, resulting in a much higher proportion of detected signals during a given time period than in traditional chromatography. By a Hadamard transformation[70] and subsequent matrix manipulations, the overlapping data could be deconvolved into individual chromatograms. Samples composed of several organic alcohols and hydrocarbons could be analyzed and an enhancement in efficiency by a factor of nearly 40 was noted.

1.3.3. On-Column Reaction Chromatography

As illustrated in Scheme 6c, the approach of on-column reaction chromatography combines catalytic activity and separation selectivity in a single column. Reaction substrates and products can be separated according to the selectivity of the stationary phase. In particular, slower reactions ($k < 10^{-2}$ s^{-1}) can be studied in great detail, because data of reaction kinetics, adsorption as well as parameters of diffusion can be obtained from temperature- and flow-dependent measurements. The observed elution profiles, characterized by a plateau formation between the reaction educt and product, can be analyzed with the unified equation of chromatography,[71, 72] which can evaluate reaction rate constants k of all kinds of first order reactions of processes taking place during a separation process. The facile handling of the catalytically active separation capillaries allows to switch between on-column reaction chromatography in a single catalytically active capillary and a chromatographic microreactor mode (Scheme 6b), which broadens the applicable time-scale window.

In 1959, Tamaru[73] reported for the first time on integrating catalysis and chromatographic separation by depositing Pd on Celite 545 and using this as packing material in GC to study the decomposition of formic acid. Further contributions on this topic were made by Bassett and Habgood,[74] who studied the catalytic isomerization of cyclopropane using Linde molecular sieve 13X exchanged with Ni^{2+} ions on a packed column. Gil-Av and Herzberg-Minzly[75] investigated Diels-Alder reactions by impregnating the stationary phase of the separation column with chloromaleic anhydride and injecting various dienes to form the Diels-Alder product. Langer et al.[76-78] studied the kinetics of the dissociation of endo-

dicyclopentadiene (retro-Diels-Alder reaction) and Marriott et al.[79] investigated the same reaction. Comparing packed with capillary columns. They reported that packed columns with larger diameters were more efficient than using coated capillary columns. This result was unexpected, as in general, high surface areas are desirable for catalyzed reactions. The specific interfacial area per volume (a_{inter} = 2/r) is high for microstructured reactors. For capillaries with inner diameters between 250 and 100 μm, the specific interfacial area per volume ranges from 16,000 to 40,000 $m^2\,m^{-3}$. Because reactions in a chromatographic system are studied in a continuous flow, kinetic evaluations are generally complex. Therefore, Phillips et al.[80-82] developed stopped flow techniques to investigate reactions with several reaction pathways and to identify the individual products. They also used displacement chromatography with a moving heater to study the formation of propadiene from the more thermodynamically favored propyne in quantities beyond the equilibrium proportions using slowly activated alumina as catalyst.[83] To perform kinetic studies, the reactor column was coupled to an analytical column with two 6-port switching valves for fast analysis.

In 2007 Trapp et al.[84, 85] reported an ht reaction rate measurement study by using the polymeric stationary phase of a chromatographic separation capillary to both immobilize catalysts and separate the products. The polymer serves as a catalyst and chromatographic separation material, so that catalysis and product separation are efficiently combined. The method was demonstrated for hydrogenations over highly active Pd nanoparticles and ring closing metathesis (RCM) reactions over Grubbs 2nd generation catalyst. For the Pd nanoparticle-catalyzed hydrogenations, a throughput of 5880 reactions in 40 h was obtained. To synthesize Pd nanoparticles with a narrow size distribution of 3.2 ± 0.7 nm for on-column hydrogenation experiments, the metal particles were embedded in a stabilizing polysiloxane matrix (Scheme 7). The obtained polysiloxane-stabilized nanoparticles were then coated onto the inner wall of microcapillaries. Substrate libraries consisting of 22 unsaturated and functionalized compounds were injected onto the column at different temperatures and carrier gas flows to vary the reaction time and to obtain temperature-dependent kinetic data. With these highly active Pd nanoparticles, extraordinarily fast hydrogenations in the range of 20 ms to 1 s were observed. Kinetic measurements were performed with a 2 cm capillary (Scheme 8). Data from conversion measurements were evaluated with kinetic models[86] based on a Langmuir-Hinshelwood mechanism to determine reaction rate constants k and activation parameters ($\Delta G^{\neq}$, $\Delta H^{\neq}$ and $\Delta S^{\neq}$).
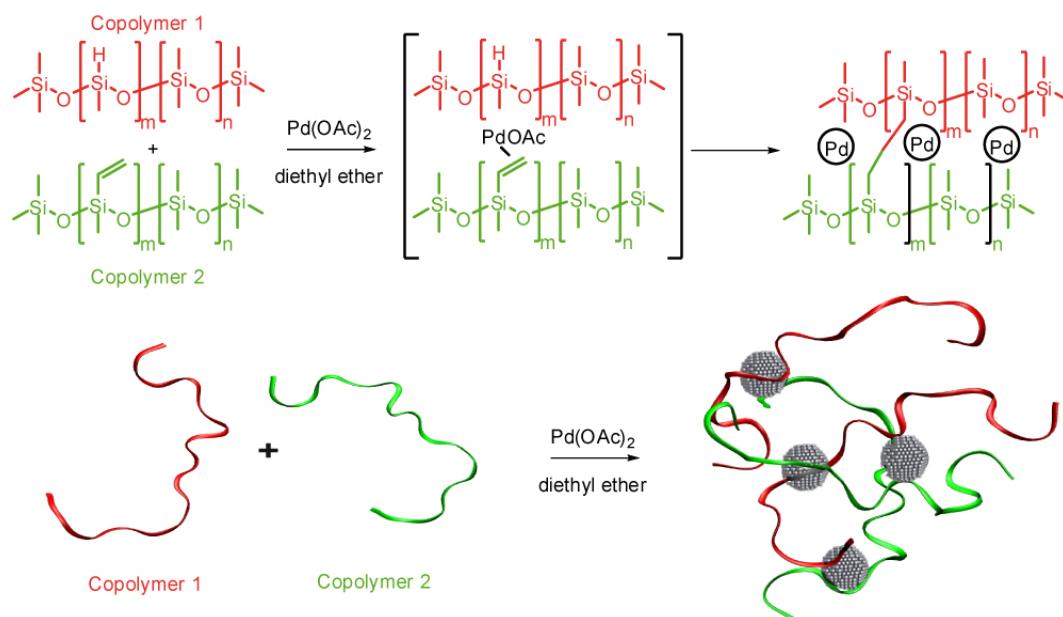
Scheme 7. Preparation of highly active Pd nanoparticles embedded in a polysiloxane matrix.

The same setup could also be used to hydrogenate cyclohex-2-enone on a preparative scale to produce 20 mg h^{-1} of cyclohexanone. An extensive study[87] including systematic TEM investigations showed that the size and morphology (crystalline or amorphous) of the nanoparticles strongly depend on the ratio of the stabilizing polysiloxanes, the conditions to immobilize the stationary phase on the surface of the fused-silica capillary, and the loading of the Pd precursor.
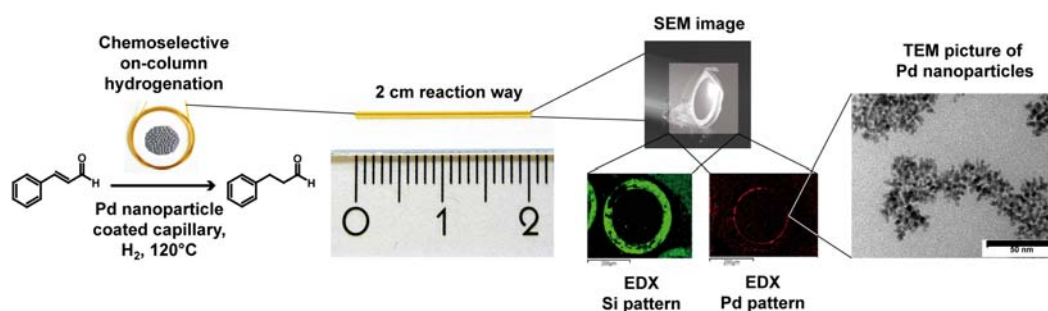
Scheme 8. On-column hydrogenation of unsaturated compounds over highly active Pd nanoparticles.

In RCM reactions, a 10 m capillary was coated with Grubbs 2nd generation catalyst dissolved in a PDMS matrix (GE SE 30, Scheme 9) with a catalyst loading of 1.6 µg cm^{-1} capillary $(1.9 \times 10^{-9}$ mol cm^{-1} capillary).
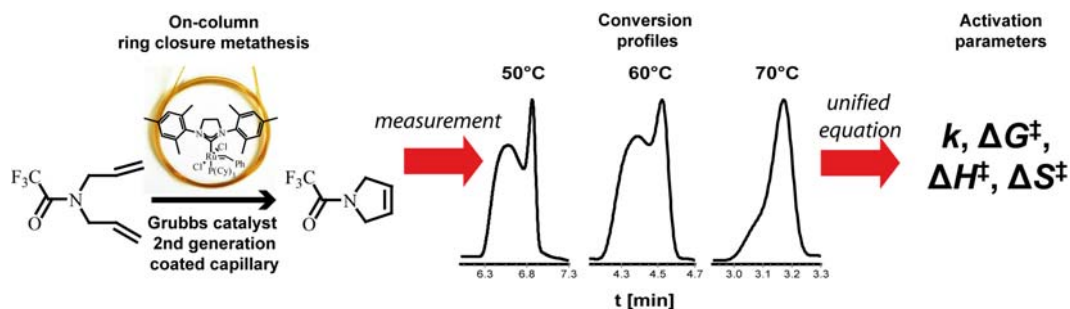
Scheme 9. On-column metathesis over the Grubbs 2nd generation catalyst.

Furthermore, substrate libraries consisting of 12 different RCM substrates were injected onto the column and elution profiles, characterized by a plateau formation between the reaction educt and product, were observed. These elution profiles were then analyzed by the unified equation of chromatography [71] to obtain reaction rate constants and activation parameters. It is remarkable that the catalyst was stable over a wide temperature range of up to 150 °C without any detectable leaching. Even cascade reaction could be performed by coupling an 80 cm column, coated with the dissolved Grubbs 2nd generation catalyst, and a 10 cm Pd nanoparticle column, followed by a separation column for product analysis. Scheme 10 shows the reaction cascade for the metathesis of *N,N*-diallyltrifluoroacetamide, followed by on-column hydrogenation to trifluoro-1-(pyrrolidin-1-yl)ethanone in less than 6 min with an overall yield of 49%.

Scheme 10. Modular design for a two-step on-column cascade reaction.

2. Objectives

The prerequisite for a directed design of catalysts is the understanding how the kinetics, i.e. the activation barrier in the catalytic mechanism is controlled by structural parameters. To identify rate-controlling elementary steps and to develop mechanistic models, comprehensive experimental kinetic data of a broad variety of substrates are needed. A precise and comprehensive kinetic characterization of transition metal catalysts requires an accurate temperature control, high reproducibility, comparability with batch tests, and short measurement cycles to characterize entire substrate libraries. Common kinetic characterization methods like online nuclear magnetic resonance (NMR) and mass spectrometry (MS) measurements sometimes do not meet all these criteria. At present, the limitation of investigating only a single reaction per run remains a bottle-neck in typical batch reactors and micro-reactors, where competing reactions lead to indefinable reaction kinetics. The combination of separation selectivity and catalytic activity in the same stationary phase of a GC capillary facilitates the precise adjustment of contact times and selectivities of the catalyst with the reaction educts. A simultaneous injection of large substrate libraries onto variable column configurations overcomes the limitation of sequential analytic measurements.

This thesis describes recent contributions to the development of on-column reaction chromatography and the understanding of the mechanism and activity of different catalyst systems. It is aimed to obtain comprehensive kinetic data from on-column reaction chromatography experiments that help to understand the factors influencing the mechanism of a catalyzed reaction. The application range of the recently described strategy[84, 85] should be extended by systematic investigations of (enantioselective) catalyst libraries, new stationary phases and covalent immobilization approaches. Widely used catalytic systems like cinchona alkaloid-modified Pt-catalysts for enantioselective hydrogenations of α-keto esters, ruthenium olefin metathesis catalysts for RCM reactions, metal-3-heptafluorobutanoylcamphorates for enantioselective intramolecular Diels-Alder reactions and metal-salen-complexes for the hydrolytic kinetic resolution (HKR) of terminal epoxides should be studied with on-column reaction chromatography.

In this context, the combination of enantioselective hydrogenations of α-keto esters over quinine-modified Pt and Pd nanoparticles and the consecutive separation of the obtained enantiomers in microcapillaries is targeted. The possibility to simultaneously determine enantiomeric excesses and reaction kinetics for entire substrate libraries should be investigated to obtain information about the mechanism from the activation parameters as well as to characterize the catalyst.

The catalytic activity of ruthenium olefin metathesis catalysts, which are widely used in several types of olefin metathesis reactions, can be significantly enhanced by a directed ligand design. A detailed kinetic investigation towards the activity of different ruthenium metathesis catalysts in RCM reactions by on-column reaction chromatography measurements should lead to reaction rate constants k and activation parameters, which are a prerequisite for a better understanding of catalytic mechanisms. The obtained activation parameters should be compared with reported literature data.

Kinetic investigations by chromatographic reaction control of catalytic transformations using room-temperature ionic liquids (RTILs) are difficult to perform due to difficult product isolation, and injection of ILs into the hot injector for GC analysis leads to accumulation of the IL and decomposition peaks or an increased noise level can be observed. Therefore, the study of RCM reactions should be extended with the combination of separation selectivity and catalysis using ILs and the Grubbs-type catalyst 1st generation to study the catalyst stability, recyclability and to efficiently determine reaction rate constants for various substrates. The comparison of activation parameters for polysiloxane- and IL-dissolved Grubbs-type catalyst should give information about the catalyst stabilization in the stationary phase.

The covalent immobilization of metal-3-heptafluorobutanoylcamphorates onto polysiloxanes is an attractive method to obtain polymers, which can be used as chiral stationary phases, chiral catalysts and NMR shift reagents. However, the known synthetic route was not widely used, because of toxic and potentially explosive reagents and limited flexibility and accessibility of the metal complex due to the short spacer. A modified synthesis route to polysiloxane-immobilized chiral camphor-based transition metal catalysts and their investigation with on-column reaction chromatography should be investigated. These

catalytically active stationary phases should be tested on their enantioselective separation efficiency as well as their catalytic activity in Diels-Alder reactions.

Cobalt- and manganese-salen-complexes are widely used catalysts for enantioselective epoxidation reactions and the HKR of terminal epoxides showing high activities and enantioselectivities in both reactions. Immobilized salen-based catalysts facilitate not only good recyclability, but also show higher activity and selectivity than their nonsupported counterparts. Therefore, the synthetic applicability of polysiloxane-supported chiral Co-salen-complexes should be studied following a modular immobilization method of monofunctionalized enantiopure unsymmetrical salen ligands with different spacer length by an ether linkage.

Chapter 3

Integration of Enantioselective Hydrogenation and Separation - Kinetic Investigations by Enantioselective On-Column Reaction Chromatography

3. Integration of Enantioselective Hydrogenation and Separation - Kinetic Investigations by Enantioselective On-Column Reaction Chromatography
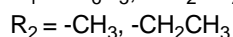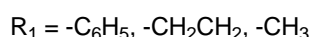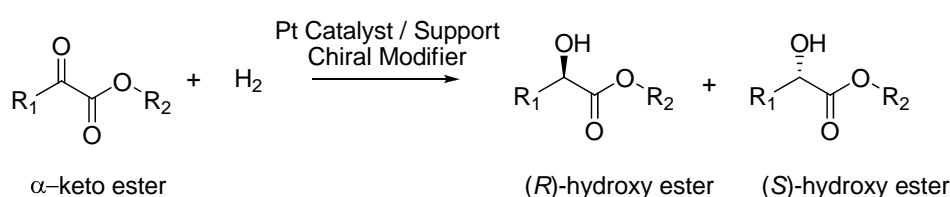
3.1. Introduction

Efficient enantioselective heterogeneous catalysts are of great economic and ecological impact, in particular, for the synthesis of enantiomerically pure drugs. The separation of the reaction product from the catalyst as an advantage of heterogeneous catalysis remains a major challenge in (enantioselective) homogeneous catalysis. The modification of heterogeneous catalysts by the addition of chiral organic ligands to influence the activity and selectivity is a common strategy to address these challenges. The early attempts to design a chiral heterogeneous catalyst focused on two strategies, namely the (i) modification of existing heterogeneous catalysts with naturally occurring chiral modifiers[88] and (ii) the usage of chiral solids such as quartz or natural fibers as supports for metallic catalysts. Even if only low enantiomeric excesses could be achieved, the proof of principle concept could be established for chiral heterogeneous catalysis.

The development of chirally modified metal catalysts started with a report of Erlenmeyer in 1922[89, 90] (Zn/fructose), followed by a Pt catalyst modified with β-methyl-cinnamic acid salt of hydrocinchonine described by Lipkin and Stewart[91] 17 years later. It was Nakamura in 1941,[92] and later Isoda[93] and Izumi,[94, 95] who described chiral acid-modified platinum and nickel catalysts. These catalytic systems, also known as the "nickel tartaric acid/NaBr system",[96, 97] found their most prominent use in the enantioselective hydrogenation of β-functionalized ketones,[98] β-diketones,[99] and sterically demanding methyl ketones[100] with optical yields as high as 92%. Reviewing all approaches for designing a chiral solid catalyst, to date the only process of industrial relevance is the application of chirally modified metal hydrogenation catalysts, namely nickel catalyst modified with tartaric acid and Pt and Pd catalysts modified with cinchona alkaloids. The "Orito catalyst" is more widely used, because it does not require a difficult catalyst preparation and, therefore, represents an attractive alternative to a soluble transition metal complex catalyst. However, the active catalyst system itself is far more complex and its understanding is challenging.

3.1.1. The Platinum-Cinchona System

In 1979, Orito, Iwai, and Niwa[101, 102] firstly reported about the asymmetric hydrogenation of α-keto esters over cinchona alkaloid modified Pt catalysts, which provided enantiomeric excesses (ee) in the range of 75–80% (Scheme 11). This catalytic system has been studied extensively in the following years leading to ee values of 97% with optimized procedures.[103-107] To get a detailed insight into rate determining elementary steps, several groups studied fundamental aspects of this reaction, e.g. the role of different substrates, metals, supports, alkaloid modifiers,[108-110] and solvents.[111, 112]

R_1 = -C$_6$H$_5$, -CH$_2$CH$_2$, -CH$_3$
R_2 = -CH$_3$, -CH$_2$CH$_3$

Support: alumina, carbon, silica, titania, zeolithe

Chiral Modifier:

quinine: R_3 = C$_2$H$_3$, R_4 = OCH$_3$
chinchonidine: R_3 = C$_2$H$_3$, R_4 = H
dihydroquinine: R_3 = C$_2$H$_5$, R_4 = OCH$_3$
dihydrochinchonidine: R_3 = C$_2$H$_5$, R_4 = H

quinidine: R_3 = C$_2$H$_3$, R_4 = OCH$_3$
chinchonine: R_3 = C$_2$H$_3$, R_4 = H
dihydroquinidine: R_3 = C$_2$H$_5$, R_4 = OCH$_3$
dihydrochinchonine: R_3 = C$_2$H$_5$, R_4 = H
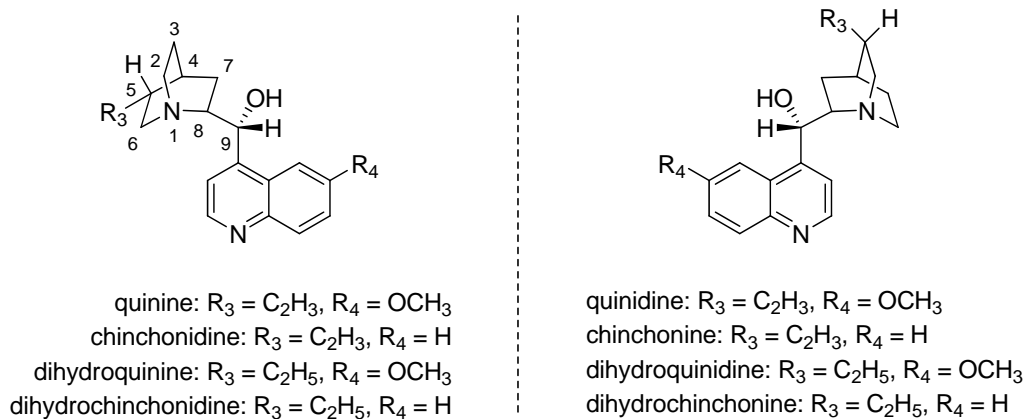
Scheme 11. Enantioselective hydrogenation of α-keto esters using Pt catalysts modified with cinchona alkaloids.

Although some of these findings resulted in a better understanding of the mechanism and led to the development of mechanistic models,[113] some experimental phenomena remain

unexplained, e.g. the influence of catalyst preparation, activation, substrate specificity and also the particle size of colloidal Pt catalysts. The role of substrates, metal catalysts, alkaloid modifiers, as well as solvent effects, kinetic studies and mechanistic models of this catalyst system are addressed briefly in the following section.

Substrates

Cinchona-modified platinum catalysts are highly substrate-specific. Only with α-keto acid derivatives high enantioselectivities could be obtained. Typically, ethyl pyruvate (**etpy**) is used as a model substrate, but also α,γ-diketo esters,[114] α-keto lactones,[115-117] α-keto acetals,[118] and α-keto ethers[119] showed high selectivities. High ee values in the enantioselective hydrogenation of trifluoromethyl ketones[120] disproved the previously postulated importance of the α-dicarbonyl fragment in the substrate. Furthermore, it could be shown that electron-withdrawing groups (EWGs) increase and electron-donating groups (EDGs) diminish the ee-value.[121]

Metal Catalysts

Various attempts were made to modify other metals with cinchona alkaloids and to extend the scope to the hydrogenation of carbon-carbon double bonds with Pd catalyst. Most of these attempts could not yield satisfactory enantioselectivities and catalytic activities.[104] Different supports like alumina, silica, carbon, titania and zeolites for chirally modified Pt catalysts were reported to give high ee values in hydrogenation reactions, although the efficiency of the benchmark (chirally modified 5% Pt/ Al_2O_3 catalysts)[122] could not be surpassed.

Additionally, the application of cinchona alkaloid modified metal nanoparticles to chiral hydrogenations has previously been reported.[123-129] Their suitability as catalyst systems arises from the possibility of precise morphology control. In particular, the distinct structure sensitivity of conventional supported Pt catalyst and the dependence of the ee on the Pt particle size in batch reactors has been studied by Baiker and Blaser and it has been reported that very small nanoparticles do not promote enantioselectivity.[130-132] A minimal diameter for good ee values was estimated to 4.0 ± 1.5 nm. Other studies revealed that catalysts with metal particles < 2 nm were less selective and showed lower turnover frequencies.[133] Therefore, it was concluded that flat surfaces are advantageous for the adsorbation of the

chiral modifier. Collier et al.[128] prepared Pt colloids by metal vapor deposition techniques and obtained optical yields up to 40% ee with an optimized preparation procedure. Bönnemann and Braun[134, 135] could show that it is possible to obtain ee values of 80% for the hydrogenation of **etpy (1)** over small Pt clusters (1.5-4.0 nm) stabilized by the protonated modifier dihydrocinchonidine. Bradley and Köhler[125, 126] prepared polyvinylpyrrolidone (PVP) stabilized colloidal Pt catalysts (3.0 nm) and could show that these catalysts are highly active in the enantioselective hydrogenation of **etpy**, but with only modest selectivity (34% ee). In their kinetic studies, reaction rates varied from $(2.0-4.9)\times10^{-2}$ s^{-1} at 50% conversion. Zuo et al.[127, 129] obtained up to 97% ee for cinchonidine-modified enantioselective hydrogenation of pyruvates in favor of (R)-lactates over PVP-stabilized Pt with a particle size less than 2.0 nm.[129] In order to extend Baiker´s 1:1 cinchona-substrate interaction model (Scheme 13a, vide infra),[136] they performed molecular mechanics calculations of the modifier-reactant interaction on the Pt surface of small Pt clusters. Assuming an adsorption of the quinoline moiety of the cinchona alkaloid on the metal surface, it has been proposed that the modifier-reactant complex requires a flat space (Pt surface) large enough (about 20 Pt atoms) to be accommodated on. Their simulations compared the interaction between reactant and modifier on large Pt surfaces and a series of small clusters with 561 Pt atoms (or 147 Pt atoms) and a particle size of 2.7 nm (or 1.6 nm) assuming a close-packed face centered cubic (fcc) structure ($10n^2+2$ packing rule with n = layer number). They validated the possibility of the recognition on small Pt clusters (1.6 nm in particle size). Furthermore, they differentiated two cases of effective recognition, where chiral modifier and substrate are (i) on the same face or (ii) on adjacent faces. According to their calculations, the recognition of the two molecules located in the adjacent faces works until the particle size is about 1.6 nm.

Alkaloid Modifiers and Reactant-Modifier Complex Structure

Different cinchona alkaloids (cinchonine, quinidine, cinchonidine, and quinine, Scheme 11) can be isolated from the bark of different cinchona trees. These molecules with chiral centers at C_3,C_4, C_8 and C_9 ((S)- and (R)-configuration at C_8 and C_9) contain an aromatic quinoline ring system and a saturated quinuclidine ring system, which are separated by a carbon atom (C_9). They are inexpensive and available in large quantities. Studies on the systematic modifications of cinchona alkaloids led to the conclusion that there are crucial structural motifs for the control of enantioselectivity, which are: (i) a basic N-atom to interact with the

substrate (ii) an extended aromatic moiety to anchor the modifier to the metal surface, (iii) the absolute configuration at the C8 position and (iv) the substituent at the C9 position (-OH or -OCH$_3$). Several experiments[108] showed that a partial hydrogenation of the chinoline system leads to a decrease in enantioinduction, whereas the *N*-alkylation led to a complete loss of selectivity. Pfaltz et al.[109, 110] synthesized relatively simple amino alcohols with just one stereogenic center, which showed good enantioselectivities. Catalytic experiments with cinchona analogues bearing different aromatic parts and chiral amino groups showed significantly higher enantioselectivities for certain modifications.[137] Further studies led to the conclusion that the flexibility and conformational rigidity are fundamental characteristics of effective modifiers.[138, 139]

Solvent Effects

The enantioselectivity of the described catalyst system is very sensitive to the nature of the solvent. Acetic acid was found to be superior to all classical solvents (up to 95% ee for **etpy**),[111] but alcohols and nonpolar solvents such as toluene (which is often chosen for production processes for technical reasons) can also be used.

Kinetic Studies

A closer look at the kinetic behavior of the modified catalyst showed that enantioselectivity is a function of pressure and temperature and that the rate of reaction is significantly higher for the modified enantioselective catalyst system than for the unmodified catalyst in a batch reactor.[140-144] This observation is also known as "ligand acceleration", a phenomenon that was firstly termed by Sharpless et al.[145] for the homogeneous asymmetric dihydroxylation of olefins catalyzed by Os complexes with cinchona alkaloid ligands. The higher reaction rates for the modified Pt catalysts were explained with a kinetic model having three different catalytic cycles, which is shown in Scheme 12. This kinetic model with a slow, racemic reaction on the unmodified catalyst and an about 10 times faster reaction with an ee around 80% on the modified sites gave a very good fit to the measured data in ethanol.[141, 146, 147] Later, it was suggested that the rate acceleration might occur due to the creation of additional active sites and not because of the modification of existing sites.[148] Further studies revealed effects of catalyst loading, modifier and substrate concentrations, hydrogen pressure, and temperature on the rate and ee of the unmodified and the modified systems.[149] It can be

concluded that the optimal modifier concentration highly depends upon the type of catalyst, the solvent, and the chiral modifier.
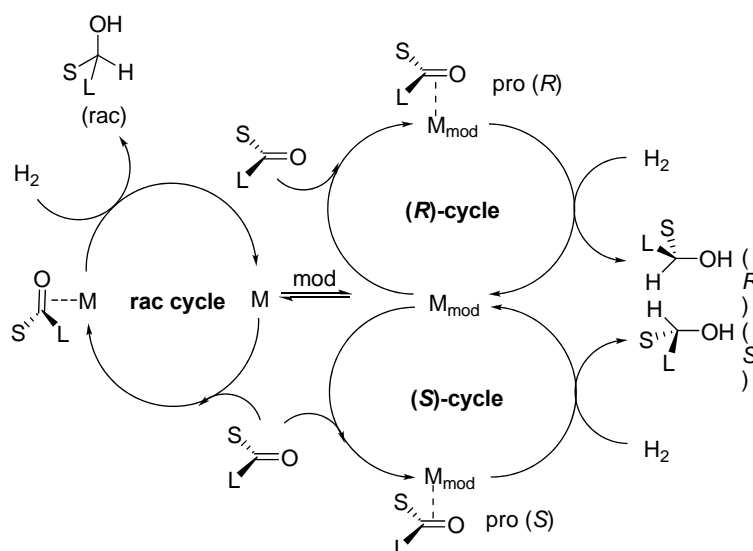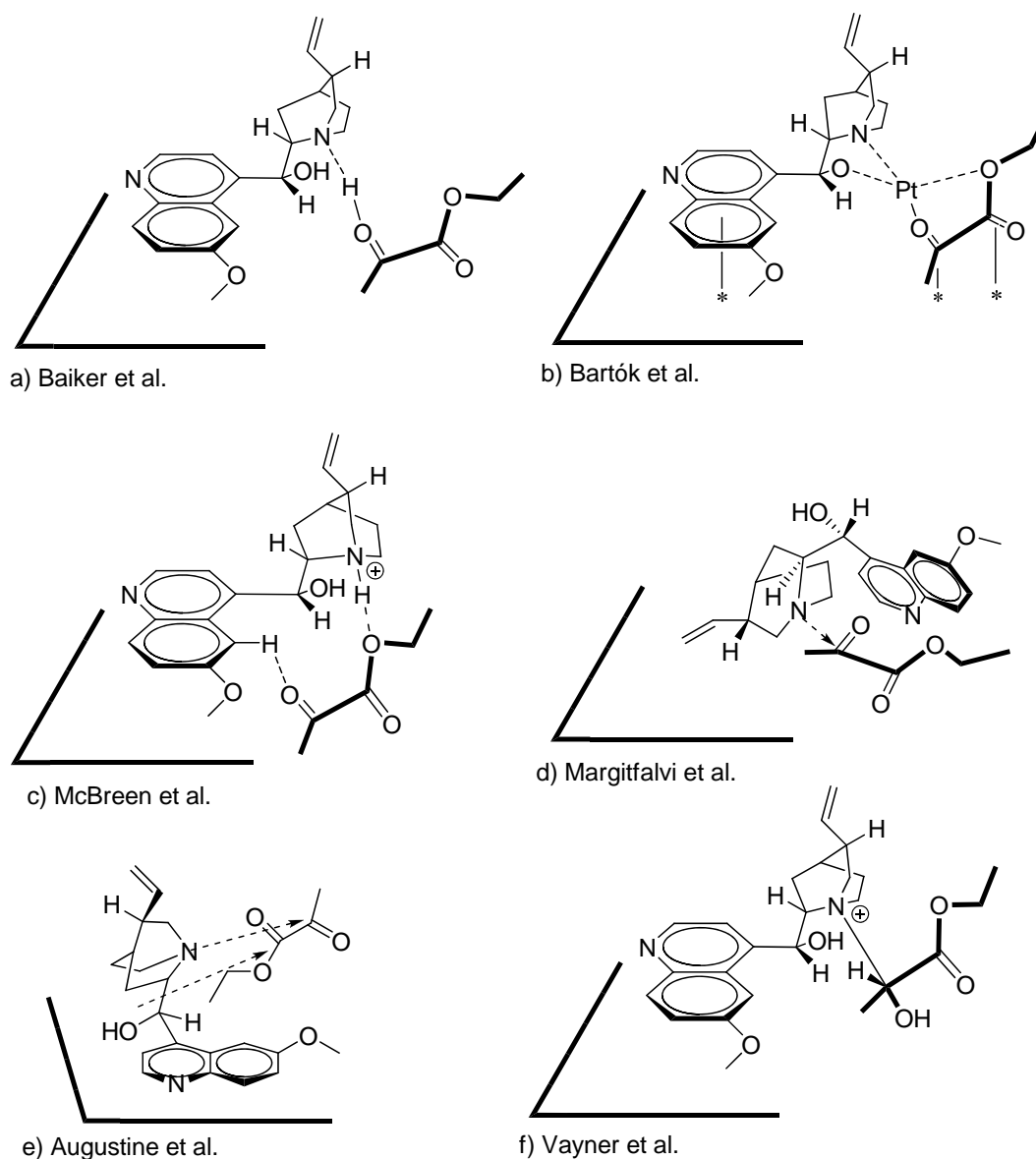

Scheme 12. Schematic catalytic cycles for the hydrogenation of ketones on a partially modified catalyst reported by Blaser,[106] where M = active site, mod = modifier, L = large substituent, S = small substituent.

The discussed kinetic models based on a Langmuir-Hinshelwood mechanism, where the basic catalytic cycle consists of (i) the adsorption of the substrate and the hydrogen on the Pt surface, (ii) the stepwise addition of the two adsorbed hydrogen atoms to the C=O bond with a half-hydrogenated intermediate, and (iii) the desorption of the product. Although various kinetic studies on Pt-catalyzed enantioselective reactions have been reported, there is no clear proof of the real nature of rate enhancement Hutchings et al.[150, 151] studied the cinchonidine-based Orito reaction in the gas phase and observed that the pre-modified catalysts showed a decrease in reaction rate compared to the unmodified reference catalyst at the gas-solid interface contrary to the proposed "ligand acceleration". This gas phase hydrogenation of methyl pyruvate in the presence of chinchonidine showed only moderate ee values (ee < 40%) and, unexpectedly, the rate of reaction was found to be about ten times lower than in the liquid phase.

Theoretical Models

Numerous theoretical and experimental observations in Pt-catalyzed hydrogenations of pyruvates with cinchonidine led to the development of three different controversially

discussed mechanistic models,[113] among these are: (i) the adsorption model,[113] (ii) the shielding model[104] and (iii) the zwitterion model[152] (Scheme 13).

a) Baiker et al.

b) Bartók et al.

c) McBreen et al.

d) Margitfalvi et al.

e) Augustine et al.

f) Vayner et al.

Scheme 13. Proposed theoretical models for the enantioselective hydrogenation of etpy on cinchona-modified Pt catalysts reported by Mallat:[107] the adsorption model (a-c), the shielding model (d) and the zwitterion model (e, f).

The first and widely accepted model assumes the adsorption of the quinoline moiety of the cinchona alkaloid on the metal surface and attractive interactions between the quinuclidine nitrogen, which is protonated in protic solvents, and the adsorbed ketone resulting in an NH⋯O hydrogen bond (Scheme 13a-c, Scheme 14a-b).
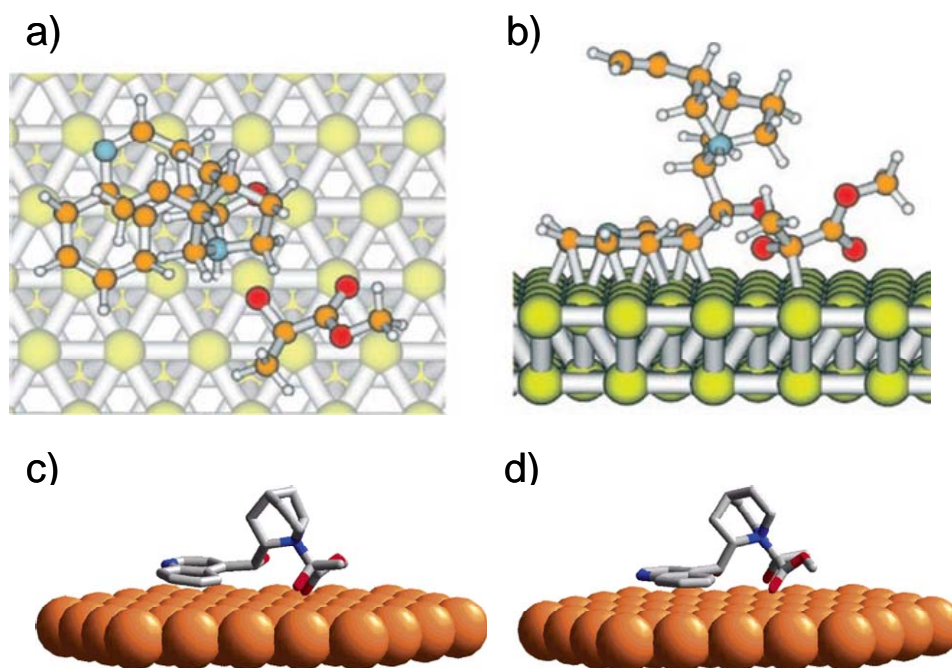
Scheme 14. (a)/(b) Adsorption model of the interaction between the Pt adsorbed chinchonidine and methyl pyruvate, based on DFT calculations, reported by Bürgi.[113] (orange = carbon, red = oxygen, blue = nitrogen). Subtle differences in geometry and energy between (c) the more stable (*S*)- and (d) (*R*)-zwitterionic cinchonidine-pyruvate adducts control enantioselectivity in hydrogenation reactions reported by Vayner et al.[152] (grey = carbon, red = oxygen, blue = nitrogen).

In apolar solvents such as toluene, the complex forms between the alkaloid and a half-hydrogenated state of the pyruvate. The adsorbed substrate, which is stabilized in this diastereomeric 1:1 complex with the adsorbed chiral modifier, is then hydrogenated predominantly from one of the two enantiotopic faces. Experimental and theoretical investigations of Baiker,[113, 153] Bartók[105] and McBreen[154, 155] refined this qualitative model (Scheme 13a-c). Margitfalvi et al.[156, 157] proposed a model assuming a supramolecular complex that is stereoselectively reduced on the Pt surface (Scheme 13d). The "shielding effect" suggests a weak complexation of the substrate and the modifier in solution. The quinoline ring is supposed to shield the opposite face of the substrate and, therefore, plays an essential role for the chiral induction in this model. A model suggested by Augustine et al.[158] implies the adsorption of the cinchona molecule either via the π-system or via the N atom of the quinoline close to a Pt ad-atom on which both hydrogen atoms and **etpy** are adsorbed. Furthermore, they proposed a nucleophilic catalytic step involving the N atom of the quinuclidine and the ketone carbonyl (Scheme 13e). In 2004, Vayner et al.[152] refined this

model by using a variety of computational techniques. The authors suggest a strong covalent bond as the key interaction between cinchonidine and the pyruvate (Scheme 13f, Scheme 14c-d). This nucleophilic addition step results in a surface-bound zwitterionic adduct between the chiral modifier and the substrate. The charged species is likely to be stabilized via H-bonding in acidic media. In the next step, the newly formed C-N bond undergoes hydrogenolysis with overall symmetry inversion.

3.1.2. Objectives

Although much progress has been made toward molecular level knowledge about chirally modified metal catalysts, the presented models cannot combine and explain all experimental and theoretical observations that have been made so far. A basic prerequisite for a wider field of applications of such systems is to understand how the structural parameters of the catalyst system affect the activation barriers during catalysis and how the selectivity and reaction kinetics can be controlled. Comprehensive experimental kinetic data of a broad variety of substrates are thus needed. One promising approach is offered by microfluidic devices for parallelized ht kinetic measurements of catalysts. Microstructured reaction systems for synthesis and kinetic studies are attractive because the effect of mass transfer between different phases is reduced by a highly specific interfacial area per volume. Furthermore, in micro structured reactors, physical processes can be more easily controlled and low operation volumes minimize reagent consumption,[49] which has already been demonstrated for asymmetric hydrogenations.[159-161] However, to determine ee values and conversions, the reaction, separation, and quantification of the educts and products have to be performed consecutively up to now and, therefore, these systems can only study one reaction per run.

The extension of the previously reported strategy of Trapp et al.[84, 85] to enantioselective hydrogenation reactions is presented in this chapter. Quinine-modified Pt and Pd nanoparticles were stabilized in a polymeric stationary phase and coated inside a chromatographic separation capillary to combine separation selectivity and catalytic activity in a single chromatographic column (Scheme 15). On-column reaction chromatography enables a systematic kinetic study for the enantioselective hydrogenation of a prochiral substrate library consisting of different α-keto esters. The obtained thermodynamic and

kinetic parameters are used for a comprehensive characterization of catalysts and materials and can be correlated with the catalyst structure to develop mechanistic models.
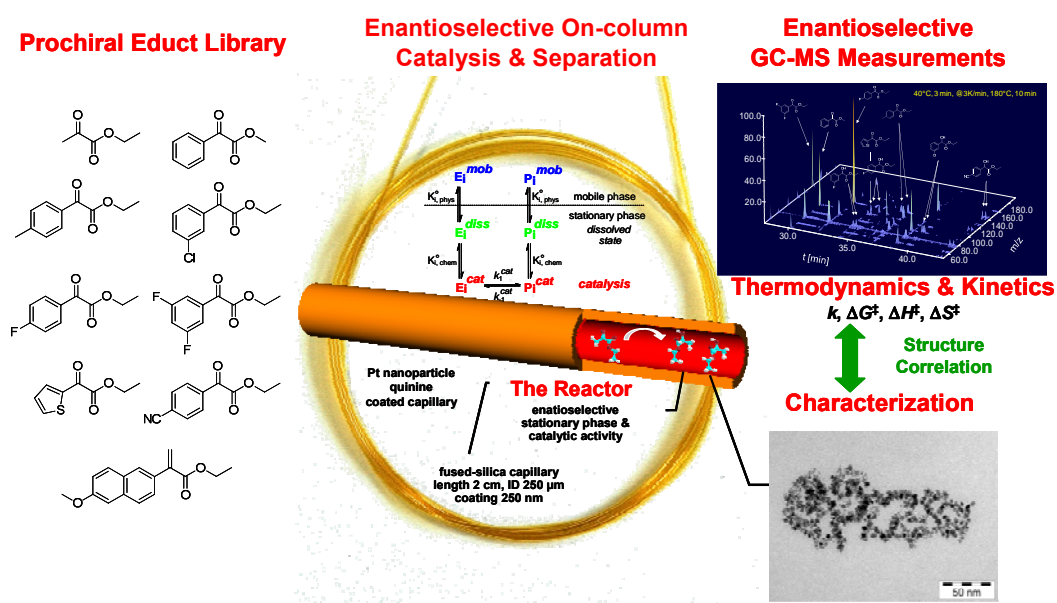

Scheme 15. Overview scheme of enantioselective on-column catalysis and separation using a quinine-modified Pt or Pd nanoparticle-coated microcapillary to investigate thermodynamic and kinetic data of prochiral substrate libraries.

3.2. Results and Discussion

3.2.1. Preparation of Catalytically Active Stationary Phases and Coating of Microcapillaries

The preparation of polymer-stabilized colloidal Pt catalysts and their usage in the chiral hydrogenation of **etpy (1)** to **etlac (2)** due to chiral modification with quinine **(3)** has been reported (Scheme 11).[125-127, 129, 162] Bradley et al.[126] noted that the stabilizing polymer in the colloidal catalyst does not hinder access of the modifier molecule to the colloidal metal surface, but that the polymer may reduce the number of surface-modified sites available for the faster enantioselective hydrogenation by adsorption at the metal surface. The preparation of transition metal colloids with silanes was firstly reported by Lewis et al.,[163-165] who demonstrated that presumably homogeneous hydrosilylation catalysts formed from Pt compounds in the presence of silanes were, in fact, colloidal in nature, raising the prospect of colloid activity in many ostensibly homogeneous catalyst systems. They used silanes and Si-H-containing polymers to reduce $Pd(hfacac)_2$ (hfacac = hexafluoroacetyl-acetonate) to colloidal Pd in organic solvents.[166] Following this approach, the previously reported strategy of Trapp et al.[84, 85, 87] was extended by using hydridomethylsiloxane-dimethylsiloxane copolymer **(4)** (HMPS) and methylvinylsiloxane-dimethylsiloxane copolymer **(5)** (MVPS), which act simultaneously as reducing agent and cross-linker, as well as chirally modified polysiloxanes to integrate enantioselective catalysis with separation selectivity. The MVPS **(5)** (4.5% $Si(O)(CH_3)(CH=CH_2)$ groups) coordinates $Pt(acac)_2$ **(6)** (acac = acetylacetonate) or $Pd(OAc)_2$ **(7)** (OAc = acetate) to the vinyl groups in dichloromethane. Quinine-modified Pt colloids were prepared from $Pt(acac)_2$ **(6)**, because both the metal precursor and the modifier are soluble in dichloromethane that was used as coating solution for the microcapillaries. HMPS **(4)** (25.7% $Si(O)(CH_3)H$ groups) was added to this mixture to reduce Pt^{2+} to Pt^0 (or Pd^{2+} to Pd^0) and to obtain an inert protecting matrix for the respective metal nanoparticles. Cross-linking with the MVPS **(5)** was achieved by hydrosilylation, catalyzed in the presence of the metal precursor or the metal nanoparticles.

In a first approach, polysiloxane-supported quinine **(10)** (Chirasil-Quinine, 5.8% $Si(O)(CH_3)$-Qn groups) was added as the chiral modifier to the HMPS/MVPS mixture (Scheme 16a).
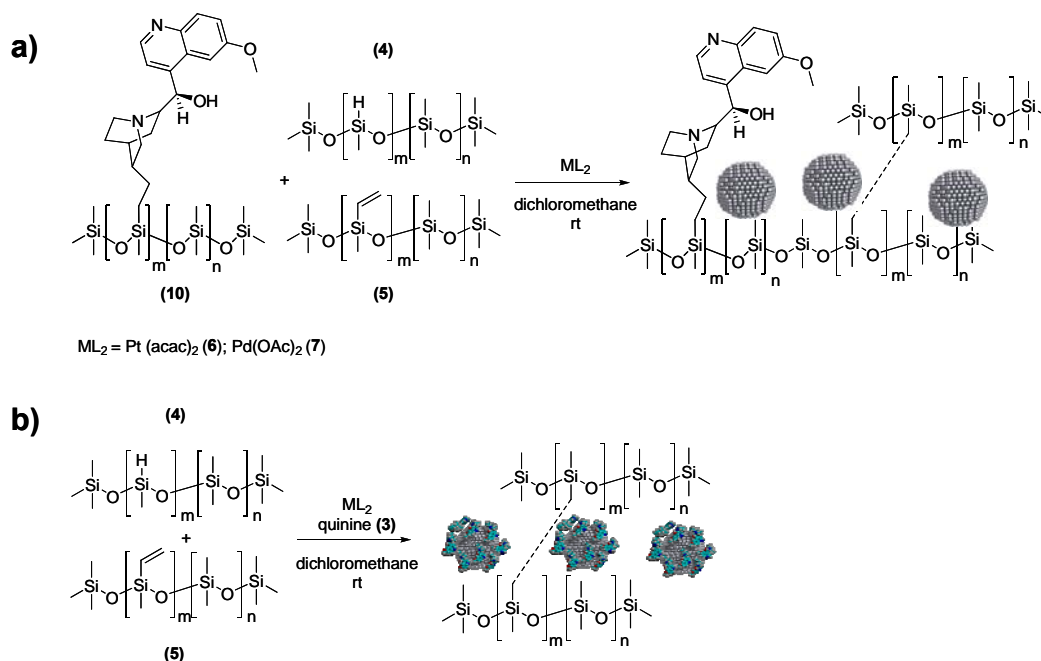
Scheme 16. Preparation of highly active Pt and Pd nanoparticles embedded in a chiral modified polysiloxane matrix. a) Metal nanoparticles embedded in polysiloxane-supported quinine embedded. b) Polysiloxane-stabilized quinine-modified metal nanoparticles.

The first immobilization of cinchona alkaloids on polysiloxanes was reported by DeClue et al.[167] They modified cinchona alkaloid with a 10-undecenoyl-spacer on its 9-O position and immobilized it via hydrosilylation using a catalytic amount of dichlorodi(cyclopentadienyl) platinum(II) (Cl$_2$Ptdcp) **(58)** on a commercially available HMPS. This modified polysiloxane was successfully tested in OsO$_4$-catalyzed asymmetric dihydroxylation (AD) reactions with excellent yield and selectivity (> 99% ee in nearly quantitative yield). Using straightforward purification techniques (i.e. precipitation, simple filtration, or ultrafiltration), these polymeric ligands were easily separated from the diol product and reused multiple times. A more convenient approach is the direct immobilization of quinidine through its ethylene group. Grunlan et al.[30] could immobilize quinine **(3)** on a siloxane support by protecting the hydroxy functionality with an acetate group **(8)** before hydrosilylation. The resulting polysiloxane-supported quinine acetate **(9)** was then deprotected with potassium carbonate (0.15 wt%) in aq. ethanol (90%) to obtain the desired polysiloxane-supported quinine **(10)** (Scheme 17). This catalyst was tested in Michael additions using thiols and α,β-unsaturated ketones and esters. Using a latent biphasic liquid/liquid separation (50:50 mixtures of *n*-heptane and EtOH) to recover the polymeric catalyst, its usage was successful through five

cycles in several examples of this reaction with varying yields (42–100%, catalyst loading 10 mol%), but only modest ee (20%).
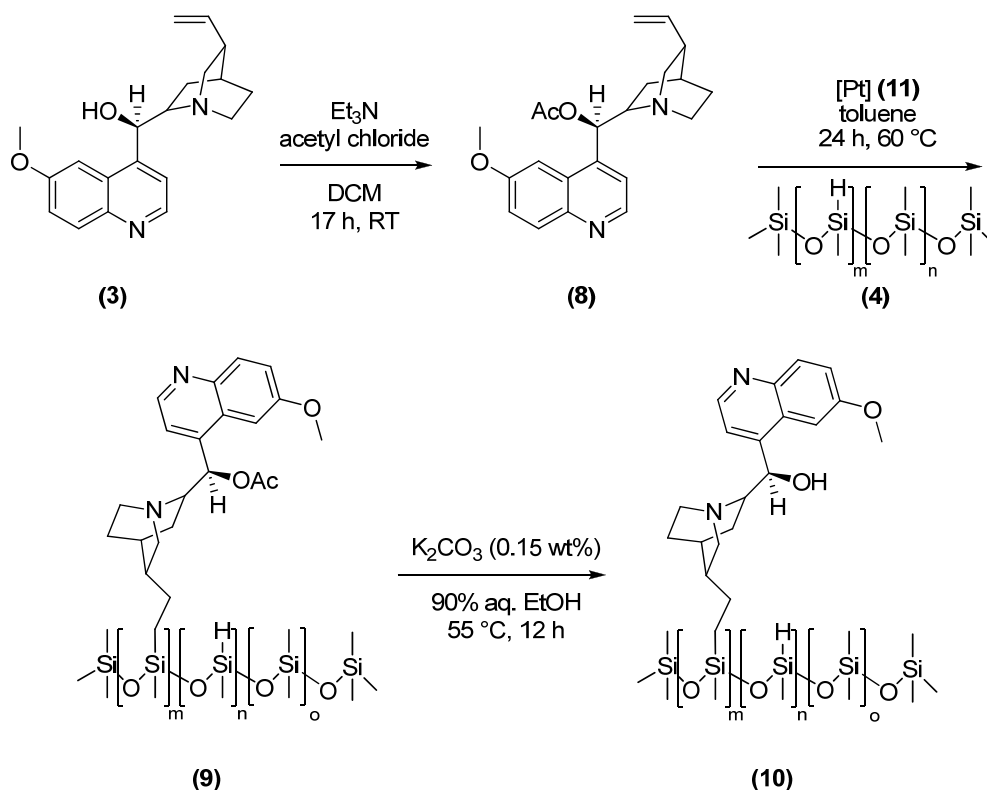
Scheme 17. Synthesis of polysiloxane-supported quinine (10).

In the present study, Chirasil-Quinine **(10)** was synthesized by immobilization of quinine acetate on HMPS **(4)** as reported by Grunlan et al.[30] (Scheme 17). The hydrosilylation reaction catalyzed by a Pt-divinyltetramethyldisiloxane complex (Karstedt´s catalyst **(11))** can be followed by ^{1}H NMR, where the disappearance of the Si-H signal at 4.6 ppm indicates a complete reaction. The obtained polymer can then be purified with column chromatography. The successful immobilization of quinine was verified by ^{1}H NMR. The disappearance of the Si-H signal at 4.6 ppm and the terminal vinyl group signal at 5.0 ppm and 5.9 ppm show the successful immobilization. Furthermore, the removal of the protecting acetate group at 2.1 ppm can be monitored (Figure 1).
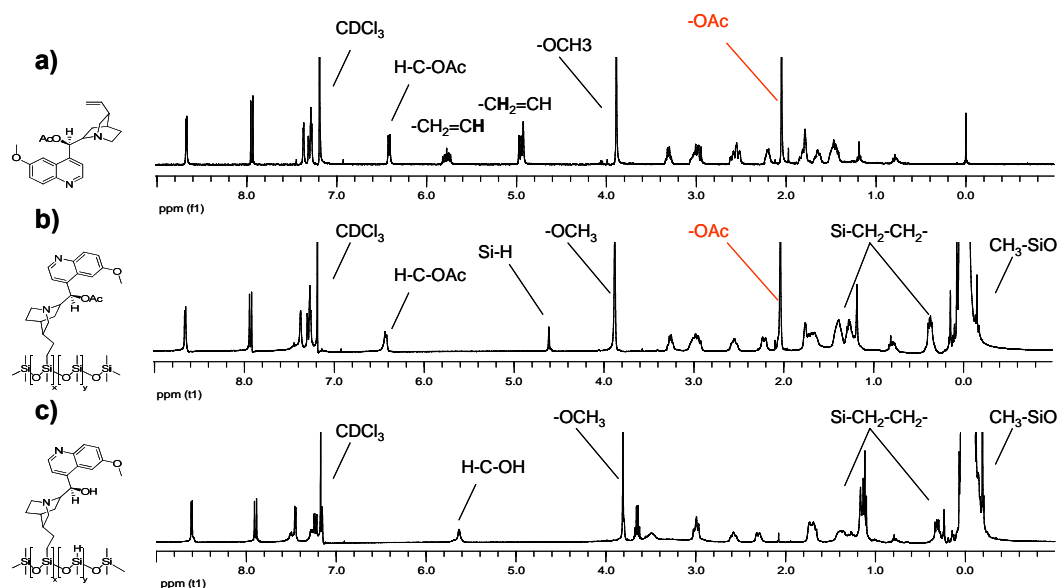
Figure 1. ^{1}H NMR spectra of (a) quinine acetate (8), (b) polysiloxane-supported quinine acetate (9) and (c) polysiloxane-supported quinine (10), (400.1 MHz, CDCl$_3$, δ = 9.0– -1.0 ppm).

In a second approach, the absorption of quinine on the polysiloxane-stabilized metal nanoparticles was investigated (Scheme 16b) by dissolving quinine, the metal precursor and the two polysiloxanes (HMPS/MVPS, 2:1 ratio) in dichloromethane. The polarity of the PDMS is comparable to a nonpolar solvent. Tuning of the polarity of stationary phases with functional groups opens the opportunity to investigate solvent effects in continuous polarity steps, as the solvent used for the liquid phase hydrogenation is known to have a marked effect on the hydrogenation. All quinine-modified Pt and Pd nanoparticles were characterized by TEM measurements. Very small, spherical and crystalline colloids with a diameter of 0.9-1.3 nm for Pd (Figure 2a) and 0.5–1.0 nm for Pt (Figure 2b) were observed. The resulting metal nanoparticle polymer solutions were then coated as a thin film of 250 nm onto the inner surface of fused-silica capillaries. The metal loading per cm of capillary was systematically varied from (0.42–4.16)×10^{-10} mol for Pt and (0.15–7.29)×10^{-10} mol for Pd. To activate the catalyst and to provide a permanently bonded polymer, the capillaries were heated to 160 °C at a rate of 0.5 K min^{-1} under slow hydrogen flow.
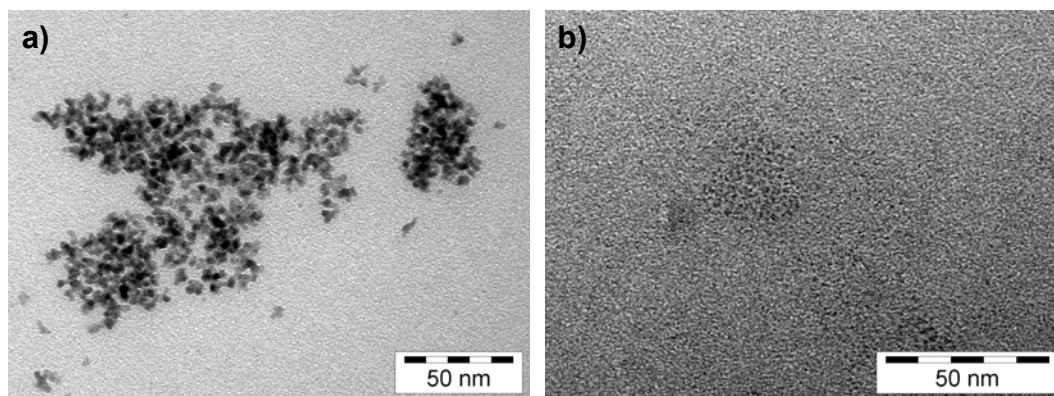
Figure 2. TEM images of polysiloxane-stabilized nanoparticles. a) Quinine-modified Pd nanoparticles (mean diameter Ø: 0.9–1.3 nm). b) Quinine-modified Pt nanoparticles (mean diameter Ø: 0.5–1.0 nm).

3.2.2. Catalytic Studies by On-Column Reaction Chromatography

On-column catalysis experiments were performed by coupling the metal nanoparticle microcapillaries between a preseparation capillary and an enantioselective separation column, which were all installed in a GC. The preseparation capillary was used to thermally equilibrate the reactants and to spatially separate the substrates of the simultaneously injected compound library. Heptakis(6-*0*-trimethylsilyl-2,3-di-*0*-methyl)-β-cyclodextrin **(12)**[168] or Chirasil-β-Dex **(13)**[169] (permethylated β-cyclodextrin linked by a monooctamethylene spacer to poly(dimethylsiloxane) (PDMS)) were used as chiral stationary phases for the enantiomer separation. Hydrogen was used as reactive carrier gas. Reaction educts and products were detected by flame ionization detection (FID) for quantification, and identified by EI quadrupole ion trap MS. To evaluate suitable reaction conditions (capillary length, metal loading, pressure, temperature) and to compare the kinetics of modified and unmodified catalyst, achiral hydrogenations over capillaries coated with non-modified Pt and Pd nanoparticles were performed by using substrate libraries consisting of different α-keto esters and naproxen precursor derivatives, which were simultaneously injected onto this column to obtain separated enantiomer peaks without any detectable catalyst leaching or deactivation as confirmed by FID and mass detector. Scheme 18 shows the achiral hydrogenation of 2-(6-methoxy-2-naphthyl)propenoic acid ethyl ester **(14)** over quinine-modified Pd nanoparticles at 155 °C and 40 kPa H$_2$ with $k = 1.8$ s^{-1} and of **etpy (1)** over quinine-modified Pt nanoparticles at 70 °C and 40 kPa H$_2$ with $k = 1.4 \times 10^{-1}$ s^{-1}.
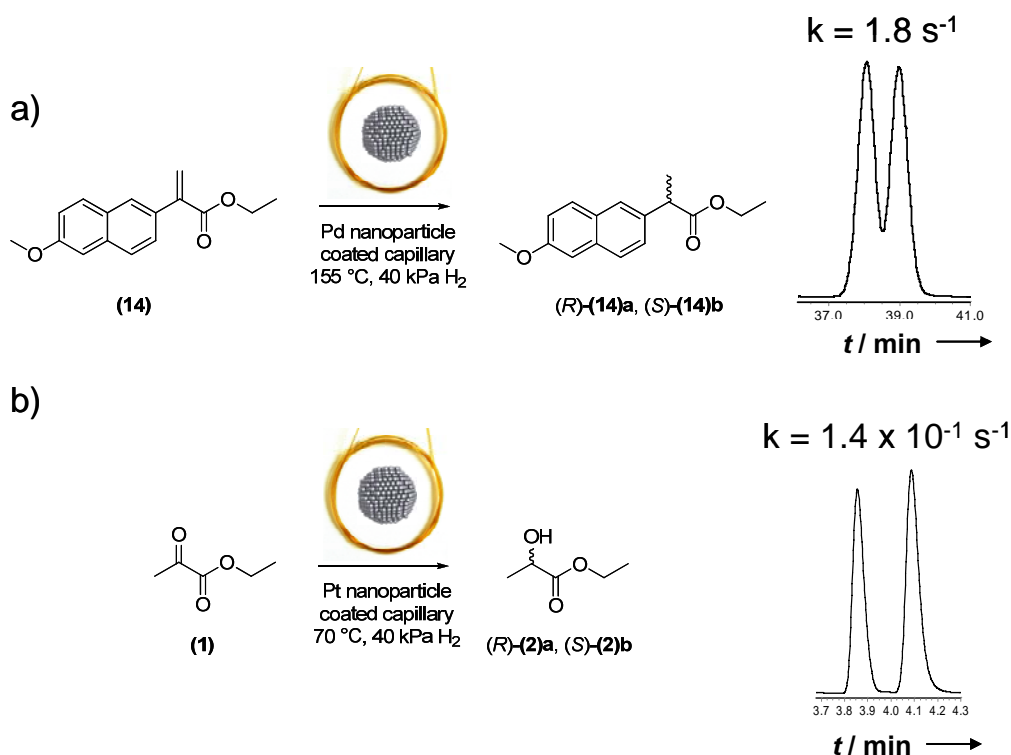
Scheme 18. GC separation of achiral on-column hydrogenation reactions of a) 2-(6-methoxy-2-naphthyl)propenoic acid ethyl ester (14) over Pd nanoparticles at 155 °C and 40 kPa and b) etpy (1) over Pt nanoparticles at 70 °C and 40 kPa. Reaction conditions: a) 2 cm Pd nanoparticle-coated fused-silica capillary i.d. 250 µm, 250 nm film thickness + 7.5 m 50% 6-TBDMS-2,3-di-Me-ß-CD in PS086, 250 nm film thickness, b) 10 cm Pt nanoparticle-coated fused-silica capillary i.d. 250 µm, 250 nm film thickness, coupled with a separation capillary, 7.5 m 50% 6-TBDMS-2,3-di-Me-ß-CD in PS086, 250 nm film thickness.

Subsequently, enantioselective on-column hydrogenations were investigated by coupling the quinine-modified Pt nanoparticle microcapillary (50–100 cm) between a 1 m long pre-separation capillary and a 25 m long chiral separation column, starting with **etpy (1)**as a model substrate (Scheme 19). The selectivity was determined from the ee of the (R)-ethyl lactate ((R)-**etlac**, **(2)a**), using the relationship ee = ([R]-[S])/([R]+[S])×100. Surprisingly, almost no enantioselectivity for hydrogenations over polysiloxane-supported quinine Pt nanoparticles was detected (Chirasil-Quinine-Pt, Scheme 16a), which might be attributed to the short and therefore rigid short spacer.
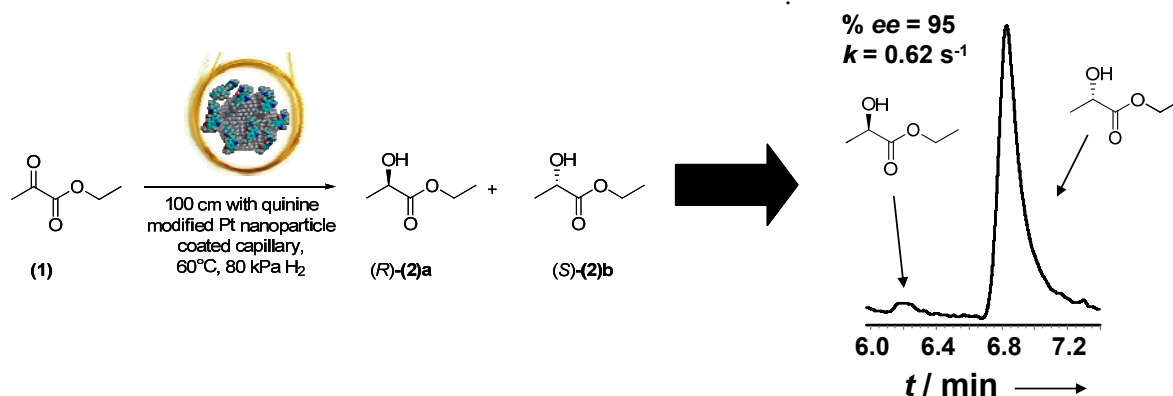
Scheme 19. Enantioselective on-column hydrogenation of etpy (1) over quinine-modified Pt nanoparticles stabilized in a polysiloxane matrix and coated onto a 100 cm long capillary, which was used as the reactor.

3.2.3.   Catalytic System

Higher selectivities towards (*R*)-**etlac (2)a** were achieved with quinine adsorbed Pt nanoparticle capillaries. Experiments with different metal loadings (8–80 ng Pt cm^{-1} capillary) at a constant modifier loading (164 ng quinine cm^{-1} capillary, 5.0×10^{-10} mol cm^{-1} capillary) clearly showed that the enantioselectivity strongly depended on the ratio of the Pt precursor, the quinine and the stabilizing polysiloxanes.
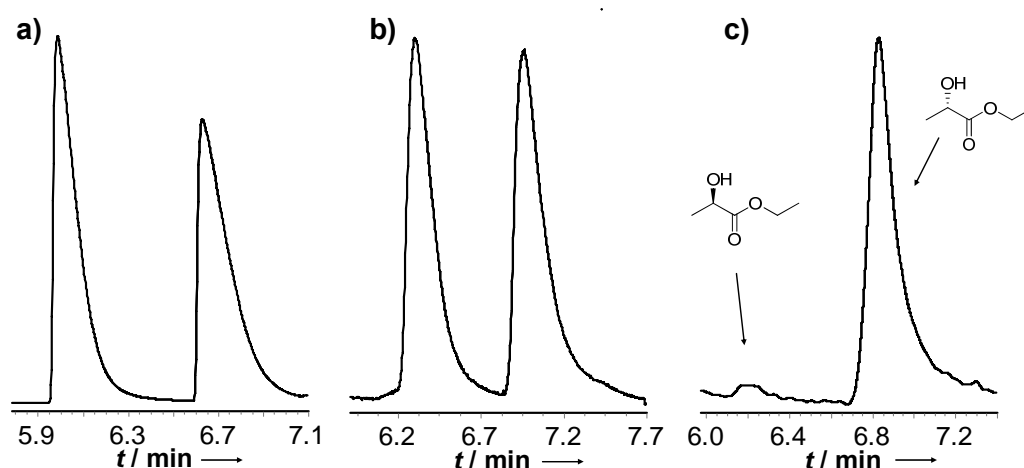
Figure 3. GC separation of enantioselective on-column hydrogenation reactions of etpy (1) over quinine-modified Pt nanoparticles at different Pt concentrations: a) 80 ng Pt cm^{-1} capillary, ee = 0%, b) 20 ng Pt cm^{-1} capillary, ee = 5%, c) 8 ng Pt cm^{-1} capillary, ee = 95%, (capillaries: 100 cm×250 μm i.d., 250 nm film thickness, 60 °C, 80 kPa H$_2$)

As shown in Figure 3, excellent ee values of up to 95% at 60 °C and 80 kPa H_2 inlet pressure could be achieved only for Pt loadings of 8 ng Pt cm^{-1} capillary (0.42×10^{-10} mol cm^{-1} capillary (Figure 3c). At higher Pt loadings (20–80 ng Pt cm^{-1} capillary, 2.1–4.2×10^{-10} mol cm^{-1} capillary, Figure 3a and b), only racemic **etlac (2)** could be detected, due to the high activity and greater contribution of non-modified and, therefore, non-enantioselective metal sites. Furthermore, this observation clearly shows the small selectivity range and hence the competition between coexisting cinchona-modified and residual unmodified catalytic sites.

Although several studies carried out in batch reactors reported that temperatures above 50 °C lead to a decrease in selectivity (probably due to desorption of the modifier from the Pt surface at higher temperatures), excellent ee values at 60 °C were observed in the microcapillary reactor. These results corroborate studies from Hutchings et al.[150] where the ee in the gas phase reaction at 60 °C was higher (42% ee) using premodified 5% Pt/γ-Al$_2$O$_3$ than in the corresponding liquid phase experiment (35% ee). Conversion rates of **etpy** to (*R*)- and (*S*)-**etlac** (**(2)a** and **(2)b**) were about 0.2–0.4% due to extremely short reaction times (2.1–3.2 s). However, it has to be emphasized that a switch to a production mode is possible by using longer capillaries, resulting in longer contact times that lead to higher yields. Furthermore, the self-condensation (aldol-condensation) of **etpy (1)** (1.4–1.6% conversion) to side product **(2)c** as a major side reaction was observed. Self-condensation occurs in the absence of the cinchona modifier, when the ratio of H atoms to adsorbed α-ketoester is too low.[170]

3.2.4. Kinetic Studies

To determine the contact time of **etpy (1)** with the catalyst, measurements were performed at different flow rates and temperatures. The enantioselective hydrogenation of C=O bonds over transition metal surfaces is typically described by a Langmuir-Hinshelwood mechanism.[149, 171] The reaction rate constants k were calculated according to pseudo first-order reaction kinetics with respect to the substrates. The Langmuir-Hinshelwood mechanism is depicted in Scheme 20, in which the substrates are represented as C=O and the catalytically active sites by an asterisk in the mechanistic description, considering the following equilibria and elementary steps: (i) adsorption of hydrogen and substrate on the active sites, (ii) fast surface

diffusion, (iii) stepwise addition of the dissociated H_2 to the C=O bond and (iv) desorption of the product.
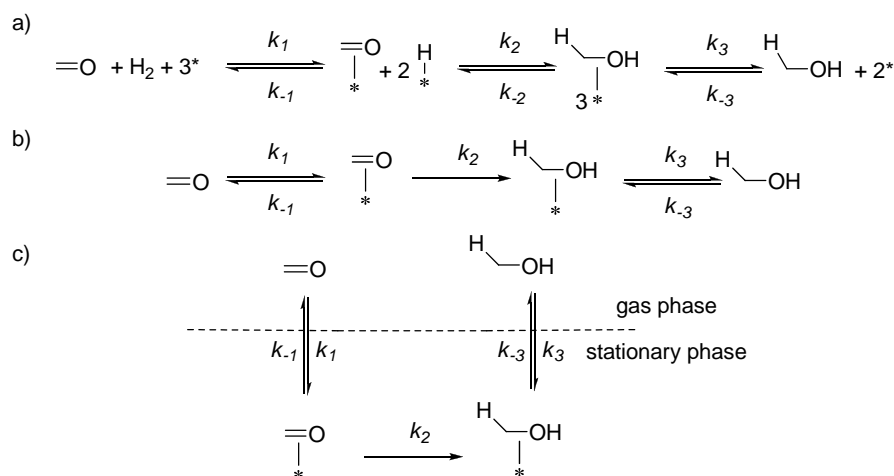
Scheme 20. Enantioselective hydrogenation of the substrates described by a Langmuir-Hinshelwood mechanism. Substrates are represented as C=O and the catalytically active sites by an asterisk (*).

Considering the experimental conditions in on-column reaction chromatography, the following assumptions can be made: (i) H_2 is used as a reactive carrier gas at a high flow rate in the range of mL min^{-1}, and thus, there is a high excess of H_2 compared to the substrates (typically H_2 / substrate: 99.99999 / 0.00001), (ii) the adsorption of H_2 on the Pt or Pd surface is fast because the activation energy for this process is very low and H_2 easily passes the polysiloxane matrix resulting in a steady state of hydrogen adsorbed on the chirally modified Pt or Pd nanoparticles, which does not influence the intrinsic hydrogenation rate of the substrate, (iii) compared to the substrate, there is an excess of quinine-modified nanoparticles, so that there are enough reactive sites available for the adsorption of the reaction educt, (iv) the hydrogenation of the substrates to the hydrogenated products can be considered as an irreversible process. Dehydrogenation in the presence of Pt or Pd is only expected at higher temperatures because the desorption of hydrogen from the metal is the limiting step. With these assumptions, it is possible to simplify the model in the on-column reaction chromatographic setup considering only the key steps depicted in Scheme 20. The advantage of this chromatographic experiment is that the transport by diffusion of the substrate to the catalytically active site can be considered orthogonal to the hydrogenation process itself. The distribution equilibria of the educts and products are obtained by the retention parameters, and diffusion coefficients can be determined by temperature-dependent measurements of the

separation efficiency by using the retention times and peak width of the individual substrates. Therefore, the model depicted in Scheme 20 can be applied to every chromatographic theoretical plate, which can be considered as a catalytic chromatographic reactor. Reaction rate constants can be calculated from the conversion data by using a first-order reaction rate law according to Equation 1, because the known retention parameters give the residence time of the substrate and hence the reaction time.

Equation 1

$$\frac{-d(substrate)}{dt} = k[substrate]$$

This equation is independent of the absolute substrate concentrations. Notably, the conversions were determined from the data for GC measurements with a flame-ionization detector (FID), which gives signal intensities that can be correlated to the ionizable carbon atoms in a specific molecule. This means that the signal intensities of the hydrogenated product and substrate are equivalent and, therefore, no correction factor has to be applied. Residence times of the hydrogenation substrates were determined with a reference column having the same composition of the stationary phase as for the catalytically active capillary columns. Reaction rate constants k of enantioselective hydrogenations were determined by application of Equation 1 to the conversion data. The rate of reaction for enantioselective hydrogenations over chirally modified metals has been reported to be significantly faster for modified enantioselective (bulk) catalyst systems (the so-called "ligand acceleration" kinetics, chapter 3.1.1.) than for the unmodified catalysts leading to a racemic product mixture.[140, 172] Contrary to these expectations, the investigated chiral Pt-cinchona catalyst showed a decrease in reaction rate compared to the unmodified catalyst. A reaction rate constant $k = 1.4 \times 10^{-1}$ s^{-1} for unmodified, unselective Pt sites and a reaction rate constant $k = 3.3 \times 10^{-2}$ s^{-1} for modified, enantioselective sites at 70 °C and 40 kPa H$_2$ was observed in this multiphase (gas-liquid-solid) reaction study corresponding to a deceleration by a factor of 10. This observation is in accord with gas phase hydrogenation studies by Hutchings et al.[150] They attributed this effect to the absence of solvent and excluded this to be a result of the pre-modification procedure. Diminished reaction rates by addition of the modifier were also detected for chirally modified Pd catalysts.[173] In summary, these results show that there are substantial differences in the behavior of this reaction at gas-liquid-solid interfaces compared to liquid-solid interfaces.

Possible reasons for the observed phenomenon are differences in the rate determining steps (e.g. desorption of the product vs. product formation on the catalyst surface) or differences in the molecular interactions on the metal surface and in solution during product formation.

3.2.5. High-Throughput Studies with Different α-Keto Esters

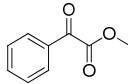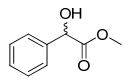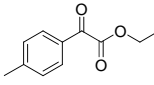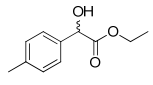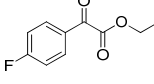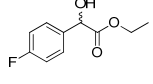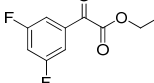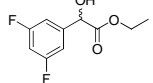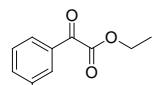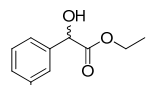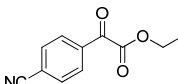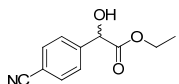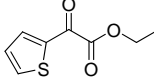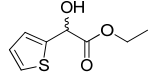To demonstrate the ht determination of ee values, a substrate library consisting of 7 different α-keto esters **(15)–(21)** (Table 1) was simultaneously injected onto capillaries coated with quinine-modified Pt and Pd nanoparticles, while applying a temperature program (Figure 4).
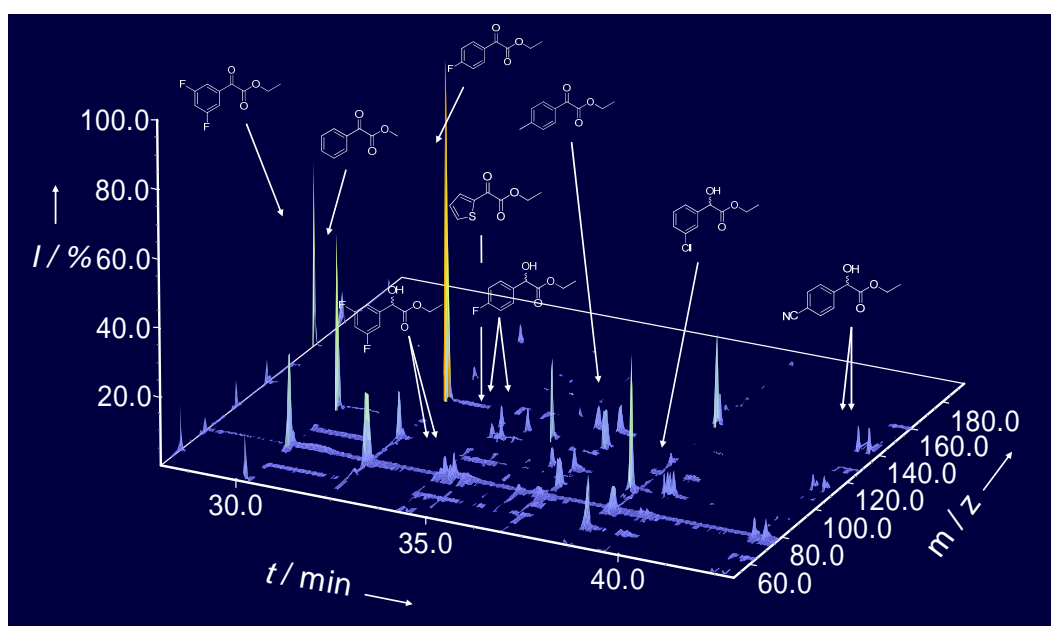
Figure 4. GC-MS measurement (retention time and mass trace) of Pt-catalyzed enantioselective on-column hydrogenations for different α-keto esters using a temperature program (40 °C, 3 min, @ 3K min⁻¹, 180 °C, 80 kPa, 10 min).

A complete and efficient separation of the reaction products could be observed after the catalytically active reactor column. Enantiomeric excesses in the range of 6–34% were observed for hydrogenations of the seven α-keto ester derivatives using capillaries coated with quinine-modified Pt or Pd nanoparticles. The low ee values can be attributed to the contribution of non-enantioselective (unmodified) sites to the product formation and also to racemization processes taking place at elevated temperatures for phenyl-substituted α-keto esters as well as to the high substrate specificity of cinchonidine (CD)-modified Pt catalysts.

Table 1. Selected results of enantioselective on-column hydrogenations over quinine-modified Pt and Pd nanoparticles.

	Substrate	Product	Pt		Pd	
			C[a]	ee[b]	C[a]	ee[b]
			[%]	[%]	[%]	[%]
(15)			82	6	quant.	11
(16)			-	-	-	-
(17)			37	13	6	22
(18)			24	27	35	34
(19)			quant.	15	quant.	6
(20)			77	31	97	8
(21)			-	-	-	-

[a] Conversion C, [b] enantiomeric excess ee. Conditions: 1 m pre-separation capillary GE SE 52 **(29)**, 50 cm quinine-modified Pt or Pd fused-silica capillary i.d. 250 μm, 500 nm film thickness, separation column (*heptakis*(6-0-trimethylsilyl-2,3-di-*O*-methyl)-1-CD **(12)**, 25.0 m×250 μm i.d. or Chirasil-β-Dex **(13)**, 25.0 m×250 μm i.d.), 40 °C, 3 min @ 3 K min⁻¹, 180 °C, 10 min, Carrier gas: H$_2$ (80 kPa).

Although several reports[146, 174-176] imply that Pd-catalyzed hydrogenations differ strongly from Pt-catalyzed hydrogenations, showing minimal activity and, sometimes, reversed enantioselectivity, the here presented ht screening indicates almost comparable activities and enantioselectivities for both Pd- and Pt-catalyzed hydrogenations. Furthermore, higher ee values for phenylglyoxylic esters **(15)**–**(21)** with EWGs were detected (e.g. nitrile substrate **(20)**: 31% ee, difluoro substrate **(18)**: 35% ee). Higher enantioselectivities for EWG-containing substrates were also reported[121, 177, 178] for the hydrogenation of α-fluorinated substrates.

3.2.6. Mechanistic Model

Despite considerable research efforts to understand the complex catalytic system of cinchona alkaloid modified Pt and Pd catalysts, the proposed mechanistic models are still under debate. In this context, it is important to distinguish between metal supported catalysts and metal colloids, as well as multiphase reactions (gas-liquid-solid) compared and two-phase reactions (liquid-solid). In the capillary microreactor used in the present study, high ee values (up to 95%) could be detected for very small Pt nanoparticles (0.5–1.0 nm, Figure 2). The polysiloxane-stabilized Pt nanoparticles of ≤ 1.0 nm investigated herein contain less than 36 atoms, but show high ee values of up to 95% in the enantioselective hydrogenation of **etpy (1)**. The fact that high ee values of up to 95% could be detected for very small Pt nanoparticles with a size of 0.5–1.0 nm, containing less than 36 atoms, leads to the conclusion that the chiral modifier-substrate complex does not require a flat Pt surface of about 20 Pt atoms to induce enantiodifferentiation and suggests an alternative mechanism than the interaction between the modifier, which is already adsorbed parallel to the flat metal surface via the quinoline ring. Up to now, the need for flat metal surfaces to induce enantioselectivity was not proven experimentally. The excellent ee values for the hydrogenation of **etpy (1)** obtained with metal colloids in this study show that the support only plays an indirect role for enantioinduction. Based on the experimental findings of this study, a mechanism for the hydrogenation of **etpy (1)** catalyzed by quinine-modified Pt nanoparticles is postulated in Scheme 21.
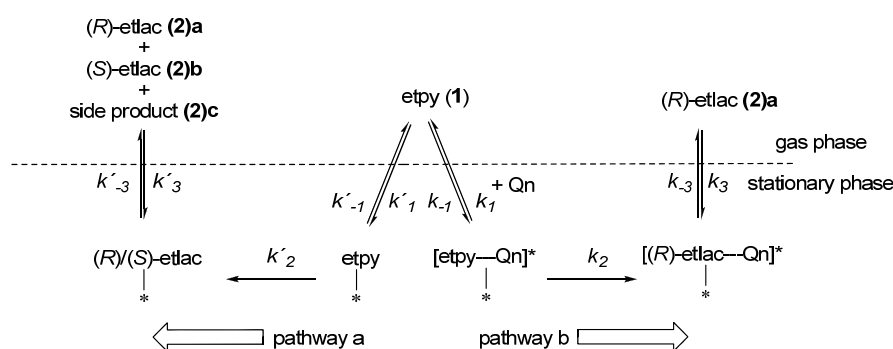
Scheme 21. Postulated mechanisms for reduction of etpy, catalyzed by a) non-modified Pt nanoparticles, and b) quinine-modified Pt nanoparticles (etpy = ethyl pyruvate (1), etlac = ethyl lactate (2)a/b, Qn = quinine (3), catalytically active sites are represented by an asterisk (*)).

The initial step is the diffusion of **etpy (2)** into the stationary phase, followed by the formation of a complex between quinine (**Qn**, **(3)**) and **etpy (2)**. **Etpy (2)** can be directly hydrogenated by unmodified, highly active Pt nanoparticles to produce a racemic mixture of **(2)a** and **(2)b**, as well as the self-condensation side-product **(2)c** (pathway a). The enantioselective pathway (pathway b) involves the complex formation between **etpy (2)** and the partially hydrogenated Qn **(3)** to form complex **[etpy---Qn]*** and the subsequent substrate adsorption with only one enantioface preferentially leading to (*R*)-**etlac (2)a**.

The formation of an NH···O-type hydrogen-bond, involving the basic nitrogen atom of the modifier and the keto oxygen atom of the substrate, is a possible substrate–modifier interaction. However, the interaction in the system investigated herein does not correspond to a hydrogen-bond between a protonated amine modifier and the keto carbonyl group, as the stabilizing polysiloxane matrix corresponds to a nonpolar, aprotic solvent. In a non-acidic medium, the basic N-atom of the modifier is able to remove a proton from the Pt nanoparticles and transfer it to the ketone substrate. During the adsorption of the quinine-substrate complex **[etpy---Qn]*** on small, highly active metal nanoparticles < 1.0 nm, the quinoline part must be tilted with respect to the surface. High quinine loading attenuates the activity of the metal nanoparticles and leads to a quinine-substrate complex **[etpy---Qn]*** that is weakly adsorbed via a quinoline N atom lone-pair bonding.[179] Taking all the results summarized above into account, the most convincing explanation for the enantiodiscrimination is the preferential stabilization of one of the two possible diastereomeric intermediates quinine-substrate complex **[etpy---Qn]***, adsorbed on the metal nanoparticle in a tilted geometry, toward the half hydrogenated **etpy**.

3.3. Conclusion

Although great progress has been made toward molecular level knowledge of the Pt-cinchona system, there are still many open questions, which need to be answered for a more complete understanding. Kinetic investigations of the enantioselective hydrogenation over chirally modified Pt catalysts are complicated by several issues demanding a careful evaluation of the experimental conditions. However, the experimental data presented in this study allow the postulation of a mechanism for enantioselective hydrogenations over small metal nanoparticles as well as the exclusion of many other reaction pathways. Contradictory results

from different experimental and theoretical studies in these surface-catalyzed asymmetric reactions, concerning adsorption geometries and thus structures of the transition states, may reflect the coexistence of several competing reaction pathways. Therefore, the mechanism of this complex catalytic system is in the focus of an ongoing debate. Indeed, the investigated Pt colloid, stabilized with polysiloxane and modified with quinine, hydrogenated **etpy** with up to 95% ee. The results of the present study reopen the debate about the optimal size and the mechanism of chirally modified metal nanoparticles in enantioselective hydrogenations of α-keto esters. In conclusion, the investigation of enantioselective hydrogenations of α-keto esters over chirally modified metal nanoparticles with on-column reaction chromatography allows detailed characterizations of catalyst and substrate libraries by means of kinetic ht studies. Together with the integrated detection of enantioselectivity and conversion measurements, the obtained experimental parameters facilitate a better mechanistic understanding.

Chapter 4

Kinetic Study of Ruthenium Olefin Metathesis Catalysts by On-Column Reaction Chromatography

4. Kinetic Study of Ruthenium Olefin Metathesis Catalysts by On-Column Reaction Chromatography

4.1. Introduction

The discovery of alkene metathesis as versatile carbon-carbon bond-forming method is one of the most important breakthroughs in synthetic chemistry.[180-184] A contributing factor for this success story was the systematic study and design of efficient and easily accessible catalyst systems by Grubbs[185] and Schrock,[186] as well as mechanistic work by Chauvin.[187, 188] These three investigators have been awarded with the Nobel Prize in Chemistry in 2005 "for the development of the metathesis method in organic synthesis". In particular, the ruthenium-based catalyst-systems of Grubbs and co-workers have to be discussed in more detail, as they show wide functional group tolerance as well as air and moisture stability. Widely used and commercially available ruthenium-based metathesis catalysts are Grubbs-type catalyst 1st (22) [189-191] and 2nd generation (23)[192-195] as well as Hoveyda-Grubbs-type catalyst 1st (24)[196] and 2nd generation (25)[197] (Scheme 22).
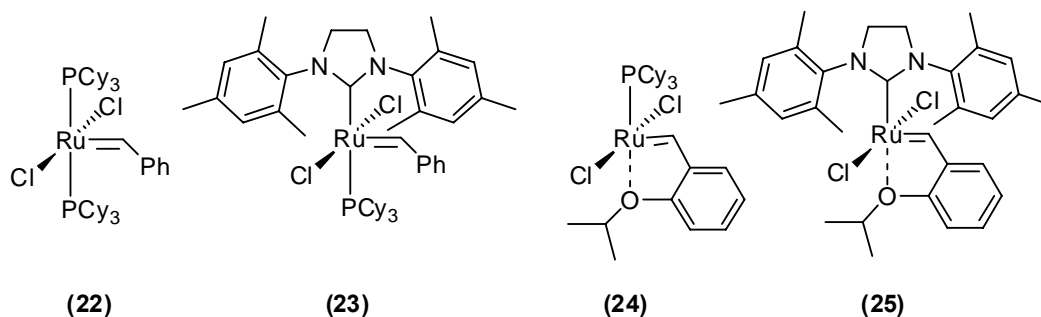
Scheme 22. Commercially available ruthenium olefin metathesis catalysts.

Additionally, ruthenium-based olefin metathesis catalysts with different *N*-heterocyclic carbene (NHC) ligands,[198-201] pyridine-ligated catalysts,[202, 203] Hoveyda-Grubbs-type related catalysts,[204-207] and dicationic ruthenium dimer analogues[208-212] are described. A significant enhancement of catalytic activity by the exchange of one PCy_3 ligand with an NHC ligand in several types of olefin metathesis reactions was reported for catalysts (23) and (25). Originally, the increased reactivity of (23) had been attributed to the ability of the NHC ligand to promote phosphine dissociation.[182] Detailed mechanistic studies by Sanford and Grubbs

demonstrated that the rate of formation (k_1) of the 14 electron-species was actually 10^2 slower for the NHC systems. The challenging question concerning the origin of the higher 2nd generation catalyst activity was addressed by several theoretical and experimental mechanistic studies. As the understanding of the fundamental reaction pathways for olefin metathesis catalysis is important to understand these catalytic activity differences, the catalytic mechanism and the catalyst decomposition pathways, as well as the recent contributions to this question will be briefly addressed in the following sections.

4.1.1. General Mechanism of Olefin Metathesis Reactions

According to the generally accepted mechanism developed by Chauvin,[187, 188] olefin metathesis of an olefin **(26)a** and a metal alkylidene **(26)b** occurs via a metallacyclobutane intermediate **(26)c** by alternating [2+2] cycloadditions and cyclo-reversions (Scheme 23).
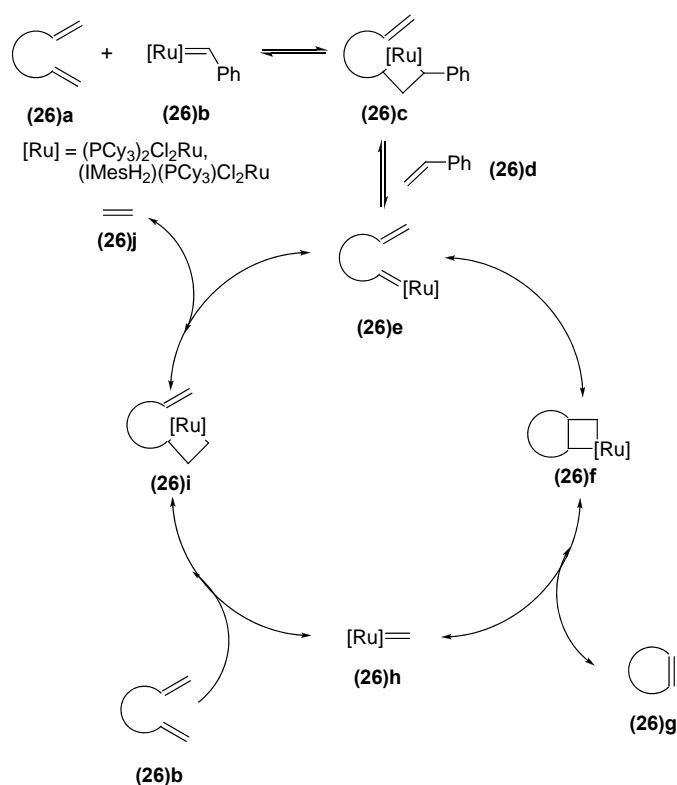
Scheme 23. Chauvin mechanism of ruthenium-catalyzed RCM reactions.[191]

The initial step of the catalytic cycle is the formation of a ruthenacyclobutane **(26)c** by the catalyst **(26)b** and the substrate **(26)a** via a [2+2] cycloaddition. Side-product **(26)d** and the new carbene complex **(26)e** are produced by a cycloreversion of intermediate **(26)c**.

Subsequently, a new ruthenacyclobutane **(26)f** is formed by an intramolecular [2+2] cycloaddition of **(26)e**. A cycloreversion leads to carbene complex **(26)h** and the ring-closing product **(26)g**. The catalytic cycle is concluded by a [2+2] cycloaddition of **(26)h** and the substrate **(26)b** to form the ruthenacyclobutane **(26)i.** Ethylene **(26)j** is released as the stoichiometric by-product. The reversible net reaction is entropically favored towards product formation due to the formation of two product molecules from one substrate molecule and the release of ethylene **(26)j** as a volatile by-product. Focusing on the specific mechanism of ruthenium-mediated olefin metathesis, initial investigations established that the pathway involves substitution of an olefin for a phosphine ligand (Scheme 24).[213, 214] The reaction proceeds predominantly via the widely accepted dissociative mechanism. This mechanism involves the rate-determining, unimolecular dissociation of one phosphine ligand before olefin coordination. An associative pathway, in which the phosphine remains bound, is thought to operate only at higher free phosphine concentrations in solution.
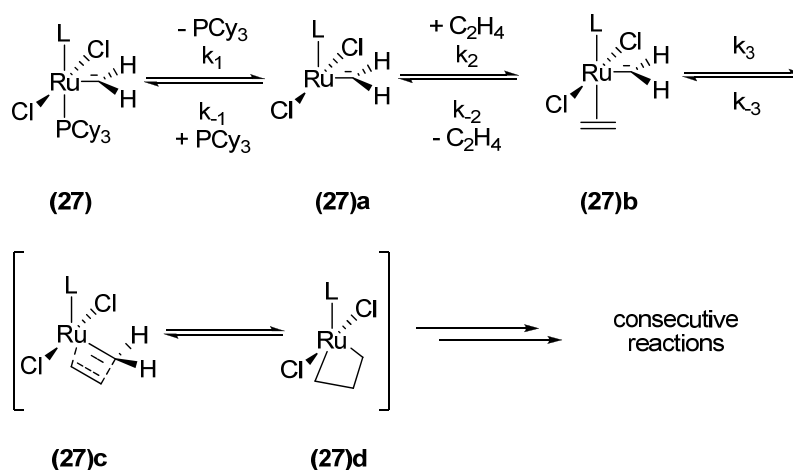
Scheme 24. Proposed dissociative mechanism of phosphine-containing Grubbs-type catalysts in olefin metathesis.

The phosphine dissociation to the naked 14-electron complex **(27)a** as catalytically active species and the following alkylidene rotation generates the 16-electron intermediate **(27)b**. This intermediate then undergoes [2+2] cycloaddition via transition state **(27)c** to the metallocyclobutane **(27)d**, followed by cleavage to release the metathesis products according to the Chauvin mechanism (Scheme 23).

4.1.2. Decomposition of Ruthenium Metathesis Catalysts

One of the major limiting factors of ruthenium carbene catalysts in many reactions is their limited lifetime and efficiency. The better understanding of the decomposition mechanisms is necessary to develop new catalysts with improved properties. Grubbs-type catalysts **(22)** and **(23)** are known to decompose with oxygen in solution to tricyclohexylphosphine oxide, benzaldehyde, and a mixture of not identified ruthenium species. Ruthenium carbene catalysts also decompose in the presence of nitriles, amines, carbon monoxide and acidic chlorinated solvents. The thermal decomposition behavior of Grubbs-type catalysts was studied by NMR.[215] Two different mechanisms are assumed to predominate, although it is agreed that the decomposition of ruthenium-alkylidene complexes most likely proceeds via a number of different pathways.[216] Decomposition studies of Grubbs et al.[215] showed that alkylidene decomposition proceeds via phosphine dissociation, followed by the bimolecular coupling of two equivalents of complex **(27)a** (Scheme 25).
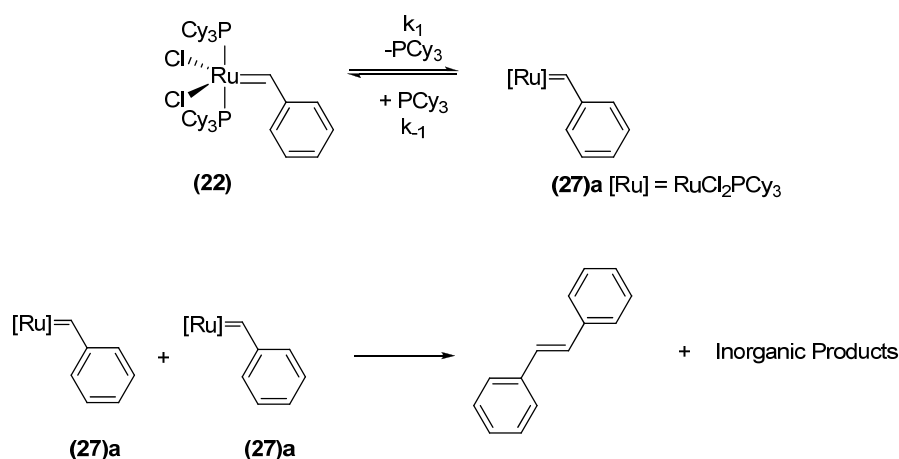
Scheme 25. Decomposition pathway of ruthenium olefin metathesis catalyst (22) reported by Grubbs.

Recent studies[217, 218] suggested that the major decomposition pathway involves a nucleophilic attack of a dissociated phosphine on the methylidene carbon. A substrate-induced decomposition mechanism for these catalysts, involving an α-hydride transfer from a ruthenacyclobutane intermediate, was suggested by van Rensburg et al.[219] The deactivation of Grubbs-Hoveyda 2nd generation type catalysts in the presence of molecular oxygen is believed to proceed by an intramolecular carbene-arene bond formation.[220, 221]

4.1.3. Mechanistic Studies

A variety of experimental and computational methods addressed a broad range of mechanistic details in ruthenium-alkylidene-catalyzed olefin metathesis applications. These studies aim to clarify the most appropriate mechanistic sequences and concentrate on the identification of relevant active intermediates in the metathesis cycle.

Nuclear Magnetic Resonance Studies

^{1}H and ^{31}P NMR kinetic studies by Sanford and Grubbs showed that the dissociative pathway is the operative mechanism.[222-226] They observed that the rate of product formation in RCM of diethyl diallylmalonat catalyzed by **(22)** was dramatically decreased by the addition of free PCy$_3$, which suggests that phosphine dissociation is necessary for catalyst turnover. Furthermore, RCM reactions proceeded with first-order kinetics in respect to both catalyst and diene. Unexpectedly, the determined phosphine dissociation barriers were low for the least catalytically active iodo-complexes of Grubbs catalyst 1st generation **(22)** compared to the catalytically highly active Grubbs-type catalyst 2nd generation **(23)** that showed a high phosphine dissociation barrier despite the expected strong *trans* influence of its NHC ligand. The high activity of the NHC coordinated catalyst **(23)** was explained with a higher fraction of the active species reacting to products compared to the 1st generation catalyst **(22)**, where a higher fraction of active species was trapped by free phosphane instead of entering the catalytic cycle. Booyens et al.[227] studied the phosphine exchange of [(IMesH$_2$)(PPh$_2$Cy)Cl$_2$Ru=CHPh] in C$_6$D$_6$ using magnetization transfer ^{31}P NMR spectroscopy and it was found to operate via a dissociative mechanism as reflected in the kinetic data showing low activation enthalpies and entropies ($k^{353} = 4.1 \pm 0.9$ s^{-1}, $\Delta H^{\ddagger} = 84 \pm 10$ kJ mol^{-1}, and $\Delta S^{\ddagger} = 4 \pm 28$ J mol^{-1} K^{-1}).

Mass Spectrometric Studies

Developments in MS ionization methods, like electrospray ionization (ESI),[228, 229] enable direct investigations of reactions by the detection and study of substrates, products and reaction intermediates, thus providing new insights into the mechanism of the studied reactions under investigation. Chen et al.[183, 211, 230, 231] studied the reaction mechanism of Grubbs-, Werner-, and Hofmann-type (carbene)ruthenium complexes with ESI-MS/MS in the

gas phase on cationized variants of these catalysts. Their gas-phase investigations with the dicationic ruthenium complex[232] $[(PCy_2(CH_2)_2N(CH_3)_3)_2(I)_2Ru=CHPh]^{2+}$ and 1-butene as collision gas in O_2 strongly favor a dissociative mechanism due to the observation of a monocationic 14-electron-complex. Reaction rates k_2 of **(27)a** are accelerated by a factor of 10^4 in the gas phase compared to solution phase due to favorable ion-induced dipole interactions and the absence of a solvent cage. The catalytic activity of these species in ion-molecule reactions with alkenes was demonstrated. Wang and Metzger could detect and characterize the catalytically active 14-electron ruthenium intermediates of two 1st generation ruthenium catalysts in solution by in situ exchange of neutral PCy_3 with a cationic phosphine using ESI-MS/MS.[233]

Theoretical Studies

The rapid development of experimental work on metathesis catalysts makes computational studies essential to allow a rational design of new efficient catalyst generations. Theoretical studies on the behavior of ruthenium metathesis catalysts have been published by the groups of Meier,[234] Thiel [235, 236] and Cavallo.[237-239] Furthermore, Chen and Adlhart[240-242] used quantum-mechanical/classical methods (QM/MM hybrid method) to compare the reaction coordinates of **(22)** and **(23)** in the degenerate metathesis of styrene, ethylene and norbonene. Calculations with catalyst **(22)** showed a high energy barrier in the middle of the reaction coordinate because of rotation of the threefold symmetric phosphane ligand, whereas this barrier was absent for catalyst **(23)** because of the twofold symmetry of its NHC ligand. They proposed that these high barriers on the potential surface after the phosphane dissociation can be eliminated by choosing ligands with twofold instead of threefold symmetry. Theoretical investigations by Straub[243-245] revealed that the electronic and steric stabilization of the active conformation of the carbene moiety in **(23)** is responsible for their exceptional alkene metathesis activity. Based on DFT calculations, a concept of active and inactive ligand conformations in ruthenium alkene carbene complexes of the Grubbs catalyst type was introduced. Scheme 26 shows the inactive alkene ligand orientation and the inactive carbene ligand orientation (red traffic lights), the inactive alkene ligand orientation and the active carbene ligand orientation and vice versa (yellow traffic lights), as well as the active alkene ligand orientation and the active carbene ligand orientation (green traffic lights). The

cycloaddition to the ruthenacyclobutane can take place without further ligand rotations with the active conformation.
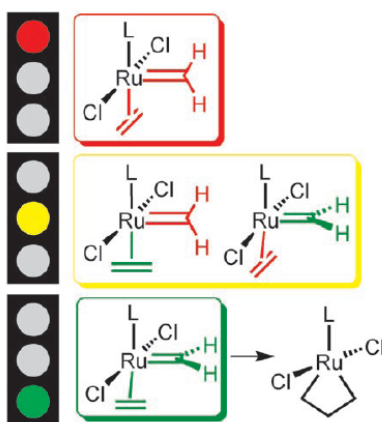
Scheme 26. "Traffic lights" concept of active and inactive ligand conformations in ruthenium alkene carbene complexes reported by Straub.[245]

Additionally, van Rensburg et al.[219, 246] studied the reaction mechanism and substrate-induced decomposition behavior of different Grubbs-type catalysts with DFT calculations and confirmed the relatively fast initiation of Grubbs-type 1st generation catalysts with progressively slower initiation for the Grubbs-type 2nd generation catalyst.

4.1.4. Activation Parameter

A comparison of the experimentally and theoretically observed reaction rate constants and activation parameters of Grubbs-type catalysts 1st **(22)** and 2nd generation **(23)** in gas-phase experiments and solution-phase studies is given in Table 2. Both the overall activity of a metathesis catalyst as well as the rates for phosphine dissociation, re-coordination and substrate coordination were studied. Because the phosphine dissociation is the rate limiting step in the catalytic cycle, these values might be correlated to each other as suggested by Grubbs. Reported Gibbs activation energies $\Delta G^{\ddagger}$ are in the range of 80.8–139.8 kJ mol^{-1} for catalyst **(22)** and 84.1–154.4 kJ mol^{-1} for catalyst **(23).** However, it is difficult to compare the activation parameters of all these studies due to different conditions (e.g. test substrates, reaction temperatures, solvents and state of aggregation).

Table 2. Comparison of reaction rate constants and activation parameters of olefin metathesis reactions catalyzed by different ruthenium metathesis catalysts of selected reports in literature.

Catalyst	$k^{[a]}$ [s^{-1}]	$E_A^{[b]}$ [kJ mol^{-1}]	$\Delta G^{\ddagger[c]}$ [kJ mol^{-1}]	$\Delta H^{\ddagger}$ [kJ mol^{-1}]	$\Delta S^{\ddagger}$ [J mol^{-1} K^{-1}]	Study/ Reference
Experimental						
(22)	9.6 ± 0.2	-	83.2 ± 2.0	99 ± 2.0	50 ± 8.0	Sanford et al.,[222] phosphine exchange ^{31}P NMR MT
(23)	0.13 ± 0.01		96.2 ± 1.7	113 ± 8.0	54 ± 25.0	
(22)	-	-	139.8 ± 9.6	-	-	Adlhart et al.,[247] phosphine dissociation ESI-MS/MS
(23)			154.4 ± 9.6			
(22)	-	62.0	-	-	-	Levebre et al.,[248] CM of *cis*-2-pentene Offline-GC
(23)	-	-	84.1	15.5 ± 0.9	-230 ± 8.0	Trapp et al.,[84, 85] RCM of (30)a On-Column GC
Theoretical						
(22)	-	-	87.0	-	-	Adlhart et al.,[240, 241] styrene metathesis QM/MM
(23)			117.2			
(22)	-	-	88.3	-	-	Adlhart et al.,[242] DFT
(23)			109.2			
(22)	-	-	80.8	69.9	61.1	Van Rensburg et al.,[246] ethylene metathesis DFT
(23)			99.6	90.0	70.7	

[a] Reaction rate constant at 353 K. [b] Activation energy E_A [c] Gibbs activation energy $\Delta G^{\ddagger}$.

4.1.5. Objectives

In fact, there are only a few detailed studies containing direct investigation of olefin metathesis reactions with online screening techniques, which give quantitative data on both elementary steps and overall kinetics.[183, 225] Nevertheless, for the systematic design of new catalysts it is important to understand how the catalytic mechanism might be controlled by structural parameters. To determine rate-controlling elementary steps and to develop and refine models, comprehensive experimental kinetic and thermodynamic data of a broad variety of catalysts and substrates are needed.

Experimental kinetic studies including NMR and MS, as well as offline GC measurements[55] are predominantly used to determine kinetic and thermodynamic data of various catalysts and substrates. However, these techniques do not have the possibility of continuous sampling in real-time and precise temperature control. Standard NMR systems with variable temperature control are usually within the range 170–390 K with a precision of ± 0.5 K, but temperature

ranges are limited due to the boiling point of the used solvent. Also in ESI-MS/MS measurements a precise temperature control is difficult. The system temperature is unknown and cannot be determined. Charge-labeled catalysts or substrates are used to improve the detection limit. Ions are thermalized or optionally treated with reagent gases in a reaction cell at pressures of approximately 0.1 Torr. The comparison of gas-phase and solution-phase experiments sometimes remains difficult. Today, the possibility of studying olefin metathesis reactions by microfluidic reactor systems[249] and ht approaches,[56, 250] including immobilized Ru metathesis catalysts,[251] allows to efficiently screen different catalysts.

In a preliminary study, Trapp et al.[84, 85] reported a strategy that allows the synchronous combination of catalysis and separation in microcapillaries to perform ht reaction rate measurements (36 rate constants/h) of a reactant library of 12 different compounds for RCM over Grubbs 2nd generation catalyst **(23)**. With this combination, it is also possible to investigate activation parameters and catalyst stability. This chapter presents a detailed activity screening of different ruthenium metathesis catalysts with on-column reaction chromatography. By temperature- and carrier gas flow-dependent conversion measurements of different Grubbs-type catalysts for RCM of *N,N*-diallyltrifluoroacetamide **(30)a** to its RCM product **(30)b**, reaction rate constants k and activation parameters ($\Delta G^{\ddagger}$, $\Delta H^{\ddagger}$, $\Delta S^{\ddagger}$, Scheme 27) are obtained. These parameters are required for a more profound understanding of the differences in catalytic activity and are a prerequisite to draw conclusions on elementary steps in metathesis reactions.
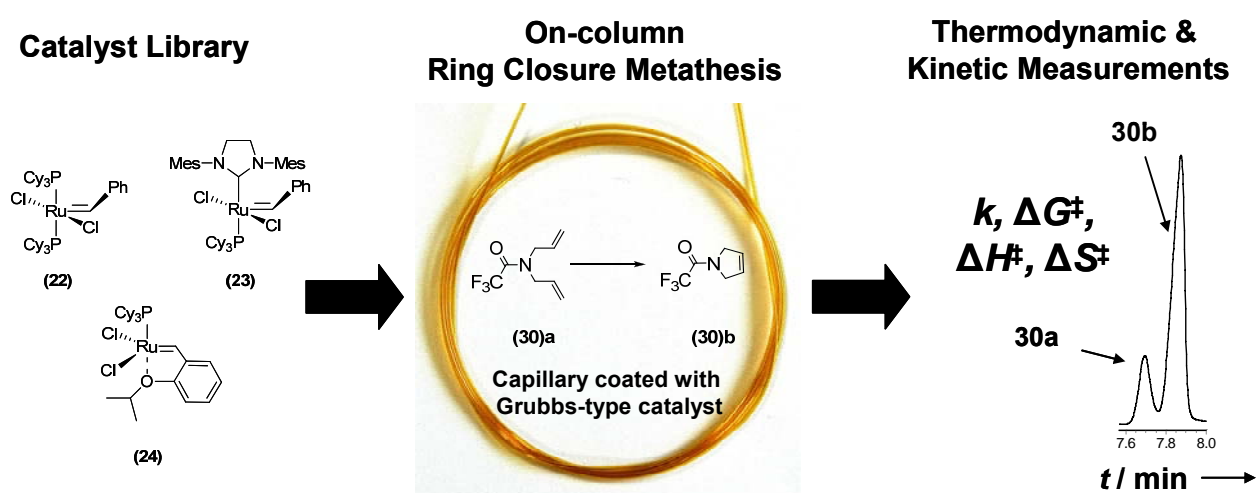
Scheme 27. On-column RCM of *N,N*-diallyltrifluoroacetamide (30)a over a Grubbs-type catalyst library.

4.2. Results and Discussion

4.2.1. Preparation of Catalytically Active Stationary Phases and Coating of Microcapillaries

Catalytically active micro columns were prepared to combine catalytic activity and separation selectivity in the polymeric stationary phase of a chromatographic separation capillary. Therefore, Grubbs-type catalysts **(22)**, **(23)** or **(24)** were dissolved with different polysiloxane (GE SE 30 **(28)** or GE SE 52 **(29)**) in absolute *n*-pentane and the resulting solutions were used to coat microcapillaries (1–3 m capillary length) under inert conditions to obtain a film thickness of 500 nm after removing the solvent. Unfortunately, catalyst **(25)** was not soluble in *n*-pentane and, therefore, could not be coated onto fused-silica capillaries, because more polar components tend to crystallize within non-polar stationary phases. The catalyst loading was only $(0.2\text{-}1.6)\times 10^{-4}$ mg cm^{-1} capillary $((0.2\text{-}2.0)\times 10^{-10}$ mol cm^{-1} capillary). ^{1}H NMR measurements confirmed that the PDMS (GE SE 30 **(28)**) did not affect the catalytic activity of catalyst **(22)**. In these experiments, the ruthenium alkylidene **(22)** and PDMS GE SE 30 **(28)** were dissolved in toluene-d$_8$ in a screw capped NMR tube. The polysiloxane-catalyst solutions were monitored by integrating the carbene proton or the *ortho* protons of the benzylidenes of **(22)** as a function of time over 24 h.

4.2.2. Catalytic Studies by On-Column Reaction Chromatography

On-column catalysis experiments were performed by coupling the ruthenium metathesis catalyst coated microcapillaries between a preseparation capillary (1 m) and a separation column (25 m), which were installed in a GC. The purpose of the pre-separation column was to thermally equilibrate the reactants and to spatially separate the substrates of the injected compound library. This enabled ht kinetic investigations due to the absence of competing reactions. Helium was used as inert carrier gas. Reaction educts and products were detected by FID for quantification and identified by quadrupole ion trap MS. By the use of substrate libraries and measurement of reaction rate constants of the spatially separated compounds, an extraordinary ht can be realized. Recently, Trapp et al. demonstrated that a throughput of 36 rate constants per hour could be achieved for a library consisting of twelve compounds.[84, 85] In this chapter, systematically varied sets of fused-silica capillaries coated with different

metathesis catalysts embedded in a polysiloxane matrix were screened by varying the stabilizing polysiloxanes and the catalyst loading under different reaction conditions (temperature, contact time). *N,N*-Diallyltrifluoroacetamide **(30)a** was chosen as a benchmark substrate for this study. Substrate **(30)a** was injected onto this column configuration at different temperatures (45-80 °C) and inlet pressures (80-120 kPa) to vary the reaction time and to obtain temperature-dependent kinetic data (Figure 5).
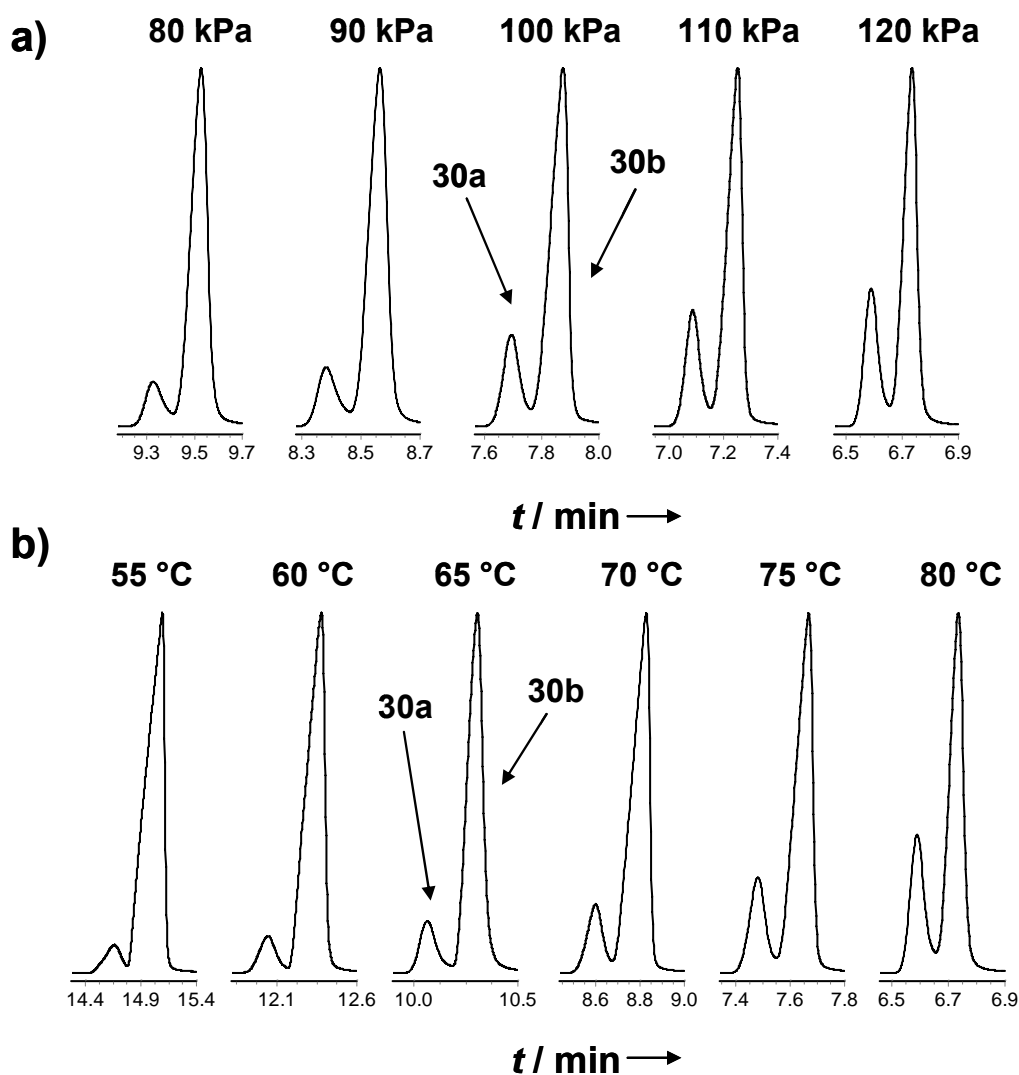
Figure 5. Pressure- (a, at 80 °C) and temperature-dependent (b, at 120 kPa) measurements of RCM of (30)a over Grubbs 1ˢᵗ generation catalyst (22) in GE SE 30 (28) for the determination of activation parameters. The first eluted peak can be assigned as the reaction educt (30)a and the second eluated peak as the reaction product (30)b. a) The carrier gas-flow is correlated to the inlet pressure and, therefore, shorter contact times with the catalyst are achieved with higher inlet pressures. b) With increasing temperature the reaction time is reduced and product formation decreases.

It is important to note that reaction temperatures above 40 °C are needed for the elution of educts and products. In these experiments, baseline-separated elution profiles of the reaction educt and product were obtained. The first eluted peak could be assigned as the reaction product *N*-trifluoroacetyl-pyrrolidine **(30)b** as proven by MS measurements. Conversions were determined by integrating the FID signals, taking a correction factor (f = 1.96 for **(30)a** → **(30)b**, chapter 8.5.2) for the relative signal ratios of the substrate and product into account. In order to investigate solvent effects in continuous polarity steps, two different PDMS were used. PDMS GE SE 30 **(28)** corresponds to a nonpolar solvent like *n*-hexane (this separation is also known as simulated distillation), whereas poly(methylphenyl)(dimethylsiloxane) (PMPS) GE SE 52 **(29)** (HP-5 column) containing 5% phenyl groups is comparable to the polarity of toluene. The elution order of reaction substrate **(30)a** and reaction product *N*-trifluoroacetyl-pyrrolidine **(30)b** depends on the separation column, which is installed after the ruthenium metathesis catalyst coated microcapillaries. The phenyl groups of the PMPS (GE SE 52 **(29)**) interact stronger with product **(30)b.** Therefore, the polar product **(30)b** elutes later than the substrate **(30)a.** A reversed elution order is obtained for PDMS (GE SE 30 **(28)**, **(30)a** elutes later than **(30)b**). By determination of the retention times for starting materials and products between 45–80 °C using both column configurations, a temperature-dependent reversal of the elution order could be excluded.

4.2.3. Determination of Reaction Rate Constants and Activation Parameters

From temperature- and carrier-gas-flow-dependent measurements (45–80 °C, 80–120 kPa), 3D datasets (p, T, k) were obtained (Figure 6a), which were evaluated with kinetic models to determine reaction rate constants k and activation parameters ($\Delta G^{\ddagger}$, $\Delta H^{\ddagger}$, $\Delta S^{\ddagger}$). These parameters can be correlated with the activity of the ruthenium metathesis catalyst. As previously described by Trapp et al.,[55] reaction rate constants k of RCM reaction were determined by application of Equation 1 (chapter 3.2.4) to the conversion data.

The Gibbs free activation energies $\Delta G^{\ddagger}$ (T) were calculated according to the Eyring equation (Equation 2) with k_B as the Boltzmann constant (k_B = 1.38×10^{-23} J K^{-1}), T as the reaction temperature in K, h as Planck's constant (h = 6.62×10^{-34} J s) and R as the gas constant (R = 8.314 J K^{-1} mol^{-1}). The statistical factor κ was set to 1.0.

Equation 2

$$\Delta G^{\neq}(T) = -RT \ln\left(\frac{k\,h}{\kappa k_B T} \right)$$

The activation enthalpy $\Delta H^{\ddagger}$ of the reaction was obtained from the slope and the activation entropy $\Delta S^{\ddagger}$ from the y-axis intercept of the Eyring plot ($\ln(k_{app}/T)$ as a function of T^{-1}. Deviations of the activation parameters $\Delta H^{\ddagger}$ and $\Delta S^{\ddagger}$ have been calculated by error band analysis of the linear regression with a level of confidence of 95%.
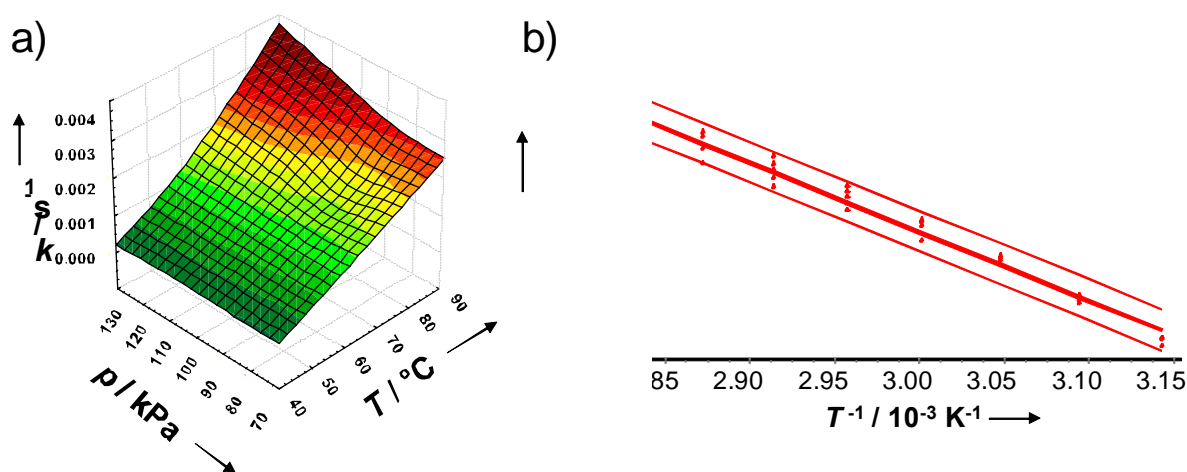
Figure 6. a) 3D plot (k / s⁻¹, p / kPa, T / °C) and b) Eyring plot ($\ln(k_{app}/T)$ as a function of T^{-1} for RCM of (30)a over Hoveyda-Grubbs catalysts 1ˢᵗ generation (24) in GE SE 30 (28) at different temperatures (45-80 °C) and inlet pressures (80–120 kPa).

Table 3 summarizes the conversions, reaction rate constants k, activation energies E_A, and activation parameters ($\Delta G^{\ddagger}$, $\Delta H^{\ddagger}$, $\Delta S^{\ddagger}$) of RCM reactions of (30)a for catalysts (22), (23), and (24) (cf. Table 1), i.e. for the Grubbs-type catalyst 1ˢᵗ generation (22) $\Delta G^{\ddagger}$(298 K) = 83.2 kJ mol⁻¹, $\Delta H^{\ddagger}$ = (18.3 ± 1.2) kJ mol⁻¹, $\Delta S^{\ddagger}$ = (-218 ± 29) J K⁻¹ mol⁻¹. The low activation enthalpies $\Delta H^{\ddagger}$ and negative activation entropies $\Delta S^{\ddagger}$ corresponds to a restraint transition state. The Gibbs activation energy in metathesis reactions of (30)a over Grubbs-type catalyst 2ⁿᵈ generation (23) (90.2 kJ mol⁻¹) was found to be 7 kJ mol⁻¹ higher than for the 1ˢᵗ generation catalysts ($\Delta G^{\ddagger}$ = 83.2 kJ mol⁻¹). Catalysts (22) and (23) have lower activation energies than catalyst (24). These parameters corroborate previous measurements from Trapp

et al.[84, 85] and are consistent with Grubbs´ experimental findings.[222, 224] The Gibbs free activation energies determined by on-column reaction chromatography for the overall activity of catalysts **(22)** and **(23)** in RCM of **(30)a** are almost identical to Gibbs free activation energies for phosphine dissociation reported by Grubbs and Sanford.[225]

Table 3. Selected results of the on-column RCM of (30)a over different Grubbs-type catalysts.

| Cat.	$k^{[a]}$ $[10^{-3} s^{-1}]$	$E_A^{[b]}$ $[kJ\ mol^{-1}]$	$\Delta G^{\ddagger[c]}$ $[kJ\ mol^{-1}]$	$\Delta H^{\ddagger}$ $[kJ\ mol^{-1}]$	$\Delta S^{\ddagger}$ $[J\ mol^{-1}\ K^{-1}]$	$r^{[d]}$ (s.d.)
(22)	7.6	21.2	83.2	18.3 ± 1.2	-218 ± 29	0.953 (0.076)
(23)	4.8	27.8	90.2	24.9 ± 0.7	-219 ± 17	0.985 (0.053)
(24)	0.6	42.5	92.7	39.6 ± 0.6	-178 ± 22	0.997 (0.041)

[a] Reaction rate constant at 50 °C and 80 kPa. [b] Activation energy E_A [c] Gibbs activation energy $\Delta G^{\ddagger}$ at 25 °C. [d] Correlation factor r and residual standard derivation (s.d.) of the linear regression of the Eyring plot. Conditions: 1 m pre-separation column (HP-5, i.d. 250 µm, 250 nm film thickness), 1–3 m microcapillary (i.d. 250 µm, 500 nm film thickness), 25 m separation column (HP-5, i.d. 250 µm, 500 nm film thickness). He was used as inert carrier gas.

This accordance might show that the activity of a metathesis catalyst may be correlated to the ratio of the rates for phosphine re-coordination (k_{-1}) and ethylene coordination (k_2) to the naked 14-electron complex **(27)a** (Scheme 20). Furthermore, the lower Gibbs activation energy of Grubbs-type catalyst 1st generation **(22)** ($\Delta G^{\ddagger} = 83.2$ kJ mol^{-1}) compared Grubbs-Hoveyda-type catalyst 1st generation **(24)** ($\Delta G^{\ddagger} = 92.7$ kJ mol^{-1}) indicates a slower initiation of catalyst **(24)**, which was also found in NMR experiments by Hoveyda et al.[196] However, the determined activation enthalpies $\Delta H^{\ddagger}$ for phosphine dissociation are about 22 kJ mol^{-1} (for catalyst **(22)**) and 79 kJ mol^{-1} (for catalyst **(23)**) higher than the activation enthalpies $\Delta H^{\ddagger}$ of this kinetic study. Also a higher reaction rate constant for catalyst **(22)** ($k = 7.6 \times 10^{-3}$ s^{-1}) than for **(23)** ($k = 4.8 \times 10^{-3}$ s^{-1}) could be observed in accordance with Sanford (**(22)**: $k_{Init} = 1.0 \times 10^{-3}$ s^{-1}, **(23)**: $k_{Init} = 5 \times 10^{-4}$ s^{-1}). No differences in conversions and rate constants for the two different stationary phases GE SE 30 **(28)** and GE SE 52 **(29)** could be detected.

4.2.4. Thermolytic Decomposition Study of Ruthenium Olefin Metathesis Catalysts

For the rational design and improvement of olefin metathesis catalysts, it is crucial to understand their decomposition behavior and their transformation into catalytically inactive

ruthenium species. In this study, the stability and recyclability of catalyst **(23)** was further characterized by performing multiple injections over 24 h at 45 °C and 60 kPa. The plot of the conversion against the time is shown in Figure 7a.
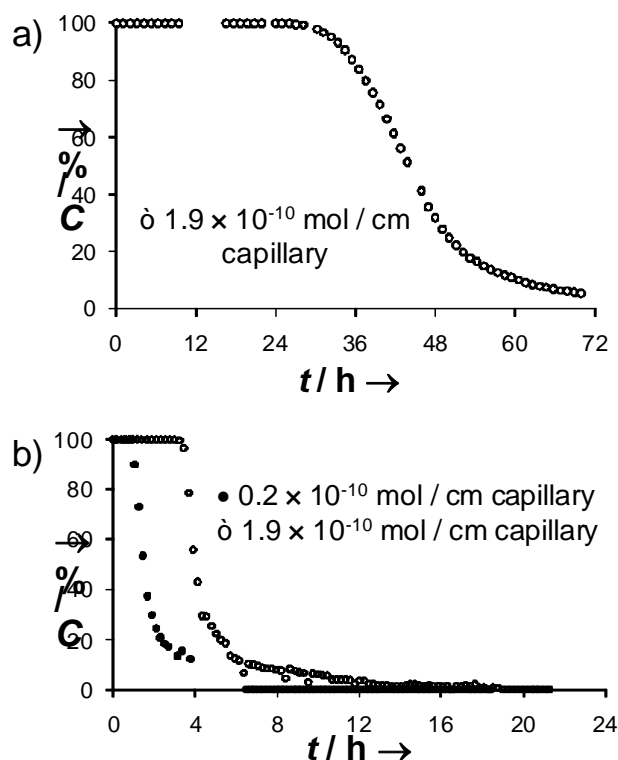
Figure 7. Conversion plot of the RCM of (30)a over Grubbs-type catalysts 2nd generation (23) in GE SE 52 (29) at a) 45 °C and 60 kPa and b) 100 °C and 60 kPa against reaction time. Reactor setup: pre-separation capillary GE SE 52 (29) (1 m, 500 nm film thickness), 2 m catalyst (23) coated capillary (2 m, 500 nm film thickness), HP–5 (25 m, 500 nm film thickness), C: Conversion, t: reaction time.

Remarkably, catalyst **(23)** proved to be incredibly stable showing full conversion for almost 36 h with a linear decrease to at least 10% conversion after 72 h in RCM of **(30)a.** In comparison, NMR decomposition studies of Grubbs and Ulman[215] reported a half-life of even about 8 days for a solution of **(22)** in their (0.023 M in C_6D_6 at 55 °C) corroborating the high stability of Grubbs-type catalysts.

To study the thermolytic decomposition behavior at forcing conditions, the same experiment was repeated at a higher temperature (100 °C, Figure 7b) For the first 16 injections over 4 h at 100 °C, no remarkable loss of catalytic activity could be determined with a catalyst loading of

1.9×10^{-10} mol cm^{-1} capillary. After this period, a remarkable decrease in the catalytic activity could be observed, resulting in almost no activity after 12 h. Hoye[252] reported that high substrate and low ruthenium metathesis concentrations might be advantageous for RCM. Therefore, the ruthenium metathesis catalyst loading of **(23)** was lowered to 0.2×10^{-10} mol cm^{-1} capillary and catalytic tests were performed, where even a faster deactivation for the low concentration was observed. The thermolytic decomposition of complexes **(22)** and **(23)** has been proposed to occur via phosphine dissociation, followed by bimolecular coupling of two four-coordinated ruthenium fragments **(27)a**.[215] In the present study, the dissociation and chromatographic removal of the PCy$_3$ ligand could not be detected, which can be explained by the fact that the phosphine ligand is dissolved in the polysiloxane and can stabilize the complex after the reaction. No leaching of the catalyst under the here investigated reaction conditions was detected by MS measurements. Instead, we detected the formation of styrene as a side-product obtained from the cycloreversion of the metallacyclobutane intermediate **(26)c**. Styrene could only be detected during the initiation period (e.g. for 30 min at 45 °C and 60 kPa) and disappeared after the full activation of the catalyst.

4.2.5. Grubbs-type Catalyst Activation

Unexpectedly, nonlinear Eyring plots [253] for RCM reactions of **(30)a** (2.3×10^{-8} mol per injection) catalyzed by **(22)** and **(23)** (1.9×10^{-9} mol, 2 m capillary) were observed (Figure 8). The plot for RCM of **(30)a** over Grubbs-type catalysts 2nd generation **(23)** in GE SE 30 **(28)** shows a nonlinear behavior for temperature-dependent measurements that apparently indicates the existence of two linear regions intersecting at 56 °C. This break point leads apparently to two sets of activation parameters with an inversion temperature at 56 °C. At first, the observed phenomena of an Eyring plot was assigned to two intersecting linear trends, namely the catalyst activation and deactivation pathways, including phosphine dissociation and re-coordination. Secondly, decomposition reactions or phase transitions that are known to occur readily in the catalytic cycle of these systems were assumed as a possible explanation for the nonlinearity of the observed Eyring plots.

On the other hand, the deactivation studies of catalyst **(23)** in the RCM of **(30)a** showed no remarkable loss of catalytic activity over 36 h (chapter 4.2.4). Therefore, the deactivation of the catalyst during the kinetic measurements at lower temperatures (45–80 °C) can be almost

excluded. Contradictorily, the negative slopes and therefore negative $\Delta H^{\ddagger}$ values for temperatures lower than 56 °C would indicate a faster reaction at lower temperatures, assuming a faster reaction rate constant k_{app} due to higher conversions.
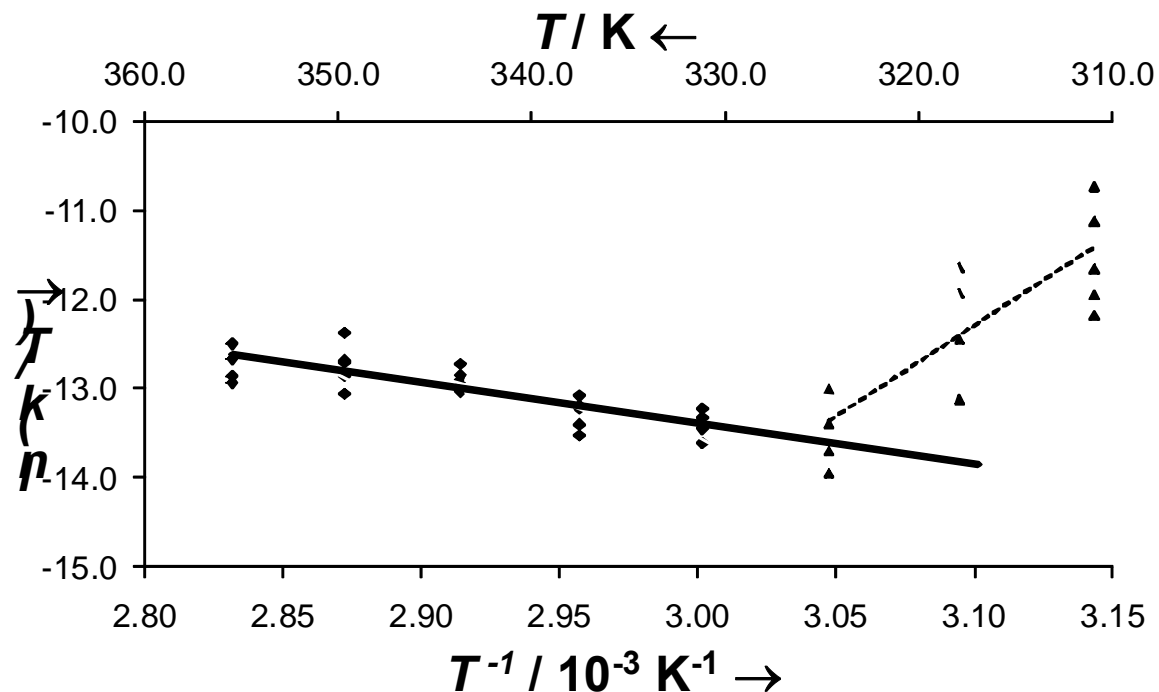
Figure 8. Nonlinear Eyring plot (*ln(k_{app}/T)* as a function of *T^{-1}* for RCM of (30)a over catalyst (23) in GE SE 30 (28) at different temperatures (318–353 K) and inlet pressures (80–120 kPa).

A closer examination of the conversion measurement data revealed a ligand exchange and catalyst activation before reaching steady state. In detail, the peak areas arising from the sum of the reaction product (A_P) and the reaction educt (A_E) were divided by the peak areas arising from the internal standard (IS, *n*-decane). Each normalized peak sum was then included in a plot of peak area versus time for each substrate and product concentration (Figure 9).

In steady state, the normalized peak areas *(A_E+A_P)/A_{IS}* (mass balance) should be constant, which is not the case below 56 °C. Due to strong interaction with the polysiloxane-supported precatalysts **(22)** and **(23)**, namely the reaction of the diene substrate with the precatalyst and removal of the benzylidene unit at low temperatures and before reaching the steady state, the majority of the substrate remains on the catalytically active microcapillary leading to

apparently higher conversions detected by the FID, which results in the nonlinear behavior of the Eyring plot.

Interestingly, this phenomenon was not observed for RCM catalyzed by Grubbs-Hoveyda-type catalyst **(24)**, which is reflected in the constant mass balance. This observation might be ascribable to the proposed release–return mechanism,[196, 197] where the diene substrate first reacts with the initial Ru complex **(24)** to remove the transition metal from the styrene ligand and release the styrene ether. Upon consumption of the diene, the active Ru-carbene reacts with the previously occupied styrenyl ether to cause reformation of the initial complex (return).
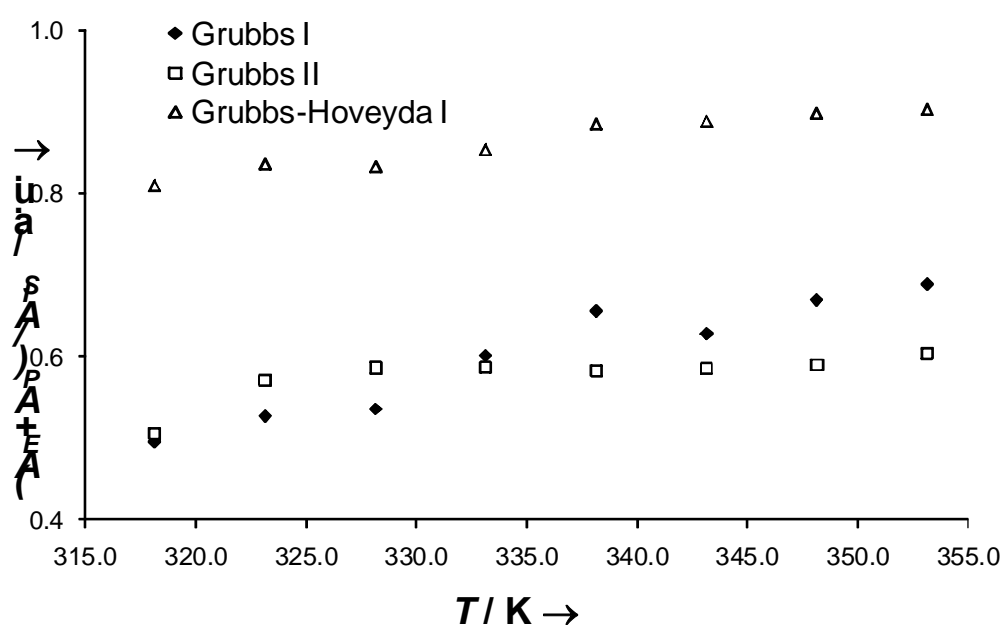
Figure 9. Normalized peak areas arising from the sum of the reaction product (A_P) and the reaction substrate (A_E), divided by the peak areas arising from the internal standard (A_{IS}, *n*-decane), as a function of the reaction temperature for RCM of (30)a over catalysts (22), (23) and (24) in GE SE 30 (28) at 120 kPa.

4.2.6.   Determination of Diffusion Coefficients

In microfluidic systems, the control of mixing is often challenging, because diffusion rates contribute to the apparent reaction rates, as reactor setups decrease in size. In the present setup, diffusion processes can be quantified and experimentally controlled by the

polysiloxane. The van Deemter equation[254-256] (Equation 3) was used to determine diffusion coefficients:

Equation 3

$$H = A + \frac{B}{u} + Cu$$

H is the height equivalent to a theoretical plate, A, the eddy diffusion, B, the coefficient of longitudinal diffusion, C, the coefficient for the mass transfer, and u, the mean velocity of the mobile phase.

Interestingly, van Deemter originally studied the heat and mass transport in fixed catalyst beds and later transferred these derivations to chromatography.[52, 254, 255] Today, the van Deemter equation is well-known to optimize and characterize the efficiency of a chromatographic system. The effective plate height $H = l/N$, where l is the capillary length of 1825 mm and N the effective plate number, was plotted as a function of the velocity u of the carrier gas at various temperatures for **(30)a** (Figure 10).
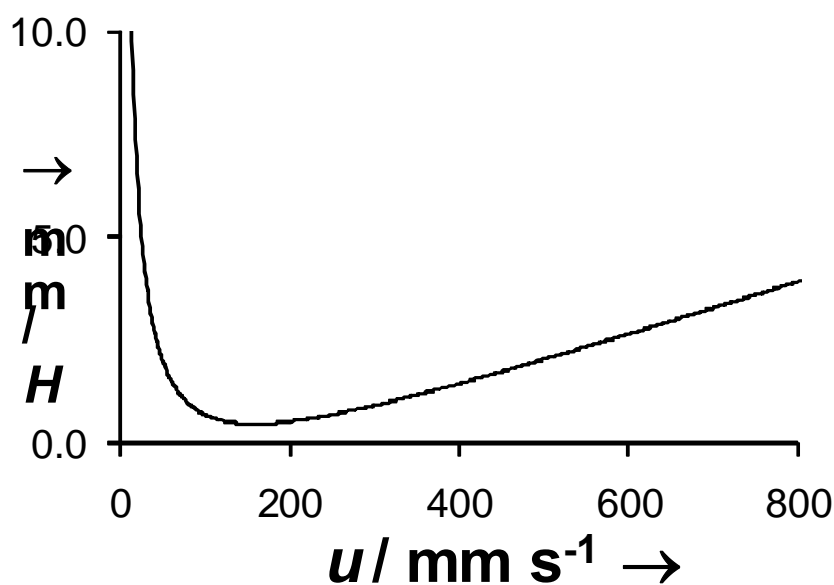

Figure 10. Determination of diffusion coefficients from van Deemter plots of (30)a at 70 °C (1825 mm fused-silica capillary, injector outlet to detector inlet, i.d. 250 μm, GE SE 30 (28), 500 nm film thickness).

The effective plate numbers, $N = 5.545 \times ((t_R - t_0)/w_h)^2$, were calculated from the retention times tR, the peak width at half height wh of the individual substrates and the hold-up time t0 determined from the injections of an internal standard. These curves were fitted with the van Deemter equation (Equation 3) to obtain the constants B and C for the individual substrates. For coated capillaries, the eddy diffusion (A term) can be neglected, because no additional migration paths caused by different particle sizes, shapes, and porosity such as in packed columns have to be considered. The B term, representing the longitudinal diffusion, directly yields the diffusion coefficients for the substrates in the mobile phase at the given temperature (Equation 4).

Equation 4

$$H = \frac{B}{u} + (C_M + C_S)u$$

$$\text{with} \quad B = 2D_M, \quad C_M = \frac{1 + 6k + 11k^2}{96(1+k)^2} \cdot \frac{d_c^2}{D_M}, \quad C_S = \frac{2k}{3(1+k)^2} \cdot \frac{d_f^2}{D_S}$$

The coefficient C for the mass transfer consists of the mass transfer coefficient in the mobile (C_M) and stationary phases (C_S). D_M and D_S are coefficients of molecular diffusion in the mobile and stationary phases, respectively, d_c the inner diameter of the capillary, and d_f the film thickness of the stationary phase. The retention factor $k' = (t_R - t_0)/t_0$ is calculated from the retention time t_R of the substrate and the hold-up time t_0, determined by co-injection of methane. From the coefficients of the van Deemter plots, the diffusion coefficients of the substrates in the mobile phase (D_M) and in the stationary phase (D_S) were calculated, e.g. for **(30)a** at 70 °C, $D_M = 0.85$ cm^2 s^{-1} and $D_S = 5.22 \times 10^{-8}$ cm^2 s^{-1}. Considering these diffusion coefficients and the small paths for the substrates to migrate into the catalytically active stationary phase, it can be concluded that the reactions are not limited by diffusion. In other words, the reaction rate constants determined in this on-column reaction chromatographic setup are directly accessible and depend only on the probability of the substrates to react with the catalytically active ruthenium complex.

4.3. Conclusion

To summarize, on-column reaction chromatography has been demonstrated to be a reliable tool in terms of characterizing different olefin metathesis catalysts. The present approach is suited to screen catalyst libraries with relatively small effort to elucidate mechanistic questions, including the catalyst activation, deactivation and decomposition. The low activation enthalpies $\Delta H^{\ddagger}$ and negative activation entropies $\Delta S^{\ddagger}$ for catalysts **(22)**, **(23)**, and **(24)** correspond to a restraint transition state. The Gibbs activation energy in metathesis reactions of **(30)a** over Grubbs-type catalyst 2nd generation **(23)** (90.2 kJ mol^{-1}) was found to be 7 kJ mol^{-1} higher than for the 1st generation catalysts ($\Delta G^{\ddagger} = 83.2$ kJ mol^{-1}). Grubbs-type 2nd generation catalyst proved to be incredibly stable showing full conversion in RCM of **(30)a** for almost 36 h. The observation of nonlinear Eyring plots gave a valuable insight into the strong interaction with the polysiloxane-supported olefin metathesis precatalysts on the catalytically active microcapillary at low temperatures and before reaching the steady state. In addition to other experimental and theoretical studies, the precise temperature control of the GC experiments investigated herein allows to obtain consistent activation parameters. From the coefficients of the van Deemter plots, the diffusion coefficients of the substrates it could be concluded that the reactions are not limited by diffusion.

Chapter 5

Reaction Kinetics of Olefin Metathesis Catalysts in Ionic Liquids - Integration of Catalysis and Separation

5. Reaction Kinetics of Olefin Metathesis Catalysts in Ionic Liquids - Integration of Catalysis and Separation

5.1. Introduction

The development of sustainable catalytic processes is of fundamental interest for basic research and for industrial applications. For a directed design of catalysts, it is essential to understand how reaction conditions influence the catalytic mechanism. This requires comprehensive experimental kinetic data to understand electronic, steric and solvent effects. Challenging tasks associated with homogeneous processes are product separation, catalyst recycling, and minimization of organic solvents. An elegant solution for these requirements is the immobilization of the active species on a support. As discussed in the introduction, variations in the catalytic activity are caused due to decreased flexibility, diffusion barriers and altered substrate selectivity of the support.

5.1.1.   Room-Temperature Ionic Liquids as Solvents

Room-temperature ionic liquids (RTILs) are attractive reaction media because of their unique solvent properties, extraordinary stability and non-volatility. In general, ILs are salts that are liquid at temperatures $< 100\,°C$ with practically no vapor pressure. Talking about the possibility of about 10^{18} anion/cation combinations, the most reported anion and cation types are shown in Scheme 28. RTILs have received considerable attention as some of them are known to be nontoxic, reusable, and compatible with many organic reactions[257] being a "safe" and "green" alternative for common organic solvents.[258, 259] Because ILs can be "tuned" with various organic and inorganic functionalities to selectively catalyze desired reactions, the term task specific ionic liquids (TSILs) was introduced in the literature.[260] Furthermore, RTILs are able to dissolve and stabilize various transition-metal catalyst precursors, thus providing an excellent support and medium for recycling,[261-265] e.g. in ruthenium-catalyzed RCM.[266-268] As shown in a recent energy balance as part of a life-cycle assessment for the cross-metathesis (CM) of oct-1-ene, the use of an IL becomes economic, as soon as six recycle runs are being performed with the same catalyst.[269] Ruthenium alkylidene-catalyzed olefin metathesis reactions can be performed (i) in pure IL, (ii) in a
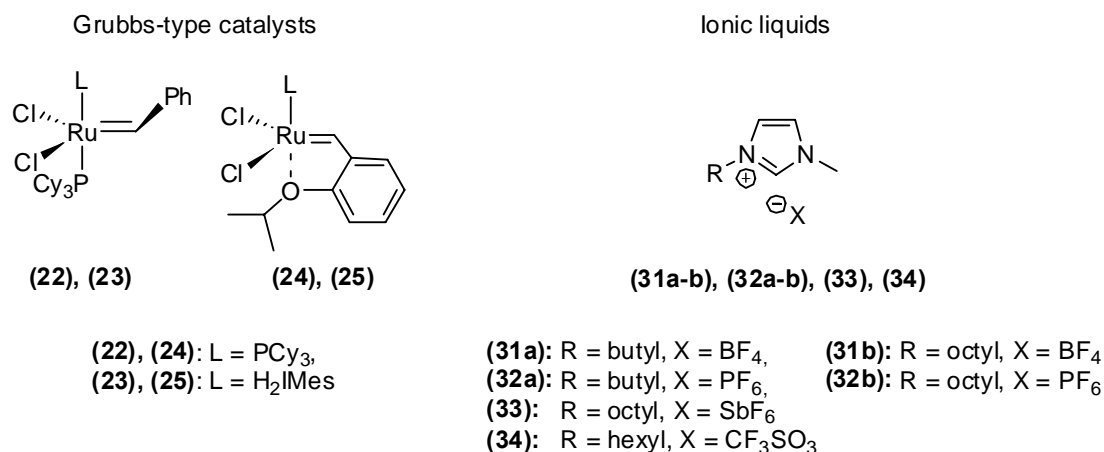
biphasic system of IL and organic solvent or (iii) in an IL with a catalytic amount of IL-supported catalyst. Recent contributions addressing these three approaches will be summarized in the following sections.
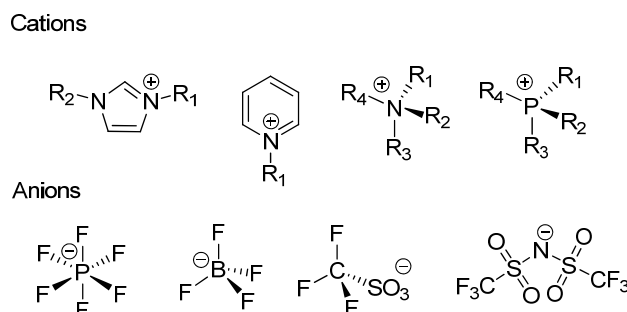
Scheme 28. ILs are composed of cations and anions. Cations (from left to right): imidazolium ion; *N*-alkylpyridinium ion; tetraalkylammonium ion; tetraalkylphosphonium ion, R$_1$, R$_2$, R$_3$, and R$_4$ = alkyl groups. Anions (from left to right): hexafluorophosphate [PF$_6$], tetrafluoroborate [BF$_4$]; trifluoromethylsulfonate [OTf]; bis(trifluoromethanesulfonyl)imide [NTf$_2$].

5.1.2. Olefin Metathesis Catalysts Dissolved in Ionic Liquids

Grubbs-type catalysts **(22)**–**(25)** that were among the first, commercially available olefin metathesis catalysts, can be stabilized in different RTILs (e.g. **(31)a/b**, **(32)a/b**, **(33)** and **(34)**) improving the overall recyclability (Scheme 29). In general, the catalyst is separated by extraction or distillation in the work-up procedure and, therefore, remains in the ionic solvent for subsequent recycling cycles. The first systematic study on practical synthetic applications of ILs as a medium for olefin metathesis was reported by Buisman et al.[270] In their study, quantitative conversion of different RCM substrates catalyzed by catalysts **(22)** and **(23)** in pure RTIL **(32)a** could be achieved after only 1 h at 80 °C. This catalyst could only be reused up to three times after diethyl ether extraction with significant loss of activity in the last cycle and significant ruthenium contamination within the final product (1300–1600 ppm). South African company SASOL investigated the potential of ILs in the CM of oct-1-ene to yield tetradec-7-ene and ethene catalyzed by **(22)**, **(23)** and **(24)**. Catalyst **(23)** dissolved in 1-ethyl-2,3-di-methylimidazolium bis[(trifluoromethyl)-sulfonyl]amide [C$_2$dmim][NTf$_2$] showed remarkable improvements compared to **(22)** with yields of tetradec-7-ene over 20% higher than with either the neat reagents or with toluene as a solvent and a high selectivity towards tetradec-7-ene.[271-273]

Grubbs-type catalysts   Ionic liquids

(22), (23)   **(24), (25)**   **(31a-b), (32a-b), (33), (34)**

(22), (24): L = PCy$_3$,   **(31a):** R = butyl, X = BF$_4$,   **(31b):** R = octyl, X = BF$_4$
(23), (25): L = H$_2$IMes   **(32a):** R = butyl, X = PF$_6$,   **(32b):** R = octyl, X = PF$_6$
                                       (33): R = octyl, X = SbF$_6$
                                       (34): R = hexyl, X = CF$_3$SO$_3$

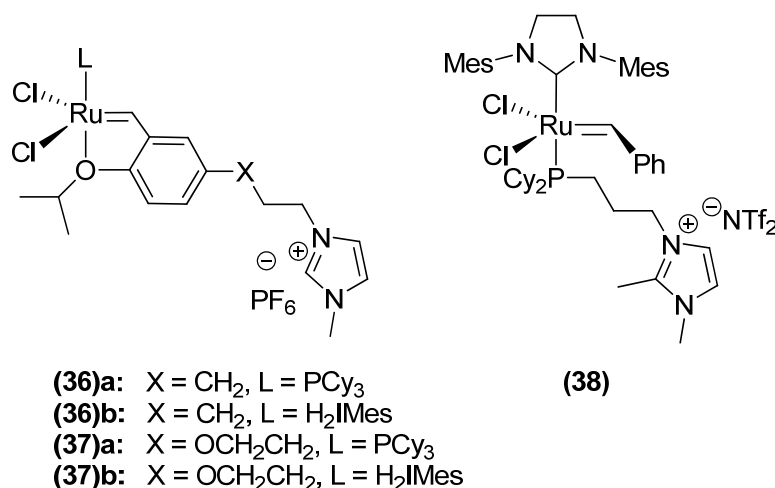**Scheme 29. Grubbs-type catalysts (22)–(25) and RTIL (31)–(34).**

Catalyst **(24)** performed even better with high activity and good recyclability at mild operating conditions from ambient temperature up to 80 °C. Ding et al.[274] reported at least four recycling cycles with 43-89% yield for the CM of styrene catalyzed by **(23)** dissolved in RTIL **(32)a**. Further studies,[275-277] reported on the use of microwaves,[278, 279] the application of continuous-flow setups,[280] and ruthenium-supported IL catalyst (Ru-SILC) in pores of amorphous alumina.[281] When discussing catalyst decomposition, not only catalyst leaching, but also various impurities stemming from the preparation of ILs, have to be taken into account.[272]

5.1.3.   Charged Olefin Metathesis Catalysts

Biphasic systems with charged ruthenium metathesis catalysts and ILs show a reduced leaching due to an increased catalyst affinity to ILs. Results obtained with the ruthenium allenylidene salt [RuCl(=C=C=CPh$_2$)-(PCy$_3$)(p-cymene)][PF$_6$] **(35)** applied in a **(31)a**-toluene mixture for RCM of *N,N*-diallyl tosylamide showed an improved catalyst activity compared to the reactions conducted in pure ionic solvent - a conversion of 96% was achieved after 5.25 h at 80 °C.[282] The allenylidene complex **(35)** was also tested in ROMP of norbornene, where up to six successful catalytic cycles in biphasic [bdmim][PF$_6$]-toluene mixtures were achieved.[283]

5.1.4. Immobilization of Olefin Metathesis Catalysts on Imidazolium Tags

Olefin metathesis catalysts can be immobilized by substituting one of the ligands with a similar ligand attached to a support via a linker and a covalent bond to a support.[284-288] The covalent anchoring of Grubbs-Hoveyda-type catalysts to imidazolium tags,[289-298] e.g. catalysts **(36)a-b**, **(37)a-b** and **(38)** (Scheme 30), resulted in further improvement towards recyclability. No significant loss in catalyst activity was observed even after ten cycles for catalyst **(36)a** dissolved in [bmim]PF$_6$ **(32)a** in RCM reaction of *N,N*-diallyl tosylamine.[289] Despite similar activity in the first cycle, catalysts **(22)** and **(24)** could not be effectively recycled for the same reaction. Furthermore, the NHC-containing analogue **(36)b** could be recycled at least eight times with low ruthenium contamination of the products (1-22 ppm).[292]


(36)a: X = CH$_2$, L = PCy$_3$
(36)b: X = CH$_2$, L = H$_2$IMes
(37)a: X = OCH$_2$CH$_2$, L = PCy$_3$
(37)b: X = OCH$_2$CH$_2$, L = H$_2$IMes

(38)

Scheme 30. IL supported Grubbs-type catalysts (36)–(38).

Similar to catalyst **(36)a**, the 1st generation catalyst **(37)a** of Yao et al.[290, 291] showed excellent recyclability and remained active for ten cycles with only a minor decrease in activity. The corresponding 2nd generation catalyst **(37)b** showed to be very active in the formation of di- and trisubstituted olefins via RCM.[299] Beside a report[295] about Grubbs-Hoveyda-type catalysts containing an IL-tag linked either to the *ortho*-oxygen substituent or to the *meta*-position of the styrenylidene ligand and an anion-tagged ruthenium complex,[300] the group of Dupont[297] prepared the ionophilic 2nd generation Grubbs-type catalysts **(38)**, which were tested in RCM reactions of several substrates and showed to be stable up to eight cycles (88–98% yield, < 2 ppm Ru contamination). The major disadvantage of this strategy is

the need for multiple functionalization steps. Furthermore, product isolation in homogeneous systems, e.g. extraction with organic solvents, remains difficult, often resulting in the deactivation of the recovered catalyst in the IL and hence in a poor recyclability or in completely inseparable mixtures. Kinetic investigations by chromatographic reaction control are difficult to perform for the same reason and injection of ILs into the hot injector for GC analysis leads to accumulation of the IL are the result. Decomposition peaks or an increased noise level can be observed.

5.1.5. Ionic Liquids as Stationary Phases

On the other hand, it is serendipity that ILs have been proven to play an important role in separation science including extractions, GC, and supported liquid membrane processes. They are used as stationary phases in GC because of their low vapor pressure and high separation efficiency.[301-308]
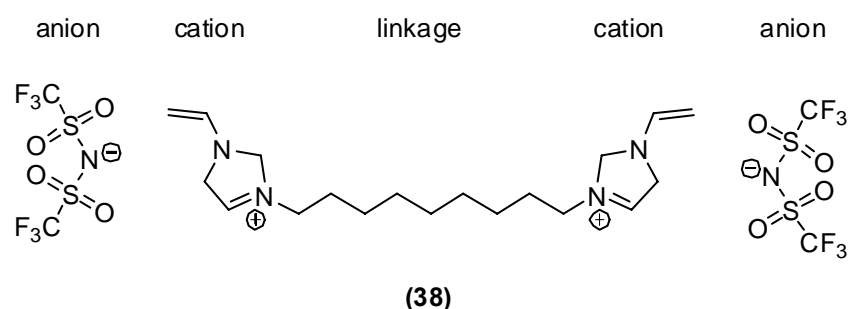
Scheme 31. A highly temperature stable geminal dicationic IL used as GC stationary phase reported by Armstrong et al.[305]

Imidazolium based ILs coated on fused-silica capillary columns are suitable candidates for GC stationary phases because of their unique properties, such as high thermostability, high viscosity, a broad liquid range, and a good wetting ability. Furthermore, it was observed that IL stationary phases show a dual-nature property meaning that they can retain and separate nonpolar compounds as well as polar compounds. Scheme 31 shows a commercially available[309] geminal dicationic IL **(39)**,[305] which is used as GC stationary phase. It can be cross-linked with a free radical initiator through its vinyl groups to provide a more durable and robust stationary phase. Additionally, ILs can be used as matrix for chiral selectors such as cyclodextrin derivatives to give a chiral stationary phase (CSPs).[304] In recent reports,

applications of ILs in microfluidic devices[310-312] and continuous-flow systems[313] are discussed.

5.1.6. Objectives

In this chapter, the concept of on-column reaction gas chromatography was used to combine separation selectivity of the ILs and catalysis by Grubbs 1st generation catalyst **(22)** in RCM reactions. With this combination, it is possible to investigate catalyst stability and recyclability for various substrates, and to efficiently determine reaction rate constants, which are hardly accessible by other techniques.

5.2. Results and Discussion

Although an improved catalytic activity and stability via the exchange of one PCy_3 ligand by an NHC ligand has been reported for Grubbs-type catalyst 2nd generation **(23)** compared to the 1st generation **(22)**, as well as for the Hoveyda-Grubbs-type catalyst 2nd generation **(25)** compared to the 1st generation **(24),** the relatively inexpensive[314] Grubbs-type catalyst **(22)** was chosen to investigate its stability in the presence of IL stationary phases. Hexyl-3-methylimidazolium trifluoromethanesulfonate ([HMIM][CF$_3$SO$_3$]) **(34)** was used as IL stationary phase, because it was reported that so far, the highest separation efficiencies in GC were achieved with RTILs consisting of trifluoromethansulfonate counter anions.[106, 303, 306]

5.2.1. Preparation of Catalytically Active Stationary Phases and Coating of Microcapillaries

Catalytically active micro columns were prepared by dissolving Grubbs-type catalyst 1st generation **(22)** in [HMIM][CF$_3$SO$_3$] **(34)** and dichloromethane to coat 5–8 m long microcapillaries with a thickness of 250 nm by the static method described by Grob[315] under strict exclusion of oxygen. IL **(34)** was dried under high vacuum at an elevated temperature to remove water before the coating procedure. After coating, helium was flushed through the capillary, the capillary ends were sealed and the capillary was directly installed into the GC oven. The catalyst loading was only 8.2×10^{-5} mg cm^{-1} capillary (9.6×10^{-11} mol cm^{-1} capillary).

5.2.2. Catalytic Studies by On-Column Reaction Chromatography

The obtained microcapillaries can be used to perform temperature-dependent measurements for RCM of different substrates for a comprehensive kinetic analysis of Grubbs-type catalyst **(22)** stabilized in [HMIM][CF$_3$SO$_3$] **(34)** (Scheme 32). The integration of separation and catalysis makes the use of an additional separation column unnecessary. Eluted compounds were identified by MS detection using an ion trap mass analyzer and quantified by flame FID. Three benchmark substrates (diethyl diallylmalonate **(40)a**, *N,N*-diallyltrifluoroacetamide **(30)a** and diallyl disulfide **(41)a**) were chosen to investigate on-column RCM by injecting the substrates dissolved in *n*-pentane into the GC. High catalytic activity of the Grubbs-type catalyst 1st generation **(22)** for these substrates was observed leading to full conversions, e.g.

for **(41)b** within 1.9 min at 70 °C, for **(30)b** within 4.3 min at 50 °C, and for **(40)b** within 20.8 min at 90 °C. Compared to RCM of the selected substrates with catalyst **(22)** in homogeneous phase (e.g. for diallyl disulfide **(41)a**: 15% yield after 12 h, 0.1 M CD$_2$Cl$_2$, 5 mol% of **(22)**),[316] these short reaction times demonstrate the high activity of these multiphase catalytic systems.
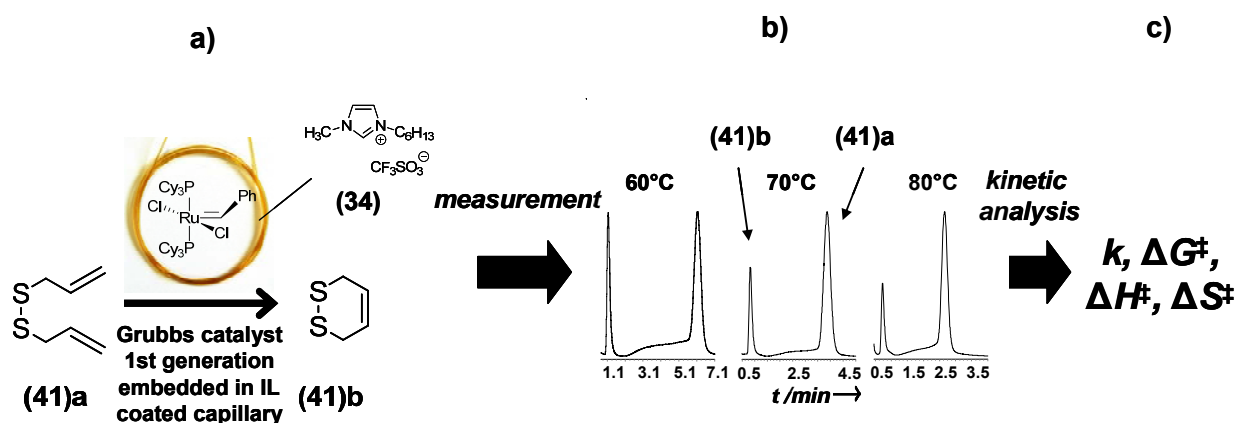
**Scheme 32. a) On-column metathesis over Grubbs 1st generation catalyst (22) dissolved in RTIL (34).**
a) In these experiments catalytic activity and separation selectivity is united in a single 8.0 m capillary by dissolving the catalyst in the IL stationary separation phase. b) Obtained elution profiles are characterized by a pronounced conversion profile from the substrate to the product. c) Activation parameters can be obtained by kinetic analysis with the unified equation of chromatography.

Dissociation and removal of the PCy$_3$ ligand or leaching of the catalyst under the reaction conditions investigated herein were not detected by FID and MS which can be explained by an effective solvation of the phosphine ligand in the IL, resulting in a stabilization of the complex after the reaction.

5.2.3. Catalyst Recycling

To further characterize the stability and hence the recyclability of the catalyst in the IL, multiple substrate injections over 24 h were performed and conversion data were determined at 50 °C and 60 kPa (Figure 11). Interestingly, for the first 8 injections over 3 h, no remarkable loss of catalytic activity could be determined. After this period, a linear decrease in the catalytic activity could be observed, which stabilized again after 12 h at an average conversion level of 51% of the activity at the beginning of these specific measurements. In

total, 63 recycling experiments with conversions of 51–91% in 24 h were carried out. Compared to the recycling experiments in the batch, only up to four recycling steps for olefin metathesis catalysts dissolved in IL and up to ten recycling steps for imidazolium-supported catalysts were reported in literature.[274]
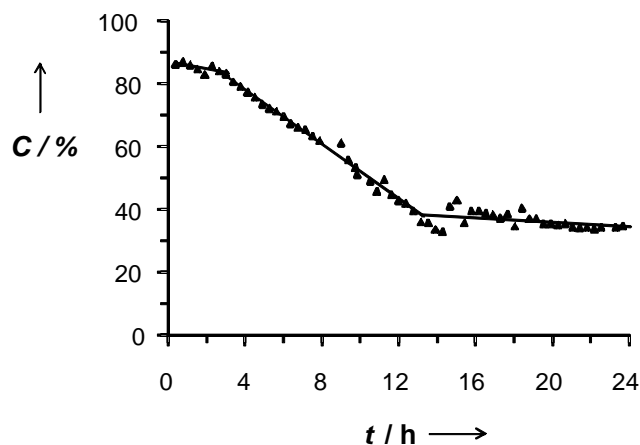

Figure 11. Stability plot of Grubbs 1st generation catalyst (22) (dissolved in [HMIM][CF$_3$SO$_3$] (34)) determined by time-dependent conversions of (30)a at 50 °C and 60 kPa inlet pressure (single 5.0 m capillary, i.d. 250 μm, film thickness 250 nm).

These experiments show that the imidazolium-containing RTIL solubilize and stabilize the active catalytic species, but remain almost unreactive toward the active catalytic site of **(22)**. Because 1,3-dialkylimidazolium ILs are considered as three-dimensional networks of anions and cations, linked together by weak interactions (such as hydrogen bonds, van der Waals, and Coulombic forces), the phosphine ligand might be dissolved in this matrix and is able to stabilize the catalytically active ruthenium species.

5.2.4. Determination of Reaction Rate Constants and Activation Parameters

To get further insights into the reaction kinetics of RCM in ILs using catalyst **(22)**, temperature-dependent measurements were performed to determine reaction rate constants from the conversion profiles for incomplete conversions (Figure 12).
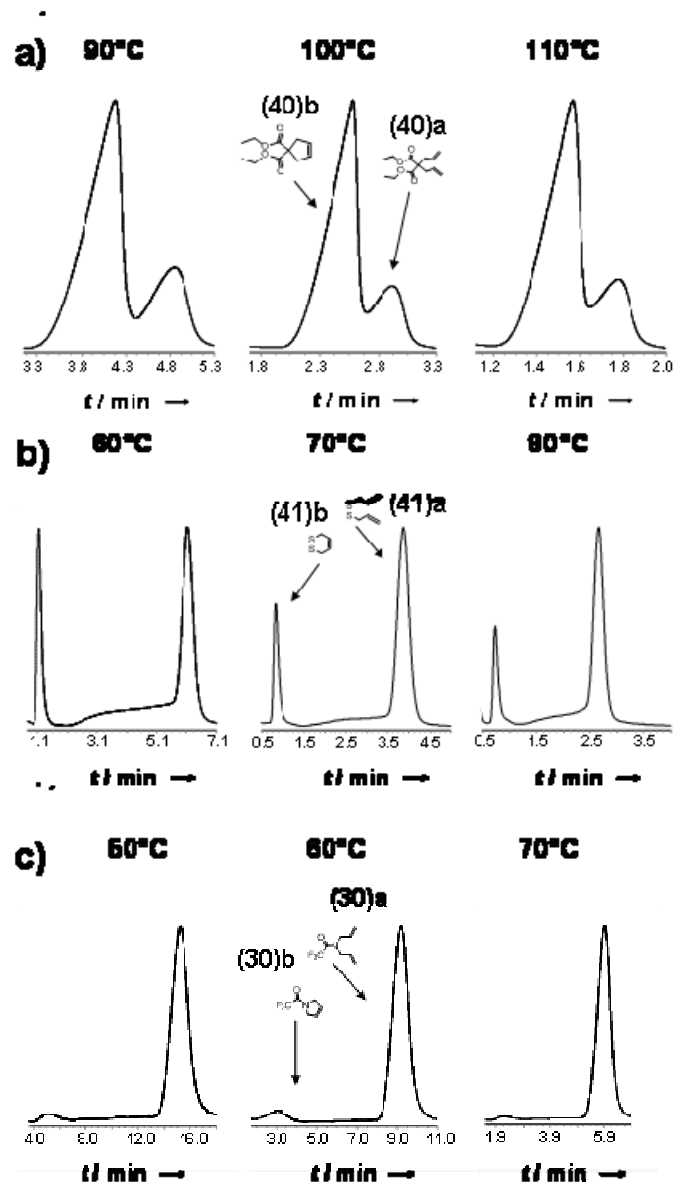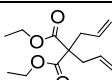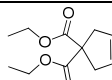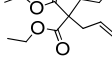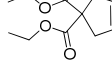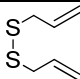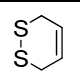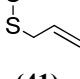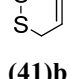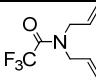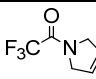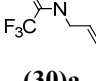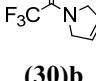
Figure 12. Selected chromatograms of the temperature-dependent measurement of RCM of a) (40)a as interconverting profile at 110 kPa, b) (41)a at 90 kPa and c) (30)a at 60 kPa for the determination of activation parameters. Conditions: a) 1.0 m catalytically active microcapillary (i.d. 250 μm, film thickness 250 nm) and 1.0 m separation capillary GE SE 52 (29) (i.d. 250 μm, film thickness 500 nm), b) /c) 8.0 m catalytically active microcapillary coated with (22) and (34) (i.d. 250 μm, film thickness 250 nm), He was used as the inert carrier gas.

The elution profiles of the substrates are characterized by a distinct plateau formation between substrate and product, which is characteristic for reaction processes taking place on the time scale of separation. Such elution profiles can be directly evaluated using the unified equation of chromatography [71] to obtain reaction rate constants of first-order reaction kinetics. As it was already observed in previous measurements,[84, 85] the contact times of diethyl

diallylmalonate **(40)a** were significantly higher than for the other test substrates. This leads to a complete conversion of reaction substrate **(40)a** on a 8 m long capillary coated with catalyst **(22)** and RTIL **(34)**. To achieve incomplete conversions, which are required for kinetic analysis for **(40)a**, the kinetic on-column measurements were performed with a 1 m capillary coupled to a 1 m separation capillary (GE SE 52 **(29)**). In this setup, reaction times were determined to be 70 s at 110 °C. The reaction rate constants of the elution profiles in this chromatographic microreactor, where the catalyst capillary is coupled with a separation capillary, were obtained via the determination of residence times of RCM substrates with a reference column using only RTIL **(34)** as the stationary phase.[55] It is important to note that the easy handling of the catalytically active separation capillaries allow to switch between on-column reaction chromatography in a single catalytically active capillary and a chromatographic microreactor mode, which broadens the applicable time-scale window.[55] Conversions were determined by integrating the FID signals, taking correction factors (f = 1.96 for **(30)a** → **(30)b**, f = 1.24 for **(40)a** → **(40)a**, f = 1.66 for **(41)a** → **(41)b**, chapter 8.5.2) for the relative signal ratios of the substrates and products into account. Table 4 summarizes the conversion data, reaction rate constants k, and activation parameters ($\Delta G^{\ddagger}$, $\Delta H^{\ddagger}$ and $\Delta S^{\ddagger}$) from temperature-dependent measurements of RCM reactions of the three substrates **(30)a**, **(40)a** and **(41)a**. These parameters agree well with recently reported experimental data (chapter 4.1.4) and corroborate theoretical calculations. The low activation enthalpies $\Delta H^{\ddagger}$ and negative activation entropies $\Delta S^{\ddagger}$ correspond to a restraint transition state for RCM reactions catalyzed by **(22)**, e.g. for diallyl disulfide **(41)a** $\Delta G^{\ddagger}$ (298 K) = 89.6 kJ mol^{-1}, $\Delta H^{\ddagger}$ = 78.1 kJ mol^{-1} and $\Delta S^{\ddagger}$ = -39 J K^{-1} mol^{-1}. Comparison of the activation parameters of RCM of **(40)a**, **(41)a** and **(30)a** shows that the metathesis reaction of *N,N*-diallyltrifluoroacetamide **(30)a** has the lowest activation enthalpy $\Delta H^{\ddagger}$ (21.8 kJ mol^{-1}) and most negative activation entropy $\Delta S^{\ddagger}$ (-215 J K^{-1} mol^{-1}) compared to the other substrates, which was also found for on-column metathesis over the Grubbs-type catalyst 2nd generation **(23)** in the nonpolar PDMS (GE SE 30 **(28)**).[84, 85] It is important to note that the Gibbs free activation energies $\Delta G^{\ddagger}(T)$ for on-column metathesis over the Grubbs-type catalyst 1st generation **(22)** in [HMIM][CF$_3$SO$_3$] **(34)** were about 4-19 kJ mol^{-1} lower than for using Grubbs-type catalyst 2nd generation **(23)** in PDMS. For RCM of diethyl diallylmalonate **(40)a** an average reaction rate constant k = 2.5×10^{-2} s^{-1} at 110 °C was determined. In comparison to measurements of the same reaction with Grubbs 2nd generation catalysts **(23)** stabilized in a nonpolar PDMS, this reaction proceeds about ten times faster in the IL.

Table 4. Selected results of the on-column metathesis reactions over Grubbs 1st generation catalyst (22) in IL (34) as a stationary phase.

	Substrate	Product	T	p	$C^{[a]}$	$k^{[b]}$	$\Delta G^{\neq[c]}$	$\Delta H^{\neq[d]}$	$\Delta S^{\neq[e]}$
			[°C]	[kPa]	[%]	[10^{-2} s^{-1}]	[kJ mol^{-1}]		[J K^{-1} mol^{-1}]
1[d]			90	110	76.5	0.8			
2[d]			100	110	81.2	1.6	95.0	63.7	-105
3[d]	(40)a	(40)b	110	110	78.8	2.5			
4[e]			60	90	30.2	2.1			
5[e]			70	90	22.5	3.8	89.6	78.1	-39
6[e]	(41)a	(41)b	80	90	19.3	10.9			
7[e]			50	60	3.3	0.6			
8[e]			60	60	5.3	0.8	86.0	21.8	-215
9[e]	(30)a	(30)b	70	60	1.7	1.0			

[a] Conversion C. [b] Reaction rate constant k. [c] Gibbs activation energy $\Delta G^{\neq}$ at 25 °C. [d] Activation enthalpy $\Delta H^{\neq}$. [e] Activation entropy $\Delta S^{\neq}$. Conditions: [d] 1.0 m catalytically active microcapillary (i.d. 250 μm, film thickness 250 nm) coupled with 1.0 m separation capillary GE SE 52 (29) (i.d. 250 μm, film thickness 500 nm), [e] 8.0 m catalytically active microcapillary coated with (22) and (34) (i.d. 250 μm, film thickness 250 nm), He was used as the inert carrier gas.

These findings show that catalyst (22) is not only efficiently stabilized in RTIL (34), but also that the conversion is considerably accelerated. A possible explanation might be that the dissociated phosphine ligand is effectively stabilized in the IL and, therefore, does not compete with the substrate to coordinate back to the ruthenium metal center. On the other hand, the catalyst is restabilized by the free phosphine ligands dissolved in the IL after the reaction.

5.3. Conclusion

The presented work confirms the possibility of an effective integration of synthesis and separation in ILs by on-column reaction chromatography and the combination of homogeneous catalysis and its advantages with heterogeneous technology including the direct access to reaction rate constants. The activation energy of $\Delta G^{\ddagger}$ (298 K) = 89.6 kJ mol^{-1} for RCM of diallyl disulfide **(41)a** added evidence for the homogeneous nature of the catalysis, i.e. for the solvation of complex **(22)** in the IL stationary phase. The obtained activation parameters showed a catalyst performance similarly to homogeneous phase. Looking at the stability of Grubbs-type catalysts 1st generation **(22)** supported on [HMIM][CF$_3$SO$_3$] **(34)**, the conversion plot revealed an effective stabilization in the IL, which was corroborated due to a stable average conversion level after 12 h. In general, the here demonstrated concept is suitable to study highly selective, heterogenized homogeneous catalysts. Here, the advantage of TSILs may also provide new opportunities for catalyst stabilization and immobilization onto microcapillaries.

Chapter 6

Synthesis of Polysiloxane-Immobilized Chiral Camphor-Based Transition Metal Catalysts and their Investigation with On-Column Reaction Chromatography
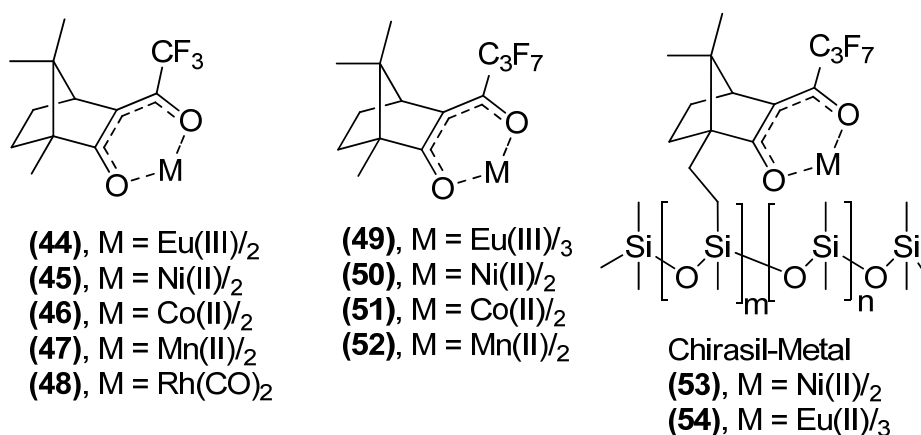
6. Synthesis of Polysiloxane-Immobilized Chiral Camphor-Based Transition Metal Catalysts and their Investigation with On-Column Reaction Chromatography

6.1. Introduction

The search for highly-efficient catalysts and reagents is of great economic and ecologic impact. In the recent years, there was a rapid method development of ht screening techniques and combinatorial processes[44, 45, 317] as convenient approaches to find and optimize efficient and selective catalysts[318] and reagents.[319, 320] Therefore, current research focuses on the combination of different disciplines in synthetic, physical and technical chemistry. First prototypes of micro-reactors were developed to realize rapid ht screenings of new molecules and catalysts with minimal amounts of material consumption. In particular, the interest of researchers was directed towards the access to enantiomerically pure compounds in the field of pharmaceuticals, agrochemicals, and flavors.[318, 321] For the synthesis of enantioselective catalysts, suitable chiral precursors are needed, which are available enantiomerically pure. Ideally, one makes use of the chiral pool,[322] meaning a stock of natural substances that are readily available as enantiopure compounds. Common chiral catalysts are amino acids, in particular, L-proline in organocatalysis,[323] tartaric acid and its derivatives,[324, 325] and ligands based on terpenes. Transition metal campherato complexes find particular use as chiral shift reagents,[326] CSPs in complexation gas chromatography (GC).[327-334] and enantioselective catalysts for numerous reactions.[29, 335, 336] Their synthesis and application will be discussed in the following sections.

6.1.1. Transition Metal Campherato Complexes as Chiral Stationary Phases in Complexation Gas Chromatography

After unsuccessful attempts in the late 1950s, the use of GC methods for enantiomer separation started in the mid 1960s, when GC was established as a standard technique. The first successful separation of enantiomeric amino acids by GC was accomplished by Gil-Av et al.[337] in 1966. Gil-Av and Schurig conjectured, whether abiotic selector-selectand systems displaying metal-organic coordination would display chiral recognition in complexation GC

in the early 1970s. Feibush et al.[338] picked up this idea in utilizing chiral camphor-derived β-diketonate anions as ligands for metal ions. In addition to their use as CSP in GC,[339] these compounds could be successfully used as paramagnetic chiral NMR shift reagents.[326, 340] Chiral camphor-derived β-diketonate metal complexes were synthesized by transferring (1R)-camphor (42) into (trifluoroacetyl)-(1R)-camphor (43) and the corresponding metal chelates (Eu(III) (44), Ni(II) (45), Co(II) (46), and Mn(II) complex (47)).[341] These metal chelates were prepared by a simple synthetic protocol, dissolved in squalane and immobilized on a GC capillary. Dicarbonylrhodium(I)-3-(trifluoroacetyl)-(1R)-camphorate (48) showed isotopic selectivity toward deuterated ethenes[327, 328] and enantioselectivity toward the racemic olefin 3-methylcyclopentene[329, 330] in complexation GC. The trifluoroacetyl group was then replaced by a stronger electron-withdrawing heptafluorobutanoyl-group resulting in stable (heptafluorobutanoyl)-(1R)-camphorato chelates of Eu(III) (49), Ni(II) (50), Co(II) (51), and Mn(II) (52). Later, squalane was replaced by PDMS as a useful solvent for the selectors.[331] High-resolution glass- or fused-silica open tubular-capillary column technology in complexation GC improved the state-of-the-art as well. Another improvement in complexation GC was the covalent linkage of the chiral selector to a polymeric backbone like polysiloxanes as exemplified with Chirasil-Val.[342]

(44), M = Eu(III)/2
(45), M = Ni(II)/2
(46), M = Co(II)/2
(47), M = Mn(II)/2
(48), M = Rh(CO)2

(49), M = Eu(III)/3
(50), M = Ni(II)/2
(51), M = Co(II)/2
(52), M = Mn(II)/2

Chirasil-Metal
(53), M = Ni(II)/2
(54), M = Eu(II)/3

Scheme 33. Chiral metal chelates (44) –(54) as selectors in stationary phases reported by Schurig et al.[29]

Chiral stationary phases, namely metal-containing polysiloxanes **(53)** and **(54)** (Chirasil-Metal), were obtained by linking 10-methylene-camphor **(55)** to a HMPS backbone via Pt-catalyzed hydrosilylation.[333, 334] As already described, Chirasil-Eu(III) **(54)** (Scheme 33) can not only be used as CSP in complexation GC, [327-334] but also as enantioselective polymeric

NMR shift reagent[326, 340] and as enantioselective polymeric homogeneous catalyst for hetero-Diels-Alder reactions.[29, 335] In the latter two cases, the chiral auxiliary can be recovered by simple precipitation.

Numerous racemic oxygen-, nitrogen- and sulphur-containing selectands can be separated into their enantiomers with complexation GC on optically active metal(II)*bis*[3-(perfluoroacyl)-(1*R*)-camphorate] selectors diluted in, or chemically bound to, an achiral stationary matrix (squalane, PDMS) without prior derivatization.[343] One important example is the separation of the aggregation pheromone of the bark beetle *Pytiogenes chalcographus*, chalcogran **(94)a–d** ((2*RS*,5*RS*)-2-ethyl-1,6-dioxaspiro[4.4]-nonane), which was firstly isolated by Francke et al.[344] It belongs to an important class of chiral spiroketals. The qualitative separation for the identification of the biologically active stereoisomers is a prerequisite for the development of suitable bio-trap sampling approaches, e.g. by using these insect sex pheromones to attract insects to traps for detection and determination of temporal distribution.[345] All four stereoisomers of chalcogran **(94)a–d** (Scheme 34) could be separated and chromatographically assigned by enantioselective complexation chromatography using nickel(II)-bis[(1*R*)-6-(heptafluorobutanoyl)-pulegonate] as CSP.[331-334, 346-356]

Z (*cis*)

(2*R*,5*R*)-**(94)a**   (2*S*,5*S*)-**(94)b**

E (*trans*)

(2*S*,5*R*)-**(94)c**   (2*R*,5*S*)-**(94)d**
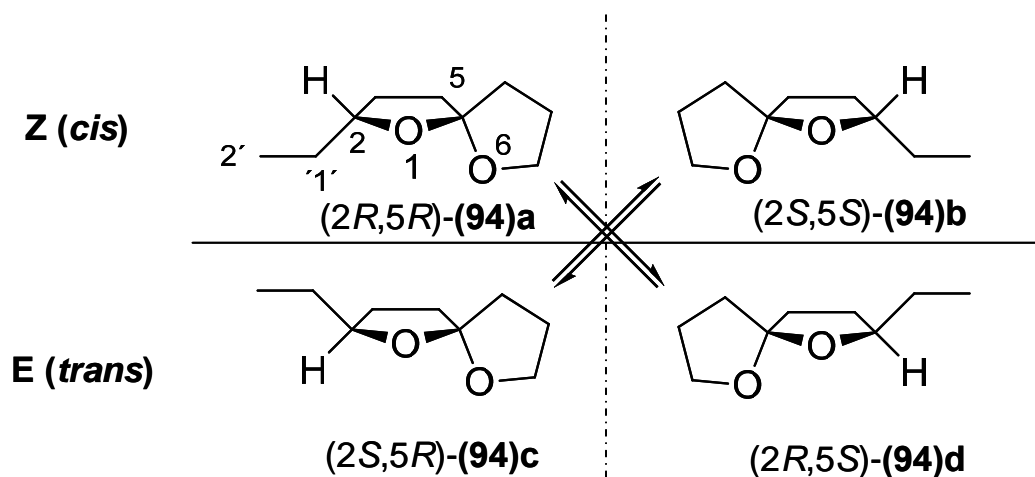
Scheme 34. Epimeric and enantiomeric pairs of chalcogran (94)a–d.

The separation of the four stereoisomers of chalcogran **(94)a–d** has been studied extensively[353, 357-361] addressing the determination of the enantioselectivity from the retention-increment, rate constants of epimerization, the isoenantioselective temperature, and the temperature-dependent reversal of the elution order.

6.1.2. Polysiloxane-Immobilized Catalysts

The immobilization of chiral catalysts has been pursued for over three decades.[15] Surprisingly, linearly functionalized polysiloxanes have found relatively little use as catalyst supports, although hydrosilylation reactions allow the immobilization of tailor-made homogeneous catalysts in a very efficient way. Their polarity and selectivity can be tuned and they are widely used as common stationary phases in capillary GC columns,[362] fluids, surfactants, release agents, membranes[363-365] and lubricants,[28] possessing good thermal, oxidative, chemical and biological stability.

Platinum-Catalyzed Hydrosilylation Reaction

The hydrosilylation reaction,[366] namely the addition of a Si-H unit to a carbon-carbon double bond to form an alkylsilane **(56)**, enables the production of silicon polymers, which are used in silicon rubbers, liquid injection molding products, paper release coatings- and pressure-sensitive adhesives. The reaction can be initiated or catalyzed in numerous ways,[367] the most widely used being Pt derivatives (Scheme 35).
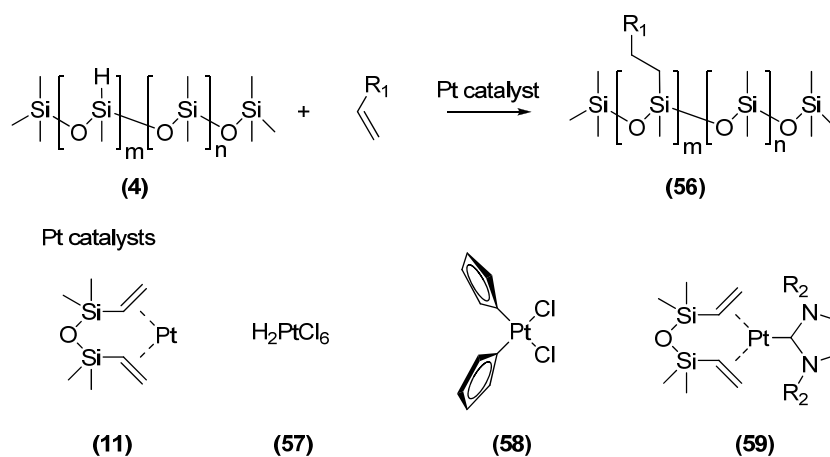
Scheme 35. Pt-catalyzed hydrosilylation reaction.

Among the catalysts known for the hydrosilylation reaction, hexachloroplatinic acid **(57)** (H_2PtCl_6) in 2-propanol (Speiers catalyst)[368] is the most common one. Sometimes, a decrease of the catalytic activity of H_2PtCl_6 **(57)**, accompanied by the precipitation of small amounts of finely dispersed Pt metal, can be detected. However, more efficient catalysts for the

polyhydrosilylation reactions have been reported like the Pt-divinyltetramethyldisiloxane complex **(11)** (Karstedt's catalyst),[369] dichlorodi-(cyclopentadienyl)platinum(II) **(58)** (Cl$_2$Ptdcp)[370, 371] or the Pt(0)-carbene complex **(59)**.[372] Toluene is often used as solvent at temperatures ranging from 25–120 °C. Ultrasonication is known to permit hydrosilylation reactions at room temperature in high yields.[373] The reaction progress is typically monitored by ^{1}H NMR and IR measurements. As most of the linear polysiloxanes are soluble in common organic solvents, they can be fully characterized by ^{1}H NMR and ^{29}Si NMR concerning purity and ligand loading. The straightforward anchoring allows the efficient, covalent attachment of tailor-made achiral[374-377] and chiral homogeneous catalysts to polysiloxanes, as reflected in the following selected examples.

Examples of Polysiloxane-Immobilized Catalysts

Wandrey et al.[378] described a polysiloxane-supported oxazaborolidine reduction catalyst. The asymmetric reduction of acetophenone, propiophenone and α-chloroacetophenone to the corresponding (*R*)- and (*S*)-alcohols with the immobilized catalyst proceeded with 89–97% ee and with 83–88% isolated yields. The authors noted that the catalyst may be quantitatively retained by a nanofiltration membrane, suggesting its potential for application in a continuously operated membrane reactor. The immobilization of cinchona alkaloids on polysiloxanes[30, 167] was already discussed in chapter 3.2. Furthermore, Grunlan et al.[30] reported an interesting liquid-liquid separation after monophasic reactions as a method to use and recover polysiloxane-supported catalysts.[30] Pini et al.[379] synthesized cross-linked PDMS-supported bis-oxazoline (box) ligands showing high ee values (91–99%) in copper-catalyzed asymmetric transformations (carbonylene reactions, Mukaiyama aldol reactions and olefin cyclopropanations). In 2000, the synthesis of an easily recoverable Ru-based siloxane catalyst was described by Garber et al.[197] (Scheme 36). Key features of the synthetic route included a Pd-catalyzed Stille-type coupling for installation of the requisite vinyl group and synthesis of the core by a Pt-catalyzed hydrosilylation / alkylation / hydroboration sequence. The final step of the synthesis of **(60)a** involved a metalation of the precursor tetraolefin by treatment with Grubbs-type catalyst **(22)** in the presence of CuCl. The more active catalyst **(60)b** was obtained by ligand exchange with the vacant structure, this time with Grubbs Hoveyda catalyst 1st generation **(24)** as the stoichiometric metal source. Efficient and catalytic RCM of *N,N*-diallyl tosylamide was achieved with 1.25 mol% **(60)a** (5 mol% Ru). The RCM

product was first isolated in 99% yield by silica gel chromatography by elution with CH_2Cl_2. Subsequent washing of the silica with Et_2O leaded to the isolation of the catalyst **(60)a**. ^{1}H NMR spectroscopy measurements revealed that 13% of the styrenyl ligands of the catalyst were vacant (13% Ru loss, 93% isolated yield of **(60)a**).

(60)a, L = PCy3, **(60)b**, L = H2IMes
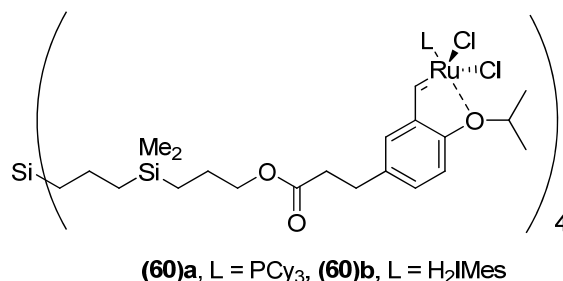
Scheme 36. Recoverable Ru-based siloxane catalysts (60)a and (60)b reported by Hoveyda.

The examples discussed above show that different immobilization strategies including the modification of the chiral ligand and the length and flexibility of the linker could be achieved. Classical methods to immobilize a chiral homogeneous ligand or its metal complex are copolymerization with a monomer or its covalent linkage to a suitable support. A modular strategy for the covalent immobilization of homogeneous (chiral) catalysts and ligands on modified polysiloxanes is shown in Scheme 37.
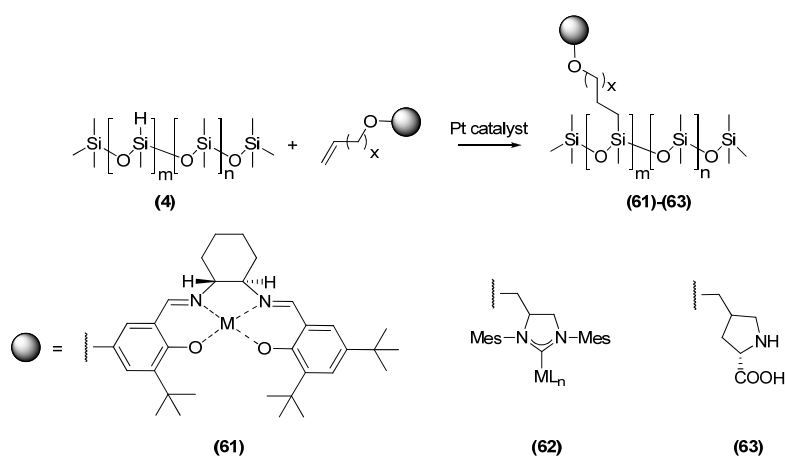
Scheme 37. A modular strategy for the covalent immobilization of homogeneous (chiral) catalysts and ligands on modified polysiloxanes.

The advantage of this approach is the possibility of the spacer length variation. Using the Williamson ether synthesis, spacers with different length bearing a terminal allyl function can be introduced. In only a few synthetic steps, supported privileged (chiral) ligands and catalysts[380] like polysiloxane-immobilized salen-complexes (61) (chapter 7), polysiloxane-immobilized NHC-complexes (62),[381] and polysiloxane-immobilized proline (63)[382] are accessible.
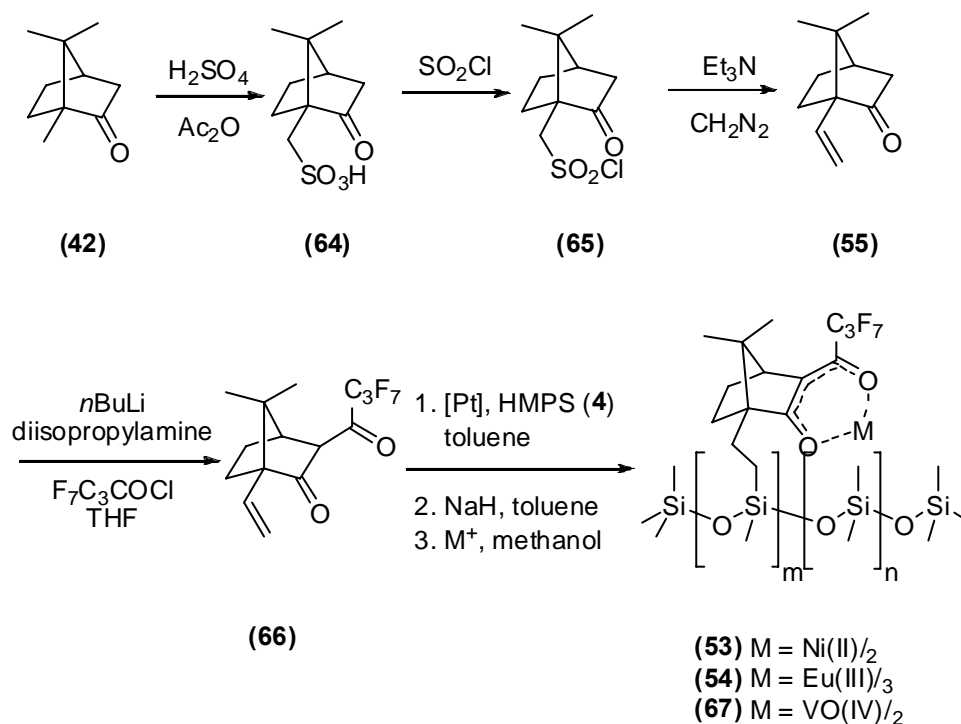
Scheme 38. Synthetic route to polysiloxane-immobilized metal 1,3-diketonates (53), (54) and (67) reported by Schurig.

The synthesis of the chemically modified chiral polysiloxanes (Chirasil-Metal), firstly described by Schurig et al.,[332] is shown in Scheme 38. Dissolving (1R)-camphor (42) in acetic anhydride and sulphuric acid leaded to (1R)-10-camphorsulfonic acid (64)[383] Treatment of (64) with thionyl chloride gave (1S)-10-camphorsulfonic acid chloride (65), which was then reacted with triethylamine to build a metastable sulfene. This sulfene reacted with diazomethane to a metastable episulfone. At higher temperatures (80-90 °C), SO_2 was eliminated to yield 10-methylene-camphor (55),[384-387] followed by an acylation with heptafluorobutanoyl chloride, which leaded to the 1,3-diketonate (66). In this synthesis step, the high acidity of the proton in the α-position of the ketone was used. To obtain the enolate

of the ketone, this proton could be abstracted with strong and sterically demanding bases (e.g. lithium diisopropylamide (LDA)). The enolate reacted with an acyl chloride under kinetic control to gave a 1,3-diketonate or at higher reaction temperatures to a thermically more stable *O*-acyl derivative. The yields of the synthesis to 1,3-diketonates using LDA as a base[326] were relatively low (only up to 35%), because of competing reactions between the acyl chloride and remaining acidic protons of the camphor molecule. Additional base leaded to bisacylation products. Furthermore, the purification of the resulting 1,3-diketonates was exceedingly difficult, because: (i) the remaining diisopropylamine can react with the acidic 1,3-diketonato-camphor derivative to form a diisopropylammonium salt, and (ii) LDA can react with the acyl chloride to the corresponding amide. Both side products are very stable and can hardly be separated by washing procedures or column chromatography from the desired product. Using sodium amide as base and DME as solvent for the acylation leaded to slightly higher yields (about 50%), because the higher boiling point of DME (85 °C) allowed higher reaction temperatures leading to a better expulsion of NH_3 and, therefore, to an equilibrium shift to the enolate.[29, 335, 388, 389]

Diels-Alder Reactions

The Diels-Alder reaction is a [4+2] cycloaddition to synthesize six-membered rings.[390] Its impact on synthetic organic chemistry was so immense that Kurt Otto and Diels-Alder were awarded with the Nobel Prize in Chemistry "for their discovery and development of the diene synthesis" in 1950.[391, 392] Many different versions of the Diels-Alder reaction were elaborated, including intramolecular [4+2] cycloadditions, hetero-Diels-Alder reactions, pressure-accelerated Diels-Alder reactions, and Lewis acid accelerated Diels-Alder reactions. The application of this reaction type not only leads to strong increase in molecular complexity (molecular size, topology, stereochemistry, functionality, and appendages), but also can result in structures increasing to additional amplification of complexity by the use of other powerful synthetic reactions.

Camphor-based polysiloxane-immobilized metal 1,3-diketonate **(67)** (Chirasil-Metal) have proven to catalyze the hetero-Diels-Alder reaction of the *trans*-1-methoxy-3-trimethylsilyloxy-1,3-butadiene (Danishefsky diene, **(68)**)[393] and benzaldehyde **(69)** (Scheme 39).[29, 335] The most efficient camphor-based catalysts were obtained, when oxovanadium(IV)

and europium(III) where used as coordinating metals. Essentially, 100% of the catalysts activity was retained through seven recycling cycles. Despite excellent chemical yields, the reaction to pyran-4-ones **(70)** only showed moderate stereoselectivities.
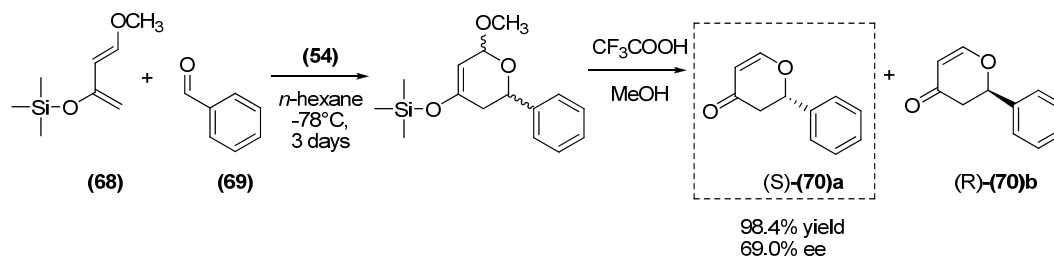
Scheme 39. Enantioselective hetero-Diels-Alder reaction of the Danishefsky diene (68) and benzaldehyde (69) to pyran-4-one (70)a/b, catalyzed by chiral camphor-based polysiloxane-immobilized metal diketonates reported by Schurig. The reaction proceeds in favor of (S)-2-phenyl-2H-pyran-4(3H)-one (70)a.

The polymeric catalysts are soluble in *n*-hexane and could be precipitated by addition of methanol. Interestingly, the polymeric oxovanadium(IV)-catalyst **(67)** induced opposite enantioselectivity compared to its monomeric counterpart. Such an altered stereoselectivity suggests significant changes in the metal coordination environment occurring in the presence of the polymer. Furthermore, intramolecular Diels-Alder reactions[394-398] that are widely used as key steps in the construction of fundamental frameworks in natural product synthesis,[399] are a suitable test-system for the catalytically activity and enantioselectivity of the polysiloxane-supported chiral Lewis acid catalysts. In particular, the intramolecular Diels-Alder reaction of furfurylfumarate derivatives to 7-oxabicyclo[2.2.1]heptene derivatives[400-402] (Scheme 40) is widely studied, because the yielded bicyclic products are important precursors in the preparation of taxol analogues.[403, 404] Jung and Gervay[400, 401] investigated the rates of cyclization of a series of substituted 2-furfuryl methyl fumarates. They discussed the *gem*-dialkyl effect, namely the acceleration of a cyclization due to the substitution of alkyl groups for hydrogen atoms on the carbons in the chain, which links the two reactive centers. The rate of cyclization was determined by monitoring the cyclization of different 2-furfuryl methyl fumarates in deuterated acetonitrile (CD$_3$CN) at room temperature by ^{1}H NMR measurements, which were used to quantify the relative amount of acyclic precursor A and cycloadduct C.
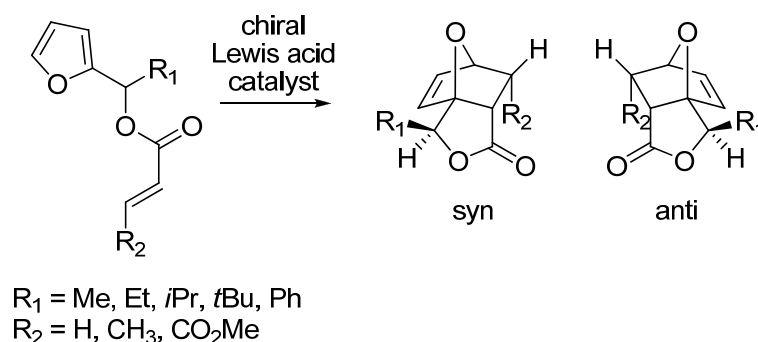
Scheme 40. Enantioselective intramolecular Diels-Alder reaction of furfurylfumarate derivatives to 7-oxabicyclo[2.2.1]heptene derivatives.

With use of simple first-order kinetics (ln [A] versus time), reaction rates were obtained and the half-life of the reaction was determined. Kita et al.[405, 406] reported a lipase-catalyzed one-pot synthesis of optically active 7-oxabicyclo[2.2.1]heptene derivatives bearing five chiral, non-racemic carbon centers, with excellent enantioselectivities in the range of 91–99% ee derived from an achiral carboxylic acid and a racemic alcohol.

6.1.3. Objectives

Immobilized transition metal campherato complexes, serving as useful asymmetric induction catalysts, offer advantages in terms of catalyst recycling. The immobilization of metal-3-heptafluorobutanoylcamphorates **(55)** to a PDMS chain via the C10 position of the camphor moiety has been described earlier.[332-334] However, this synthetic route was not widely used, as diazomethane as a carcinogenic and potentially explosive reagent has to be used in equimolar amounts. Furthermore, the flexibility and accessibility of the metal complex is limited due to the short spacer between the catalytically active center and the support. Hence, the catalytic activity of the polysiloxanes is reduced. Within this chapter, a new immobilization strategy of metal 1,3-diketonates, is introduced. The camphor ligand can be attached by hydrosilylation to the polysiloxane via an ether or thioether functionality on the C10 position of the (1*R*)-10-hydroxycamphor **(74)**[407] or the (1*S*)-10-camphorthiol **(75).** The advantage of this approach is the flexibility in the length of the spacer as well as the less hazardous synthetic route. The obtained polysiloxane-immobilized chiral catalysts are then investigated in their enantioselective separation efficiency as well as in their catalytic activity by on-column reaction chromatography experiments.

6.2. Results and Discussion

6.2.1. Synthesis of 1,3-Diketonato Camphor Ligands

Commercially available (1*S*)-camphorsulfonic acid **(64)** was converted to the corresponding potassium sulfonate **(71)**, which reacted with phosphorus pentabromide to the acid bromide **(72).** Elimination of sulfur dioxide yielded (1*S*)-10-bromocamphor **(73)**, which was converted into the corresponding acetate intermediate **(73)a** using potassium acetate in acetic acid. Alkaline saponification with potassium hydroxide in methanol yielded (1*R*)-10-hydroxycamphor **(74)**. An alternative preparation of **(74)** from *α*-pinene oxide in 72% yield[408] or in a three-step synthesis from 1-methylnorbornan-2-one via a regioselective tandem C=C double-bond addition/stereo-controlled Wagner-Meerwein rearrangement has been reported.[409] The treatment of camphorsulfonic acid **(64)** with thionyl chloride leaded to the corresponding sulfonic acid chloride **(65)**, which could be converted to camphorthiol **(75)** using triphenylphosphine. Following the modular spacer strategy described above, **(74)** and **(75)** were converted to ligands **(76), (77), (78)** and **(79)** bearing a terminal allyl function. This vinyl group is necessary for the Pt-catalyzed immobilization on HMPS. The acylation of ligands **(76)–(79)** with heptafluorobutanoyl chloride leaded to 1,3-diketonate camphor derivatives **(80),(81),(82)** and **(83)**. A strong and sterically demanding base (LDA) is required to selectively deprotonate the 3-position of **(80)-(83)**. Here, the high acidity of the proton in the α-position of the ketone has a markedly favorable effect on the deprotonation. Acyl chloride was added at low temperatures (-78 °C) to react with the obtained enolate to the 1,3-diketonates. As described in chapter 6.1.2., the yields of the acylation using LDA as a base were relatively low (only up to 35%). The formation of the very stable and hardly removable side products – perfluoro-*N,N*-diisopropylbutanamide **(84)**, *O*-acylcamphor derivative **(85)**, bisacylated camphor derivative **(86)**, and unreacted starting material – resulted in low yields (only up to 15%). The reagent quality turned out to be the most prominent factor influencing the reaction yield. Strictly anhydrous conditions proved to be crucial (anhydrous THF, anhydrous acylation reagent, LDA prepared freshly before each reaction).
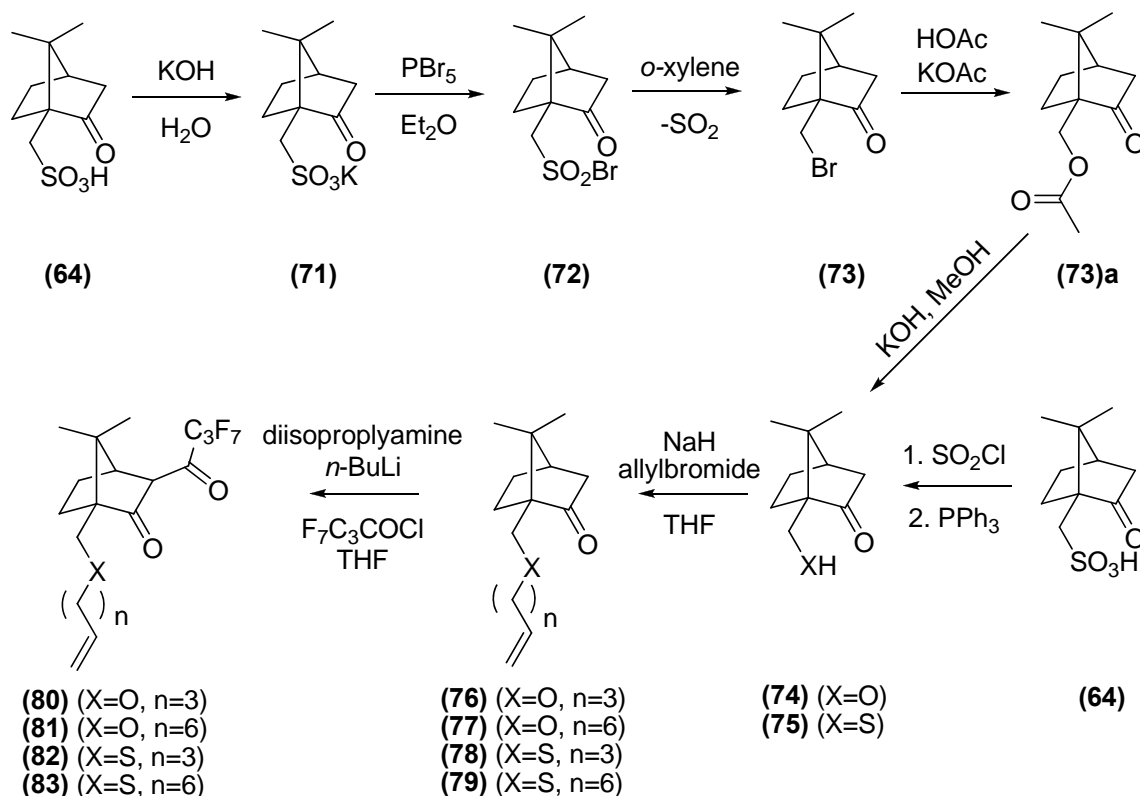
Figure 13. Synthetic route to chiral 1,3-diketonato camphor ligands (80)–(83).

The selectivity of the organolithium reaction and its possible multiple reaction pathways is shown in Scheme 41: (i) LDA substrate complexation leaded to perfluoro-N,N-diisopropylbutanamide **(84)** and starting material **(76)** (ii) the thermodynamically stable O-acyl derivate **(85)** was obtained at higher reaction temperatures and (iii) the bisacylated camphor derivative **(86)** was obtained at higher base concentrations. Therefore, the purification process of the obtained 1,3-diketonates was exceedingly difficult.[29, 335] Different separation methods as column chromatography, distillation, ion-exchanger as well as preparative GC or HPLC were used. The separation with column chromatography was not successful, as with this technique, the perfluoro-N,N-diisopropylbutanamide is inseparable from the product. To separate the amide from the desired camphor derivative, the crude mixture was distilled with a Kugelrohr apparatus. The obtained fractions were further purified with preparative GC to obtain 3-(heptafluorobutanoyl)-(1R)-10-(prop-2-enyloxy)-camphor **(80)** in 98% purity.
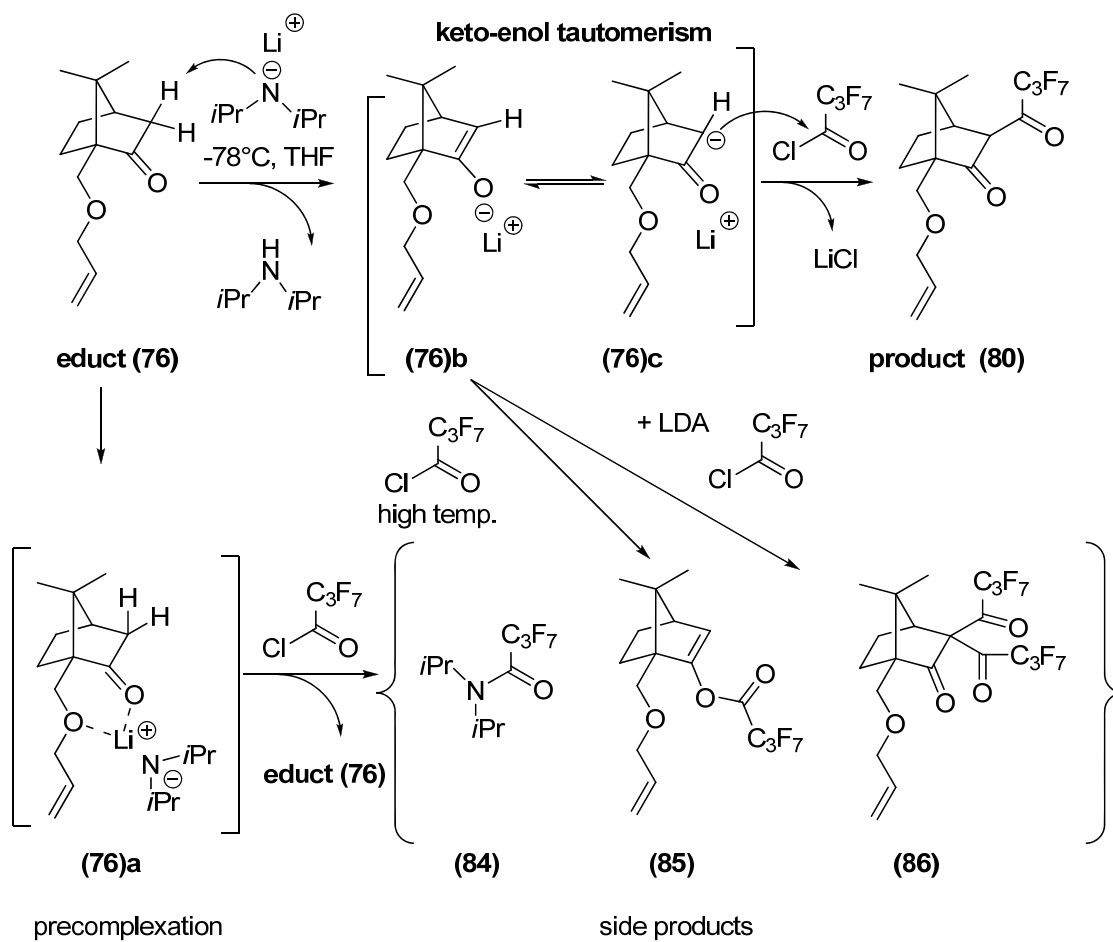
Scheme 41. Acylation of camphor derivative (76) with perfluorobutanoyl chloride including side-reactions leading to (84)-(86).

Ligand **(80)** was characterized with ^{1}H NMR, ^{13}C NMR, ^{19}F NMR, IR and HRMS measurements. The ^{1}H NMR spectra of the camphor ligand **(80)** is shown in Figure 14. The vinyl protons gave rise to the predicted ABX pattern and spin-spin coupling constants of the trans-, cis-, and gem-protons of the terminal vinyl group were detected to be J_{trans} = 17.3 Hz, J_{cis} = 10.4 Hz and J_{gem}= 17.2 Hz, respectively. The perfluoropropyl-group is a ten spin system of the type ABCX$_3$Y$_2$Z$_2$. ^{19}F NMR measurements reveal two CF$_2$ signals at 117–120 ppm and 126–127 ppm with multiplets assigned as CF$_2$ resonances, and one CF$_3$ signal at -80 ppm. Only weak perfluoropropyl-carbon-resonances from 118-108 ppm and perfluoropropyl-carbonyl-carbon-resonances at ~208 ppm could be obtained by ^{13}C NMR. To obtain stronger carbon resonances of the perfluoropropyl-group, it is necessary to use a ^{19}F noise decoupling technique (^{13}C(^{19}F)), which was not used in the present study due to the fact that the attachment of the perfluoropropyl-group could be verified by ^{19}F NMR.
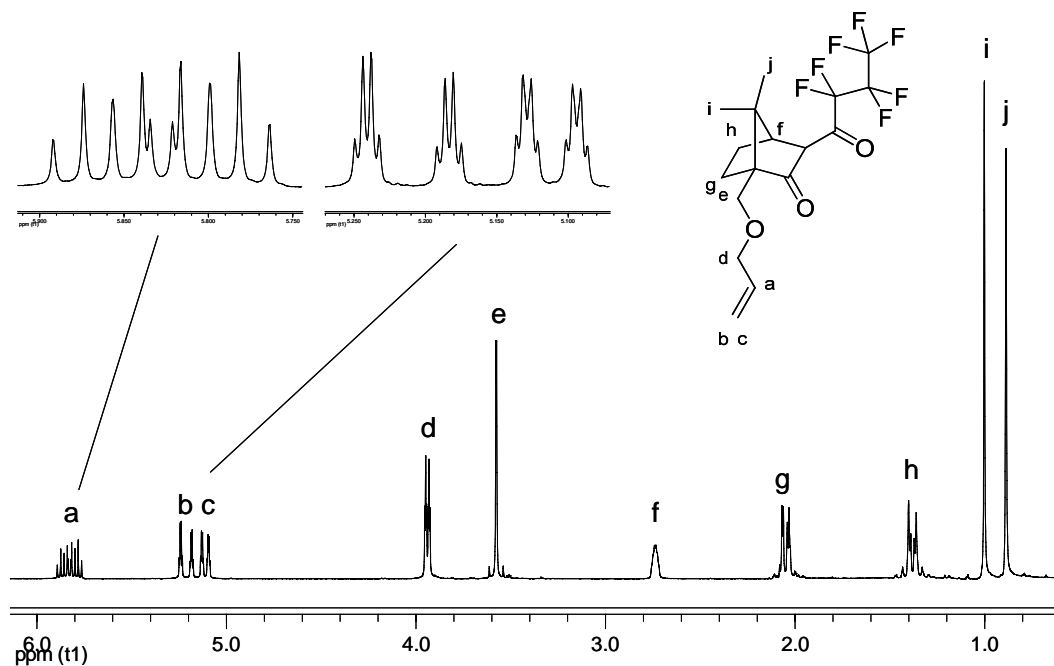
Figure 14. ^{1}H NMR spectra of the camphor ligand **(80)** (400.1 MHz, CDCl$_3$, δ = 6.2–0.5 ppm).

6.2.2. Synthesis of Modified HMPS Copolymers

HMPS **(4)** was synthesized by an acid-catalyzed thermic equilibration of hexamethyldisiloxane **(87)**, octamethyldisiloxane**(88)** and polyhydridomethylsiloxane **(89)** (Scheme 42).[169] Polymers with different molecular weight distributions (2840-3100 g mol^{-1}) and different total contents of statistically distributed Si(O)(CH$_3$)H groups (10.2-28.4%) could be synthesized depending on the educt stoichiometry. The total content of Si(O)(CH$_3$)H groups could be determined by integration of the signals of the ^{1}H NMR spectrum.
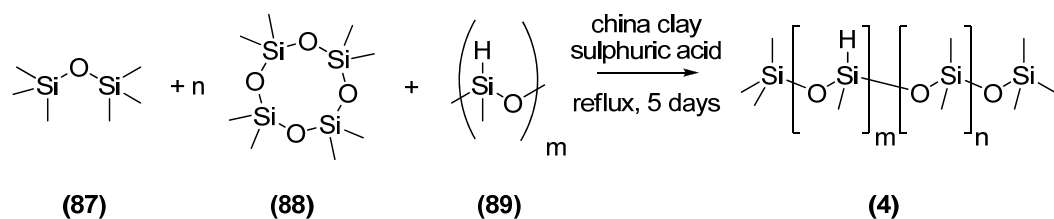
Scheme 42. Synthesis of modified HMPS (4).

6.2.3. Immobilization of 1,3-Diketonato Camphor Ligands on Modified Polysiloxanes

The immobilization of camphor ligands **(80)**–**(83)** was achieved by Pt-catalyzed hydrosilylation reaction of polysiloxane **(4)** (HMPS, 10.2–28.4% Si(O)(CH$_3$)H-groups) using H$_2$PtCl$_6$ **(57)** dissolved in anhydrous THF or 2-propanol (Speiers catalyst) or Karstedt's catalyst **(11)** in anhydrous toluene (Scheme 43).
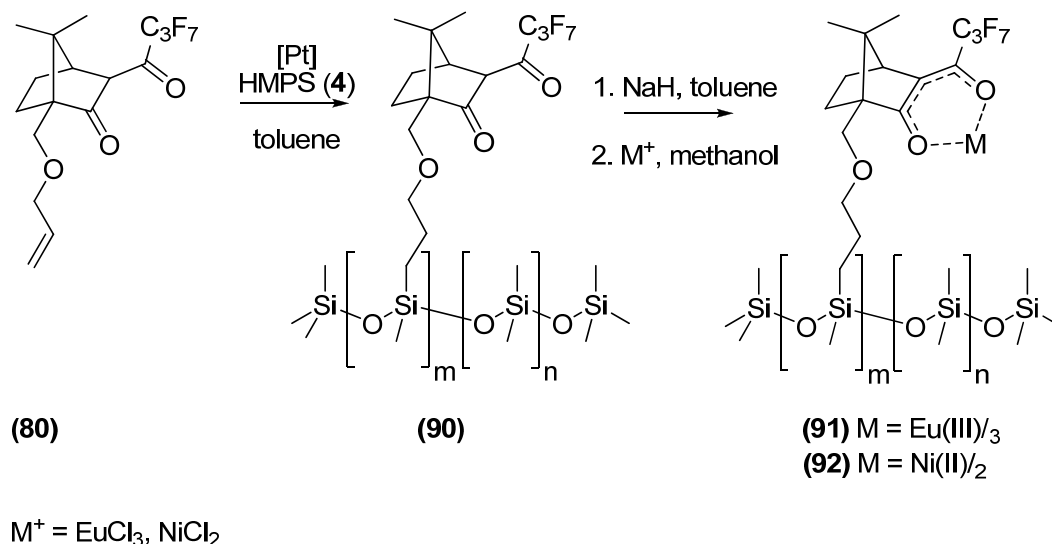
Scheme 43. Synthetic route to polysiloxane-supported metal 1,3-diketonato camphor complexes (91)–(92).

No colloidal Pt species were formed during the reaction with Karstedt's catalyst (**(11)**, 0.1 M solution in xylene). This catalyst **(11)** showed high activity towards the hydrosilylation of camphor ligands **(80)**–**(83)** and HMPS **(4)**. The reaction progress was monitored by ^{1}H NMR and FT-IR measurements after a reaction time of ~12 h at elevated temperatures. The complete covalent linkage between polysiloxane and ligand with no remaining Si-H functions was indicated by the disappearance of the silanic protons at 4.6 ppm in the ^{1}H NMR spectrum and the fading of the silane band (Si-H) at 2160 cm^{-1} in the FT-IR spectrum. In the case of an incomplete reaction, additional Pt catalyst (50% of the original volume) was added to the reaction solution and allowed to proceed for another ~12 h. The reaction conditions were varied depending on the starting materials: reaction times were typically between 12 h and 72 h under an argon atmosphere and reaction temperatures from room temperature (using ultrasonication) to 125 °C. The polymers could be purified with a short chromatography column. [3-(heptafluorobutanoyl)-(1*S*)-10-propoxy-camphorate]-PDMS **(90)** was obtained as

a slightly colored, viscous polymer. Purifications through precipitation in methanol or centrifugation with methanol as described by Keller[29, 335] were not performed, as lower molecular weight polysiloxanes (2840–3100 g mol^{-1}) used herein showed a lower tendency to precipitate in methanol. After the purification step, the modified polysiloxanes were dried under high vacuum at elevated temperature. The obtained polymers were soluble in many organic solvents like THF, toluene and chloroform. The successful immobilization of the 1,3-diketonates was verified with ^{1}H and ^{19}F NMR as well as EI-MS and ESI-MS. The ^{1}H NMR spectra of ligand **(80)**, HMPS **(4)** and PS-supported ligand **(90)** showed the completion of the reaction with the disappearance of the Si-H signal at 4.6 ppm and the terminal vinyl group signal at 5.7 ppm and 5.1 ppm (Figure 15).
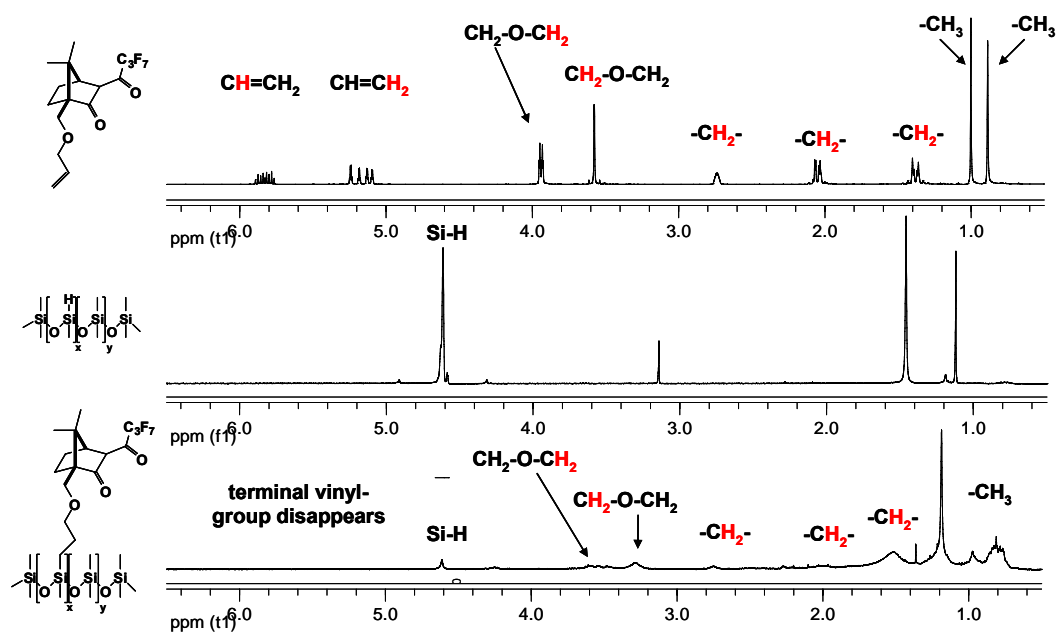
Figure 15. ^{1}**H NMR spectra of the camphor ligand (80), HMPS (4) and the polysiloxane-supported camphor ligand (90) (400.1 MHz, CDCl$_3$, δ = 6.5–0.5 ppm).**

The degree of substitution could be determined from the ^{1}H NMR spectra. These measurements confirmed that the amount of Si(O)(CH$_3$)H groups decreased to 2.1% (starting from 25.8% in HMPS **(4)**). Another possibility to detect the ligand loading is ^{19}F NMR measurements (Figure 16). Both ^{19}F NMR spectra of ligand **(80)** and polysiloxane-supported ligand **(90)** showed a CF$_3$ signal at -80 ppm, a CF$_2$ signal at 117–120 ppm, and a CF$_2$-CO-signal at 126–127 ppm.
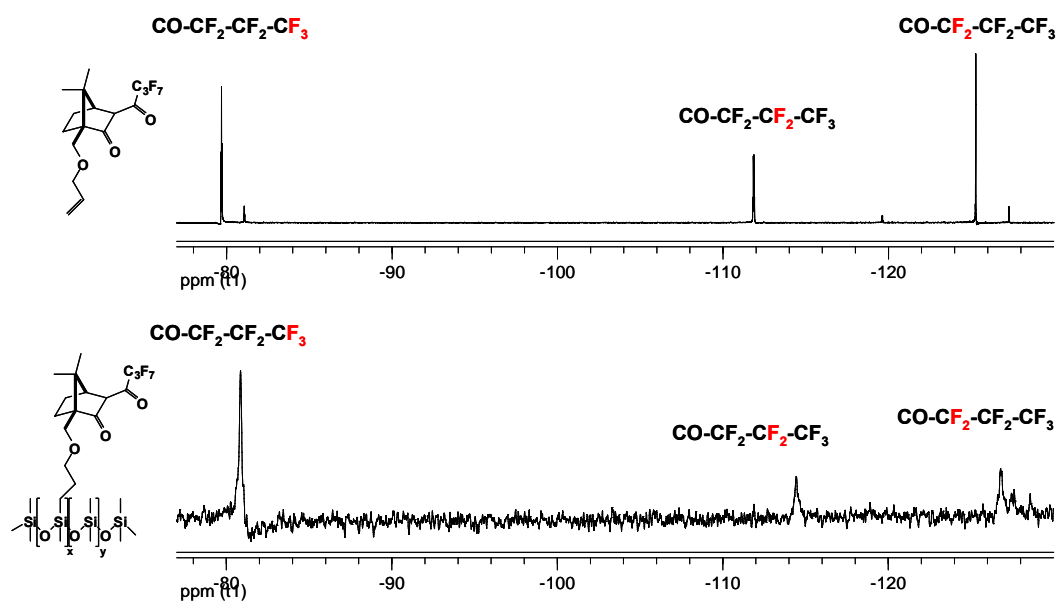
Figure 16. ^{19}**F NMR spectra of the camphor ligand (80) and the polysiloxane-supported camphor ligand (90) (300.1 MHz, CDCl$_3$, δ = -75– -130 ppm).**

The positive-ion ESI spectrum of [3-(heptafluorobutanoyl)-(1*S*)-10-propoxy-camphorate]-PDMS **(90)** showed its molecular weight distribution with peaks apparent in the range between *m/z* 170 and 1365 [M$^+$], centered around *m/z* 860. Figure 17 shows an enlarged spectrum ranging from *m/z* 600 to 1100. The *m/z* values of the more intense peaks are considered to reflect differences in the number of methylpolyoxypropylsiloxane units. Also in this spectrum, the intense peaks show a regular difference of 74 Da.
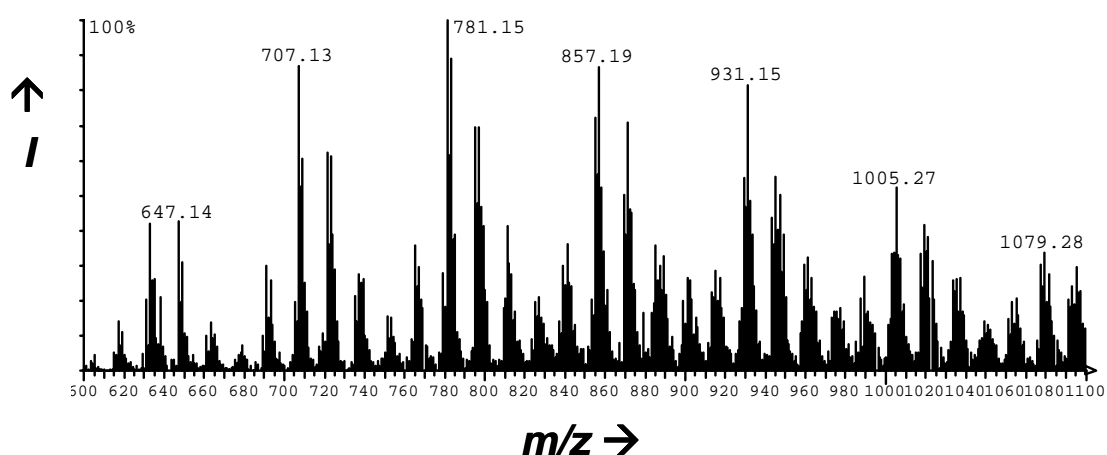
Figure 17. Enlarged positive-ion ESI spectrum of polysiloxane-supported [3-(HFB)-(1*S*)-10-propoxy-camphorate] (90) (solvent: CH$_2$Cl$_2$, *m/z*: 600–1100).

6.2.4. Metalation of Immobilized 1,3-Diketonates

Stable metal chelates of 3-acylcamphor compounds are known since 1894.[338, 410-413] Because of the electron-withdrawing properties of heptafluorobutanoyl-group, stable 1,3-diketonato metal chelates can be obtained. For chelate formation of the sodium or barium salts[341] of the acetylcamphor, the derivatives are treated with metal salts in methanolic solution. Additionally, the immobilized camphor derivative **(90)** can be transformed into the corresponding enolate under basic conditions and into the corresponding metal chelates europium(III)-tris[3-(heptafluorobutanoyl)-(1*S*)-10-propoxycamphorate]-PDMS (Chirasil-Eu(III)-Propoxy-Camphor, **(91))** and nickel(II)-bis[3-(heptafluorobutanoyl)-(1*S*)-10-propoxy-camphorate]-PDMS (Chirasil-Ni(II)-Propoxy-Camphor, **(92))** by adding metal salts (EuCl$_3$, NiCl$_2$,) dissolved in methanol. Bivalent metal cations lead to a linear polymer complex with two metal atoms sharing two oxygen atoms in a bridged structure, whereas tri- or multivalent metal cations lead to three-dimensional cross-linked complexes. Similar to the positive-ion ESI spectrum of polysiloxane **(90)**, the main peaks in the positive-ion ESI spectrum of Chirasil-Eu(III)-Propoxy-Camphor **(91)** were centered around 930 ranging from *m/z* 500-1700 with the most intensive peak at 708. Again, the peaks showed a regular difference of 74 Da (one DMS unit) as pointed out in the enlarged positive ion ESI spectrum from *m/z* 550-2000 (Figure 18). A low signal-to-noise ratio did not allow the detection of europium isotope effects.
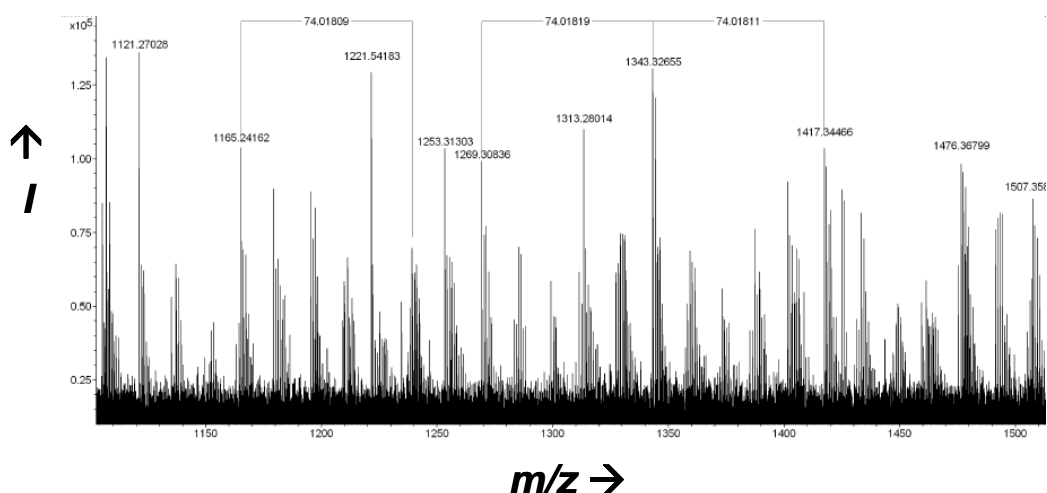
Figure 18. Enlarged positive-ion ESI spectrum of Chirasil-Eu(III)-Propoxy-Camphor (91)
(solvent: CH$_2$Cl$_2$, *m/z*: 1100–1600).

6.2.5. Coating of Microcapillaries

The catalytically active micro columns were prepared by dissolving **(91)** or **(92)** in absolute diethyl ether and coating untreated 25 m long microcapillaries dynamically with a film thickness of 250 nm using static methods described by Grob.[315] Afterwards, the columns were dried in a stream of nitrogen and then conditioned at 90 °C for 3 h. Furthermore, a reference column was coated with octamethylen-permethyl-ß-cyclodextrin-PDMS (Chirasil-β-Dex **(13)**)[169, 333, 334].

6.2.6. Separation Efficiency of Chirasil-Metal-Propoxy-Camphor as Chiral Stationary Phase

The separation efficiency of the novel stationary phase was tested by injecting a doped mixture of menthone racemates ((+)-menthone **(93)a** and (-)-menthone **(93)b**) and diastereomers of the two enantiomeric pairs of Z- and *E*-2-ethyl-dioxaspiro[4,4]nonane chalcogran **(94)**. The menthone enantiomers could be separated running a temperature program (50–180 °C @ 4 K min^{-1} with a inlet pressure of 80 kPa, Figure 19).
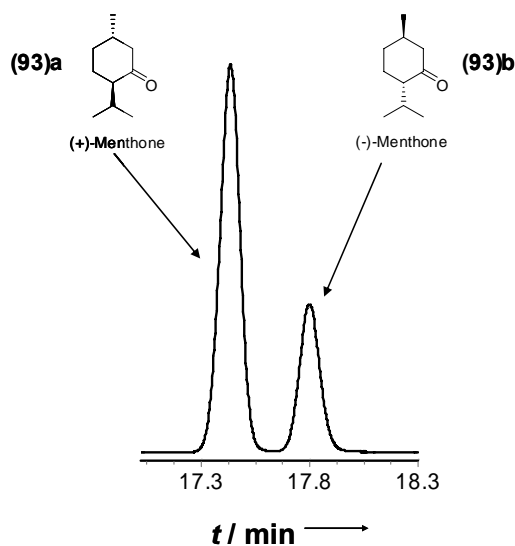
Figure 19. Separation of menthone enantiomers (93)a and (93)b by complexation GC on Chirasil-Eu(III)-Propoxy-Camphor (91) at 50–180 °C @ 4 K min^{-1}. Column: 25 m x 250 µm i.d., fused-silica capillary, 500 nm film thickness, He was used as carrier gas, inlet pressure: 80 kPa.

As described by Jiang and Schurig,[361] the GC enantiorecognition of the two enantiomeric pairs of *Z*- and *E*-chalcogran **(94)a-d**, respectively, critically depends on whether the chiral selector Ni(II)-bis[3-(heptafluorobutanoyl)-(1*R*)-camphorate] **(50)** is chemically linked via a methylene spacer to PDMS (Chirasil-Nickel **(53)**), or is only dissolved in PDMS (Chira-Nickel). Using Chirasil-β-Dex **(13)**[169] as CSP, the four stereoisomers of **(94)a-d** could be separated by enantioselective GC. The elution order of **(94)a-d** on **(13)** was (2*R*,5*S*)-**(94)a**, (2*R*,5*R*)-**(94)b**, (2*S*,5*S*)-**(94)c**, and (2*S*,5*R*)-**(94)d,** which could be determined by co-injection of enantiomerically enriched (2*S*,5*RS*)-**(94)c/d**. To evaluate the separation efficiency of the prepared columns coated with Chirasil-β-Dex **(13)**, Chirasil-Ni(II)-Propoxy-Camphor **(92)** and Chirasil-Eu(III)-Propoxy-Camphor **(91),** a mixture of both *Z*- and *E*-chalcogran **(94)a-d** was injected. Because the polymers **(91)** and **(92)** were coated without an achiral matrix (PDMS), the concept of the retention-increment[343, 352] was not applied. The four stereoisomers of **(94)a-d** could be separated by enantioselective GC on Chirasil-β-Dex **(13)** as shown in Figure 20. Chalcogran **(94)a-d** shows typical interconversion plateaus between the epimers (2*R*,5*S*)-**(94)a**/(2*R*,5*R*)-**(94)b** and (2*S*,5*S*)-**(94)a**/(2*S*,5*R*)-**(94)b** between 60–120 °C. It can be concluded that the epimerization process takes only place at the spiro center (C5). The temperature-dependent GC measurement of both *Z*- and *E*-chalcogran **(94)** on Chirasil-Ni(II)-Propoxy-Camphor **(92)** is depicted in Figure 21.
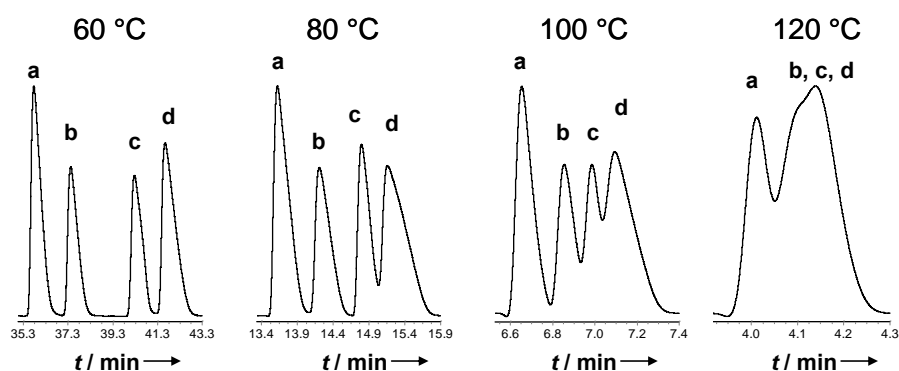
Figure 20. Separation of enantiomers of chalcogran (94) by complexation GC between 60–120 °C on Chirasil-β-Dex (13). Column: 25 m×250 μm i.d., 250 nm film thickness, fused-silica capillary; He was used as carrier gas, inlet pressure: 100 kPa, a= *Z*-(2*S*,5*S*)-chalcogran (94)a, b= *Z*-(2*R*,5*R*)-chalcogran (94)b, c= *E*-(2*R*,5*S*)-chalcogran (94)c, d= *E*-(2*S*,5*R*)-chalcogran (94)d.

The four stereoisomers of **(94)a-d** could not be separated by using Chirasil-Ni(II)-Propoxy-Camphor **(92)** (Figure 21).
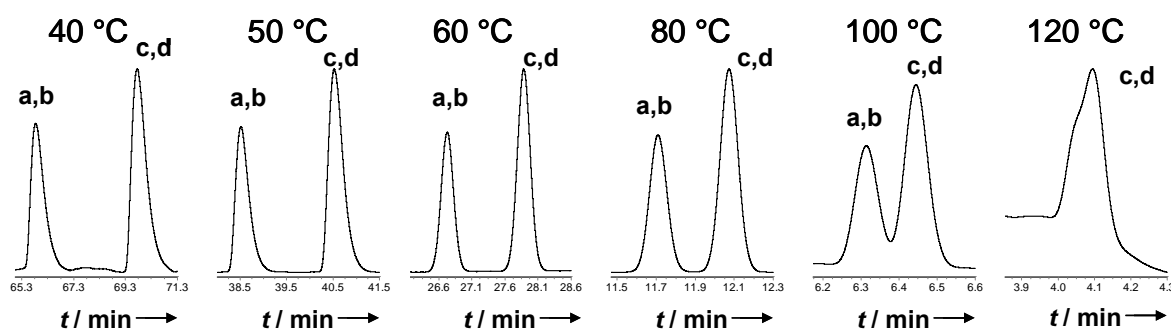
Figure 21. GC separation of chalcogran epimers (94) on Chirasil-Ni(II)-Propoxy-Camphor (92) between 40–120 °C, Column: 25 m×250 µm i.d., 250 nm film thickness, fused-silica capillary, He was used as carrier gas, inlet pressure: 100 kPa.

Only low chiral separation of the enantiomers was observed with Chirasil-Eu(III)-Propoxy-Camphor **(91)** as stationary phase at temperatures between 40–60 °C (Figure 22).
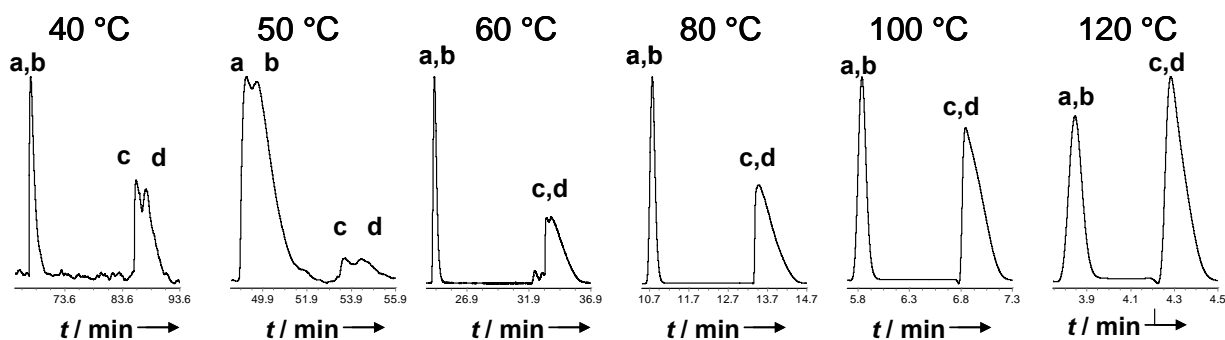
Figure 22. GC separation of chalcogran epimers (94) on Chirasil-Eu(III)-Propoxy-Camphor (91) between 40–120 °C. Column: 25 m×250 µm i.d., 250 nm film thickness, fused-silica capillary, He was used as carrier gas, inlet pressure: 100 kPa.

The low enantiomeric separation efficiency for all four stereoisomers may be attributed to the low chiral selector loading **(80)**. On the other hand, the menthone racemates (+)-**(93)a** and (-)-**(93)b** could be successful immobilized. In general, the separation efficiency highly depends on the purity of the used stationary phase and the quality of the capillary coating.

6.2.7. Catalytic Studies by On-Column Reaction Chromatography

A suitable test-system for the catalytically activity and enantioselectivity of the polysiloxane-supported Lewis acid derivative Chirasil-Eu(III)-Propoxy-Camphor **(91)** is the intramolecular

Diels-Alder reaction of furfurylfumarate derivatives. Furfurylfumarate derivatives were synthesized by the Schotten-Baumann reaction of furfuryl alcohol **(95)** and the corresponding acyl chlorides **(96)**, **(97)** and **(98)** to obtain derivatives **(99)**, **(100)** and **(101)** (Scheme 44).

(95)	**(96)** R_1 = H, R_2 = H	**(99)** R_1 = H, R_2 = H
	(97) R_1 = CH$_3$, R_2 = CH$_3$	**(100)** R_1 = CH$_3$, R_2 = CH$_3$
	(98) R_1 = H, R_2 = CO$_2$Et	**(101)** R_1 = H, R_2 = CO$_2$Et
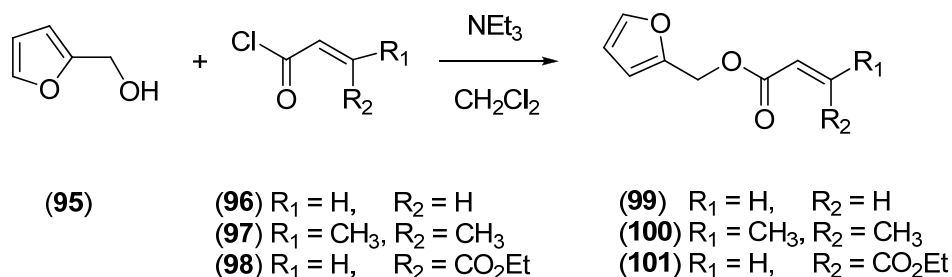
Scheme 44. Synthesis of 2-furanyl-methylacrylate derivatives (99)-(101).

On-column catalysis was performed by using a 25 m long microcapillary coated with the polymeric Lewis acid catalyst **(91)** facilitating the advantage of precise temperature control. Helium was used as carrier gas. Starting materials and products were quantified by FID and identified by MS. The 2-furanyl-methylacrylate derivatives **(99)-(101)** were injected onto this column to investigate the catalytic activity of the polymer-bound catalyst. Intramolecular Diels-Alder reaction leading to almost complete conversion (> 95%) of starting material **(99)** to 7-oxabicyclo[2.2.1]hept-2-ene **(102)a/b** were observed in on-column reaction chromatography experiments (Figure 23) without detection of any side-products. Nevertheless, the separation efficiency of the stationary phase did not allow the separation of enantiomers **(102)a** and **(102)b** due to poor selectivity of the immobilized camphor derivate towards the 7-oxabicyclo[2.2.1]hept-2-ene derivatives. Although, the two enantiomers could be separated using Chirasil-β-Dex **(13)** as CSP, the combination of catalytic activity and separation selectivity in a single chromatographic stationary phase was not fulfilled. On the other hand, the catalytic effect of the polymeric Lewis acid catalyst **(91)** on the Diels-Alder reaction broadens the applicability of on-column reaction chromatography studies and is part of ongoing investigations.
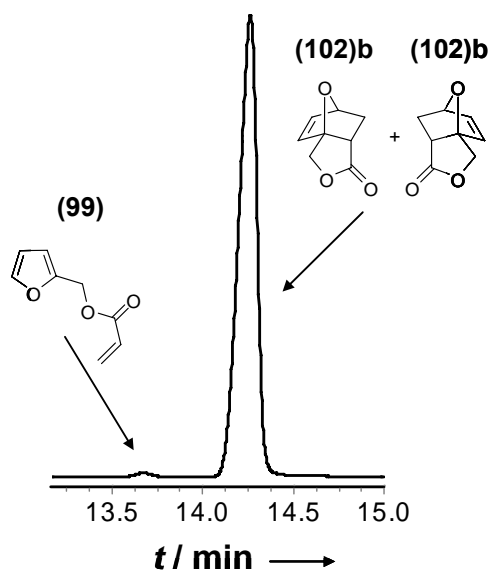
Figure 23. On-column reaction chromatography of furfurylfumarate (99) to 7-oxabicyclo[2.2.1]hept-2-ene (102)a/b at 50–180 °C @ 4 K min^{-1}. Column: 25 m×250 μm i.d., fused-silica capillary, He was used as carrier gas, inlet pressure: 80 kPa.

6.3. Conclusion

The synthetic applicability of polysiloxane-supported chiral camphor-based transition metal catalysts with a modular, flexible linker system and their separation selectivity and catalytic activity could be demonstrated. The synthetic strategy featuring the attachment of alkane spacers on the C10 position of (1*R*)-10-hydroxycamphor ligands or the (1*S*)-10-camphorthiol ligands via an ether or thioether functionality facilitates the control of the distance between the catalytically active center and the support. With this method, novel polysiloxane-immobilized Lewis acid catalysts could be successfully prepared and the ligand immobilization could be verified by NMR and MS measurements. The chiral separation selectivity of these modified polysiloxanes was tested showing good selectivity towards menthone racemates but only poor selectivity towards the epimers of chalcogran. Catalytic activity was obtained for intramolecular Diels-Alder reactions of furfuryl derivatives on a 25 m microcapillary with conversions > 95%. The chiral selectivity of the Lewis-acid catalysts coated onto the capillary did not allow separating of the formed enantiomers. In general, complexation chromatography and on-column reaction chromatography surpass other method since educt purification and derivatization are unnecessary and only a small sample size is required.

Chapter 7

Synthesis of Polysiloxane-Supported Chiral Salen-Complexes

7. Synthesis of Polysiloxane-Supported Chiral Salen-Complexes

7.1. Introduction

The covalent attachment of homogeneous catalysts to soluble and insoluble polymer supports has been widely studied to overcome the problem of catalyst separation in homogeneous catalysis.[15] This strategy combines advantages of both heterogeneous and homogeneous catalysis, namely the improvement of catalyst separation and recycling and the application of the immobilized catalyst in continuous flow processes. Ideally, the investigation of immobilized catalysts by parallelized ht kinetic measurements can provide insights into the catalytic mechanism and identify rate-determining elementary steps in order to develop theoretical models. Therefore, comprehensive experimental kinetic data of a broad variety of substrates are necessary. Chiral, salen-based catalysts are attractive candidates for immobilization, because of their high reactivity, selectivity and recyclability shown for enantioselective epoxidations,[414] enantioselective ring-opening of *meso* epoxides[415] and kinetic resolution of terminal epoxides.[416]

7.1.1. Chiral Salen-Based Metal Complexes

Epoxides are arguably one of the most important building blocks in organic synthesis as the ring opening of epoxides permits straightforward elaboration to useful new functionality including new carbon-carbon bonds.[417] Furthermore, strained three-membered ring units are found in a number of natural products.[418-420] The discovery of titanium-tartrate-catalyzed asymmetric epoxidation reactions by the group of Sharpless provided general access to highly enantioenriched epoxyalcohols and arguably had the a profound impact on asymmetric catalysis.[421-423] Sharpless achievements were honored with the Nobel Prize in Chemistry together with William S. Knowles and Ryorji Noyori, "for their work on chirally catalyzed hydrogenation reactions" in 2001. The epoxidation of unfunctionalized conjugated olefins by manganese salen ligands, developed independently by the groups of Jacobsen[424, 425] and Katsuki[426] in the 1990s, has enabled the practical synthesis of certain classes of enantiomerically enriched epoxides. Both transformations involve the generation of new sp^3 stereocenters from prochiral sp^2-hybridized precursors. Even though stereospecific

substitution reactions of sp³-hybridized substrates seem to represent a less straightforward target for asymmetric catalysis, this type of transformation can be applied in two important contexts: the desymmetrization of meso substrates and the hydrolytic kinetic resolution (HKR) of racemic compounds. As mentioned above, the Co-salen-complex (*R,R*)-**(103)b** and Mn-salen-complex (*R,R*)-**(103)d**, derived from chiral salen ligand (*R,R*)-**(103)a**, was successfully used in enantioselective epoxidation reactions and the HKR of terminal epoxides showing high activities and enantioselectivities in both reactions (Scheme 45).

(*R,R*)-**(103)a**: X, Y = *t*-Bu, M = H, H
(*R,R*)-**(103)b**: X, Y = *t*-Bu, M = Co
(*R,R*)-**(103)c**: X, Y = *t*-Bu, M = Co(OAc)
(*R,R*)-**(103)d**: X, Y = *t*-Bu, M = Mn
(*R,R*)-**(103)e**: X = OH, Y = *t*-Bu, M = H, H
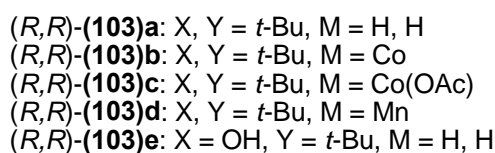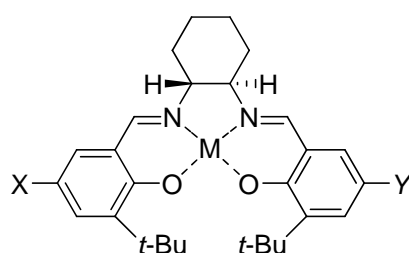
Scheme 45. Chiral salen ligands and complexes (103)a-e.

7.1.2. Immobilization of Salen-Complexes

Supported salen catalysts can be roughly classified into three categories based on their synthetic design, which are: (i) symmetrical salen ligands functionalized with monomeric units, (ii) symmetrical salen ligands incorporated into the polymer main chain through condensation of diamine and aldehyde salen precursors, and (iii) unsymmetrical salen ligands attached to resins, dendrimers, or linear polymers.[24] A detailed understanding of the catalytic behavior of salen-based transition metal catalysts, following either a monometallic or a bimetallic reaction mechanism, allows the design of tailor-made supported catalysts. These catalysts facilitate not only good recyclability, but also show higher activity and selectivity than their nonsupported counterparts. One of the first synthetic protocols for the immobilization of Co-salen-complex (*R,R*)-**(103)b** was developed by Jacobsen and Annis.[35, 427] They used a modified hydroxymethylpolystyrene resin **(104)a** to immobilize an unsymmetrically substituted salen ligand such as (*R,R*)-**(103)e** to obtain the polymer-bound chiral Co-salen-complex (*R,R*)-**(104)b** (Scheme 46). Furthermore, ligand (*R,R*)-**(103)e** could

be successfully immobilized on silica beads to give catalyst (R,R)-**(104)c**. These two solid-supported chiral Co-salen-complexes (R,R)-**(104)b/c** proved to be particularly advantageous in the HKR of epichlorohydrins and epoxyalcohols showing high yields and high ee values and facilitated product purification, catalyst recycling, and adaptation to continuous flow methodologies.

(104)a   **(104)b**

= 90 µm Hydroxymethylpolystyrene
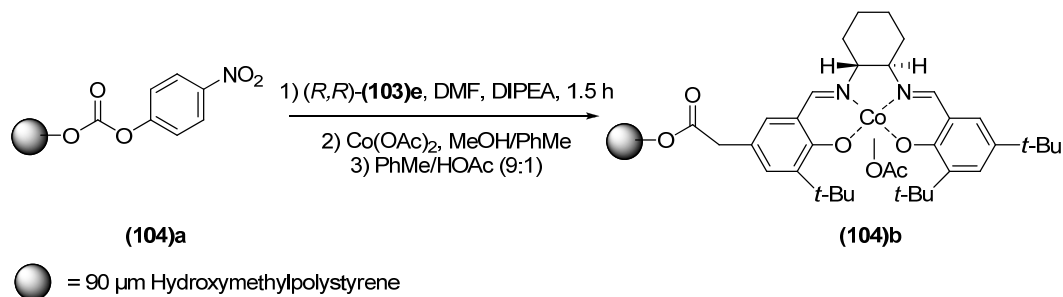
Scheme 46. Polystyrene-bound chiral Co-salen-complex (104)b.

Weck et al.[428] reported a synthetic approach to polystyrene-supported chiral salen ligands (R,R)-**(105)b** by the free radical polymerization of an unsymmetrical styryl-substituted salen monomer (H$_2$salen=bis(salicylidene)ethylenediamine (R,R)-**(105)a**). Remarkably, the copolymer-supported Co-salen-complex (R,R)-**(105)b** showed a better catalytic performance (> 99% ee, 54% conversion, 1 h) compared to the homopolymeric analogue (R,R)-**(105)c** and the monomeric Co-salen-complex (R,R)-**(103)b**. The soluble poly(styrene)-supported catalyst (R,R)-**(105)b** was recovered by precipitation after the catalytic reactions and was recycled three times without apparent loss of selectivity and slightly reduced reaction rates. Additionally, the immobilization of the chiral salen-complex (R,R)-**(103)a** and (R,R)-**(103)b** on several other organic[429-437] and inorganic supports[438] has been reported. Developments in supported metal-salen-complexes have recently been reviewed.[24, 439] In particular, applications of metal-salen catalysts in continuous-flow processes[35, 41] are of great interest for ht screening approaches.

So far, only few polysiloxane-embedded and -supported salen-complexes were reported. In 1996, Vankelecom et al.[363] occluded N,N-bis(3,5-di-tert-butyl-salicylidene)chloro-1,2-cyclohexanediaminemangan catalyst (R,R)-**(106)** in an elastomeric type PDMS membranes, which were tested in the enantioselective epoxidation of olefins and could be regenerated by a

simple washing procedure. The authors did not detect any significant differences to the homogeneous catalysts concerning activity, product selectivity, and enantiomeric selectivity.

(107)
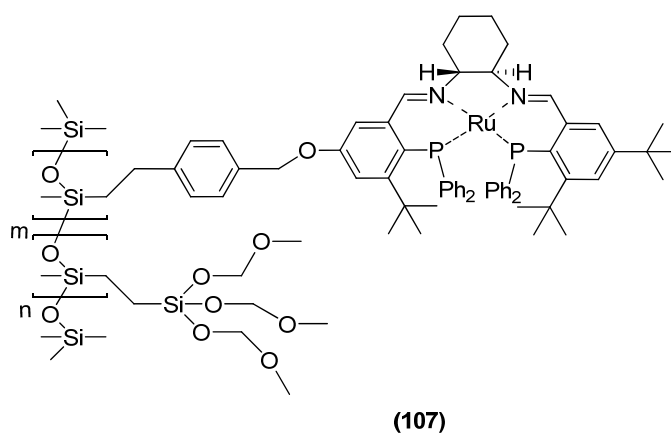
Figure 24. Polysiloxane-immobilized chiral salen ruthenium catalysts.

Laue et al.[440] reported the preparation of chiral salen ruthenium catalysts (R,R)-**(107)** tethered to polysiloxanes (Figure 24). They were also used in continuously operated membrane reactors using ultra or nanofiltration techniques. A molecular weight of $22\,\mathrm{kg\,mol^{-1}}$ and a metal loading of $0.3\,\mathrm{mmol\,g^{-1}}$ turned out to be the best obtainable parameters, yielding up to 97% ee in the hydrogen transfer reduction of acetophenone in *i*PrOH

7.1.3. Hydrolytic Kinetic Resolution of Terminal Epoxides Catalyzed by Co(III)-Salen-Complexes

A wide variety of asymmetric reactions such as epoxide kinetic resolutions, epoxidations, hetero-Diels-Alder reactions, and conjugate additions have been catalyzed by metal-salen-complexes. In particular, the HKR of readily available and inexpensive epoxide racemates catalyzed by Co(III)-salen-complexes (R,R)-**(103)c** represents a powerful approach to the preparation of enantioenriched terminal epoxides and found widespread use in both academic and industrial applications (Scheme 47). [441-444] As this solventless process generates no waste, it is an extreme example of "atom economy" using low catalyst loadings (0.0001 mol% Co), starting out with 1 eq. of racemic epoxide **(108)a/b** to 0.55 eq. of water, and yielding approximately 0.5 eq. of enantiopure epoxide **(108)a** together with about 0.5 eq. of nearly enantiopure diol **(108)c**.
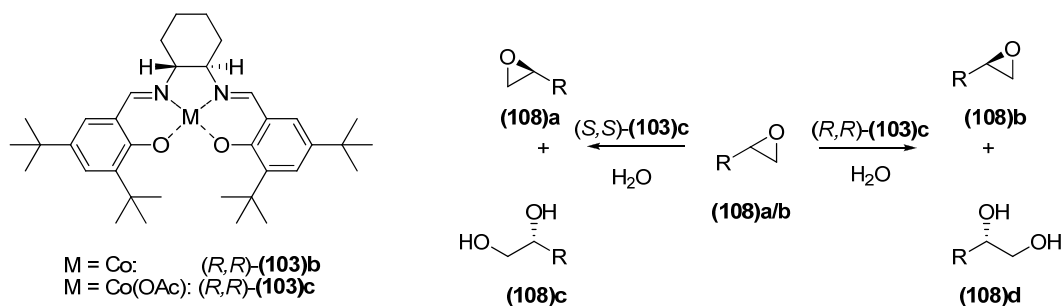
Scheme 47. HKR of epoxide racemates catalyzed by Co(III)-salen-complexes.

As pointed out by Nielsen et al.,[445] paradoxically, the metal-catalyzed HKR "has not received the level of green attention - either scientific or semantic - that has been devoted to the environmentally and economically unproven organocatalytic reactions carried out in the presence of water."
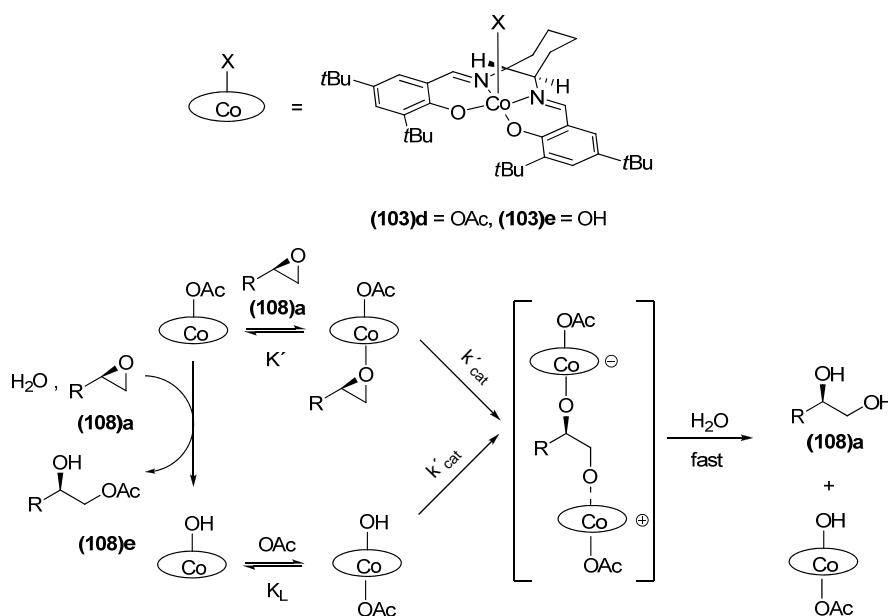
Scheme 48. Dominant bimetallic catalytic cycle in HKR reactions by Nielsen et al.[445]

Kinetic studies on the HKR indicate a second-order dependence on Co(III)-catalyst (R,R)-**(103)c**, which supports a cooperative bimetallic catalytic mechanism with a head-to-tail arrangement corresponding to rotation of one of the salen units by 180° (Scheme 48).[445-447] According to these findings, the dimerization,[446-448] oligomerization,[446, 447, 449] dendrimerization,[450] and polymerization[35, 451-453] of Co-salen ligand (R,R)-**(103)b** leads to catalytic systems with similar enantioselectivity and substantially enhanced reactivity relative

to the monomeric species. Furthermore, the covalent immobilization of Co-salen ligand (*R*,*R*)-**(103)b** on organic[35, 454] and inorganic support[35, 454-456] simplifies the separation of the catalyst from by-products and reaction products, the catalysts recycling, as well as the possible application of the immobilized catalyst in continuous-flow processes.[35, 454] A high ligand-loading support may be beneficial to the reactivity because of the assumed cooperative bimetallic catalytic mechanism in the HKR of terminal epoxides.

7.1.4. Objectives

The immobilization of Co-salen ligands on polysiloxanes has not been described so far. Herein, the synthesis of polysiloxane-immobilized chiral Co-salen-complexes with variable spacer length is reported. The development of a straightforward immobilization method of monofunctionalized enantiopure unsymmetrical salen ligands by an ether linkage is targeted. These covalently immobilized Co(III)-salen-OAc catalysts might be beneficial in the HKR of terminal epoxides due to the assumed cooperative bimetallic catalytic mechanism.

7.2. Results and Discussion

The Co-salen-complex (*R,R*)-**(103)b** has been demonstrated to be a highly efficient and enantioselective catalyst for the HKR of terminal epoxides. Jacobsen and Annis[427] could show that the immobilization through the 3-substituent of the salicaldehyde has no adverse effect of the enantioselectivity of the asymmetric ring opening of terminal epoxides. Therefore, the synthesis and immobilization of unsymmetrical salen ligands through the flexible linker strategy (Scheme 37, chapter 6) was chosen.

7.2.1. Synthesis of Unsymmetrical Salen Ligands

The Williamson ether synthesis of 2-*tert*-butyl hydroquinone **(109)** and allylbromides with different chain length (3-bromoprop-1-ene **(110)a,** 6-bromohex-1-ene **(110)b** or 8-bromooct-1-ene **(110)c**) affords the corresponding ethers **(111)a-c**. Using 1 eq. of the corresponding allybromide, the ether synthesis yields a mixture of the desired ethers **(111)a-c** and only minor amounts of undesired disubstituted products (< 15%). Compounds **(111)a-c** were subsequently formylated using paraformaldehyde **(112)**, tin tetrachloride **(113)** and 2,6-lutidine **(114)** to obtain the corresponding salicaldehyde derivatives **(115)a-c** (Scheme 49).
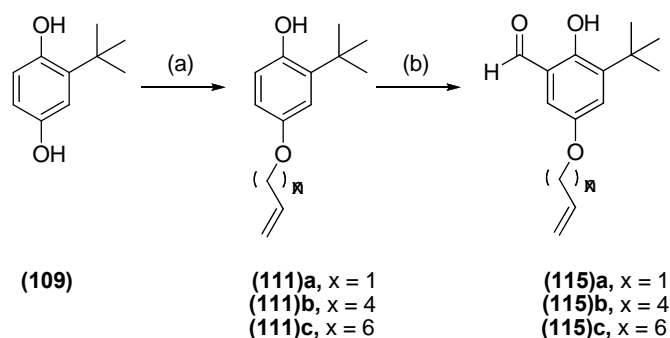
Scheme 49. Synthesis of salicaldehyde derivatives. Reagents: (a) 1.0 eq. 3-bromoprop-1-ene (110)a,
6-bromohex-1-ene (110)b or 8-bromooct-1-ene (110)c, sodium hydride, THF, 60 °C, 5 h
(b) 4 eq. paraformaldehyde(112), 0.3 eq. SnCl₄ (113), 1.2 eq. 2,6-lutidine (114), toluene, 90 °C, 6 h.

The synthesis of the unsymmetrically substituted salen ligands **(116)a-c** by utilization of an excess of di-*tert*-butyl salicaldehyde **(117)** (3 eq.) relative to salicaldehyde derivatives **(115)a-c** (1 eq.) and (*R,R*)-1,2-diammoniumcyclohexane mono-(+)-tartrate salt **(118)** (2 eq.)

yields a statistical 9:6:1 ratio of salen ligand (*R,R*)-**(103)a** to vinyl-terminated ligands (*R,R*)-**(116)a-c** to the disubstituted ligand (*R,R*)-**(116)d-f** (Scheme 50).
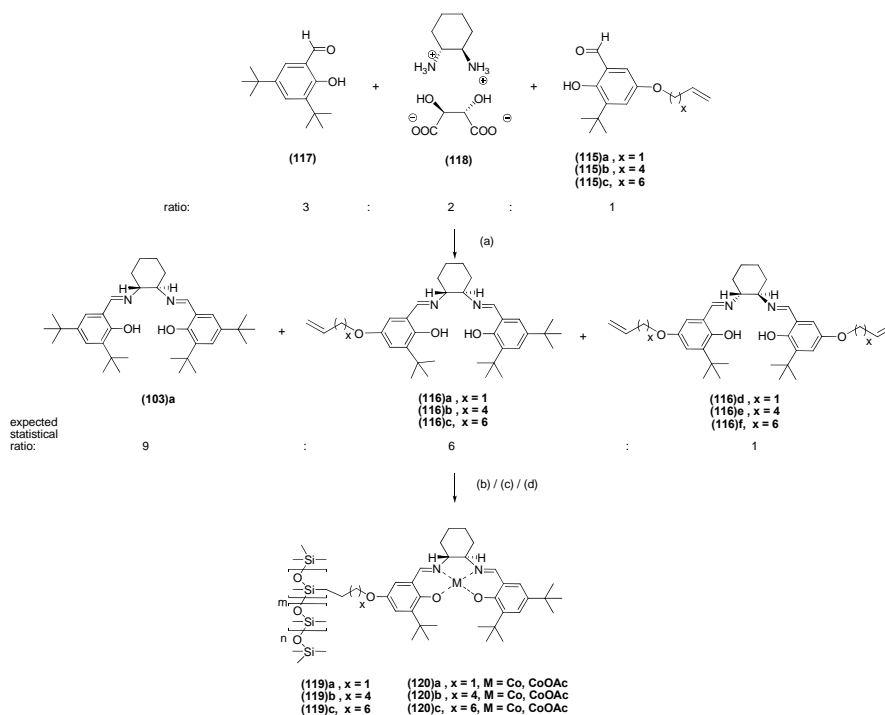
Scheme 50. Synthesis route to polysiloxane-supported chiral Co-salen-complexes.
Reagents: (a) ethanol/H$_2$O, K$_2$CO$_3$, 2 h, reflux, (b) HMPS (4), H$_2$PtCl$_6$ (57) or Karstedt's catalyst (11),
toluene:THF, ultrasonication, 3 days (c) Co(OAc)$_2$·4 H$_2$O, toluene, 2 h, reflux. (d) HOAc, toluene.

Since the condensations of the two amino groups should proceed with comparable rates, the reaction yields the desired unsymmetrical salen (*R,R*)-**(116)a-c** and two undesired symmetrical salens (*R,R*)-**(103)a** and (*R,R*)-**(116)d-f**. Table 5 shows the ratio of the obtained salen ligands at different precursor ratios. Synthesis of the salen ligand precursor by utilization of an excess of di-*tert*-butyl salicaldehyde **(117)** (3 eq.) relative to **(115)a** (1 eq.) and tartrate salt (*R,R*)-**(118)** (2 eq.) yielded only a 1:1 ratio of the desired monoallylic ligand (*R,R*)-**(116)a** (7.4%) to the diallylic ligand (*R,R*)-**(116)d** (7.2%, Table 5, Entry 1) instead of the expected statistical 6:1 ratio.

Table 5. Statistical ratio of unsymmetrical substituted ligand (116)a-c to ligand (R,R)-(103)a to the disubstituted ligand (116)d-f.

Entry	Synthesis	(R,R)-(103)a [%]	(R,R)-(116) [%]	(R,R)-(116) [%]
1*	1 eq. (115)a, 3 eq. (117), 2 eq. (118)	65.7	7.4 (a)	7.2 (d)
2**	2 eq. (115)a, 2 eq. (117), 1 eq. (118)	21.9	34.8 (b)	12.6 (e)
3**	1 eq. (115)a, 3 eq. (117), 2 eq. (118)	70.9	19.9 (c)	3.7 (f)

* analyzed by GC (15 m RTX 1, 0.5 bar H_2),
**analyzed by HPLC (125 mm Nucleodur 100-5-C18ec, 4.0 mm i.d., MeOH:H_2O (95:5), 0.8 mL min^{-1}, 5.6 MPa, 308 K, UV, 220 nm).

Experiments with a higher ratio of **(115)a** (1 eq.) to **(117)** (2 eq.) and **(118)** (1 eq.) (Table 5, Entry 2) yielded a 3:1 ratio of (R,R)-**(116)b** (34.8%) to (R,R)-**(116)e** (12.5%, Table 5, Entry 1) as confirmed by HPLC measurements (Figure 25). The obtained mixtures could be separated by preparative HPLC to yield unsymmetrical ligands (R,R)-**(116)a-c** with different chain length (**a:** C3, **b**: C6, **c:** C8).
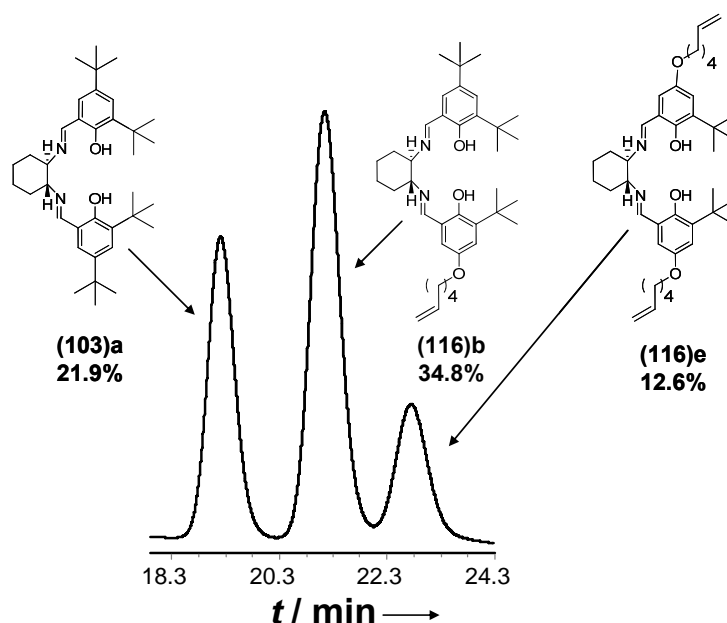
Figure 25. HPLC separation of salen ligand (103)a (12.6%), monoallylic salen ligand (116)a (34.8%) and diallylic salen ligand (116)d (12.6%). Conditions: 125 mm Nucleodur 100-5-C18ec, 4.0 mm i.d., MeOH:H_2O (95:5), 0.8 mL min^{-1}, 5.6 MPa, 308 K, UV, 220 nm.

An alternative route to enantiopure unsymmetrical salen ligands using hydrogen chloride as a protecting group for one amine group of the cyclohexyldiamine was described by Weck et

al.[457] This one-pot synthesis giving 60–85% yields for different monofunctionalized unsymmetrical salen ligands was not applied in the present study, but might be a straightforward approach to ligands (*R,R*)-**(116)a-c**. Specific optical rotation angles of the unsymmetrical salen ligands were detected by using polarimetry. Compared to the levorotatory Jacobsen ligand (*R,R*)-**(103)a** ($[\alpha]_{20}^{D}$ = -315° (c = 1, CH$_2$Cl$_2$)), showing negative values, the specific rotation absolute values of the polysiloxane-immobilized ligands were lower than those of the monomers ((*R,R*)-**(116)a**: $[\alpha]_{20}^{D}$ = -288,7° (c = 1, CHCl$_3$), (*R,R*)-**(116)b**: $[\alpha]_{20}^{D}$ = -267.5° (c = 0.75, CHCl$_3$), and (*R,R*)-**(116)c**: $[\alpha]_{20}^{D}$ = -232.5° (c = 0.55, CHCl$_3$)).

7.2.2. Immobilization of Salen Ligands on Modified Polysiloxanes

HMPS copolymer **(4)** was synthesized by an acid-catalyzed thermic equilibration of hexamethyldisiloxane **(87)**, octamethyldisiloxane **(88)** and polyhydridomethylsiloxane **(89)** as described in chapter 6.2.2. The Pt-catalyzed hydrosilylation of HMPS **(4)** and the ligand mixture allowed the capture of the vinyl-terminated ligands (*R,R*)-**(116)a-c** and (*R,R*)-**(116)d-f**, while the soluble tetra-*tert*-butyl-substituted ligand (*R,R*)-**(103)a** was washed away from the polysiloxane-immobilized product. With this approach, the mixture of ligands (*R,R*)-**(116)a-c**, (*R,R*)-**(116)d-f**, and (*R,R*)-**(103)a** required no chromatographic separation. However, ligands (*R,R*)-**(116)a-c**, (*R,R*)-**(116)d-f**, and (*R,R*)-**(103)a** could be isolated by preparative HPLC to only immobilize the unsymmetrical ligands (*R,R*)-**(116)a-c** on HMPS **(4)**. The polysiloxane-immobilized salen ligands (*R,R*)-**(119)a-c** were purified with column chromatography over silica gel and activated carbon to remove the residual Pt catalyst, which might coordinate to the immobilized salen ligand. Furthermore, unwanted catalyst residues can be removed with the anion exchange resin Levathit S 100. Inductively-coupled-plasma mass-spectrometry (ICP-MS) measurements confirmed that no Pt was left after the purification process. To verify the successful immobilization of ligands (*R,R*)-**(116)a-c**, ^{1}H NMR measurements were performed. These measurements showed the completion of the reaction with the disappearance of the Si-H signal at 4.6 ppm as well as the terminal vinyl group signals at 5.8 ppm and 5.0 ppm (Figure 26).
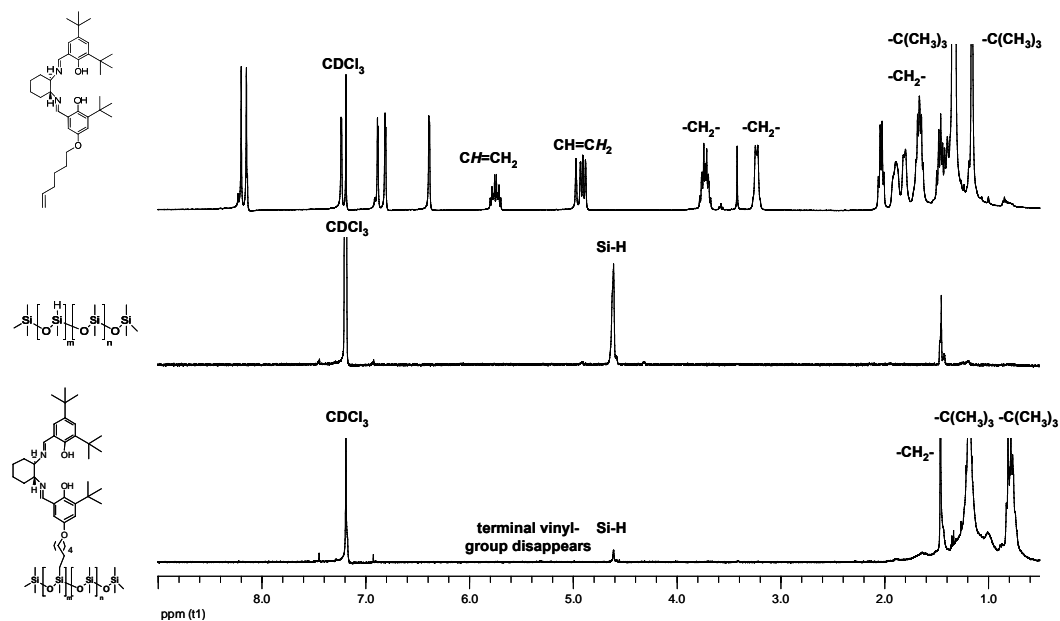
Figure 26. ^{1}H NMR spectra of the modified ligand (*R,R*)-**(116)b**, the HMPS (**4**), and the polysiloxane-supported ligand (*R,R*)-**(119)b** (400.1 MHz, CDCl$_3$, δ = -9.0– -0.5 ppm).

7.2.3. Metalation of Immobilized Salen Ligands

Metal insertion was accomplished by adding a solution of Co(OAc)$_2$ in methanol and toluene to yield polysiloxanes (*R,R*)-**(120)a-c**. Elemental analysis measurements detected a cobalt loading of 0.5%. An aerobic oxidation of the Co(II)-salen precatalyst (*R,R*)-**(120)a-c** to the catalytically active Co(III) state was achieved by dissolving the polysiloxane in a toluene / acetic acid mixture (9:1). After 30 min of gentle stirring, all volatiles were removed in vacuum to afford the polysiloxane immobilized Co(III)-salen-OAc catalysts (*R,R*)-**(121)a-c** as slightly colored, viscous polymers. Catalytic tests with the immobilized catalysts towards the HKR of terminal epoxides will be part of further studies and are currently being continued.

7.3. Conclusion

The present work demonstrates the synthetic applicability of polysiloxane-supported chiral Co-(III)-salen-complexes. The systematically variation of the alkane spacer length leaded to three different chiral salen ligands that were covalently bounded to modified polysiloxanes. Furthermore, the terminal vinyl group of the unsymmetrical salen ligands offers other immobilization possibilities via copolymerization. The benefits usually postulated to be associated with immobilization of soluble catalysts facilitated product purification, catalyst recycling, and adaptation to continuous flow methodology are targeted to be realized using biphasic liquid/liquid separation techniques or on-column reaction chromatography experiments. The use of these immobilized catalysts might particularly be advantageous in the HKR of terminal epoxides, where purification had proven problematic with homogeneous catalysts. These catalytic tests are the subject of ongoing investigations.

8. Experimental Section

8.1. General Methods and Materials

Unless otherwise indicated, all operations were performed under an argon atmosphere using standard Schlenk technique and flame-dried glassware. All solvents were dried through distillation using standard techniques and kept under an argon atmosphere (THF, diethyl ether (Mg-Anthracen); CH_2Cl_2, acetonitrile, DMSO, Et_3N, ethyl acetate (CaH_2); DMF (Desmodur®, dibutyl tin dilaurate); MeOH, EtOH (Mg); acetone (3Å molsieve); *n*-hexane, *n*-pentane, toluene, benzene, *o*-xylene (Na/K).

All starting materials were purchased from commercial sources (ABCR (Karlsruhe, Germany), ChemPur Feinchemikalien (Karlsruhe, Germany), Fluka (Buchs, Switzerland), Macherey & Nagel (Düren, Germany), Sigma-Aldrich (Steinheim, Germany), Strem Chemicals (Newburyport, USA). Unless otherwise indicated, the following chemicals were used as received: acetic acid, 3-bromoprop-1-ene **(110)a**, 2-*tert*-butyl hydroquinone **(109),** 3-di-*tert*-butyl-2-hydroxybenzaldehyde **(117)**, (1*R*)-10-camphorsulfonic acid **(64)**), 4-cyano-phenylglyoxylic acid ethyl ester **(20),** diallyl disulfide **(41)a**, diethyl diallylmalonate **(40)a**, diisopropylamine,   3,3-dimethyl-acrylchloride,   PDMS   GE SE 30   **(28)**, ethyl 3-chlorobenzoylformate   **(19)**,   (*E*)-ethyl 3-(chlorocarbonyl)acrylate,   ethyl 4-fluorobenzoylformate **(17)**, diastereomers of chalcogran **(94)a–d**, (2*RS*,5*RS*)-2-ethyl-1,6-dioxaspiro[4.4]-nonane (Boehringer Ingelheim), ethyl α-oxothiophen-2-acetate **(21),** ethyl pyruvate **(1)** (distilled and kept at 5 °C before use), ethyl-3,5-difluorophenylglyoxylat **(18)**, ethyl-4-methylbenzoylformate **(16)**, ethyldiisopropylamine, europium chloride hexahydrate, 2-furylmethanol, Grubbs catalyst 1st generation [($PCy_3)_2Cl_2Ru=CHPh$] **(22)**, Grubbs catalyst 2nd generation [($H_2IMes)(PCy_3)Cl_2Ru=CHPh$] **(23)**, heptafluorobutanoyl chloride (98%, Aldrich, in ampule under argon), H_2PtCl_6 **(57)** (stored under argon), 1-hexyl-3-methylimidazolium trifluoromethansulfonate ([HMIM][CF_3SO_3]) **(34)**, Hoveyda-Grubbs catalyst 1st generation [($PCy_3)_2Cl_2Ru=CHC_6H_4$-O-*i*Pr] **(24)**, 2,6-lutidine **(114)**, menthone enantiomers **(93)a–b**, methyl 2-oxo-2-phenylacetate **(15)**, mono-ethyl fumarate, *N,N*-diallyltrifluoroacetamide **(30)a**, *n*BuLi (1.6 M in anhydrous THF), nickel(II)-chloride, palladium(II) acetate **(7)**, paraformaldehyde **(112)**, (5% phenyl)-methylpolysiloxane GE SE 52 **(29)**, platin-divinyltetramethylsiloxane (Karstedt's catalyst) **(11)**, platinum(II)

acetylacetonate **(6),** potassium acetate, potassium hydroxide, quinine **(3)**, thionyl chloride, and tin tetrachloride **(113)**. IL **(34)** was stored under argon atmosphere and was dried under high vacuum over night at an elevated temperature to remove water before the coating procedure**.** 6-Bromohex-1-ene **(110)b**, 8-bromooct-1-ene **(110)c**,[458] (*R,R*)-1,2-diammoniumcyclohexane mono-(+)-tartrate salt **(118)**,[459] the 2-furanylmethylacrylate derivatives **(99)-(101)**,[400, 401] HMPS **(4)**,[84, 85] 2-(6-methoxy-2-naphthyl)propenoic acid ethyl ester **(122)**,[460] MVPS **(5)**,[84, 85] and phosphorus pentabromide[461] were prepared as described elsewhere. Fused-silica capillaries (i.d. 250 μm, o.d. 365 μm) were purchased from Microquartz (Munich, Germany).

8.2. Analytical Techniques

Analytical thin-layer chromatography (TLC) was performed on commercially available silica gel plates with F-254 indicator (Polygram® SIL G/UV254 or Polygram® ALOX N/UV254 (Marcherey-Nagel). Visualization was accomplished by an ultraviolet lamp (254 nm). **Silica gel column chromatography** was carried out with Silica Gel Type 9385 (230–400 mesh, 60 Å pore diameter, Merck) as stationary phase. **NMR spectra** were recorded on a DPX 300 (^{1}H: 300.1 MHz, ^{13}C: 75.5 MHz, ^{19}F: 300.1 MHz) or an AV 400 (^{1}H: 400.1 MHz, ^{13}C: 100.6 MHz) spectrometer (Bruker) in the assigned deuterated solvents. Chemical shifts (δ) are reported in parts per million (ppm) using residual solvents protons as internal standards. The coupling constants are reported in Hertz (Hz). The corresponding solvent peaks were used as reference peaks (CDCl$_3$: dC 77.0 ppm, dH 7.26 ppm; CD$_2$Cl$_2$: dC 54.0 ppm, dH 5.32 ppm; C$_6$D$_6$: dC 128.1 ppm, dH 7.16 ppm), for ^{19}F spectra CFCl$_3$ was used as external reference. Splitting patterns are designated as s (singlet), d (doublet), t (triplet), q (quartet), bs (broad singlet), m (multiplet) and bm (broad multiplet). **GC measurements** were performed on a Thermo Trace PolarisQ GC-MS (San Jose, California, USA), equipped with a split injector (250 °C) and a FID (250 °C) on a HP 6890 or HP 5890, or on a FINNIGAN SSQ 7000. Helium was used as inert carrier gas. **Preparative GC** was performed on a Dr. Hupe APG 402 Prototyp. **LC/MS spectra** were recorded on a Shimadzu LCMS 2010. **Preparative HPLC** was performed on a Shimadzu LC-8A. **Mass spectra** were recorded on a quadrupole ion trap MS Trace GC PolarisQ (EIMS, 70 eV, ion source temperature 200 °C, San Jose, California, USA), on a FINNIGAN MAT 8200 or a FINNIGAN MAT 8400 (EI), a FINNIGAN MAT 95 (ESI, HR) and a Bruker FT-ICR Apex-Qe (ESI). **FT-IR spectra** were recorded on a Nicolet Magna FT-IR 560 Spectrometer. Characteristic absorption bands are

given in wave-numbers (cm^{-1}) with the relative intensities designated as vs (very strong), s (strong), m (medium), and w (weak). **Optical rotation angles** were measured on a Perkin Elmer Model 343. **Melting points** were determined using a Gallenkamp melting point apparatus. **Transmission electron micrographs** (TEM) were obtained on a Hitachi 7500 transmission electron microscope operating at an acceleration voltage of 100 kV. High-resolution transmission electron microscopy (HRTEM) images were obtained on a Hitachi HF 2000 microscope with a cold field emission source operating at 200 keV. **Elemental analysis** was performed at „Mikroanalytisches Labor H. Kolbe", Mülheim a. d. Ruhr, Germany. A **Kugelrohr Distillation** Oven from Büchi was used for the distillation of small sample volumes.

8.3. Software

The following software programs were used: ChemBioDraw® Ultra 11.0, ChemOrganizer MMVII 1.0.0.4,[462] DCXPlorer,[463, 464] Endnote 9.0, MestRec® 4.7.0.0, Microsoft® Office 2003, RCXPlorer,[465] and XCalibur®.

8.4. Experimental Section - Chapter 3

### 8.4.1. Synthesis of Polysiloxane-Supported Quinine (10) (Chirasil-Quinine)[30]

Quinine Acetate (8)[30, 466, 467], (1R)-(6-methoxyquinolin-4-yl)((4S,8R)-8-vinylquinuclidin-2-yl)methyl acetate
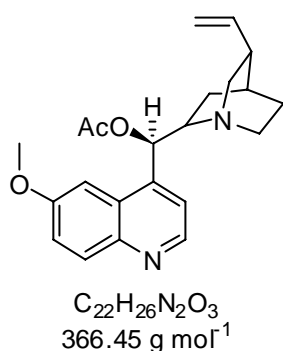
Quinine **(3)** (2.0 g, 6.2 mmol, 1 eq.) and Et$_3$N (0.94 g, 9.3 mmol, 1.5 eq.) were dissolved in dichloromethane (45 mL). After cooling to 0 °C, a solution of acetyl chloride (0.65 g, 8.3 mmol) was added over 1 h. The reaction mixture was allowed to stir 17 h at RT, and then sat. aq. NaHCO$_3$ solution was added, and the aq. layer extracted with dichloromethane. The combined organic layer was dried with MgSO$_4$, filtered, the volatiles were evaporated, and purified via column chromatography with ethyl acetate:MeOH (10:1) as the eluent. This provided quinine acetate **(8)** (1.83 g, 81%). ^{1}H NMR (400.1 MHz, CDCl$_3$, 300 K) δ: 8.75 (d, 1H, J = 4.8 Hz, Ar-H), 8.02 (d, 1H, J = 9.0 Hz, Ar-H), 7.45 (d, 1H, J = 2.7 Hz, Ar-H), 7.40-7.36 (m, 2H, Ar-H), 6.50 (d, 1H, H-C-OCOCH$_3$, J = 7.2 Hz), 5.91-5.79 (m, 1H, CH=CH$_2$), 5.06-5.02 (m, 1H, CH=CH_2), 5.01-4.98 (m, 1H, CH=CH_2), 3.96 (s, 3H, -OCH$_3$), 3.39 (q, 1H, J = 8.4 Hz), 3.16–3.02 (m, 2H, N-CH$_2$), 2.72-2.58 (m, 2H, N-CH_2), 2.34-2.23 (m, 1H, CH-CH=CH$_2$), 2.13 (s, 3H, O-CO-CH_3), 1.78-1.68 (m, 1H, CH$_2$-CH-CH$_2$), 1.93-1.85 (m, 2H, CH_2-CH-CH$_2$), 1.60-1.49 (m, 2H, CH$_2$-CH-CH_2) ppm.

Polysiloxane-Supported Quinine Acetate (9)[30], [(1R)-(8-ethylquinuclidin-2-yl)(6-methoxyquinolin-4-yl)methyl acetate]-poly(dimethylsiloxane)
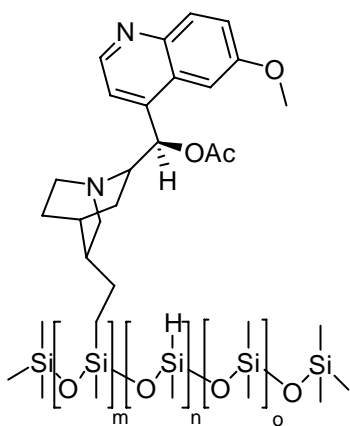
HMPS **(4)** (9.0 g), quinine acetate **(8)** (1.13 g, 3.1 mmol), and platin-divinyltetramethylsiloxane (Karstedt's catalyst) **(11)** (30 µL) were dissolved in anhydrous toluene (120 mL) and heated at 65 °C for 24 h under an argon atmosphere. The progress of the reaction was monitored with ^{1}H NMR spectroscopy or IR spectroscopy by the disappearance of the Si-H signal at δ = 4.6 ppm or the Si-H absorbance at ~2100 cm^{-1}. In the case of an incomplete reaction, additional catalyst (50% of

the original volume) was added to the reaction solution and allowed to proceed for another ~12 h before reaction control. When necessary, this cycle was repeated until no Si-H signal in the NMR spectrum or Si-H absorbance in the IR spectrum was observed. Typically, no additional Pt catalyst was required to complete the reaction. After a complete reaction, the reaction mixture was allowed to cool to RT and the toluene removed under reduced pressure. A small amount of DCM:ethyl acetate (2:1) was added to the residue and the solution passed through a short silica gel column with similar eluent to remove the residual Pt. Volatiles were removed under reduced pressure. This provided polysiloxane-supported quinine acetate (9) (6.8 g, 67%). ^{1}H NMR (400.1 MHz, CDCl$_3$, 300 K): δ = 8.67–8.65 (m, 1H, Ar-H), 7.96–7.92 (m, 1H, Ar-H), 7.39–7.38 (m, 1H, Ar-H), 7.32–7.25 (m, 2H, Ar-H), 6.47–6.43 (m, 1H, H-C-OCOCH$_3$), 4.97–4.92 (m, 1H), 4.61 (bs, 0.2H, Si-H), 3.90 (s, 3H, -OCH$_3$), 3.43–3.38 (q, 1H, J = 7.0 Hz), 3.33–3.24 (m, 1H, N-CH), 3.04–2.95 (m, 2H, N-CH$_2$-), 2.63–2.52 (m, 2H, N-CH$_2$), 2.24–2.19 (m, 1H, CH-CH=CH$_2$), 2.05 (s, 3H, O-CO-CH$_3$), 1.84–1.18 (m, 6H, CH$_2$), 0.82–0.74 (m, 1H), 0.39–0.35 (m, 1H), 0.01– -0.03 (bm, 59H, CH$_3$-Si-O-) ppm.

Polysiloxane-Supported Quinine (10)[30] (Chirasil-Quinine), [(1R)-(8-ethylquinuclidin-2-yl)(6-methoxyquinolin-4-yl)methanol]-poly(dimethylsiloxane)
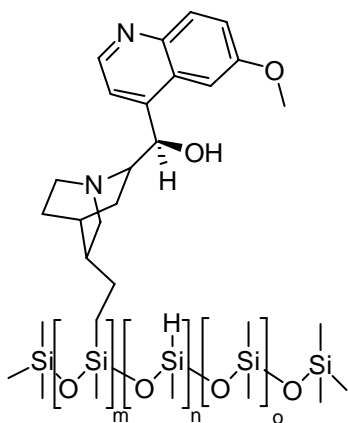
Polysiloxane-supported quinine acetate (9) (5.1 g) was dissolved in a 0.15 wt% K$_2$CO$_3$ in 90% aq. EtOH (150 mL). The mixture was allowed to stir at 55 °C for 12 h. The solvent was evaporated, the residue was dissolved in n-heptane (300 mL) and washed three times with water. Afterwards, the organic layer was dried with MgSO$_4$, filtered, and solvents were removed under reduced pressure. This provided polysiloxane-supported quinine (10) (4.1 g, 81%). ^{1}H NMR (400.1 MHz, CDCl$_3$, 300 K): δ = 8.61–8.60 (d, 1H, J = 4.5 Hz, Ar-H), 7.91–7.89 (d, 1H, J = 9.2 Hz, Ar-H), 7.52–7.45 (m, 1H, Ar-H), 7.28–7.21 (m, 2H, Ar-H), 5.63 (bm, 1H, H-C-OH), 3.81 (s, 3H, -OCH$_3$), 3.69–3.62 (m, 1H), 3.03–2.97 (m, 3H,), 2.62–2.55 (m, 1H), 2.32–2.29 (m, 1H), 1.74–1.10 (m, 12H), 0.34–0.30 (m, 2H), 0.07– -0.19 (m, 107H, CH$_3$-Si-O) ppm.

8.4.2. Preparation of Quinine-Modified Platinum Nanoparticles in a Polysiloxane Matrix and Coating of Microcapillaries

Platinum(II)acetylacetonate **(6)** ((0.1–1.0) mg, (4.5–44.5)×10^{-4} mmol)), quinine **(3)** (12.0 mg, 3.70×10^{-2} mmol), HMPS **(4)** (8 mg) and MVPS copolymer **(5)** (4 mg) were mixed in absolute dichloromethane (3 mL). For the preparation of the TEM samples, the solvent was slowly evaporated and the polymeric samples were again dissolved and evaporated on a grid. Fused-silica capillaries (0.5 m×250 µm i.d., thermally deactivated at 220 °C for 24 h) were coated with the solutions to obtain a film thickness of 250 nm. They were coated by the static method described by Grob.[315] Capillaries were filled with the solution and the solvent removed under high vacuum after one end of the capillary was closed. Then, the capillaries were flushed with argon and subsequently the polymer film was immobilized in a slow hydrogen stream by heating the capillary from 25–160 °C at a rate of 0.5 K min^{-1}. The temperature was maintained for 10 h at 160 °C.

8.4.3. Preparation of Quinine-Modified Palladium Nanoparticles in a Polysiloxane Matrix and Coating of Microcapillaries

Quinine-modified Pd nanoparticles were prepared according to the described procedure (chapter 8.4.2.) using Pd(OAc)$_2$ **(7)** (0.1-1.0 mg, 2.5-25.4×10^{-4} mmol), quinine **(3)** (12.0 mg, 3.7×10^{-2} mmol), HMPS **(4)** (8 mg) and MVPS **(5)** (4 mg).

8.4.4. Enantioselective On-Column Hydrogenation Experiments over Quinine-Modified Pt and Pd Nanoparticles

On-column hydrogenation experiments were performed on a Thermo Trace PolarisQ GC-MS equipped with a split injector (250 °C), a FID (250 °C) and a quadrupole ion trap MS. For the hydrogenation of different substrates (α-keto esters), a fused-silica capillary coated with quinine-modified Pt or Pd nanoparticles in a polysiloxane matrix (0.5 m×250 µm i.d., 250 nm film thickness) were used. The reaction mixture was quantified by coupling the coated microcapillary between a pre-separation capillary (GE SE 52 **(29)**, 1.0 m×250 µm i.d., 250 nm film thickness) and a chiral separation column (heptakis(6-*O*-trimethylsilyl-2,3-di-*O*-methyl)-β-cyclodextrin **(12)**,[168] 25.0 m×250 µm i.d. or Chirasil-β-Dex **(13)**,[169]

25.0 m×250 µm i.d.). Hydrogen was used as reactive carrier gas. All measurements were repeated at least three times. Conversions were determined by integrating the FID signals with the software tool DCXplorer.[463, 464]

8.5. Experimental Section - Chapter 4

8.5.1. Dissolving of Grubbs-type Catalysts in a Polysiloxane Matrix and Coating of Microcapillaries

Capillaries were coated by the static method described by Grob[315] to obtain a uniform film with a thickness of 500 nm. Therefore, fused-silica capillaries (i.d. 250 µm, 1–3 m) were filled with the solutions of the respective Grubbs-type catalyst **(22)**, **(23)**, or **(24)** (0.1–1.0 mg) and the respective polysiloxane (24 mg; GE SE 30 **(28)** or GE SE 52 **(29)**) dissolved in absolute *n*-pentane (3 mL) under strict exclusion of oxygen. The solvent was removed by high vacuum after closing one end of the capillary. Afterwards, the capillary was flushed with argon.

8.5.2. Correction Factors for Ring-Closing Olefin Metathesis Substrates

Conversions were determined from the data for GC with FID, which gives signal intensities that can be correlated to the ionizable carbon atoms in a specific molecule. Response correction factors for the relative signal ratios of the educts and products were taken into account. Correction factors ((peak area of substrate/peak area of internal standard)×(peak area of product/peak area of internal standard)) were determined by integrating the FID signals of the corresponding substrate and product and an internal standard (*n*-decane) to give $f = 1.96$ for **(30)a** → **(30)b**, $f = 1.24$ for **(40)a** → **(40)a** and $f = 1.66$ for **(41)a** → **(41)b**). GC measurements were performed on a separation column (GE SE 30 **(28)**, 25 m, i.d. 250 µm). Helium was used as inert carrier gas. The measurements were performed in steps of 5 K between 45–80 °C and pressures in steps of 10 kPa between 80–120 kPa.

8.5.3. Recycling Experiments over Grubbs-type Catalyst Stabilized in a Polysiloxane Matrix

Stability measurements were performed after installation of the prepared columns (Reactor setup: pre-separation capillary GE SE 52 **(29)** (1 m, 500 nm film thickness), 2 m Grubbs-type 2nd generation catalyst **(23)** coated capillary (2 m, 500 nm film thickness), HP–5 (25 m, 500 nm film thickness) by injection of **(30)a**. Measurements were performed at 45 °C and 60 kPa (67 measurements, 63 min per cycle) as well as 100 °C and 60 kPa (110 measurements, 13.5 min per cycle) by performing multiple injections. Conversions were determined by integrating the FID signals with the software tool RCXplorer,[465] taking correction factors (chapter 8.5.2.) for the relative signal ratios of the substrate and product into account.

8.5.4. On-Column Ring-Closing Olefin Metathesis Experiments over Grubbs-type Catalysts

On-column RCM experiments were performed on a Thermo Trace PolarisQ GC-MS equipped with a split injector (250 °C), a FID (250 °C) and a quadrupole ion trap MS. For RCM of *N,N*-diallyltrifluoroacetamide **(30)a**, fused-silica capillaries (1–3 m, i.d 250 μm) coated with the different Grubbs-type catalysts **(22)**, **(23)**, or **(24)** dissolved in a PDMS (GE SE 30 **(28)** or GE SE 52 **(29)**, 500 nm film thickness) were used. These capillaries were coupled between a preseparation column (HP-5, 1 m, i.d. 500 μm, 500 nm film thickness) and a separation column (HP-5, 25 m, i.d. 500 μm, 500 nm film thickness) to quantify the reaction mixture. Helium was used as inert carrier gas. The measurements were performed in steps of 5 K between 45–80 °C and pressures in steps of 10 kPa between 80–120 kPa. All measurements were repeated at least three times. A total of 120 measurements for each catalyst were considered for the statistical analysis of the reaction rate constants to obtain activation parameters.

8.5.5. Determination of Activation Parameters with Contact Times for Ring-Closing Olefin Metathesis Experiments over Grubbs-type Catalysts

Residence times of the metathesis substrate **(30)a** were determined with a reference column using only GE SE 30 **(28)** or GE SE 52 **(29)** as the stationary phase and were compared with

the catalytically active column using the reactor setup described above. An internal standard (*n*-decane), assumed not to undergo any chemical interaction with the catalyst and substrates, was used. Methane was usually co-injected to measure the gas hold-up (dead-volume) if the solvent peak did not overlap with the methane peak. Otherwise the retention time of methane was measured in a separate experiment. From the retention difference the contact times can be precisely determined. Reaction rate constants *k* of metathesis reactions were determined by application of Equation 1 (chapter 3.2.4) to the conversion data. The Gibbs free activation energies $\Delta G^{\ddagger}(T)$ were calculated according to the Eyring equation (Equation 3, chapter 4.2.3.)

8.6. Experimental Section - Chapter 5

8.6.1. Dissolving of Grubbs-type 1st Generation Catalysts in an Ionic Liquid and Coating of Microcapillaries

Grubbs catalyst 1st generation **(22)** (0.5 mg, 6.08×10^{-4} mmol) and [HMIM][CF$_3$SO$_3$] **(34)** (24.0 mg, 0.07 mmol) were dissolved in anhydrous dichloromethane (3.0 mL) under an argon atmosphere. Fused-silica capillaries (1.0–8.0 m×250 µm i.d.) were coated with these solutions under strict exclusion of oxygen. Capillaries were coated by the static method described by Grob[315] to obtain a film thickness of 250 nm. Therefore, capillaries were filled with the respective solution and the solvent was removed by high vacuum after closing one end of the capillary. After complete removal of the solvent the capillaries were flushed with argon, the capillary ends were sealed and the capillary was directly installed in the GC.

8.6.2. On-Column Metathesis Experiments over Grubbs-type Catalysts 1st Generation Stabilized in an Ionic Liquid

On-column metathesis experiments were performed after installation of the prepared column (for substrate **(30)a** / **(41)a**: 8.0 m×250 µm i.d., 250 nm film thickness; for substrate **(40)a**: 1.0 m×250 µm i.d., 250 nm film thickness and separation capillary GE SE 52 **(29),** 0.1 m×250 µm i.d., 250 nm film thickness) by injection of the individual diallylic compounds **(30)a**, **(40)a** and **(41)a**. All measurements were repeated two times at each temperature in steps of 10 K between 50–70 °C at 60 kPa for *N,N*-diallyltrifluoroacetamide **(30)a**, 60–80 °C

at 90 kPa for diallyl disulfide **(41)a**, and 90–110 °C at 110 kPa for diethyl diallylmalonate **(40)a**.

8.6.3. Recycling Experiments over Grubbs-type Catalyst 1st Generation Stabilized in an Ionic Liquid

Stability measurements were performed after installation of the prepared column (6.0 m×250 µm i.d., 250 nm film thickness) by injection of **(41)a**. This measurement was repeated 63 times at 50 °C at 60 kPa (24 h). Conversions were determined by integrating the FID signals with the software tool RCXplorer[465] taking correction factors (chapter 8.5.2.) for the relative signal ratios of the substrate and product into account.

8.6.4. Determination of Activation Parameters for Ring-Closing Olefin Metathesis Experiments over Grubbs-type Catalyst 1st Generation Stabilized in an Ionic Liquid with the Unified Equation of Chromatography

The recently described unified equation of chromatography[71] allows the direct calculation of reaction rate constants k_1 and k_{-1} and Gibbs activation energies $\Delta G^{\ddagger}(T)$ for all types of first-order reactions, regardless of the initial concentrations of the interconverting analytes A and B and the equilibrium constant $K_{A/B}$. To determine the reaction rate constants and to obtain the activation parameters from the temperature-dependent measurements, the computer program DCXplorer[463, 464] was used.

8.6.5. Determination of Activation Parameters with Contact Times for Ring-Closing Olefin Metathesis Experiments over Grubbs-type Catalyst 1st Generation Stabilized in an Ionic Liquid

Residence times of the metathesis substrates were determined with a reference column using only IL **(34)** as the stationary phase and were compared with the residence times of the metathesis substrates on a catalytically active column. From the retention difference, the contact times can be precisely determined as described in chapter 8.5.5.

8.7. Experimental Section - Chapter 6

8.7.1. Synthesis of Chiral 1,3-Diketonates

Potassium-(1*S*)-camphor-10-sulfonate (71), (potassium ((1*S*,4*R*)-7,7-dimethyl-2-oxobicyclo [2.2.1]heptan-1-yl)methanesulfonate)
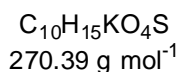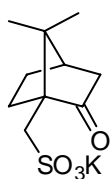
(1*S*)-10-Camphorsulfonic acid **(64)** (350.0 g, 1.51 mol) was suspended in H$_2$O (150 mL) and then slowly neutralized by adding a solution of potassium hydroxide (84.5 g, 1.51 mol) in H$_2$O (200 mL) under ice bath cooling. The solvent was removed under reduced pressure and under high vacuum. The product was dried two times over phosphorus pentoxide for 24 h to yield **(71)** (391.7 g, 1.45 mol, 96%) as a white salt. ^{1}H NMR (300.1 MHz, CDCl$_3$, 300 K): δ = 3.45 (d, 1H, *J* = 20.0 Hz, CH$_2$SO$_3$), 3.13 (d, 1H, *J* = 20.0 Hz, CH$_2$SO$_3$), 2.66–2.67 (m, 1H), 2.24–2.02 (m, 5H), 1.59–1.49 (m, 1H), 1.02 (s, 3H, CH$_3$), 1.00 (s, 3H, CH$_3$) ppm. ^{13}C NMR (75.5 MHz, CDCl$_3$, 300 K): δ = 213.1, 58.3, 54.6, 48.4, 42.9, 42.8, 27.5, 26.9, 19.7, 19.6 ppm. FT-IR [cm^{-1}]: 3454 (s), 2954 (s), 2232 (s), 2082 (s), 1740 (vs), 1728 (vs), 1469 (m), 1414 (m), 1374 (w), 1284 (w), 1217 (w), 1186 (w), 1166 (w), 1103 (w), 1040 (w), 973 (w), 934 (w), 936 (w), 851 (w), 780 (w), 710 (w), 686 (w), 619 (w). m$_p$ 320-328 °C.

The structure formula beside this text shows: C$_{10}$H$_{15}$KO$_4$S, 270.39 g mol^{-1}, with SO$_3$K group.

(1*S*)-10-Camphorsulfonic acid bromide (72), ((((1*S*,4*R*)-7,7-dimethyl-2-oxobicyclo[2.2.1] heptan-1-yl)methanesulfonyl bromide)
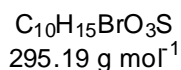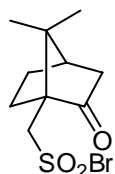
In a three-necked flask equipped with a mechanical stirrer, potassium-(1*S*)-camphor-10-sulfonate **(71)** (350.0 g, 1.2 mol) was suspended in anhydrous diethyl ether (1.5 L) at 0 °C under an argon atmosphere. Phosphorus pentabromide (561.4 g, 1.3 mol) was added rapidly under mechanical stirring and ice bath cooling. The red mixture was allowed to warm up to RT for 30 min and then it was refluxed for additional 30 min. Afterwards, the solution was poured into ice water. The organic phase was separated and washed with water and dried over CaCl$_2$. The organic phase was removed under reduced pressure to yield colorless crystalline product **(72)** (272.5 g, 71%). ^{1}H NMR (300.1 MHz, CDCl$_3$, 300 K): δ = 4.50 (d, 1H, *J* = 14.7 Hz, CH$_2$SO$_2$Br), 3.90 (d, 1H, *J* =14.7 Hz, CH$_2$SO$_2$Br), 2.53–2.39 (m,

The structure formula beside this text shows: C$_{10}$H$_{15}$BrO$_3$S, 295.19 g mol^{-1}, with SO$_2$Br group.

2H), 2.16–2.04 (m, 2H), 1.99 (d, 1H, J = 18.3 Hz, CH), 1.83–1.74 (m, 1H), 1.52–1.43 (m, 1H), 1.14 (s, 3H, CH$_3$), 0.93 (s, 3H, CH$_3$) ppm. ^{13}C NMR (75.5 MHz, CDCl$_3$, 300 K): δ = 212.4, 69.1, 60.5, 48.0, 42.7, 42.2, 26.8, 25.4, 19.7, 19.6 ppm. LR-MS (EI, m/z): 41 (41), 81 (80), 109 (82), 151 (100) [M$^+$]-SO$_2$Br, 187 (7), 229 (10). FT-IR [cm^{-1}]: 2954 (s), 2891 (s), 1739 (vs), 1456 (m), 1414 (m), 1392 (m), 1376 (m), 1279 (w), 1182 (w), 1127 (w), 1094 (w), 1038 (w), 967 (w), 933 (w), 853 (w), 794 (w), 764 (w), 710 (w), 679 (w), 642 (w), 616 (w).

(1S)-10-Bromocamphor (73), ((1S,4R)-1-(bromomethyl)-7,7-dimethylbicyclo[2.2.1] heptan-2-one)
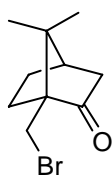
(1S)-Camphorsulfonic acid bromide **(72)** (249.8 g, 846.2 mmol) was dissolved in anhydrous o-xylene. A small amount of calcium chloride was added and the mixture was stirred for 48 h under strict exclusion of light. Then, the mixture was filtered and the filtrate was heated under reflux till the generation of SO$_2$ was decreasing. The organic phase was removed under reduced pressure. The residue was recrystallized with EtOH:H$_2$O (1:1) to yield colorless crystalline product **(73)** (136.9 g, 70%). ^{1}H NMR (400.1 MHz, CDCl$_3$, 300 K): δ = 3.62 (d, 1H, J = 11.2 Hz, CH$_2$Br), 3.41 (d, 1H, J = 11.2 Hz, CH$_2$Br), 2.44–2.37 (m, 1H), 2.16–2.09 (m, 2H), 2.06–1.98 (m, 1H), 1.90 (d, 1H, J = 18.4 Hz), 1.59–1.52 (m, 1H), 1.44–1.37 (m, 1H), 1.10 (s, 3H, CH$_3$), 0.94 (s, 3H, CH$_3$) ppm. ^{13}C NMR (100.6 MHz, CDCl$_3$, 300 K): δ = 215.5, 60.3, 48.2, 44.0, 43.0, 29.3, 27.7, 26.7, 20.5, 20.3 ppm. LR-MS (EI, m/z): 41 (37), 53 (18%), 67 (41), 81 (72), 93 (20), 109 (74), 123 (38), 133 (7), 151 (100) [M$^+$]-Br, 173 (1), 230 (7) [M$^+$]. HRMS spec. calcd. for C$_{10}$H$_{15}$OBr: 230.0306; found: 230.0302. FT-IR [cm^{-1}]: 2967 (s), 2935 (s), 2884 (s), 1744 (vs), 1465 (m), 1451 (m), 1421 (m), 1382 (m), 1328 (m), 1287 (m), 1234 (w), 1215 (w), 1195 (w), 1167 (w), 1071 (w), 1043 (w), 1018 (w), 961 (w), 934 (w), 910 (w), 873 (w), 851 (w), 809 (w), 775 (w), 745 (w), 708 (w), 671 (w), 629 (w). $[\alpha]^D_{20}$ = +17.5° (c = 1, CHCl$_3$). m$_p$: 66–69 °C.

C$_{10}$H$_{15}$BrO
231.13 g mol^{-1}

(1*R*)-10-Hydroxycamphor (74), ((1*R*,4*R*)-1-(hydroxymethyl)-7,7-dimethylbicyclo[2.2.1]heptan-2-one)

C$_{10}$H$_{16}$O$_2$
168.23 g mol^{-1}

(1*S*)-10-Bromocamphor **(73)** (51.8 g, 0.31 mol), potassium acetate (192.2 g, 1.96 mol) and acetic acid (122 mL, 2.13 mol) were stirred under reflux heating for 10 h. Afterwards, the mixture was dissolved in water and neutralized with potassium carbonate and then extracted with diethyl ether. The phases were separated and the organic phase was dried over magnesium sulfate and then removed under reduced pressure. The obtained product **(73)a** (44.8 g, 0.21 mol) was dissolved in a methanolic KOH solution (10%, 500 mL) and heated under reflux for 6 h. Afterwards, the mixture was poured into water (1000 mL). The phases were separated and the aqueous phase was washed with diethyl ether. The combined organic phases were dried over magnesium sulfate and removed under reduced pressure to yield **(74)** (32.5 g, 63%). ^{1}H NMR (400.1 MHz, CDCl$_3$, 300 K): δ = 3.88 (d, 1H, *J* = 12.0 Hz, C*H*$_2$OH), 3.65 (d, 1H, *J* = 12.0 Hz, C*H*$_2$OH), 2.56-2.46 (bs, 1H, -OH), 2.45–2.38 (m, 1H), 2.08 (t, 1H, *J* = 4.4 Hz), 2.05–1.96 (m, 1H), 1.87 (d, 1H, *J* = 18.4 Hz), 1.84 (ddd, 1H, *J* = 4.0 Hz, *J* = 17.2 Hz, *J* = 29.2 Hz), 1.61 (ddd, 1H, *J* = 4.8 Hz, *J* = 9.2 Hz, *J* = 14.0 Hz), 1.40 (ddd, 1H, *J* = 4.0 Hz, *J* = 9.6 Hz, *J* = 12.8 Hz), 1.01 (s, 3H, CH$_3$), 0.99 (s, 3H, CH$_3$) ppm. ^{13}C NMR (100.6 MHz, CDCl$_3$, 300 K): δ = 221.0, 61.7, 60.7, 46.8, 44.0, 43.5, 26.7, 26.0, 20.8, 19.3 ppm. LR-MS (EI, m/z): 29 (20), 41 (48), 55 (28), 67 (33), 81 (40), 95 (95), 108 (100), 125 (13), 137 (8) [M$^+$]-CH$_3$O, 153 (39) [M$^+$]-CH$_3$, 168 (18) [M$^+$]. FT-IR [cm^{-1}]: 3442 (s), 2955 (s), 2876 (s), 1729 (vs), 1610 (s), 1457 (m), 1417 (m), 1390 (m), 1370 (m), 1323 (m), 1300 (m), 1288 (m), 1272 (m), 1217 (m), 1201 (m), 1178 (m), 1162 (m), 1143 (m), 1107 (w), 1060 (w), 1028 (w), 1009 (w), 997 (w), 950 (w), 930 (w), 919 (w), 871 (w), 852 (w), 808 (w), 769 (w), 753 (w), 710 (w), 675 (w), 651 (w), 631 (w). [α]$^D_{20}$ = +8.0°(c = 1, CHCl$_3$). m$_p$: 216-218 °C. $[\alpha]^D_{20}$ =+21.8 (c = 1, CHCl$_3$).

(1*S*)-10-Camphorthiol (75), ((1*S*,4*R*)-1-(mercaptomethyl)-7,7-dimethylbicyclo[2.2.1]
heptan-2-one)

C$_{10}$H$_{16}$OS
184.30 g mol^{-1}

(1*S*)-10-Camphorsulfonic acid **(64)** (100.0 g, 0.43 mol) and thionyl chloride
(62.7 mL, 0.86 mol) were heated up to 80 °C. After 3 h, the excess of thionyl
chloride was removed in vacuum. The mixture was allowed to cool down to
RT and was powdered afterwards. The obtained (1*S)*-camphor-10-sulfonic
acid chloride **(65)** and triphenylphosphine (338.74 g, 1.29 mol) were
dissolved in a mixture of water (100 mL) and 1,4-dioxane (400 mL). This mixture was heated
under reflux for 2 h. Then water was added (600 mL) and the mixture was extracted with *n*-
pentane. The organic phase was washed with water, dried with magnesium sulfate and the
solvent was removed under reduced pressure. The product was purified with column
chromatography (*n*-pentane: ethyl acetate, 98:2) to yield crystalline product **(75)** (72.2 g,
91%). ^{1}H NMR (300.1 MHz, CDCl$_3$, 300 K): δ = 2.88 (d, 1H, *J* = 12.0 Hz, C*H*$_2$SH), 2.63 (d,
1H, *J* = 12.0 Hz, C*H*$_2$SH), 2.39–1.36 (m, 8H, CH$_2$), 1.01 (s, 3H, CH$_3$), 0.90 (s, 3H, CH$_3$) ppm.
^{13}C NMR (75.5 MHz, CDCl$_3$, 300 K): δ = 218.1, 67.4, 48.2, 44.1, 27.6, 27.4, 27.0, 21.8, 20.7,
20.2 ppm. LR-MS (EI, m/z): 42 (100.0), 67 (10), 81 (23), 107 (57), 109 (28), 133 (34), 151
(55), 184 (26) [M$^+$], $[\alpha]_{20}^{D}$ = +2.6° (c = 1, CHCl$_3$).

(1*R*)-10-(prop-2-enyloxy)camphor (76), ((1*R*,4*R*)-1-(allyloxymethyl)-7,7-dimethylbicyclo
[2.2.1]heptan-2-one)
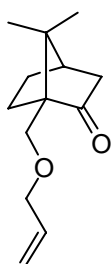
C$_{13}$H$_{20}$O$_2$
208.30 g mol^{-1}

Sodium hydride (1.85 g, 77.3 mmol) was dissolved in anhydrous THF
(100 mL) at 0 °C. (1*R*)-10-hydroxycamphor **(74)** (10.0 g, 59.4 mmol) was
dissolved in anhydrous THF (30 mL) and added through a dropping funnel to
this mixture. Afterwards, the 3-bromoprop-1-ene (5.8 mL, 68.4 mmol)
dissolved in anhydrous THF (100 mL) was added. The solution was stirred for
5 h at 60 °C. The mixture was quenched with ethanol (1 mL), extracted with *n*-
pentane and washed with water. The organic phase was dried over calcium
chloride and removed under reduced pressure. The product was purified with column
chromatography (*n*-pentane: ethyl acetate, 8:2) to yield colorless oil **(76)** (8.0 g, 65%).
^{1}H NMR (400.1 MHz, CDCl$_3$, 300 K): δ = 5.88–5.75 (tdd, 1H, *J* = 5.3 Hz, *J* = 10.6 Hz,
J = 17.2 Hz, C*H*=CH$_2$), 5.23–5.15 (dd, 1H, *J* = 1.7 Hz, *J* = 17.3 Hz, CH=C*H*$_2$) 5.10–5.05 (dd,

1H, J = 1.4 Hz, J = 10.4 Hz, CH=CH_2), 3.92–3.89 (td, 2H, J = 1.5 Hz, J = 5.3 Hz, O-CH_2-CH=CH$_2$), 3.51–3.50 (m, 2H, CH$_2$-O), 2.35–2.28 (ddd, 1H, CH), 2.15–1.35 (m, 6H), 1.00 (s, 3H, CH$_3$), 0.89 (s, 3H, CH$_3$) ppm. ^{13}C NMR (100.6 MHz, CDCl$_3$, 300 K): δ = 217.9, 135.4, 116.7, 72.9, 70.8, 66.8, 61.7, 47.4, 43.9, 27.2, 26.9, 20.6, 20.5 ppm. LR-MS (EI, m/z): 28 (10), 41 (62) [C$_3$H$_5$]$^+$, 55 (25), 67 (29), 81 (28), 95 (35), 109 (100) [C$_8$H$_{13}$]$^+$, 123 (15), 151 (33) [C$_{10}$H$_{15}$O]$^+$, 165 (5) [C$_{10}$H$_{13}$O$_2$]$^+$, 167 (2) [C$_{10}$H$_{15}$O$_2$]$^+$, 179 (3) [C$_{11}$H$_{18}$O$_2$]$^+$, 193 (1) [C$_{12}$H$_{17}$O$_2$]$^+$, 208 (7) [M$^+$]. HRMS spec. calcd. for C$_{13}$H$_{20}$O$_2$: 208.1463; found: 208.1504. $[\alpha]_{20}^{D}$ = +9.7° (c = 1, CHCl$_3$).

(1R)-10-(oct-7-enyloxy)camphor (77), ((1R,4R)-7,7-dimethyl-1-((oct-7-enyloxy)methyl) bicyclo [2.2.1]heptan-2-one)
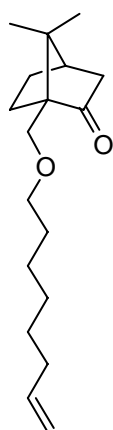
C$_{18}$H$_{30}$O$_2$
278.43 g mol^{-1}

Compound **(77)** was prepared like compound **(76)** using sodium hydride (1.63 g 68.0 mmol) dissolved in anhydrous THF (100 mL), *(1R)*-10-hydroxycamphor (74) (8.80 g, 52.3 mmol) dissolved in anhydrous THF (30 mL) and 8-bromooct-1-ene (10.1 mL, 60.2 mmol) to yield colorless oil **(77)** (8.4g, 58%). ^{1}H NMR (400.1 MHz, CDCl$_3$, 300 K): δ = ppm. 5.80–5.67 (tdd, 1H, J = 6.7 Hz, J = 10.2 Hz, J = 13.4 Hz, CH=CH$_2$), 4.96–4.84 (m, 2H, CH=CH_2), 4.09–4.02 (m, 2H, CH$_2$-O), 3.51–3.31 (m, 2H, O-CH_2-CH=CH$_2$), 2.01–1.92 (m, 5H), 1.52–1.45 (m, 10H), 1.33–1.22 (m, 2H), 0.99 (s, 3H, CH$_3$), 0.88 (s, 3H, CH$_3$). ^{13}C NMR (100.6 MHz, CDCl$_3$, 300 K): δ = 218.1, 139.5, 114.5, 72.1, 67.2, 61.7, 47.4, 44.2, 43.9, 34.1, 29.9, 29.3, 29.2, 27.1, 26.4, 25.6, 21.1, 20.7 ppm. HRMS spec. calcd. for C$_{18}$H$_{30}$O$_2$: 278.2245, found: 278.2241. LR-MS (EI, m/z): 67 (55), 79 (45), 109 (100) [C$_8$H$_{13}$]$^+$, 125 (15), 169 (14), 209 (4), 222 (8), 249 (6), 278 (4) [M$^+$]. $[\alpha]_{20}^{D}$ = +25.4° (c = 1, CHCl$_3$).

(1*S*)-10-(prop-2-enylthio)camphor (78), ((1*S*,4*R*)-1-(allylthiomethyl)-7,7-dimethylbicyclo [2.2.1]heptan-2-one)
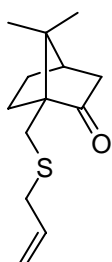
C$_{13}$H$_{20}$OS
224.36 g mol^{-1}

Compound **(78)** was prepared like compound **(76)** using sodium hydride (1.56 g, 65 mmol) dissolved in anhydrous THF (100 mL), (1*S*)-10-camphorthiol **(75)** (9.22 g, 50 mmol) dissolved in anhydrous THF (30 mL) and 3-bromoprop-1-ene (4.9 mL, 57.5 mmol). The solution was stirred for 5 h at RT. After the work-up procedure a colorless oil **(78)** was obtained (6.00 g, 53%). ^{1}H NMR (400.1 MHz, CDCl$_3$, 300 K): δ = 5.80–5.66 (m, 1H, C*H*=CH$_2$), 5.09–5.02 (m, 2H, CH=C*H$_2$*), 3.10–3.07 (m, 2H, S-C*H$_2$*-CH=CH$_2$), 2.70–2.37 (m, 2H, CH$_2$-S), 2.26–1.30 (m, 7H), 0.98 (s, 3H, CH$_3$), 0.84 (s, 3H, CH$_3$) ppm. ^{13}C NMR (100.6 MHz, CDCl$_3$, 300 K): δ = 217.9, 134.0, 117.5, 68.4, 61.3, 48.2, 43.5, 37.4, 28.1, 27.3, 26.0, 20.6, 20.6 ppm. HRMS spec. calcd. for C$_{13}$H$_{20}$OS: 224.1232; found: 224.1235. $[\alpha]_{20}^{D}$ = +10.5° (c = 1, CHCl$_3$).
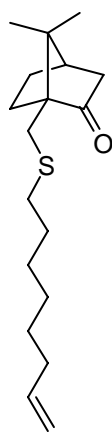
(1*S*)-10-(oct-7-enylthio)camphor (79), ((1*S*,4*R*)-7,7-dimethyl-1-((oct-7-enylthio)methyl) bicyclo[2.2.1]heptan-2-one)

C$_{18}$H$_{30}$OS
294.50 g mol^{-1}

Compound **(79)** was prepared like compound **(76)** using sodium hydride (0.56 g, 23.2 mmol) dissolved in anhydrous THF (100 mL), (1*S*)-10-camphorthiol **(75)** (3.0 g, 17.8 mmol) dissolved in anhydrous THF (30 mL) and 8-bromooct-1-ene (3.4 mL, 20.5 mmol). The solution was stirred for 5 h at RT. After the work-up procedure a colorless oil **(79)** was obtained (4.2 g, 80%). ^{1}H NMR (400.1 MHz, CDCl$_3$, 300 K): δ = 5.84–5.67 (m, 1H, C*H*=CH$_2$), 4.97–4.85 (m, 2H, CH=C*H$_2$*), 2.49–2.45 (m, 2H, S-C*H$_2$*-CH=CH$_2$), 2.35–2.26 (m, 2H, CH$_2$-S), 2.18–2.16 (m, 2H, C*H$_2$*-CH=CH$_2$), 2.15–1.90 (m, 2H, CH$_2$), 1.99–1.97 (m, 4H), 1.43–1.29 (m, 9H), 0.99 (s, 3H, CH$_3$) 0.84 (s, 3H, CH$_3$) ppm. ^{13}C NMR (100.6 MHz, CDCl$_3$, 300 K): δ = 218.0, 139.4, 114.6, 61.3, 72.0, 48.1, 43.8, 35.0, 34.3, 33.1, 29.9, 29.0, 28.6, 28.4, 27.3, 27.0, 20.6, 14.6 ppm. HRMS spec. calcd. for C$_{18}$H$_{30}$OS: 294.2017; found: 294.2025. $[\alpha]_{20}^{D}$ = +28.7° (c = 0.5, CHCl$_3$).

3-(heptafluorobutanoyl)-(1*R*)-10-(prop-2-enyloxy)camphor (80), ((1*R*,4*R*)-1-(allyloxy-methyl)-3-(2,2,3,3,4,4-hexafluorobutanoyl)-7,7-dimethylbicyclo[2.2.1]heptan-2-one)
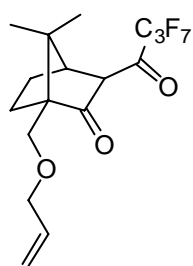
C$_{17}$H$_{19}$F$_7$O$_3$
404.32 g mol^{-1}

Diisopropylamine was dried over calcium hydride and distilled. To *n*BuLi (1.6 M in anhydrous THF, 37.8 mL, 60.5 mmol) in anhydrous THF, freshly distilled diisopropylamine (8.5 mL, 60.5 mmol) was added at -20 °C. After 30 min at -20 °C, (1*R*)-10-(prop-2-enyloxy)camphor **(76)** (10.5 g, 50.4 mmol) dissolved in anhydrous THF (20 mL) was added slowly and the temperature was allowed to rise up to -20 °C to give a slightly yellow solution. Then, the reaction mixture was cooled down to -60 °C and the heptafluorobutanoyl chloride (7.5 mL, 50.4 mmol) was added dropwise. The mixture was stirred at RT for 12 h. The solution was poured into ice and hydrochloric acid (1 M) was added. After extraction with diethyl ether, the organic phase was washed with aqueous solution of hydrochloric acid (1 M) and water and was dried over magnesium sulfate. Afterwards, the organic phase was removed under reduced pressure to yield a dark-red oil. The crude product was then distilled in a Kugelrohr apparatus (180 °C, 0.1 mbar). Further purification was obtained by preparative GC (HP 6890N; 28 m ZB-1; temperature program: 230/60, 8/min, 280, 10 min iso/350; 0.6 bar H$_2$, retention time, %Total): 14.26 min, 98.5%) to yield a slightly yellow to colorless oil **(80)** (3.1 g, 15%). ^{1}H NMR (400.1 MHz, CDCl$_3$, 300 K): δ = 5.79–5.76 (tdd, 1H, *J* = 5.4 Hz, *J* = 10.6 Hz, *J* = 17.2 Hz, C*H*=CH$_2$); 5.25–5.17 (dd, 1H, *J* = 1.7 Hz, *J* = 17.3 Hz, 1H, CH=C*H*$_2$) 5.14–5.05 (dd, 1H, *J* = 1.4 Hz, *J* = 10.4 Hz, CH=C*H*$_2$); 3.95–3.93 (td, 2H, *J* = 1.5 Hz, *J* = 5.4 Hz, O-C*H*$_2$-CH=CH$_2$); 3.58–3.57 (m, 2H, C*H*$_2$-O); 2.36–2.28 (ddd, 1H, *J* = 2.7 Hz, *J* = 4.5 Hz, *J* = 18.2 Hz), 2.07–2.03 (m, 2H, CH$_2$), 1.32–1.26 (m, 2H, CH$_2$), 1.00 (s, 3H, CH$_3$), 0.89 (s, 3H, CH$_3$) ppm. ^{13}C NMR (100.6 MHz, CDCl$_3$, 300 K): δ = 212.0, 134.3, 120.2, 116.3, 72.2, 65.0, 61.1, 48.9, 47.8, 26.0, 25.2, 21.0, 19.0 ppm (-COC$_3$F$_7$ carbon resonances could not be detected). ^{19}F NMR (300.1 MHz, CDCl$_3$, 302 K): δ = -127.4– -127.3 (m, 2F, CF$_2$-CO), -120.1– -117.6 (q, 2F, *J* = 9.0 Hz, CF$_2$), -81.3– -81.2 (t, 3F, *J* = 8.8 Hz, CF$_3$) ppm. HRMS spec. calcd. for C$_{17}$H$_{19}$F$_7$NaO$_3$: 427.1109; found: 427.1114. Preparative GC (HP 6890N; 28 m ZB-1; temperature program: 230/60, 8/min, 280, 10 min iso/350; 0.6 bar H$_2$, retention time, %Total): 14.26 min, 98.5%.

3-(heptafluorobutanoyl)-(1*R***)-10-(oct-7-enyloxy)camphor (81),** ((1*R*,4*R*)-3-(2,2,3,3,4,4-hexafluorobutanoyl)-7,7-dimethyl-1-((oct-7-enyloxy)methyl)bicyclo[2.2.1]heptan-2-one)

C_3F_7
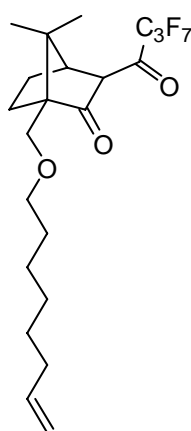
$C_{22}H_{29}F_7O_3$
474.45 g mol-1

Compound **(81)** was prepared like compound **(80)** using *n*BuLi (1.6 M in *n*-hexane, 10.7 mL, 17.1 mmol) dissolved in anhydrous THF (20 mL), freshly distilled diisopropylamine (2.4 mL, 17.1 mmol), (1*R*)-10-(oct-2-enyloxy)-camphor **(76)** (3.2 g, 14.3 mmol) dissolved in anhydrous THF (5 mL), heptafluorobutanoyl chloride (2.1 mL, 14.3 mmol) dissolved in anhydrous THF (10 mL) to yield a slightly yellow to colorless oil **(81)** (0.8 g, 12%). ^{1}H NMR (300.1 MHz, CDCl$_3$, 300 K): δ = 5.80–5.67 (m, 1H, C*H*=CH$_2$), 4.95–4.83 (m, 2H, CH=C*H$_2$*), 4.96–4.84 (m, 2H, CH=C*H$_2$*), 4.09–4.02 (m, 2H, CH$_2$-O), 3.51–3.31 (m, 2H, O-C*H$_2$*-CH=CH$_2$), 2.07-2.03 (m, 1H), 2.01–1.92 (m, 2H, CH$_2$), 1.52–1.45 (m, 8H, CH$_2$), 1.33–1.22 (m, 2H, CH$_2$-) 0.99 (s, 3H, CH$_3$), 0.88 (s, 3H, CH$_3$) ppm. ^{13}C NMR (75.5 MHz, CDCl$_3$, 300 K): δ = 213.1, 139.5, 114.5, 72.1, 67.2, 48.2, 44.2, 34.1, 30.1, 29.9, 29.9, 29.3, 27.1, 27.0, 26.4, 21.1, 20.9, 20.7 ppm (-COC$_3$F$_7$ carbon resonances could not be detected). ^{19}F NMR (300.1 MHz, CDCl$_3$, 302 K): δ = -127.4 – -127.3 (m, 2F, CF$_2$-CO), -120.2– -117.5 (q, 2F, *J* = 9.0 Hz, CF$_2$), -81.3– -81.2 (t, 3F, *J* = 8.8 Hz, CF$_3$) ppm. LR-MS (EI, m/z): 69 (50), 109 (100) [C$_8$H$_{13}$]$^+$, 152 (10), 222 (13), 278 (7) [C$_{18}$H$_{29}$O$_2$]$^+$, 333 (4), 475 (5) [M$^+$]. $[\alpha]_{20}^D$ = +21.3° (c = 1, CHCl$_3$).

3-(heptafluorobutanoyl)-(1*S***)-10-(prop-2-enylthio)camphor (82),** ((1*S*,4*R*)-1-(allylthio-methyl)-3-(2,2,3,3,4,4-hexafluorobutanoyl)-7,7-dimethylbicyclo[2.2.1]heptan-2-one)

C_3F_7
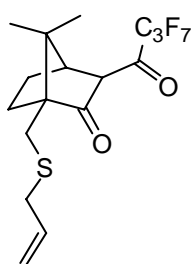
$C_{17}H_{19}F_7O_2S$
420.39 g mol-1

Compound **(82)** was prepared like compound **(80)** using *n*BuLi (1.6 M in *n*-hexane, 10.7 mL, 17.1 mmol) dissolved in anhydrous THF (20 mL), freshly distilled diisopropylamine (2.4 mL, 17.1 mmol), (1*S*)-10-(prop-2-enylthio)camphor **(78)** (3.2 g, 14.3 mmol) dissolved in anhydrous THF (5 mL), heptafluorobutanoyl chloride (2.1 mL, 14.3 mmol) dissolved in anhydrous THF (10 mL) to yield a slightly yellow to colorless oil **(82)** (0.9 g, 13%). ^{1}H NMR (400.1 MHz, CDCl$_3$, 300 K): δ = 5.80–5.66 (m, 1H, C*H*=CH$_2$); 5.09–5.02 (m, 2H, CH=C*H$_2$*), 3.10–3.07 (m, 2H, S-C*H$_2$*-CH=CH$_2$), 2.91–2.89 (m, 1H), 2.70–2.37 (m, 2H, CH$_2$-S), 2.26–1.30 (m, 5H, CH$_2$) 0.98 (s, 3H, CH$_3$), 0.84 (s, 3H, CH$_3$) ppm. ^{13}C NMR (100.6 MHz, CDCl$_3$, 300 K): δ = 212.4, 139.2, 118.0, 115.6, 71.0, 68.0, 51.7,

40.9, 30.4 26.1, 25.6, 22.6, 22.1 ppm (COC_3F_7 carbon resonances could not be detected). ^{19}F NMR (300.1 MHz, $CDCl_3$, 302 K): δ = -127.5 – -127.4 (m, 2F, $-CF_2$-CO), -120.1– -117.6 (q, 2F, J = 9.0 Hz, CF_2), -81.2– -81.1 (t, 3F, J = 8.8 Hz, CF_3) ppm. LR-MS (EI, m/z): 109 (30) $[C_8H_{13}]^+$, 251 (25), 291 (40), 329 (38), 374 (25) $[C_{14}H_{14}F_7O_2]^+$, 379 (52) $[C_{14}H_{14}F_7O_2S]^+$, 419 (100) $[M^+$-H], 420 (19) $[M^+]$.

3-(heptafluorobutanoyl)-(1S)-10-oct-7-enylthio)camphor (83), ((1S,4R)-3-(2,2,3,3,4,4-hexafluorobutanoyl)-7,7-dimethyl-1-((oct-7-enylthio)methyl)bicycle [2.2.1]heptan-2-one)
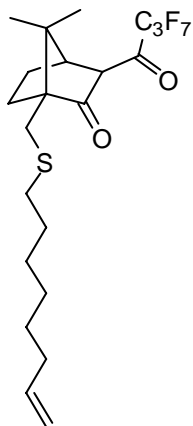

$C_{22}H_{29}F_7O_2S$
490.52 g mol^{-1}

Compound **(83)** was prepared like compound **(80)** using nBuLi (1.6 M in n-hexane, 10.7 mL, 17.1 mmol) dissolved in anhydrous THF (20 mL), freshly distilled diisopropylamine (2.4 mL, 17.1 mmol), (1S)-10-(oct-7-enylthio)camphor **(79)** (4.2 g, 14.3 mmol) dissolved in anhydrous THF (5 mL), heptafluorobutanoyl chloride (2.1 mL, 14.3 mmol) dissolved in anhydrous THF (10 mL) to yield a slightly yellow to colorless oil **(83)** (0.9 g, 14%). ^{1}H NMR (400.1 MHz, $CDCl_3$, 300 K): δ = 5.82–5.60 (m, 1H, CH=CH_2); 5.07–5.02 (m, 2H, CH=CH_2); 2.91–2.89 (m, 1H), 2.49–2.45 (m, 2H, S-CH_2-CH=CH$_2$), 2.35–2.26 (m, 2H, CH_2-S), 2.19–2.17 (m, 2H, CH_2-CH=CH$_2$), 2.15-1.90 (m, 2H, CH_2), 1.99–1.97 (m, 4H, CH_2), 1.43–1.29 (m, 5H, CH_2), 1.09 (s, 3H, CH_3), 0.98 (s, 3H, CH_3) ppm. ^{13}C NMR (100.6 MHz, $CDCl_3$, 300 K): δ = 213.5, 139.1, 118.0, 115.7, 106.8, 100.6, 69.3, 51.0, 40.2, 33.9, 33.5, 33.0, 30.6, 29.6, 29.2, 28.6, 21.9, 21.4 ppm (-COC_3F_7 carbon resonances could not be detected). ^{19}F NMR (300.1 MHz, $CDCl_3$, 302 K): δ = -127.5 – -127.4 (m, 2F, CF_2-CO), -120.0 – -117.6 (q, 2F, J = 9.0 Hz, CF_2), -81.2 – -81.1 (t, 3F, J = 8.8 Hz, CF_3) ppm. LR-MS (EI, m/z): 69 (55), 109 (32) $[C_8H_{13}]^+$, 238 (12), 280 (36), 294 (9), 322 (28), 339 (21), 430 (12), 458 (20), 491 (17) $[M^+]$.

8.7.2. Immobilization of 1,3-Diketonates

[3-(heptafluorobutanoyl)-(1*S*)-10-propoxy-camphorate]-poly(dimethylsiloxane) (90),
[(1*S*,4*R*)-3-(2,2,3,3,4,4,4-heptafluorobutanoyl)-7,7-dimethyl-1-(propoxymethyl)bicyclo
[2.2.1]heptan-2-one]-poly(dimethylsiloxane)
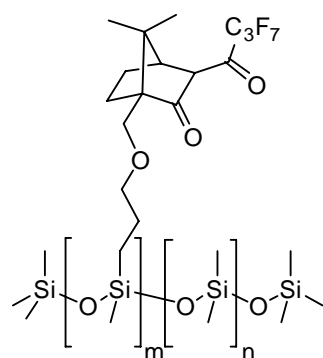
3-(heptafluorobutanoyl)-(1*R*)-10-(prop-2-enyloxy)camphor (166 mg, 0.4 mmol) **(80)** was added to a solution of HMPS **(4)** (10.2% SiH, 1.64 g, 1 mmol) in anhydrous toluene. After 15 min of stirring at RT, the Pt catalyst (Karstedt's catalyst **(11)**, (0.1 M in xylene, 0.05 eq.) or H_2PtCl_6 **(58)** (8 mg, 0.02 mmol, 0.05 eq.) dissolved in anhydrous THF (1 mL)) was added dropwise and the solution was refluxed (alternatively, ultrasonication at RT) for 24 h under an argon atmosphere. The hydrosilylation procedure was continued as described in chapter 8.4.1. (compound **(9)**). Purification of the crude polymer and, in particular, removing the rest of the catalyst was performed by passing the polymer dissolved in toluene through a short column of activated charcoal. Volatiles were removed under reduced pressure. The solution was filtered and the solvent was evaporated to yield yellow-brown polysiloxane **(90)** (1.60 g). ^{1}H NMR (400.1 MHz, CDCl$_3$, 300 K): δ = 3.55–3.30 (m), 3.14 (s), 1.48–0.76 (m), 0.19– -0.19 (bs, Si-CH$_3$) ppm. ^{19}F NMR (300.1 MHz, CDCl$_3$, 302 K): δ = -127.3 – -127.2 (m, 2F, CF$_2$-CO), -120.2– -117.7 (m, 2F, CF$_2$), -81.4 – -81.3 (m, 3F, CF$_3$) ppm. LR-MS (EI, m/z): 73 (100) [C$_4$H$_9$Si]$^+$, 163 (32) [C$_5$H$_{15}$O$_2$Si$_2$]$^+$, 237 (100) [C$_{27}$H$_{21}$O$_3$Si]$^+$, 281 (35) [C$_8$H$_{25}$O$_3$Si$_4$]$^+$, 355 (33) [C$_{10}$H$_{31}$O$_4$Si$_5$]$^+$, 503 (10) [C$_{14}$H$_{43}$O$_6$Si$_7$]$^+$, 593 (6) [C$_{16}$H$_{49}$O$_8$Si$_8$]$^+$, 667 (5), 1217 (3), 1365 (2) [M$^+$]. LR-MS (ESI pos, CH$_2$Cl$_2$, m/z): 170 (13), 389 (53), 647 (72), 781 (65), 931 (53).

8.7.3. Metalation of Polysiloxane-Immobilized 1,3-Diketonates

Europium(III)-tris[3-(heptafluorobutanoyl)-(1*S*)-10-propoxy-camphorate]-poly(dimethylsiloxane), Chirasil-Eu(III)-Propoxy-Camphor (91), europium(III)-tris[(1*S*,4*R*)-3-(2,2,3,3,4,4,4-heptafluorobutanoyl)-7,7-dimethyl-1-(propoxymethyl)bicyclo[2.2.1]heptan-2-one]-poly(dimethylsiloxane)
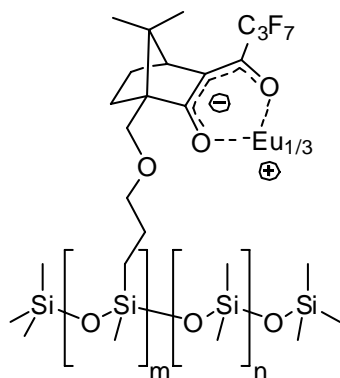
To a solution of sodium hydride (263 mg, 11.0 mmol) dissolved in anhydrous toluene (10 mL), the polymer ligand **(90)** (0.99 g, 0.7 mmol) dissolved in anhydrous toluene (20 mL) was added slowly under an argon atmosphere. The solution was stirred for 10 h at RT. Afterwards the solution was filtered through a glass frit (G3). To the filtrate, europium chloride hexahydrate (0.54 g, 1.5 mmol) dissolved in methanol (20 mL) was added. The solution was stirred for 30 min at RT and 2 h under reflux. Afterwards, the solvent was removed under reduced pressure and the residue was taken up in *n*-hexane. The solution was filtered and washed with H_2O, dried over magnesium sulfate and the solvent was removed under reduced pressure to yield viscous, light yellow polysiloxane **(91)** (0.98 g). ^{1}H NMR (400.1 MHz, CDCl$_3$, 300 K): δ = 3.44–2.86 (m), 1.49-0.76 (m), 0.19– -0.19 (bs, Si-CH$_3$) ppm. ^{19}F NMR (300.1 MHz, CDCl$_3$, 302 K): δ = -127.4 – -127.3 (m, 2F, CF$_2$-CO), -120.1 – -117.6 (m, 2F, CF$_2$), -81.3 – -81.2 (m, 3F, CF$_3$) ppm. LR-MS (EI, m/z): 73 (32) [C$_4$H$_9$Si]$^+$, 147 (35), 221 (100), 281 (13), 355 (33) [C$_{10}$H$_{31}$O$_4$Si$_5$]$^+$, 429 (11), 503 (35) [C$_{14}$H$_{43}$O$_6$Si$_7$]$^+$, 563 (67), 741 (83), 815 (80), 903 (72), 963 (56), 1067 (34), 1127 (25), 1201 (13) [M$^+$]. LR-MS (ESI pos, THF, m/z): 552, 614, 634, 664, 692, 708, 738, 762, 782, 798, 817, 856, 872, 886, 902, 930, 946, 976, 990, 1004, 1020, 1034, 1050, 1064, 1078, 1108, 1124, 1152, 1168, 1182, 1198, 1221, 1256, 1272, 1330, 1346, 1388, 1404, 1425, 1462, 1494, 1536, 1552, 1568, 1585, 1611, 1626, 1644, 1684, 1701, 1717, 1760, 1776, 1793, 1832, 1849, 1865, 1906, 1923, 1940, 1996, 2013, 2072.
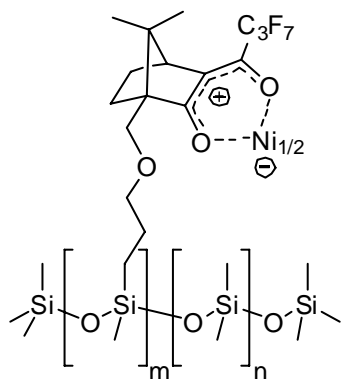
**Nickel(II)-bis[3-(heptafluorobutanoyl)-(1*S*)-10-propoxy-camphorate]-
poly(dimethylsiloxane), Chirasil-Ni(II)-Propoxy-Camphor (92),** nickel(II)-bis[(1*S*,4*R*)-3-
(2,2,3,3,4,4,4-heptafluorobutanoyl)-7,7-dimethyl-1-(propoxymethyl)bicyclo[2.2.1]heptan-2-
one]-poly(dimethylsiloxane)

Polysiloxane **(92)** was prepared like polysiloxane **(91)** using sodium hydride (300 mg, 12.4 mmol) dissolved in anhydrous toluene (10 mL), the polymer ligand **(90)** (1.0 g, 0.7 mmol) dissolved in anhydrous toluene (20 mL) and nickel(II)-chloride (200 mg, 1.5 mmol) dissolved in methanol (20 mL) to yield a viscous green-brown polysiloxane **(92)** (0.98 mg). ^{1}H NMR (400.1 MHz, CDCl$_3$, 300 K): δ = 3.43–2.83 (m), 1.45–0.77 (m), 0.19 − -0.19 (bs, Si-CH$_3$) ppm. ^{19}F NMR (300.1 MHz, CDCl$_3$, 302 K): δ = -127.4 − -127.3 (m, 2F, CF$_2$-CO), -120.1 − -117.6 (m, 2F, CF$_2$), -81.3 − -81.2 (m, 3F, CF$_3$) ppm.

8.7.4. Separation of Chalcogran

The separation of enantiomers of chalcogran **(94)a–d** a was performed on a Thermo Trace PolarisQ GC-MS equipped with a split injector (250 °C), a FID (250 °C) and a quadrupole ion trap MS using a chiral separation column (Chirasil-β-Dex **(13)**,[169, 333, 334] Chirasil-Eu(III)-Propoxy-Camphor **(91)**, or Chirasil-Ni(II)-Propoxy-Camphor **(92)**, 25.0 m×250 μm i.d., 250 nm film thickness). Capillaries were coated by the static method described by Grob.[315] Helium was used as carrier gas (100 kPa). The measurements were repeated three times at each temperature in steps of 10 K between 40–120 °C.

8.7.5. On-Column Intramolecular Diels-Alder Experiments

On-column intramolecular Diels-Alder experiments were performed on a Thermo Trace PolarisQ GC-MS equipped with a split injector (250 °C), a FID (250 °C) and a quadrupole ion trap MS. For the intramolecular Diels-Alder reaction of 2-furanylmethylacrylate derivatives **(99)**, **(100)** and **(101)**, a fused-silica capillary (Chirasil-Eu(III)-Propoxy-Camphor **(91)** (25 m×250 μm i.d., 250 nm film thickness)) was used. Capillaries were coated by the static method described by Grob.[315] Helium was used as carrier gas. The measurements were

repeated three times at each temperature in steps of 4 K between 50–180 °C and a inlet pressure of 80 kPa.

8.8. Experimental Section - Chapter 7

8.8.1. Salen Ligand Synthesis

4-(allyloxy)-2-*tert*-butylphenol (111)a
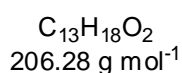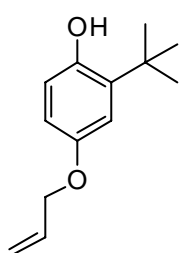
A mixture of 2-*tert*-butyl hydroquinone **(109)** (5.5 g, 33.1 mmol) and anhydrous potassium carbonate (2.2 g, 16.2 mmol) in anhydrous acetonitrile (75 mL) was stirred for 30 min at RT. Subsequently, 3-bromoprop-1-ene **(110)a** (3.9 g, 32.1 mmol) and potassium iodide (0.3 g, 1.8 mmol) were added and the mixture was allowed to reflux for 3 h under an argon atmosphere. The mixture was cooled to RT, poured into H_2O (200 mL) and extracted with diethyl ether (3×100 mL). The organic layers were combined, washed with brine (2×100 mL), dried over magnesium sulfate and concentrated. The product was purified by silica gel chromatography (*n*-hexane:ethyl acetate, 7:3) to yield product **(111)a** as a colorless oil (5.9 g, 87%). ^{1}H NMR (300.1 MHz, CDCl$_3$, 300 K): δ = 6.82–6.46 (m, 3H, Ar-H), 5.95 (m, 1H, C*H*=CH$_2$), 5.36–5.21 (m, 2H, CH=C*H$_2$*), 4.41–4.38 (m, 2H, O-CH$_2$), 1.31 (s, 9H, C(CH$_3$)$_3$) ppm. ^{13}C NMR (75.5 MHz, CDCl$_3$, 300 K): δ = 152.8, 148.8, 137.9, 134.2, 117.9, 117.1, 112.6, 112.0, 69.9, 34.4, 29.9 ppm. LR-MS (EI, m/z):207 (100) [M+H]. FT-IR [cm^{-1}]: 3368 (s), 2957 (s), 2868 (s), 1706 (vs), 1651 (s), 1590 (m), 1505 (m), 1485 (m), 1419 (m), 1390 (m), 1363 (m), 1257 (m), 1194 (m), 1077 (m), 1040 (w), 996 (w), 930 (w), 872 (w), 806 (w), 775 (w).

$C_{13}H_{18}O_2$
206.28 g mol^{-1}

2-*tert*-butyl-4-(hex-4-enyloxy)phenol (111)b
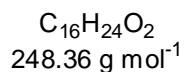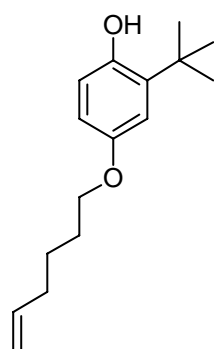
Compound **(111)b** was prepared like compound **(111)a** using 2-*tert*-butyl hydroquinone **(109)** (4.0 g, 24.1 mmol), anhydrous potassium carbonate (1.6 g, 11.8 mmol), 6-bromohex-1-ene **(110)b** (3.8 g, 23.3 mmol) and potassium iodide (0.2 g, 1.2 mmol). The product was purified by silica gel chromatography (*n*-hexane:ethyl acetate, 7:3) to yield product **(111)b** as colorless oil (5.1 g, 85%). ^{1}H NMR (300.1 MHz, CDCl$_3$, 300 K): δ = 6.82-6.46 (m, 3H, Ar-H), 5.82-5.69 (tdd, 1H, *J* = 5.3 Hz, *J* = 10.6 Hz, *J* = 17.3 Hz, C*H*=CH$_2$) 4.99–4.87 (m, 2H, CH=C*H$_2$*), 4.10–4.02 (m, 2H, O-CH$_2$), 2.08–1.65 (m, 6H), 1.31 (s, 9H, C(CH$_3$)$_3$) ppm. ^{13}C NMR

$C_{16}H_{24}O_2$
248.36 g mol^{-1}

(75.5 MHz, CDCl$_3$, 300 K): δ = 153.2, 148.7, 139.0, 138.0, 117.5, 115.2, 112.7, 111.0, 68.8, 35.1, 33.9, 30.1, 30.1, 30.1, 25.8, 21.4 ppm. LR-MS (EI, m/z): 249 (100) [M+H]. FT-IR [cm^{-1}]: 3391 (s), 2953 (s), 2867 (s), 1707 (vs), 1652 (s), 1590 (m), 1506 (m), 1437 (m), 1389 (m), 1364 (m), 1287 (w), 1258 (w), 1195 (w), 1076 (w), 1042 (w), 995 (w), 931 (w), 910 (w), 872 (w), 806 (w), 775 (w).

2-*tert*-butyl-4-(oct-4-enyloxy)phenol (111)c
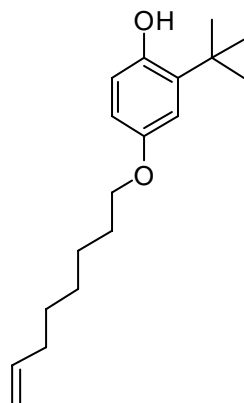
C$_{18}$H$_{28}$O$_2$
276.41 g mol^{-1}

Compound (111)c was prepared like compound (111)a using 2-*tert*-butyl hydroquinone (109) (5.0 g, 30.1 mmol), anhydrous potassium carbonate (2.0 g, 14.7 mmol), 8-bromooct-1-ene (110)c (4.9 mL, 29.2 mmol) and potassium iodide (250 mg, 1.5 mmol). The product was purified by silica gel chromatography (*n*-hexane:ethyl acetate, 85:15) to yield (111)c (7.1 g, 85%) as a colorless oil. ^{1}H NMR (300.1 MHz, CDCl$_3$, 300 K): δ = 6.80–6.58 (m, 3H, Ar-H), 5.82–5.73 (tdd, 1H, *J* = 6.7 Hz, *J* = 10.1 Hz, *J* = 16.9 Hz), 5.00–4.88 (m, 2H, CH=C*H$_2$*), 3.86–3.79 (m, 2H, O-CH$_2$-), 2.00–1.29 (m, 10H), 1.31 (s, 9H, C(CH$_3$)$_3$) ppm. ^{13}C NMR (75.5 MHz, CDCl$_3$, 300 K): δ = 153.3, 148.5, 139.4, 138.6, 117.1, 115.2, 114.7, 114.6, 68.9, 35.0, 34.3, 29.8, 29.8, 29.8, 29.6, 26.3 ppm. FT-IR [cm^{-1}]: 3523 (s), 3416 (s), 3076 (s), 2996 (s), 2930 (s), 2859 (s), 1710 (vs), 1640 (s), 1587 (m), 1506 (m), 1484 (m), 1462 (m), 1424 (m), 1389 (m), 1363 (m), 1330 (m), 1289 (m), 1273 (m), 1254 (m), 1195 (w), 1143 (w), 1044 (w), 995 (w), 909 (w), 873 (w), 854 (w), 800 (w), 776 (w), 754 (w), 726 (w). HRMS (ESIpos) calcd for C$_{18}$H$_{28}$Na$_1$O$_2$ [M]$^+$ 299.198078, found 299.198147.

5-(allyloxy)-3-*tert*-butyl-2-hydroxybenzaldehyde (115)a
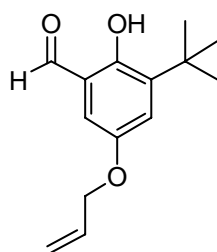
C$_{14}$H$_{18}$O$_3$
234.29 g mol^{-1}

2,6-Lutidine (114) (3.1 g, 29.1 mmol) and compound (111)a (5.0 g, 24.2 mmol) were dissolved in anhydrous toluene (200 mL). The resulting yellow heterogeneous mixture was stirred at RT under an argon atmosphere for 10 min, followed by the addition of paraformaldehyde (112) (2.9 g) and tin tetrachloride (1.9 g, 7.3 mmol). The mixture was heated under reflux at 90 °C for 6 h and the reaction progress was monitored by TLC. The reaction mixture was allowed to cool to RT and water (200 mL) and diethyl ether (200 mL) were added. The resulting emulsion was filtered through a pad of ceolite and the layers were separated. The organic layer was washed with

water, brine, dried over anhydrous magnesium sulfate and was then concentrated. The product was purified by silica gel chromatography (*n*-hexane:ethyl acetate, 7:3) or by preparative HPLC (MeOH/H_2O (8:2), Nucleodur 100-10-C18/A, NW50, 48 mm i.d., 198×48 mm, 06/01, 35.0 mL min^{-1}, 65.3 mg mL^{-1}, 3.8 MPa, 308 K, SPD-20A, 220 nm, 0.1 mm) to yield product **(115)a** as a yellow oil (3.0 g, 53%). ^{1}H NMR (300.1 MHz, $CDCl_3$, 300 K): δ = 11.51 (s, 1H), 9.84 (s, 1H, CHO), 7.10–7.09 (d, 1H, *J* = 3.0 Hz, Ar-H), 6.74–6.73 (d, 1H, *J* = 3.1 Hz, Ar-H) 6.15–6.02 (tdd, 1H, *J* = 5.3 Hz, *J* = 10.6 Hz, *J* = 17.3 Hz, C*H*=CH$_2$), 5.49–5.41 (dd, 1H, *J* = 1.6 Hz, *J* = 17.3 Hz, CH=C*H*$_2$), 5.36–5.31 (dd, 1H, J = 1.4 Hz, J = 10.5 Hz, CH=C*H*$_2$), 4.56–4.53 (td, 2H, *J* = 1.5 Hz, *J* = 5.3 Hz, O-CH$_2$-), 1.43 (s, 9H, C(CH$_3$)$_3$) ppm. ^{13}C NMR (75.5 MHz, $CDCl_3$, 300 K): 196.0, 153.3, 149.8, 139.5, 133.5, 129.8, 118.2, 117.8, 112.3, 70.2, 34.4, 31.6 ppm. FT-IR [cm^{-1}]: 3077(s), 2999 (s), 2929 (s), 2857 (s), 1651 (m), 1611 (m), 1455 (m), 1435 (m), 1391 (m), 1361 (m), 1325 (m), 1278 (m), 1255 (m), 1227 (m), 1211 (m), 1190 (m), 1147 (m), 1051 (m), 996 (w), 909 (w), 859 (w), 836 (w), 808 (w), 797 (w), 762 (w), 719 (w). HRMS (EI) calcd for $C_{14}H_{18}O_3$ [M]$^+$ 234.125747, found 234.125594.

3-*tert*-butyl-2-hydroxy-5-(hex-4-enyloxy)benzaldehyde (115)b
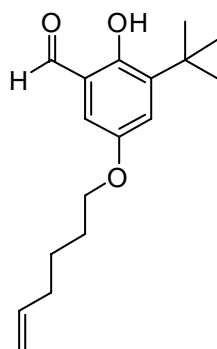
C$_{17}$H$_{24}$O$_3$
276.37 g mol^{-1}

Compound **(115)b** was prepared like compound **(115)a** using 2,6-lutidine **(114)** (2.6 g, 24.6 mmol), compound **(111)b** (5.1 g, 20.5 mmol), paraformaldehyde **(112)** (2.5 g) and tin tetrachloride (1.6 g, 6.2 mmol). The product was purified by silica gel chromatography (*n*-hexane:ethyl acetate, 7:3) or by preparative HPLC (DCM:MeOH, 8:30, Nucleodur 100-10-C18/A, NW50, 48 mm i.d., 198×48 mm, 06/01, 35.0 mL min^{-1}, 80.0 mg mL^{-1}, 4.1 MPa, 308 K, UV, 220 nm, 0.2 mm) to yield product **(115)b** as a yellow oil (2.9 g, 52%). HPLC-MS (125 mm Nucleodur 100-5-C18ec, 2.0 mm i.d., MeOH:H_2O (85:15), 0.2 mL min^{-1}, 6.0 Pa, 308 K, DAD, 220 nm, retention time, %Total): 4.52 min ($C_{16}H_{24}O_2$), 23.6%, 9.60 min ($C_{17}H_{24}O_3$), 9.7% 27.76 min ($C_{22}H_{34}O_2$) 3.8%. ^{1}H NMR (300.1 MHz, $CDCl_3$, 300 K): δ = 11.41 (s, 1H), 9.75 (s, 1H, CHO), 7.10–7.09 (d, 1H, *J* = 3.0 Hz, Ar-H), 6.74–6.73 (d, 1H, *J* = 3.0 Hz, Ar-H), 5.84–5.70 (tdd, 1H, *J* = 5.3 Hz, *J* = 10.6 Hz, *J* = 17.3 Hz, C*H*=CH$_2$) 5.01–4.94 (dd, 1H, *J* = 1.6 Hz, *J* = 17.3 Hz, CH=C*H*$_2$), 4.93–4.89 (dd, 1H, J = 1.4 Hz, J = 10.5 Hz, CH=C*H*$_2$), 3.89-3.81 (m, 2H, O-CH$_2$-), 2.11–2.04 (m, 2H, C*H*$_2$-CH=CH$_2$), 1.79-1.68 (m, 2H, O-CH$_2$-C*H*$_2$-), 1.57–1.47 (m, 3H), 1.34 (s, 9H, C(CH$_3$)$_2$) ppm. ^{13}C NMR (75.5 MHz, $CDCl_3$, 300 K): 196.0, 150.1, 149.1, 139.1, 139.1, 129.4, 117.9, 116.7, 112.4, 68.8, 34.4, 33.9, 31.6, 28.7, 25.9

ppm. FT-IR [cm^{-1}]: 3077 (s), 2946 (s), 2870 (s), 2740 (s), 1651 (s), 1611 (m), 1436 (m), 1392 (m), 1361 (m), 1325 (m), 1278 (m), 1255 (m), 1227 (w), 1190 (w), 1148 (w), 1051 (w), 995 (w), 961 (w), 911 (w), 837 (w), 809 (w), 797 (w), 762 (w), 718 (w). HRMS (EI) calcd for C$_{17}$H$_{24}$O$_3$ [M]$^+$ 276.172256, found 276.172546.

3-*tert*-butyl-2-hydroxy-5-(oct-7-enyloxy)benzaldehyde (115)c
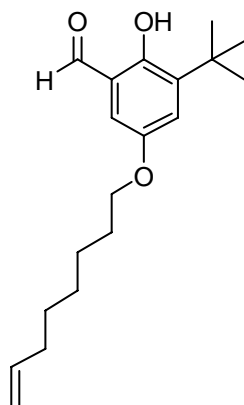
Compound **(115)c** was prepared like compound **(115)a** using 2,6-lutidine **(114)** (2.5 g, 23.3 mmol), **(111)c** (4.0 g, 19.4 mmol), paraformaldehyde **(112)** (2.3 g) and tin tetrachloride (1.5 g, 5.8 mmol) The product was purified by silica gel chromatography (*n*-hexane:ethyl acetate, 85:15) to yield product **(115)c** as a yellow oil (3.8 g, 64%). HPLC-MS (125 mm Nucleodur 100-5-C18ec, 2.0 mm i.d., MeOH:H$_2$O (80:20), 0.2 mL min^{-1}, 7.1 MPa, 308 K, DAD, 220 nm, retention time, %Total): 35.04 min (C$_{19}$H$_{28}$O$_3$), 94.0%. ^{1}H NMR (300.1 MHz, CDCl$_3$, 300 K): δ = 11.41 (s, 1H), 9.75 (s, 1H, CHO), 7.10–7.09 (d, 1H, *J* = 3.0 Hz, Ar-H), 6.74–6.73 (d, 1H, *J* = 3.0 Hz, Ar-H), 5.82–5.67 (dd, 1H, *J* = 1.7 Hz, *J* = 17.3 Hz, CH=C*H*$_2$), 4.97–4.85 (dd, 1H, *J* = 1.4 Hz, *J* = 10.5 Hz, CH=C*H*$_2$), 3.88–3.84 (m, 2H, O-CH$_2$), 2.03–1.97 (m, 2H, C*H*$_2$-CH=CH$_2$), 1.76–1.67 (m, 2H, O-CH$_2$-C*H*$_2$), 1.57–1.47 (m, 7H), 1.34 (s, 9H, C(CH$_3$)$_2$) ppm. ^{13}C NMR (75.5 MHz, CDCl$_3$, 300 K): δ = 197.0, 156.46, 140.4, 139.4, 124.7, 120.2, 114.8, 114.7, 113.0, 35.4, 33.1, 29.6; 29.5, 29.2, 28.6, 28.4, 26.3 ppm. FT-IR [cm^{-1}]: 3084 (s), 2959 (s), 2913 (s), 2871 (s), 1650 (s), 1611 (s), 1483 (m), 1435 (m), 1422 (m), 1391 (m), 1361 (m), 1323 (m), 1276 (m), 1256 (m), 1225 (m), 1211 (m), 1191 (m), 1145 (m), 1100 (w), 1044 (w), 1020 (w), 986 (w), 964 (w), 926 (w), 898 (w), 837 (w), 813 (w), 796 (w), 762 (w), 722 (w). HRMS (EI) calcd for C$_{19}$H$_{28}$O$_3$ [M]$^+$ 304.203790, found 304.203843.

Unsymmetrical Salen Ligand (R,R)-(116)a, 4-(allyloxy)-2-*tert*-butyl-6-((*E*)-((1*R*,2*R*)-2-((*E*)-3,5-di-*tert*-butyl-2-hydroxybenzylideneamino)cyclohexylimino)methyl)phenol
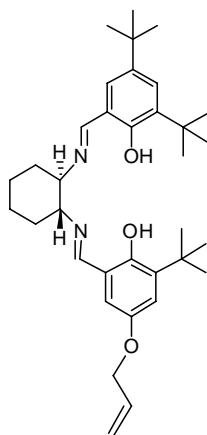
$C_{35}H_{50}N_2O_3$
546.78 g mol^{-1}

A three-necked flask equipped with a stirrer, a reflux condenser, and an addition funnel was charged with (*R,R*)-1,2-diammoniumcyclohexane mono-(+)-tartrate salt **(118)** (0.86 g, 3.2 mmol), K_2CO_3 (0.90 g, 6.5 mmol) and distilled H_2O (1.5 mL). The mixture was stirred until dissolution was achieved and then ethanol (6 mL) was added. The resulting cloudy mixture was heated to reflux (75–80 °C) and a solution of 3-di-*tert*-butyl-2-hydroxybenzaldehyd **(117)** (1.15 g, 4.9 mmol) and compound **(115)a** (0.38 g, 1.6 mmol) dissolved in ethanol (5 mL) was added dropwise. The funnel was rinsed with ethanol and the yellow slurry was stirred at reflux for 2 h before heating was discontinued. The organic phase was washed with water and brine. After drying over magnesium sulfate the solvent was removed under vacuum to give a mixture of the desired product (*R,R*)-**(116)a** (7.4%), the ligand (*R,R*)-**(103)a** (65.7%) as well as the symmetric disubstituted ligand (*R,R*)-**(116)d** (7.2%) as a yellow crystalline powder. GC (15 m RTX 1, 240/80, 8/min, 330, 10 min, 360, 0.5 bar H_2, retention time, %Total): 23.28 min ($C_{36}H_{54}N_2O_2$), 65.7%, 24.04 min ($C_{35}H_{50}N_2O_3$), 7.4%, 24.69 min ($C_{34}H_{46}N_2O_4$), 7.2%. The mixture of salen ligands could be separated by preparative HPLC (MeOH:H_2O (95:5), Nucleodur 100-10-C18/A, NW50, 48 mm i.d., 198×48 mm, 06/01, 35.0 mL min^{-1}, 115.0 mg mL^{-1}, 2.1 MPa, 308 K, SPD-20A, 220 nm, 0.1 mm) to give (*R,R*)-**(116)a** as a yellow powder. ^{1}H NMR (400.1 MHz, CDCl$_3$, 300 K): δ = 13.57 (s, 2H), 8.32-8.27 (d, 2H, *J* = 20.8 Hz, CH=N), 7.35 (s, 1H, Ar-H), 7.01–6.96 (m, 2H, Ar-H), 6.54 (bs, 1H, Ar-H), 6.08–5.98 (tdd, 1H, *J* = 6.7 Hz, *J* = 10.1 Hz, *J* = 16.9 Hz), 5.41–5.36 (dd, 1H, *J* = 1.7 Hz, *J* = 17.3 Hz, CH=C*H*$_2$), 5.28–5.26 (dd, 1H, *J* = 1.4 Hz, *J* = 10.4 Hz, CH=C*H*$_2$), 4.45–4.36 (m, 2H, O-CH$_2$), 2.02–1.50 (m, 10H), 1.44 (s, 9H, C(CH$_3$)$_3$), 1.42 (s, 9H, C(CH$_3$)$_3$), 1.26 (s, 9H, C(CH$_3$)$_3$) ppm. ^{13}C NMR (100.6 MHz, CDCl$_3$, 300 K): δ = 165.7, 165.1, 157.6, 133.2, 125.6, 117.4, 117.1, 112.2, 71.8, 69.2, 34.6, 34.5, 33.7, 32.7, 32.6, 31.0, 29.1, 28.9, 23.9 ppm. FT-IR [cm^{-1}]: 2951 (s), 2859 (s), 1627 (s), 1596 (s), 1467 (m), 1437 (m), 1389 (m), 1360 (m), 1329 (m), 1273 (m), 1252 (m), 1203 (m), 1173 (m), 1156 (m), 1141 (m), 1096 (m), 1049 (w), 981 (w), 927 (w), 878 (w), 861 (w), 827 (w), 800 (w), 772 (w), 764 (w), 731 (w), 712 (w). HRMS (ESIpos) calcd for $C_{35}H_{51}N_2O_3$ [M]$^+$ 547.389276, found 547.389421. $[\alpha]_{20}^D$ = -288,7° (c = 1, CHCl$_3$).

Unsymmetrical Salen Ligand (*R,R*)-(116)b, 2,4-di-*tert*-butyl-6-((*E*)-((1*R*,2*R*)-2-((*E*)-3-*tert*-butyl-5-(hex-5-enyloxy)-2-hydroxybenzylideneamino)cyclohexylimino)methyl)phenol

$C_{38}H_{56}N_2O_3$
588.86 g mol^{-1}
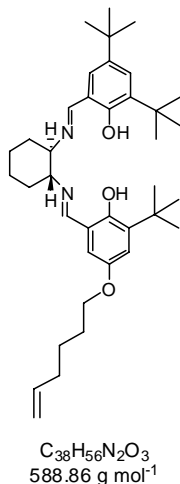
Compound (*R,R*)-(116)b was prepared like compound (*R,R*)-(116)a using (*R,R*)-1,2-diammoniumcyclohexane mono-(+)-tartrate salt (118) (0.34 g, 0.7 mmol), K$_2$CO$_3$ (0.27 g, 1.9 mmol), 3-di-*tert*-butyl-2-hydroxybenzaldehyd (117) (0.34 g, 4.9 mmol) and compound (115)b (0.40 g, 1.5 mmol) to give a mixture of the desired product (*R,R*)-(116)b (34.8%), the ligand (*R,R*)-(103)a (21.9%) as well as the symmetric disubstituted ligand (*R,R*)-(116)e (12.5%) as a yellow crystalline powder. HPLC-MS (125 mm Nucleodur 100-5-C18ec, 4.0 mm i.d., MeOH:H$_2$O (95:5), 0.8 mL min^{-1}, 5.6 MPa, 308 K, UV, 220 nm, retention time, %Total): 19.21 min (C$_{36}$H$_{54}$N$_2$O$_2$), 21.9%, 21.14 min (C$_{38}$H$_{56}$N$_2$O$_3$), 34.8%, 22.75 min (C$_{38}$H$_{56}$N$_2$O$_3$), 12.6%. The mixture of salen ligands could be separated by preparative HPLC (DCM:MeOH, 7:5, Nucleodur 100-10-C18/A, NW50, 48 mm i.d., 198×48 mm, 06/01, 35.0 mL min^{-1}, 117.6 mg mL^{-1}, 2.1 MPa, 308 K, SPD-20A, 220 nm, 0.1 mm) to give (*R,R*)-(116)b as a yellow powder. ^{1}H NMR (400.1 MHz, CDCl$_3$, 300 K): δ = 13.57 (s, 2H), 8.30 (d, 2H, *J* = 19.8 Hz, CH=N), 7.23 (d, 1H, *J* = 2.2 Hz, Ar-H), 6.91 –6.87 (m, 2H, Ar-H) 6.38 (d, 1H, *J* = 2.8 Hz, Ar-H), 5.79–5.69 (tdd, 1H, *J* = 6.7 Hz, *J* = 10.1 Hz, *J* = 16.9 Hz), 4.97–4.92 (dd, 1H, *J* = 1.7 Hz, *J* = 17.3 Hz, CH=C*H*$_2$), 4.90–4.88 (dd, 1H, *J* = 1.4 Hz, *J* = 10.4 Hz, CH=C*H*$_2$), 3.78–3.67 (m, 2H, O-CH$_2$), 2.05–2.00 (dd, 2H, *J* = 7.1 Hz, *J* = 14.2 Hz), 1.95–1.85 (m, 2H), 1.85–1.75 (m, 2H), 1.69–1.62 (m, 4H) 1.49–1.39 (m, 6H) 1.34 (s, 9H, C(CH$_3$)$_3$), 1.32 (s, 9H, C(CH$_3$)$_3$), 1.15 (s, 9H, C(CH$_3$)$_3$) ppm. ^{13}C NMR (100.6 MHz, CDCl$_3$, 300 K): δ = 165.6, 165.0, 157.5, 154.3, 150.1, 139.6, 138.2, 135.9, 126.4, 125.6, 118.3, 117.5, 117.4, 114.3, 111.9, 72.1, 71.9, 67.9, 34.6, 34.5, 33.6, 33.1, 32.8, 32.7, 31.0, 29.0, 28.9, 28.5, 25.0, 24.0 ppm. FT-IR [cm^{-1}]: 3000 (s), 2934 (s), 2861 (s), 1628 (s), 1467 (m), 1438 (m), 1390 (m), 1360 (m), 1330 (m), 1274 (m), 1252 (m), 1241 (m), 1213 (m), 1173 (w), 1156 (w), 1141 (w), 1096 (w), 1052 (w), 992 (w), 973 (w), 911 (w), 878 (w), 862 (w), 848 (w), 828 (w), 803 (w), 755 (w), 713 (w). HRMS (ESIpos) calcd for C$_{38}$H$_{56}$N$_2$NaO$_3$ [M]$^+$ 611.418498, found 611.418315. $[\alpha]_{20}^{D}$ = -267.5° (c = 0.75, CHCl$_3$).

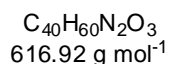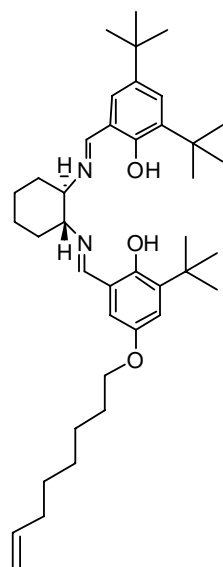**Unsymmetrical Salen Ligand (*R,R*)-(116)c,** 2,4-di-*tert*-butyl-6-((*E*)-((1*R*,2*R*)-2-((*E*)-3-*tert*-butyl-2-hydroxy-5-(oct-7-enyloxy)benzylideneamino)cyclohexylimino)methyl)phenol

Compound (*R,R*)-(116)c was prepared like compound (*R,R*)-(116)b using (*R,R*)-1,2-diammoniumcyclohexane mono-(+)-tartrate salt (118) (860 mg, 3.2 mmol, 0.66 eq.), K_2CO_3 (900 mg, 6.5 mmol), 3-di-*tert*-butyl-2-hydroxybenzaldehyd (117) (1.15 g, 4.9 mmol, 1 eq.) and compound (115)c (380 mg, 1.6 mmol, 0.33 eq.) to give a mixture of the desired product (*R,R*)-(116)c (19.9%), the ligand (*R,R*)-(103)a (70.9%) as well as the symmetric disubstituted ligand (*R,R*)-(116)f (3.7%) as a yellow crystalline powder. HPLC-MS (125 mm Nucleodur 100-5-C18ec, 4.0 mm i.d., MeOH, 0.8 mL min^{-1}, 5.6 MPa, 308 K, UV, 220 nm, retention time, %Total): 5.79 min ($C_{36}H_{54}N_2O_2$), 70.9%, 7.51 min ($C_{40}H_{60}N_2O_3$), 19.9%, 9.7 min ($C_{44}H_{66}N_2O_4$), 3.7%. The mixture of salen ligands could be separated by preparative HPLC (DCM:MeOH, 4:5, Nucleodur 100-10-C18/A, NW50, 48 mm i.d., 198×48 mm, 06/01, 35.0 mL min^{-1}, 26.5 mg mL^{-1}, 2.8 MPa, 308 K, SPD-20A, 220 nm, 0.1 mm) to give (*R,R*)-(116)c as a yellow powder. ^{1}H NMR (400.1 MHz, CDCl$_3$, 300 K): δ = 13.57 (s, 2H), 8.30 (d, 2H, *J* = 19.8 Hz, CH=N), 7.23 (d, 1H, *J* = 2.2 Hz, Ar-H), 6.91–6.87 (m, 2H, Ar-H) 6.38 (d, 1H, *J* = 2.8 Hz, Ar-H), 5.82–5.73 (tdd, 1H, *J* = 6.7 Hz, *J* = 10.1 Hz, *J* = 16.9 Hz), 5.00–4.94 (dd, 1H, *J* = 1.7 Hz, *J* = 17.3 Hz, CH=C*H*$_2$), 4.92–4.88 (dd, 1H, *J* = 1.4 Hz, *J* = 10.4 Hz, CH=C*H*$_2$), 3.93–3.83 (m, 2H, O-CH$_2$), 2.05–2.00 (dd, 2H, *J* = 7.1 Hz, *J* = 14.2 Hz) 1.95–1.85 (m, 2H), 1.85–1.75 (m, 2H), 1.69–1.62 (m, 4H) 1.49–1.39 (m, 10H) 1.34 (s, 9H, C(CH$_3$)$_3$), 1.32 (s, 9H, C(CH$_3$)$_3$), 1.15 (s, 9H, C(CH$_3$)$_3$) ppm. ^{13}C NMR (100.6 MHz, CDCl$_3$, 300 K): δ = 165.6, 165.0, 157.5, 154.3, 150.1, 139.6, 138.2, 135.9, 126.4, 125.6, 118.3, 117.5, 117.4, 114.3, 111.9, 72.1, 71.9, 67.9, 34.6, 34.5, 33.6, 33.1, 32.8, 32.7, 31.0, 29.0, 28.9, 28.5, 25.0, 24.0 ppm. FT-IR [cm^{-1}]: 2930 (s), 2858 (s), 1628 (s), 1596 (m), 1465 (m), 1437 (m), 1389 (w), 1360 (w), 1330 (w), 1273 (w), 1252 (w), 1241 (w), 1203 (w), 1173 (w), 1155 (w), 1141 (w), 1096 (w), 1055 (w), 982 (w), 933 (w), 909 (w), 878 (w), 861 (w), 827 (w), 801 (w), 772 (w), 764 (w), 731 (w), 712 (w). HRMS (ESIpos) calcd for $C_{40}H_{61}N_2O_3$ [M]$^+$ 617.467560, found 617.467667. $[\alpha]_{20}^D$ = -232.5° (c = 0.55, CHCl$_3$).

$C_{40}H_{60}N_2O_3$
616.92 g mol^{-1}

8.8.2. Immobilization of Chiral Salen Derivatives

Chirasil-Propoxy-Salen **(119)a,** [2,4-di-*tert*-butyl-6-((*E*)-((1*R*,2*R*)-2-((*E*)-3-*tert*-butyl-2-hydroxy-5-propoxybenzylideneamino)cyclohexylimino)methyl)phenol]-poly(dimethylsiloxane)
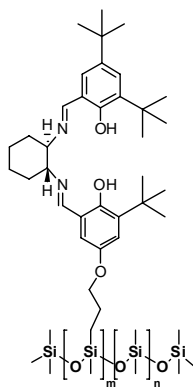
The unsymmetrical salen ligand **(116)a** (500 mg, 0.9 mmol) was added to a solution of HMPS **(4)** (5.6 g, total content of $Si(O)(CH_3)H$ groups: 25.7%) in anhydrous toluene. After 15 min of stirring at RT, the Pt catalyst (Karstedt's catalyst **(11)** (0.1 M in xylene, 0.05 eq.) or H_2PtCl_6 **(57)** (8 mg, 0.02 mmol, 0.05 eq.) in anhydrous THF (1 mL)) was added and the solution was refluxed (alternatively, ultrasonication at RT) for 24 h under an argon atmosphere. The hydrosilylation procedure was continued as described in chapter 8.4.1. (Compound **(9)**). Purification of the crude polymer and, in particular, removing the rest of the catalyst was performed by passing the polymer dissolved in toluene through a short column of activated charcoal. Volatiles were removed under reduced pressure. The solution was filtered and the solvent was evaporated to yield yellow-brown polysiloxane **(119)a** (5.4 g). ^{1}H NMR (400.1 MHz, CDCl$_3$, 300 K): δ = 8.27–8.24 (bm, CH=N), 7.25–7.08 (m, Ar-H), 1.33 (bs, C(CH$_3$)$_3$), 1.14 (bs, C(CH$_3$)$_3$) 0.19– -0.19 (bs, Si-CH$_3$) ppm. FT-IR [cm^{-1}]: 2962 (s), 2160 (s), 1412 (m), 1258 (w), 1013 (w), 910 (w), 841 (w), 789 (w), 703 (w).

Chirasil-Hexyloxy-Salen **(119)b,** [2,4-di-*tert*-butyl-6-((*E*)-((1*R*,2*R*)-2-((*E*)-3-*tert*-butyl-5-(hexyloxy)-2-hydroxybenzylideneamino)cyclohexylimino)methyl)phenol]-poly(dimethyl-siloxane)
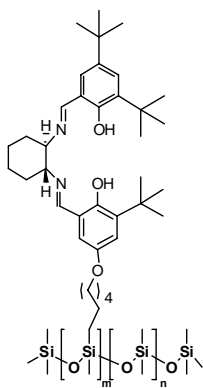
Polysiloxane **(119)b** was prepared like polymer **(119)a** using unsymmetrical salen ligand **(116)b** (79 mg, 0.1 mmol) and HMPS **(4)** (344 mg, total content of $Si(O)(CH_3)H$ groups: 25.7%). (Yield: 320 mg). ^{1}H NMR (400.1 MHz, CDCl$_3$, 300 K): δ = 8.27–8.24 (bm, CH=N), 7.25–7.08 (m, Ar-H), 1.33 (bs, C(CH$_3$)$_3$), 1.14 (bs, C(CH$_3$)$_3$) 0.19 – -0.19 (bs, Si-CH$_3$).

Chirasil-Octyloxy-Salen (119)c, [2,4-di-*tert*-butyl-6-((*E*)-((1*R*,2*R*)-2-((*E*)-3-*tert*-butyl-2-hydroxy-5-(octyloxy)benzylideneamino)cyclohexylimino)methyl)phenol]-poly(dimethyl-siloxane)
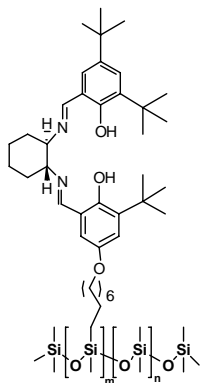
Polysiloxane **(119)c** was prepared like polymer **(119)a** using unsymmetrical salen ligand **(116)c** (100 mg, 0.2 mmol) and HMPS **(4)** (2.43 g, total content of Si(O)(CH$_3$)H groups: 25.7%). (Yield: 2.20 g). ^{1}H NMR (300.1 MHz, CDCl$_3$, 300 K): δ = 8.27–8.23 (bm, CH=N), 7.25-7.08 (m, Ar-H), 1.33 (bs, C(CH$_3$)$_3$), 1.14 (bs, C(CH$_3$)$_3$), 0.19 − -0.19 (bs, Si-CH$_3$) ppm.

8.8.3. Metalation of Polysiloxane-Immobilized Salen Ligands

Chirasil-Co(II)-Propoxy-Salen (120)a, Co(II)-[2,4-di-*tert*-butyl-6-((*E*)-((1*R*,2*R*)-2-((*E*)-3-*tert*-butyl-2-hydroxy-5-propoxybenzylideneamino)cyclohexylimino)methyl)phenol]-poly-(dimethylsiloxane)
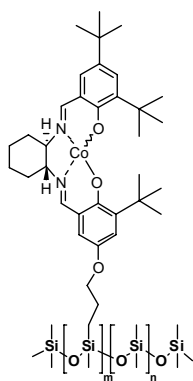
Cobalt insertion into the polysiloxane-immobilized ligand Chirasil-Propoxy-Salen **(119)a** (200 mg) was accomplished by adding a solution of Co(OAc)$_2$*4 H$_2$O (654 mg, 2.6 mmol) dissolved in toluene (20 mL) with gentle stirring at RT for 30 min and refluxing for 2 h. Afterwards, the solvent was removed under vacuum and the polymer was dissolved in *n*-hexane and filtered. The organic phase was washed with water, dried over magnesium sulfate and the solvent was removed under vacuum to yield **(120)a** (0.190 g). The catalyst can be oxidized to the Co(III) state by dissolving the polysiloxane toluene:acetic acid (9:1) in air with gentle stirring for 3 h and removing the solvent afterwards. ^{1}H NMR (400.1 MHz, CDCl$_3$, 300 K): δ = 8.06–8.00 (bm, CH=N), 7.47-7.43 (m, Ar-H), 1.35 (bs, C(CH$_3$)$_3$), 1.17 (bs, C(CH$_3$)$_3$), 0.19– -0.19 (bs, Si-CH$_3$) ppm. FT-IR [cm^{-1}]: 2962 (s), 2155 (s), 1412 (m) 1258 (w), 1014 (w), 911 (w), 840 (w), 790 (w), 757 (w). $[\alpha]_{20}^{D}$ = -19.4° (c = 0.67, CHCl$_3$). Elemental analysis: anal. found Co: 0.5%.

Chirasil-Co(II)-Hexyloxy-Salen (120)b, Co(II)-[2,4-di-*tert*-butyl-6-((*E*)-((1*R*,2*R*)-2-((*E*)-3-*tert*-butyl-5-(hexyloxy)-2-hydroxybenzylideneamino)cyclohexylimino)methyl)phenol]-poly-(dimethylsiloxane)
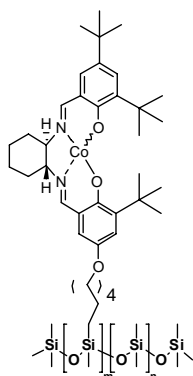
Polymer **(120)b** was prepared like polymer **(120)a** using Co(OAc)$_2$·4 H$_2$O (623 mg, 2.5 mmol) and Chirasil-Hexyloxy-Salen **(119)b** (200 mg). (Yield: 610 mg). ^{1}H NMR (400.1 MHz, CDCl$_3$, 300 K): δ = 8.24–8.20 (bm, CH=N), 7.25–7.08 (m, Ar-H), 1.34 (bs, C(CH$_3$)$_3$), 1.16 (bs, C(CH$_3$)$_3$), 0.19 – -0.19 (bs, Si-CH$_3$) ppm. -12.5° (c = 0.80, CHCl$_3$). $[\alpha]_{20}^{D}$ = -15.4° (c = 0.60, CHCl$_3$). Elemental analysis: anal. found Co: 0.5%.

Chirasil-Co(II)-Octyloxy-Salen (120)c, Co(II)-[2,4-di-*tert*-butyl-6-((*E*)-((1*R*,2*R*)-2-((*E*)-3-*tert*-butyl-2-hydroxy-5-(octyloxy)benzylideneamino)cyclohexylimino)-methyl)phenol]-poly-(dimethylsiloxane)
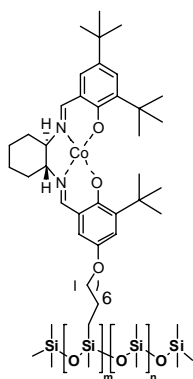
Polymer **(120)c** was prepared like polymer **(120)a** using Co(OAc)$_2$·4 H$_2$O (271 mg, 1.1 mmol) and Chirasil-Octyloxy-Salen **(119)c** (500 mg). (Yield: 260 mg). ^{1}H NMR (400.1 MHz, CDCl$_3$, 300 K): δ = 8.24–8.20 (bm, CH=N), 7.25-7.08 (m, Ar-H), 1.34 (bs, C(CH$_3$)$_3$), 1.16 (bs, C(CH$_3$)$_3$), 0.19 – -0.19 (bs, Si-CH$_3$) ppm. FT-IR [cm^{-1}]: 2962 (s), 1412 (w), 1258 (w), 1013 (w), 842 (w), 790 (w), 701. $[\alpha]_{20}^{D}$ = -7,7° (c = 0.85, CHCl$_3$). Elemental analysis: anal. found Co: 0.5%.

9. Summary

In the present thesis, recent contributions to the development, theory and application of on-column reaction chromatography have been described. The understanding of the mechanism and activity of different catalyst systems has been expanded by detailed kinetic studies of catalyst and materials.

In the first part, different α-keto esters were used to investigate enantioselective hydrogenation reactions over quinine-modified Pt and Pd nanoparticles by the synchronous combination of catalysis and separation in microcapillaries. In this capillary microreactor high ee values (up to 95% ee) were detected for the enantioselective hydrogenation of ethyl pyruvate over very small quinine-modified Pt nanoparticles (0.5-1.0 nm). With enantioselective on-column reaction chromatography, it was possible to optimize noble metal to modifier ratios and to perform ht reaction rate and enantioselectivity measurements for entire substrate libraries at gas/liquid/solid interfaces. Substantial differences in the behavior of this reaction at gas-liquid-solid interfaces compared to liquid-solid interfaces for the enantioselective hydrogenation of ethyl pyruvate at 70 °C and 40 kPa lead to higher reaction rate constant for unmodified, unselective Pt sites ($k = 1.4 \times 10^{-1}$ s^{-1}) than for reaction rate constant for modified, enantioselective sites ($k = 3.3 \times 10^{-2}$ s^{-1}) . This experimental result might be ascribable to differences in the rate determining steps (e.g. desorption of the product *vs.* product formation on the catalyst surface) or differences in the molecular interactions on the metal surface and in solution during product formation.

Furthermore, the reactivity of different ruthenium metathesis catalysts in RCM reactions has been studied in detail by a synchronous combination of catalysis and separation in microcapillaries for different stationary phases and different catalyst loadings. These on-column chromatographic experiments led to comprehensive kinetic data from temperature-dependent measurements. The here obtained activation parameters, i.e. for RCM of *N,N*-diallyltrifluoroacetamide over Grubbs-type catalyst 1$^{\text{st}}$ generation $\Delta G^{\ddagger}(298 \text{ K}) = 83.2 \text{ kJ mol}^{-1}$, $\Delta H^{\ddagger} = (18.3 \pm 1.2) \text{ kJ mol}^{-1}$, $\Delta S^{\ddagger} = (-218 \pm 29) \text{ J K}^{-1} \text{mol}^{-1}$ corroborate recently reported experimental and theoretical calculations. On-column reaction chromatography investigations of different ruthenium carbene complexes have been

demonstrated to obtain reliable results comparable to solution phase experiments. The low activation enthalpies $\Delta H^{\ddagger}$ and negative activation entropies $\Delta S^{\ddagger}$, correspond to a restraint transition state. These parameters help to understand the multi-step nature of olefin metathesis reaction as well as the catalyst initiation and activity in these ruthenium-based systems. Furthermore, the comparison of the obtained $\Delta G^{\ddagger}$ values for different Grubbs-type catalysts reveals their different catalytic activity. The observed phenomena of nonlinear Eyring plots proved the exchange of the benzylidene unit and the diene substrate on the Ru metal center at temperatures below 56 °C before the catalyst reaches its more active steady-state condition. In conclusion, on-column reaction chromatography makes it possible to screen not only a large set of olefin metathesis catalysts and substrates with relatively small effort, but also to obtain mechanistic information.

The synchronous combination of catalysis and separation in microcapillaries also allowed the efficient study of RCM reactions catalyzed by 1st generation Grubbs-type catalyst embedded in an IL for different reaction temperatures and substrates. The challenging isolation of reaction educts and products from ILs has been solved by making use of the intrinsic separation selectivity. Comprehensive kinetic data were obtained from the direct evaluation of the elution profiles using the unified equation of chromatography. Grubbs-type 1st generation catalyst could be efficiently stabilized in an IL. Up to ten times faster RCM reactions were observed in the IL compared to on-column reaction chromatography measurements with PDMS as a stabilizing matrix. Furthermore, the presented concept of on-column reaction chromatography can be generally applied to characterize various metathesis catalysts stabilized by or covalently attached to different RTILs in comprehensive kinetic ht screenings without any additional isolation step, which is typically difficult to perform for batch reactors.

Covalently immobilized, polysiloxane-supported, asymmetric metal-[3-heptafluorobutanoyl-camphorates and their application in on-column reaction chromatography has been synthesized and investigated in chapter 6. These novel polymeric chiral metal-1,3-diketonatocamphor complexes with a flexible linker could be synthesized and characterized with NMR and MS studies. The obtained polysiloxane-immobilized chiral catalysts were investigated in their enantioselective separation efficiency of menthone racemates and Z- and E-chalcogran. Although the menthone racemates could be separated and the polymeric catalyst showed activity in the on-column intramolecular Diels-Alder reactions

of furfuryl derivatives, the enantiomers of chalcogran and 7-oxabicyclo[2.2.1]hept-2-ene could not be separated which is might be ascribable to the low ligand loading of the metal-1,3-diketonatocamphor complexes.

In the last chapter, the flexible and straightforward immobilization strategy of chiral catalysts on modified polysiloxanes was extended to the synthetic applicability of polysiloxane-supported chiral Co-salen-complexes. Monofunctionalized enantiopure unsymmetrical salen ligands were immobilized by an ether linkage onto a polysiloxane support. Concerning selectivity and reactivity, the covalent immobilized Co(III)-salen-OAc catalysts might be beneficial in the HKR of terminal epoxides because of the assumed cooperative bimetallic catalytic mechanism. The polysiloxane support simplifies the separation of the catalyst from by-products and reaction products using biphasic liquid/liquid separation techniques, the catalysts recycling, as well as the possible application of the immobilized catalyst in continuous-flow processes using on-column chromatography.

The investigation of enantioselective hydrogenations, olefin metathesis and Diels-Alder reactions illustrate the widespread applicability and, additionally, the (r)evolution of chemist's toolkits from flasks and beakers to miniaturized reactors with highly efficient and selective catalysts inherently combined with separation techniques. According to biological systems, where reactions efficiently take place at miniaturized interfaces, the development of chemical micro plants for the production of fine chemicals can be envisaged as a natural step with such continuous-flow reactors in terms of energy efficiency and environmental impact.

10.   References

[1]   E. K. Rideal, H. S. Taylor, *Catalysis in Theory and Practice*, Macmillan, London, **1919**.

[2]   R. J. Farrauto, C. H. Bartholomew, *Fundamentals of Industrial Catalytic Processes*, Chapman & Hall, London, **1997**.

[3]   J. Hagen, *Industrial Catalysis - A Practical Approach*, 2 ed., WILEY-VCH Verlag GmbH & Co. KGaA, Weinheim, **2006**.

[4]   S. C. Stinson, *Chem. Eng. News* **2001**, *79*, 79.

[5]   J. M. Thomas, W. J. Thomas, *Principles and Practice of Heterogeneous Catalysis*, WILEY-VCH Verlag GmbH & Co. KGaA, Weinheim, **1997**.

[6]   G. Ertl, H. Knözinger, F. Schüth, J. Weitkamp, *Handbook of Heterogeneous Catalysis*, 2 ed., WILEY-VCH Verlag GmbH & Co. KGaA, Weinheim, **2008**.

[7]   B. Cornils, W. A. Herrmann, *Applied Homogeneous Catalysis with Organometallic Compounds: A Comprehensive Handbook in Three Volumes*, 2 ed., WILEY-VCH Verlag GmbH & Co. KGaA, Weinheim, **2002**.

[8]   *National Research Council Panel on New Directions in Catalytic Sciences and Technology - Catalysis Looks to the Future*, National Academy Press, Washington D.C., **1992**.

[9]   C. C. Leznoff, *Chem. Soc. Rev.* **1974**, *3*, 65.

[10]   R. H. Grubbs, *Chem. Tech.* **1977**, 512.

[11]   F. R. Hartley, P. N. Vezey, *Adv. Organomet. Chem.* **1977**, *15*, 189.

[12]   F. R. Hartley, *Supported Metal Complexes. A New Generation of Catalysts*, Reidel, Dordrecht, **1985**.

[13]   Y. Iwasawa, *Tailored Metal Catalysts*, Reidel, Dordrecht, **1986**.

[14]   W. Keim, B. Driessen-Hölscher, in *Handbook of Heterogeneous Catalysis, Vol. 1* (Eds.: G. Ertl, H. Knözinger, J. Weitkamp), WILEY-VCH Verlag GmbH & Co. KGaA, Weinheim, **1997**, p. 231.

[15]   D. E. D. Vos, I. F. J. Vankelecom, P. A. Jacobs, *Chiral Catalyst Immobilization and Recycling*, WILEY-VCH Verlag GmbH & Co. KGaA, Weinheim, **2000**.

[16]   P. McMorn, G. J. Hutchings, *Chem. Soc. Rev.* **2004**, *33*, 108.

[17]   F. Cozzi, *Adv. Synth. Catal.* **2006**, *348*, 1367.

[18]   M. Heitbaum, F. Glorius, I. Escher, *Angew. Chem., Int. Ed.* **2006**, *45*, 4732.

[19]   M. Heitbaum, F. Glorius, I. Escher, *Angew. Chem.* **2006**, *118*, 4850.

[20]   J. N. H. Reek, P. W. N. M. Van Leeuwen, A. G. J. Van Der Ham, A. B. De Haan, in *Catalyst Separation, Recovery and Recycling, Vol. 30*, Springer Amsterdam, **2006**, pp. 39.

[21]   R. B. Merrifield, *Nature* **1965**, *150*, 178.

[22]   D. E. Bergbreiter, *Chem. Rev.* **2002**, *102*, 3345.

[23]   J. Lu, P. H. Toy, *Chem. Rev.* **2009**, doi:10.1021/cr8004444.

[24]   N. Madhavan, C. W. Jones, M. Weck, *Acc. Chem. Res.* **2008**, *41*, 1153.

[25]   G. G. Wildgoose, C. E. Banks, R. G. Compton, *Small* **2006**, *2*, 182.

[26]   W. Miao, T. H. Chan, *Acc. Chem. Res.* **2006**, *39*, 897.

[27]   I. F. J. Vankelecom, P. A. Jacobs, in *Chiral Catalyst Immobilization and Recycling* (Ed.: D. E. V. De Vos, Ivo F. J.; Jacobs, Pierre A.), WILEY-VCH Verlag GmbH & Co. KGaA, Weinheim, **2000**, pp. 19.

[28] M. J. Owen, in *Silicon-Containing Polymers* (Eds.: R. G. Jones, W. Ando, J. Chojnowski), Kluwer Publishers, Dordrecht, The Netherlands, **2000**, pp. 213–231.

[29] F. Keller, H. Weinmann, V. Schurig, *Chem. Ber./Recueil* **1997**, *130*, 879.

[30] M. A. Grunlan, K. R. Regan, D. E. Bergbreiter, *Chem. Commun.* **2006**, 1715.

[31] C. Wiles, P. Watts, *Eur. J. Org. Chem.* **2008**, *2008*, 1655.

[32] F. A. Karnatz, F. C. Whitmore, *J. Am. Chem. Soc.* **1932**, *54*, 3461.

[33] J. L. Dye, M. T. Lok, F. J. Tehan, J. M. Creaso, K. J. Voorhees, *J. Org. Chem.* **1973**, *38*, 1773.

[34] C. R. Harrison, P. Hodge, *J. Chem. Soc., Perkin Trans. I* **1976**, 2252.

[35] D. A. Annis, E. N. Jacobsen, *J. Am. Chem. Soc.* **1999**, *121*, 4147.

[36] V. Skelton, G. M. Greenway, S. J. Haswell, P. Styring, D. O. Morgan, B. H. Warrington, S. Y. F. Wong, *Analyst* **2001**, *126*, 11.

[37] M. T. Reetz, W. Wiesenhöfer, G. Franció, W. Leitner, *Adv. Synth. Catal.* **2003**, *345*, 1221.

[38] C. Wiles, P. Watts, S. J. Haswell, E. Pombo-Villar, *Tetrahedron Lett.* **2003**, *59*, 10173.

[39] S. Saaby, K. R. Knudsen, M. Ladlow, S. V. Ley, *Chem. Commun.* **2005**, 2909.

[40] I. R. Baxendale, C. M. Griffiths-Jones, S. V. Ley, G. K. Tranmer, *Synlett* **2006**, 427.

[41] A. Kirschning, W. Solodenko, K. Mennecke, *Chem. Eur. J.* **2006**, *12*, 5972.

[42] G. Shore, S. Morin, M. G. Organ, *Angew. Chem. Int. Ed.* **2006**, *45*, 2761.

[43] W. Solodenko, G. Jas, U. Kunz, A. Kirschning, *Synthesis* **2007**, *4*, 583.

[44] M. T. Reetz, K. M. Kühling, A. Deege, H. Hinrichs, D. Belder, *Angew. Chem.* **2000**, *112*, 4049.

[45] M. T. Reetz, K. M. Kühling, A. Deege, H. Hinrichs, D. Belder, *Angew. Chem. Int. Ed.* **2000**, *39*, 3891.

[46] D. Janasek, J. Franzke, A. Manz, *Nature* **2006**, *442*, 374.

[47] A. J. deMello, *Nature* **2006**, *442*, 394.

[48] J. Kobayashi, Y. Mori, K. Okamoto, R. Akiyama, M. Ueno, T. Kitamori, S. Kobayashi, *Science* **2004**, *304*, 1305.

[49] H. R. Sahoo, J. G. Kralj, K. F. Jensen, *Angew. Chem. Int. Ed.* **2007**, *46*, 5704.

[50] G. M. Whitesides, *Nature* **2006**, *442*, 368.

[51] P. A. Auroux, Y. Koc, A. deMello, A. Manz, P. J. R. Day, *Lab Chip* **2004**, *4*, 534.

[52] J. J. van Deemter, F. J. Zuiderweg, A. Klinkenberg, *Chem. Eng. Sci.* **1956**, *5*, 271.

[53] M. J. E. Golay, *Anal. Chem.* **1957**, *29*.

[54] R. Daw, J. Finkelstein, *Nature* **2006**, *442*, 367.

[55] O. Trapp, *J. Chromatogr. A* **2008**, *1184*, 160.

[56] J. M. Blacquiere, T. Jurca, J. Weiss, D. E. Fogg, *Adv. Synth. Catal.* **2008**, *350*, 2849.

[57] C. Cai, J. Y. L. Chung, J. C. McWilliams, Y. Sun, C. S. Shultz, M. Palucki, *Org. Process Res. Dev.* **2007**, *11*, 328

[58] C. Hoffmann, H.-W. Schmidt, F. Schüth, *J. Catal.* **2001**, *198*, 348.

[59] S. Vukojevic, O. Trapp, J.-D. Grunwaldt, C. Kiener, F. Schüth, *Angew. Chem.* **2005**, *117*, 8192.

[60] H. F. M. Boelens, D. Iron, J. A. Westerhuis, G. Rothenberg, *Chem. Eur. J.* **2003**, *9*, 3876.

[61] F. Schüth, in *Handbook of Heterogeneous Catalysis* (Eds.: G. Ertl, H. Knözinger, F. Schüth, J. Weitkamp), WILEY-VCH Verlag GmbH & Co. KGaA, Weinheim, **2008**, p. 2053.

[62] M. J. E. Golay, *J. Chromatogr.* **1975**, *8*, 421.

[63]   W. S. Cooke, *Today Chem. Work* **1996**, *1*, 16.

[64]   B. Rosenkranz, J. Bettmer, *Anal. Bioanal. Chem.* **2002**, *373*, 461.

[65]   H. J. Huebschmann, *Handbook of GC/MS. Fundamentals and Applications*, WILEY-VCH Verlag GmbH & Co. KGaA, Weinheim, **2001**.

[66]   O. Trapp, *Angew. Chem., Int. Ed.* **2007**, *46*, 5609

[67]   O. Trapp, *Angew. Chem.* **2007**, *119*, 5706

[68]   O. Trapp, **2007**, *PCT Patent Application WO2007045224A2*.

[69]   O. Trapp, *Nachr. Chem.* **2006**, *54*, 1111.

[70]   R. R. Ernst, W. A. Anderson, *Rev. Sci. Instrum.* **1966**, *37*, 93.

[71]   O. Trapp, *Electrophoresis* **2006**, *27*, 2999.

[72]   O. Trapp, *Anal. Chem.* **2006**, *78*, 189.

[73]   K. Tamaru, *Nature* **1959**, *183*, 319.

[74]   D. W. Bassett, H. W. Habgood, *J. Phys. Chem.* **1960**, *64*, 769.

[75]   E. Gil-Av, Y. Herzberg-Minzly, *Chem. Commun.* **1961**, 316.

[76]   G. L. Pratt, S. H. Langer, *J. Phys. Chem.* **1969**, *73*, 209.

[77]   S. H. Langer, J. E. Patton, *J. Phys. Chem.* **1972**, *76*, 2159.

[78]   S. H. Langer, T. D. Griffith, *J. Phys. Chem.* **1978**, *82*, 1327.

[79]   H. K. Lee, S. F. Y. Li, P. J. Marriott, *Bull. Sing. N. I. Chem.* **1990**, *18*, 109.

[80]   C. S. G. Phillips, A. J. Hart-Davis, R. G. L. Saul, J. Wormald, *J. Gas Chromatogr.* **1967**, *5*, 424.

[81]   K. F. Scott, C. S. G. Phillips, *J. Chromatogr.* **1975**, *112*, 61.

[82]   J. R. Conder, C. L. Young, *Physicochemical Measurement by Gas Chromatography*, WILEY-VCH Verlag GmbH & Co. KGaA, Chichester, **1979**.

[83]   P. M. Lyne, C. S. G. Phillips, *J. Chromatogr.* **1989**, *471*, 145.

[84]   O. Trapp, S. K. Weber, S. Bauch, W. Hofstadt, *Angew. Chem.* **2007**, *119*, 7447.

[85]   O. Trapp, S. K. Weber, S. Bauch, W. Hofstadt, *Angew. Chem. Int. Ed.* **2007**, *46*, 7307.

[86]   A. Schmidt, R. Schomäcker, *Ind. Eng. Chem. Res.* **2007**, *46*, 1677.

[87]   O. Trapp, S. K. Weber, S. Bauch, T. Bäcker, W. Hofstadt, B. Spliethoff, *Chem. Eur. J.* **2008**, *14*, 4657.

[88]   T. Mallat, E. Orglmeister, A. Baiker, *Chem. Rev.* **2007**, *107*, 4863.

[89]   E. Erlenmeyer, H. Erlenmeyer, *Biochem. Zeitschr.* **1922**, *133*, 52.

[90]   The paper of Erlenmeyer [89] did not reported, if the catalyst was really heterogeneous.

[91]   D. Lipkin, T. D. Stewart, *J. Am. Chem. Soc.* **1939**, *61*, 3295.

[92]   Y. Nakamura, *Bull. Chem. Soc. Jpn.* **1941**, *16*, 367.

[93]   T. Isoda, A. Ichikawa, T. Shimamoto, *Rikagaku Kenkyusho Hokuku* **1958**, *34*, 134.

[94]   Y. Izumi, M. Imaida, H. Fukawa, S. Akabori, *Bull. Chem. Soc. Jpn.* **1963**, 36.

[95]   Y. Izumi, *Adv. Cat.* **1983**, *32*, 215.

[96]   A. Tai, T. Sagimura, in *Chiral Catalyst Immobilization and Recycling* (Eds.: D. E. De Vos, I. F. J. Vankelecom, P. A. Jacobs), WILEY-VCH Verlag GmbH & Co. KGaA, Weinheim, **2000**, p. 173.

[97]   T. Osawa, T. Harada, O. Takayasu, *Top. Catal.* **2000**, *13*, 155.

[98]   T. Sagimura, S. Nakagawa, A. Tai, *Bull. Chem. Soc. Jpn.* **2002**, *75*, 355.

[99]   A. Kai, K. Ito, T. Harada, *Bull. Chem. Soc. Jpn.* **1981**, *54*, 223.

[100] T. Osawa, T. Harada, A. Tai, *J. Mol. Catal.* **1994**, *87*, 333.

[101] Y. Orito, S. Imai, S. Niwa, *J. Chem. Soc. Jpn.* **1979**, 1118.

[102] Y. Orito, S. Imai, S. Niwa, *J. Chem. Soc. Jpn.* **1980**, 670.

[103] P. B. W. Wells, Richard P. K., *Enantioselective hydrogenation catalyzed by platinum group metals modified by natural alkaloids*, WILEY-VCH Verlag GmbH & Co. KGaA, Weinheim, **2000**.

[104] M. Studer, H. U. Blaser, C. Exner, *Adv. Synth. Catal.* **2003**, *345*, 45.

[105] M. H. Bartók, *Curr. Org. Chem.* **2006**, *10*, 1533.

[106] H.-U. Blaser, M. Studer, *Acc. Chem. Res.* **2007**, *40*, 1348.

[107] T. Mallat, S. Diezi, A. Baiker, in *Handbook of Heterogeneous Catalysis* (Eds.: G. Ertl, H. Knözinger, F. Schüth, J. Weitkamp), WILEY-VCH Verlag GmbH & Co. KGaA, Weinheim, **2008**, p. 3603.

[108] H.-U. Blaser, H. P. Jalett, D. M. Monti, A. Baiker, J. T. Wehrli, *Stud. Surf. Sci. Catal.* **1991**, *67*, 147.

[109] A. Pfaltz, T. Heinz, *Top. Catal.* **1998**, *4*, 229.

[110] M. Schürch, T. Heinz, R. Aeschimann, T. Mallat, A. Pfaltz, A. Baiker, *J. Catal.* **1998**, *173*, 187.

[111] H. U. Blaser, H. P. Jalett, J. Wiehl, *J. Mol. Catal.* **1991**, *68*, 215.

[112] J. L. Margitfalvi, E. Tálas, *Appl. Catal., A* **2006**, *301*, 187.

[113] T. Bürgi, A. Baiker, *Acc. Chem. Res.* **2004**, *37*, 909.

[114] M. Studer, S. Burkhardt, A. F. Indolese, H. U. Blaser, *Chem. Commun.* **2000**, 1327.

[115] N. Künzle, A. Szabo, M. Schürch, G. Wang, T. Mallat, A. Baiker, *Chem. Commun.* **1998**, 1377.

[116] S. Niwa, J. Imamura, K. Otsuka, , **1987**, *JP 62158268, (CAN 108, 128815)*.

[117] N. Künzle, R. Hess, T. Mallat, A. Baiker, *J. Catal.* **1999**, *186*, 239.

[118] M. Studer, S. Burkhardt, H. U. Blaser, *Chem. Commun.* **1999**, 1727.

[119] M. Studer, H. U. Blaser, S. Burkhardt, *Adv. Synth. Catal.* **2002**, *344*, 511.

[120] T. Mallat, M. Bodmer, A. Baiker, *Catal. Lett..* **1997**, *44*, 95.

[121] R. Hess, T. Mallat, A. Baiker, *J. Catal.* **2003**, *218*, 453.

[122] Platinum, 5% on alumina powder, reduced, dry: E 4759, 4522 from Engelhard (BASF: Escat™ 2941) and JMC 94 from Johnson Matthey

[123] P. J. G. Collier, T.; Iggo, J. A.; Whyman, R. , in *Chiral Reactions in Heterogeneous Catalysis* (Eds.: G. Jannes, V. Dubois), Plenum Press, New York, **1995**, p. 105.

[124] H.-U. Blaser, D. Imhof, M. Studer, *Stud. Surf. Sci. Catal.* **1997**, *108*, 175.

[125] J. U. Köhler, J. S. Bradley, *Catal. Letters* **1997**, *45*, 203.

[126] J. U. Köhler, J. S. Bradley, *Langmuir* **1998**, *14*, 2730.

[127] X. Zuo, H. Liu, M. Liu, *Tetrahedron Lett.* **1998**, *39*, 1941.

[128] P. J. Collier, J. A. Iggo, R. Whyman, *J. Mol. Catal. A: Chem.* **1999**, *146*, 149.

[129] X. Zuo, H. Liu, D. Guo, X. Yang, *Tetrahedron Lett.* **1999**, *55*, 7787.

[130] J. T. Wehrli, A. Baiker, D. M. Monti, H.-U. Blaser, *J. Mol. Catal.* **1989**, *49*, 195.

[131] J. T. Wehrli, A. Baiker, D. M. Monti, H.-U. Blaser, *J. Mol. Catal.* **1990**, *61*, 207.

[132] Blaser stated in a recent review article (Acc. Chem. Res. 2007, 40, 1348) that: "...even though colloids are not well-suited for technical applications [the results of Liu et. al. (Tetrahedr. 1999, 55, 7787)] of course reopen the debate about the optimal size of the Pt crystallites."

[133] G. Webb, P. B. Wells, *Catal. Today* **1992**, *12*, 319.

[134] H. Bönnemann, G. A. Braun, *Angew. Chem., Int. Ed.* **1996**, *35*, 1992.

[135] H. Bönnemann, G. A. Braun, *Angew. Chem.* **1996**, *108*, 2120.

[136] A. Baiker, *J. Mol. Catal. A.* **1997**, *115*, 473.

[137] C. Exner, PhD thesis, University of Basel (Basel, Switzerland), **2002**.

[138] E. Orglmeister, T. Bürgi, T. Mallat, A. Baiker, *J. Catal.* **2005**, *232*, 137.

[139] A. Vargas, D. Ferri, A. Baiker, *J. Catal.* **2005**, *236*, 1.

[140] M. Garland, H.-U. Blaser, *J. Am. Chem. Soc.* **1990**, *112*, 7048.

[141] I. M. Sutherland, A. Ibbotson, R. B. Moyes, P. B. Wells, *J. Catal.* **1990**, *125*, 77.

[142] P. A. Meheux, A. Ibbotson, P. B. Wells, *J. Catal.* **1991**, *128*, 387.

[143] J. Wang, Y. Sun, C. LeBlond, R. N. Landau, D. G. Blackmond, *J. Catal.* **1996**, *161*, 752.

[144] J. Margitfalvi, E. Tálas, E. Tfirst, *Top. Catal.* **2006**, *39*, 77.

[145] E. N. Jacobsen, I. Marko, W. S. Mungall, G. Schröder, K. B. Sharpless, *J. Am. Chem. Soc.* **1988**, *110*, 1968.

[146] H.-U. Blaser, H. P. Jalett, D. M. Monti, J. F. Reber, J. T. Wehrli, *Stud. Surf. Sci. Catal.* **1988**, *41*, 153.

[147] H.-U. Blaser, M. Garland, H. P. Jalett, *J. Catal.* **1993**, *144*, 569.

[148] D. J. Jenkins, A. M. S. Alabdulrahman, G. A. Attard, K. G. Griffin, P. Johnston, P. B. Wells, *J. Catal.* **2005**, *234*, 230.

[149] H.-U. Blaser, H.-P. Jalett, M. Garland, M. Studer, H. Thies, A. Wirth-Tijani, *J. Catal.* **1998**, *173*, 282.

[150] M. von Arx, N. Dummer, D. J. Willock, S. H. Taylor, R. P. K. Wells, P. B. Wells, G. J. Hutchings, *Chem. Commun.* **2003**, 1926.

[151] N. F. Dummer, G. J. Hutchings, S. H. Taylor, *EUROPACAT VII. Seventh European Congress on Catalysis* **2005**, Sofia, Bulgaria.

[152] G. Vayner, K. N. Houk, Y.-K. Sun, *J. Am. Chem. Soc.* **2004**, *126*, 199.

[153] N. Bonalumi, T. Burgi, A. Baiker, *J. Am. Chem. Soc.* **2003**, *125*, 13342.

[154] S. Lavoie, M. A. Laliberte, P. H. McBreen, *J. Am. Chem. Soc.* **2003**, *125*, 15756.

[155] S. Lavoie, M. A. Laliberte, I. Temprano, P. H. A. McBreen, *J. Am. Chem. Soc.* **2006**, *128*, 7588.

[156] J. L. Margitfalvi, M. Hegedüs, E. Tfirst, *Tetrahedron: Asymmetry* **1996**, *7*, 571.

[157] J. L. Margitfalvi, M. Hegedüs, E. Tfirst, *Stud. Surf. Sci. Catal.* **1996**, *101*, 241.

[158] R. L. Augustine, S. K. Taneilyan, L. K. Doyle, *Tetrahedron: Asymmetry* **1993**, *4*, 1803.

[159] C. de Bellefon, N. Pestre, T. Lamouille, P. Grenouillet, V. Hessel, *Adv. Synth. Catal.* **2003**, *345*, 190.

[160] C. Jäkel, R. Paciello, *Chem. Rev.* **2006**, *106*, 2912.

[161] R. Abdallah, B. Fumey, V. Meille, C. de Bellefon, *Catal. Today* **2007**, *125*, 34.

[162] A. Bykov, V. Matveeva, M. Sulman , P. Valetskiy , O. Tkachenko, L. Kustov , L. Bronstein , E. Sulma, *Catal. Today* **2009**, *140*, 64.

[163] L. N. Lewis, N. Lewis, *J. Am. Chem. Soc.* **1986**, *108*, 7228.

[164] L. N. Lewis, N. Lewis, *Chem. Mater.* **1989**, *1*, 106.

[165] L. N. Lewis, *J. Am. Chem. Soc.* **1990**, *112*, 5998.

[166] L. Fowley, D. Michos, X. Liang, R. H. Crabtree, *Tetrahedron Lett.* **1993**, *34*, 3075.

[167] M. S. DeClue, J. S. Siegel, *Org. Biomol. Chem.* **2004**, *2*, 2287.

[168] B. Maas, A. Dietrich, V. Karl, A. Kaunzinger, D. Lehmann, T. Köpke, A. Mosandl, *J. Microcol. Sep* **1993**, *5*, 421.

[169] H. Cousin, O. Trapp, V. Peulon-Agasse, X. Pannecoucke, L. Banspach, G. Trapp, Z. Jiang, J. C. Combret, V. Schurig, *Eur. J. Org. Chem.* **2003**, 3273.

[170] J. M. Bonello, R. M. Lambert, N. Kunzle, A. Baiker, *J. Am. Chem. Soc.* **2000**, *122*, 9864.

[171] E. Toukoniitty, P. Mäki-Arvela, J. Wärnå, T. Salmi, *Catal. Today* **2001**, *66*, 411.

[172] G. Szöllösi, S. Cserényi, F. Fülöp, M. Bartók, *J. Catal.* **2008**, *260*, 245.

[173] W. R. Huck, T. Bürgi, T. Mallat, A. Baiker, *J. Catal.* **2003**, *219*, 41.

[174] T. J. J. Hall, P.; Vermeer, W. A. H.; Watson, S. R.; Wells, P. B., *Studies in Surface Science and Catalysis, 101(Pt. A, 11th International Congress on Catalysis - 40th Anniversary, 1996, Pt. A)* **1996**

[175] A. Tungler, K. Fodor, T. Mathe, R. A. Sheldon, *Stud. Surf. Sci. Catal.* **1997**, *108*, 157.

[176] A. Tungler, G. Fogassy, *J. Mol. Catal. A: Chem.* **2001**, *173*, 231.

[177] M. von Arx, T. Bürgi, T. Mallat, A. Baiker, *Chem. Eur. J.* **2002**, *8*, 1430.

[178] K. Szori, G. Szöllosi, M. Bartók, *Adv. Synth. Catal.* **2006**, *348*, 515.

[179] D. Ferri, T. Burgi, *J. Am. Chem. Soc.* **2001**, *123*, 12074.

[180] A. Fürstner, *Angew. Chem. Int. Ed.* **2000**, *39*, 3012.

[181] A. Fürstner, *Angew. Chem.* **2000**, *112*, 3140.

[182] T. M. Trnka, R. H. Grubbs, *Acc. Chem. Res.* **2001**, *34*, 18.

[183] C. Adlhart, P. Chen, in *Handbook of Metathesis, Vol. 1* (Ed.: R. H. Grubbs), WILEY-VCH Verlag GmbH & Co. KGaA, Weinheim, **2003**, pp. 132.

[184] D. Astruc, *New. J. Chem.* **2005**, *29*, 42.

[185] R. H. Grubbs, *Nobel Lecture* **2005**.

[186] R. R. Schrock, *Nobel Lecture* **2005**.

[187] J.-L. Hérisson, Y. Chauvin, *Makromolekulare Chemie* **1970**, *141*, 161.

[188] Y. Chauvin, *Nobel Lecture* **2005**.

[189] S. T. Nguyen, R. H. Grubbs, J. W. Ziller, *J. Am. Chem. Soc.* **1993**, *115*, 9858.

[190] P. Schwab, R. H. Grubbs, J. W. Ziller, *J. Am. Chem. Soc.* **1996**, *118*, 100.

[191] A. S. K. Hashmi, *J. Prakt. Chem.* **1997**, *339*, 195.

[192] M. Scholl, T. M. Trnka, J. P. Morgan, R. H. Grubbs, *Tetrahedron Lett.* **1999**, *40*, 2247.

[193] M. Scholl, S. Ding, C. W. Lee, R. H. Grubbs, *Org. Lett.* **1999**, *1*, 953.

[194] C. W. Bielawski, R. H. Grubbs, *Angew. Chem. Int. Ed.* **2000**, *39*, 2903.

[195] J. P. Morgan, R. H. Grubbs, *Org. Lett.* **2000**, *2*, 3153.

[196] J. S. Kingsbury, J. P. A. Harrity, J. Bonitatebus, P. J. , A. H. Hoveyda, *J. Am. Chem. Soc.* **1999**, *121*, 791.

[197] S. B. Garber, J. S. Kingsbury, B. L. Gray, A. H. Hoveyda, *J. Am. Chem. Soc.* **2000**, *122*, 8168.

[198] J. Huang, E. D. Stevens, S. P. Nolan, J. L. Petersen, *J. Am. Chem. Soc.* **1999**, *121*, 2674.

[199] T. Weskamp, F. J. Kohl, W. Hieringer, D. Gliech, W. A. Herrmann, *Angew. Chem. Int. Ed.* **1999**, *38*, 2416.

[200] T. Weskamp, F. J. Kohl, W. Hieringer, D. Gleich, W. A. Herrmann, *Angew. Chem.* **1999**, *111*, 2573.

[201] E. Colacino, J. Martinez, F. Lamaty, *Coord. Chem. Rev.* **2007**, *251*, 726.

[202] J. A. Love, J. P. Morgan, T. M. Trnka, R. H. Grubbs, *Angew. Chem., Int. Ed.* **2002**, *41*, 4035.

[203] J. A. Love, J. P. Morgan, T. M. Trnka, R. H. Grubbs, *Angew. Chem.* **2002**, *114*, 4207.

[204] K. Grela, S. Harutyunyan, A. Michrowska, *Angew. Chem.* **2002**, *114*, 4210.

[205] K. Grela, S. Harutyunyan, A. Michrowska, *Angew. Chem., Int. Ed.* **2002**, *41*, 4038.

[206] H. Wakamatsu, S. Blechert, *Angew. Chem.* **2002**, *114*, 832.

[207] H. Wakamatsu, S. Blechert, *Angew. Chem., Int. Ed.* **2002**, *41*, 2403.

[208] S. M. Hansen, F. Rominger, M. Metz, P. Hofmann, *Chem. Eur. J.* **1999**, *5*, 557.

[209] S. M. Hansen, M. A. O. Volland, F. Rominger, F. Eisenträger, P. Hofmann, *Angew. Chem., Int. Ed.* **1999**, *38*, 1273.

[210] S. M. Hansen, M. A. O. Volland, F. Rominger, F. Eisenträger, P. Hofmann, *Angew. Chem.* **1999**, *111*, 1360.

[211] C. Adlhart, M. A. O. Volland, P. Hofmann, P. Chen, *Helv. Chim. Acta* **2000**, *83*, 3306.

[212] M. A. O. Volland, S. M. Hansen, F. Rominger, P. Hofmann, *Organometallics* **2004**, *23*, 800.

[213] E. L. Dias, S. T. Nguyen, R. H. Grubbs, *J. Am. Chem. Soc.* **1997**, *119*, 3887.

[214] M. Ulman, R. H. Grubbs, *Organometallics* **1998**, *17*, 2484.

[215] M. Ulman, R. H. Grubbs, *J. Org. Chem.* **1999**, *64*, 7202.

[216] M. B. Dinger, J. C. Mol, *Organometallics* **2003**, *22*, 1089.

[217] S. H. Hong, M. W. Day, R. H. Grubbs, *J. Am. Chem. Soc.* **2004**, *126*, 7414.

[218] S. H. Hong, A. G. Wenzel, T. T. Salguero, M. W. Day, R. H. Grubbs, *J. Am. Chem. Soc.* **2007**, *129*, 7961.

[219] W. J. van Rensburg, P. J. Steynberg, W. H. Meyer, M. M. Kirk, G. S. Forman, *J. Am. Chem. Soc.* **2004**, *126*, 14332.

[220] K. Vehlow, S. Gessler, S. Blechert, *Angew. Chem., Int. Ed.* **2007**, *46*, 8082

[221] K. Vehlow, S. Gessler, S. Blechert, *Angew. Chem.* **2007**, *119*, 8228.

[222] M. S. Sanford, J. A. Love, R. H. Grubbs, *J. Am. Chem. Soc.* **2001**, *123*, 6543.

[223] M. S. Sanford, M. Ulman, R. H. Grubbs, *J. Am. Chem. Soc.* **2001**, *123*, 749.

[224] M. S. Sanford, California Institute of Technology (Pasadena, California), **2001**.

[225] M. S. Sanford, J. A. Love, in *Handbook of Metathesis, Vol. 1* (Ed.: R. H. Grubbs), WILEY-VCH Verlag GmbH & Co. KGaA, Weinheim, **2003**, p. 112.

[226] J. A. Love, M. S. Sanford, M. W. Day, R. H. Grubbs, *J. Am. Chem. Soc.* **2003**, *125*, 10103.

[227] S. Booyens, A. Roodt, O. F. Wendt, *J. Organomet. Chem.* **2007**, *692*, 5508.

[228] R. D. Cole, *Electrospray Ionization Mass Spectrometry* Wiley, New York, **1997**.

[229] C. M. Whitehouse, R. N. Dreyer, M. Yamashita, J. B. Fenn, *Anal. Chem.* **1985**, *57*, 675.

[230] C. Hinderling, C. Adlhart, P. Chen, *Angew. Chem., Int. Ed.* **1998**, *37*, 2685.

[231] C. Hinderling, C. Adlhart, P. Chen, *Angew. Chem.* **1998**, *110*, 2831.

[232] B. Mohr, D. M. Lynn, R. H. Grubbs, *Organometallics* **1996**, *15*, 4317.

[233] H. Wang, J. O. Metzger, *Organometallics* **2008**, *27*, 2761.

[234] O. M. Aagaard, R. J. Meier, F. Buda, *J. Am. Chem. Soc.* **1998**, *120*, 7174.

[235] S. F. Vyboishchikov, M. Bühl, W. Thiel, *Chem. Eur. J.* **2002**, *8*, 3962.

[236] S. F. Vyboishchikov, W. Thiel, *Chem. Eur. J.* **2005**, *11*, 3921.

[237] L. Cavallo, *J. Am. Chem. Soc.* **2002**, *124*, 8965.

[238] C. Costabile, L. Cavallo, *J. Am. Chem. Soc.* **2004**, *126*, 9592.

[239] A. Correa, L. Cavallo, *J. Am. Chem. Soc.* **2006**, *128*, 13352.

[240] C. Adlhart, P. Chen, *Angew. Chem. Int. Ed.* **2002**, *41*, 4484.

[241] C. Adlhart, P. Chen, *Angew. Chem.* **2002**, *114*, 4668.

[242] C. Adlhart, P. Chen, *J. Am. Chem. Soc.* **2004**, *126*, 3496.

[243] B. F. Straub, *Angew. Chem., Int. Ed.* **2005**, *44*, 5974

[244] B. F. Straub, *Angew. Chem.* **2005**, *117*, 6129.

[245] B. F. Straub, *Adv. Synth. Catal.* **2006**, *349*, 204

[246] W. J. van Rensburg, P. J. Steynberg, M. M. Kirk, W. H. Meyer, G. S. Forman, *J. Organomet. Chem.* **2006**, *691*, 5312.

[247] S. Torker, D. Merki, P. Chen, *J. Am. Chem. Soc.* **2008**, *130*, 4808.

[248] F. Levebre, X. Bories-Azeau, J. M. Basset, *Study of the activity and steroselectivity of some metathesis catalysts with acyclic internal olefins*, Kluwer Academic Publishers, **2002**.

[249] N. Schwesinger, G. Pieper, H. Wurziger, **2001**, *WO0170387*.

[250] M. Stoyanova, U. Rodemerck, U. Bentrup, U. Dingerdissen, D. Linke, R.-W. Mayer, H. G. J. Lansink Rotgerink, T. Tacke, *Appl. Catal., A* **2008**, *340*, 242.

[251] J. S. Kingsbury, A. H. Hoveyda, in *Polymeric Materials in Organic Synthesis and Catalysis* (Ed.: M. R. Buchmeiser), **2005**, pp. 467.

[252] T. R. Hoye, S. M. Donaldson, T. J. Vos, *Org. Lett.* **1999**, *1*, 277.

[253] D. Heller, H. Buschmann, *Top. Catal.* **1998**, *5*, 159.

[254] J. J. van Deemter, *Ind. Eng. Chem. Res.* **1953**, *45*, 1227.

[255] J. J. van Deemter, *Ind. Eng. Chem. Res.* **1954**, *46*, 2300.

[256] S. J. Hawkes, *J. Chem. Educ.* **1983**, *60*, 393.

[257] Z. C. Zhang, *Adv. Synth. Catal.* **2006**, *49*, 153.

[258] M. Smiglak, W. M. Reichert, J. D. Holbrey, J. S. Wilkes, L. Sun, J. S. Thrasher, K. Kirichenko, S. Singh, A. R. Katritzky, R. D. Rogers, *Chem. Commun.* **2006**, 2554.

[259] N. V. Plechkova, K. R. Seddon, *Chem. Soc. Rev.* **2008**, *37*, 123.

[260] S.-G. Lee, *Chem. Commun.* **2006**, 1049.

[261] T. Welton, *Chem. Rev.* **1999**, *99*, 2071.

[262] P. Wasserscheid, W. Keim, *Angew. Chem. Int. Ed.* **2000**, *39*, 3772.

[263] R. Sheldon, *Chem. Commun.* **2001**, 2399.

[264] J. Dupont, R. F. de Souza, P. A. Z. Suarez, *Chem. Rev.* **2002**, *102*, 3667.

[265] P. Wasserscheid, T. Welton, *Ionic Liquids in Synthesis*, WILEY-VCH Verlag GmbH & Co. KGaA, Weinheim, **2003**.

[266] C. Fischmeister, in *Metathesis Chemistry, From Nanostructure Design to Synthesis of Advanced Materials* (Eds.: Y. Imamoglu, V. Dragutan, S. Karabulut), Springer, Berlin, **2007**, pp. 483.

[267] V. I. Parvulescu, C. Hardacre, *Chem. Rev.* **2007**, *107*, 2615.

[268] P. Sledz, M. Mauduit, K. Grela, *Chem. Soc. Rev.* **2008**, *37*, 2433.

[269] D. Kralisch, A. Stark, S. Korsten, G. Kreisel, B. Ondruschka, *Green Chem.* **2005**, *7*, 301.

[270] R. C. Buijsman, E. van Vuuren, J. G. Sterrenburg, *Org. Lett.* **2001**, *3*, 3785.

[271] A. Ranwell, C. L. Dwyer, M. Ajam, *IP.com Journal* **2004**, *4*, 4.

[272] A. Stark, M. Ajam, M. Green, H. G. Raubenheimer, A. Ranwell, B. Ondruschka, *Adv. Synth. Catal.* **2006**, *348*, 1934.

[273] D. B. G. Williams, M. Ajam, A. Ranwell, *Organometallics* **2006**, *25*, 3088.

[274] X. Ding, X. Lv, B. Hui, Z. Chen, M. Xiao, B. Guo, W. Tang, *Tetrahedron Lett.* **2006**, *47*, 2921.

[275] V. Martinez, J.-C. Blais, D. Astruc, *Org. Lett.* **2002**, *4*, 651.

[276] H. Han, F. Chen, J. Yu, J. Dang, Z. Ma, Y. Zhang, M. Xie, *J. Polymer. Sci. Polymer. Chem.* **2007**, *45*, 3986.

[277] A. V. Vasnev, A. A. Greish, L. M. Kustov, *Mendeleev Communications* **2004**, *14*, 59.

[278] K. G. Mayo, E. H. Nearhoof, J. J. Kiddle, *Org. Lett.* **2002**, *4*, 1567.

[279] S. Garbacia, B. Desai, O. Lavastre, C. O. Kappe, *J. Org. Chem.* **2003**, *68*, 9136.

[280] A. Fürstner, L. Ackermann, K. Beck, H. Hori, D. Koch, K. Langemann, M. Liebl, C. Six, W. Leitner, *J. Am. Chem. Soc.* **2001**, *123*, 9000.

[281] H. Hagiwara, N. Okunaka, T. Hoshi, T. Suzuki, *Synlett* **2008**, *2008*, 1813.

[282] D. Sémeril, H. Olivier-Bourbigou, C. Bruneau, P. H. Dixneuf, *Chem. Commun.* **2002**, 146

[283] S. Csihony, C. Fischmeister, C. Bruneau, I. T. Horváth, P. H. Dixneuf, *New J. Chem.* **2002**, *26*, 1667

[284] M. R. Buchmeiser, *New. J. Chem.* **2004**, *28*, 549.

[285] C. Copéret, J. M. Basset, *Adv. Synth. Catal.* **2007**, *349*, 78.

[286] M. R. Buchmeiser, *Chem. Rev.* **2008**, DOI:10.1021/cr800207n.

[287] I. Dragutan, V. Dragutan, *Platinum Metals Rev.* **2008**, *52*, 71.

[288] I. Dragutan, V. Dragutan, *Platinum Metals Rev.* **2008**, *52*, 157.

[289] N. Audic, H. Clavier, M. Mauduit, J. C. Guillemin, *J. Am. Chem. Soc.* **2003**, *125*, 9248.

[290] Q. Yao, Y. Zhang, *Angew. Chem. Int. Ed.* **2003**, *42*, 3395.

[291] Q. Yao, Y. Zhang, *Angew. Chem.* **2003**, *115*, 3517.

[292] H. Clavier, N. Audic, M. Mauduit, J.-C. Guillemin, *Chem. Commun.* **2004**, 2282

[293] D. Rix, H. Clavier, Y. Coutard, L. Gulajski, K. Grela, M. Mauduit, *J. Organomet. Chem.* **2006**, *691*, 5397.

[294] D. Rix, F. Caijo, I. Laurent, L. Gulajski, K. Grela, M. Mauduit, *Chem. Commun.* **2007**, 3771.

[295] C. Thurier, C. Fischmeister, C. Bruneau, H. Olivier-Bourbigou, P. H. Dixneuf, *J. Mol. Catal. A: Chem.* **2007**, *268*, 127.

[296] H. Clavier, S. P. Nolan, M. Mauduit, *Organometallics* **2008**.

[297] C. S. Consorti, G. L. P. Aydos, G. Ebeling, J. Dupont, *Org. Lett.* **2008**, *10*, 237.

[298] H. Wakamatsu, Y. Saito, M. Masubuchi, R. Fujita, *Synlett* **2008**, 1805.

[299] Q. Yao, M. Sheets, *J. Organomet. Chem.* **2005**, *690*, 3577.

[300] G. Liu, J. Zhang, B. Wu, J. Wang, *Org. Lett.* **2007**, *9*, 4263.

[301] D. W. Armstrong, L. He, Y.-S. Liu, *Anal. Chem.* **1999**, *71*, 3873.

[302] A. Berthod, L. He, D. W. Armstrong, *Chromatographia* **2001**, *53*, 63.

[303] J. L. Anderson, D. W. Armstrong, *Anal. Chem.* **2003**, *75*, 4851.

[304] J. Ding, T. Welton, D. W. Armstrong, *Anal. Chem.* **2004**, *76*, 6819.

[305] J. L. Anderson, R. Ding, A. Ellern, D. W. Armstrong, *J. Am. Chem. Soc.* **2005**, *127*, 593.

[306] J. L. Anderson, D. W. Armstrong, *Anal. Chem.* **2005**, *77*, 6453.

[307] X. Han, D. W. Armstrong, *Acc. Chem. Res.* **2007**, *40*, 1079–1086.

[308] J. Seeley, S. Seeley, E. Libby, Z. Breitbach, D. Armstrong, *Anal. Bioanal. Chem.* **2008**, *390*, 323.

[309] D. Vitkuske, Supelco Ionic Liquids, in *Reporter* **2008**, www.sigmaaldrich.com/supelco/the_reporter/t208002.pdf, 2009.

[310] D. Chatterjee, B. Hetayothin, A. R. Wheeler, D. J. King, R. L. Garrell, *Lab Chip* **2006**, *6*, 199.

[311] P. Dubois, G. Marchand, Y. Fouillet, J. Berthier, T. Douki, F. Hassine, S. Gmouh, M. Vaultier, *Anal. Chem.* **2006**, *78*, 4909.

[312] Y. S. Nanayakkara, H. Moon, T. Payagala, A. B. Wijeratne, J. A. Crank, P. S. Sharma, D. W. Armstrong, *Anal. Chem.* **2008**, *80*, 7690.

[313] W. Leitner, N. Theyssen, Z. Hou, K. Kottsieper, M. Solinas, D. Giunta, **2006**, *2006-EP50195*.

[314] Compared to Grubbs-type catalyst 1st generation the 2nd generation catalysts are about four to five times more expensive. Source: Sigma-Aldrich (Materia Inc.), 2009.

[315] K. Grob, *Making and Manipulating Capillary Columns for Gas Chromatography*, Huthig Verlag, Heidelberg, **1986**.

[316] G. Spagnol, M. P. Heck, S. P. Nolan, C. Mioskowski, *Org. Lett.* **2002**, *4*, 1767.

[317] M. T. Reetz, *Angew. Chem.* **2002**, *114*, 1391.

[318] R. Noyori, *Angew. Chem. Int. Ed.* **2002**, *41*, 2008.

[319] H. C. Kolb, M. G. Finn, K. B. Sharpless, *Angew. Chem. Int. Ed.* **2001**, *40*, 2004.

[320] H. C. Kolb, M. G. Finn, K. B. Sharpless, *Angew. Chem.* **2001**, *113*, 2056.

[321] R. Noyori, *Asymmetric Catalysis in Organic Synthesis, Vol. 1*, WILEY-VCH Verlag GmbH & Co. KGaA, Weinheim, **1994**.

[322] H.-U. Blaser, *Chem. Rev.* **1992**, *92*, 935.

[323] B. List, *Acc. Chem. Res.* **2004**, *37*, 548.

[324] K. B. Sharpless, *Angew. Chem., Int. Ed.* **2002**, *41*, 2024.

[325] K. B. Sharpless, *Angew. Chem.* **2002**, *114*, 2126.

[326] M. D. McCreary, D. W. Lewis, D. L. Wernick, G. M. Whitesides, *J. Am. Chem. Soc.* **1974**, *96*, 1038.

[327] V. Schurig, *Angew. Chem. Int. Ed.* **1976**, *15*, 304.

[328] V. Schurig, *Angew. Chem.* **1976**, *88*, 336.

[329] V. Schurig, *Angew. Chem., Int. Ed.* **1977**, *16*, 110.

[330] V. Schurig, *Angew. Chem.* **1977**, *89*, 113.

[331] V. Schurig, R. Weber, *J. Chromatogr.* **1981**, *217*, 51.

[332] V. Schurig, R. Link, in *Chiral Separations* (Eds.: D. Stevenson, I. D. Wilson), Plenum Press, New York and London, **1988**, pp. 91.

[333] V. Schurig, D. Schmalzing, M. Schleimer, *Angew. Chem. Int. Ed. Engl.* **1991**, *30*, 987.

[334] V. Schurig, D. Schmalzing, M. Schleimer, *Angew. Chem.* **1991**, *103*, 994.

[335] F. Keller, Eberhard-Karls-Universität Tübingen (Tübingen), **1997**.

[336] A. Togni, *Organometallics* **1990**, *9*, 3106.

[337] E. Gil-Av, B. Feibush, R. Charles-Sigler, *Tetrahedron Lett.* **1966**, 1009.

[338] B. Feibush, R. E. Sievers, C. S. Springer, M. F. Richards, *J. Am. Chem. Soc.* **1972**, *94*, 6717.

[339] V. Schurig, R. C. Chang, A. Zlatkis, B. Feibush, *J. Chromatogr.* **1974**, *99*, 147.

[340] G. R. Sullivan, *Stereochem.* **1978**, *10*, 287.

[341] V. Schurig, *Inorg. Chem.* **1972**, *11*, 736.

[342] H. Frank, G. J. Nicholson, E. Bayer, *J. Chromatogr. Sci.* **1977**, *15*, 174.

[343] V. Schurig, *J. Chromatogr. A* **2002**, *965*, 315.

[344] W. Francke, V. Heemann, B. Gerken, J. A. A. Renwick, J. P. Vité, *Naturwissenschaften* **1977**, *64*, 590.

[345] K. Mori, in *Methods in Chemical Ecology, Vol. 1* (Eds.: J. G. Millar, K. F. Haynes), Kluwer Academic Publisher, Boston, **1998**.

[346] V. Schurig, B. Koppenhöfer, W. Bürkle, *Angew. Chem.* **1978**, *90*, 993.

[347] V. Schurig, B. Koppenhöfer, W. Bürkle, *Angew. Chem. Int. Ed. Engl.* **1978**, *17*, 937.

[348] B. Koppenhoefer, K. Hintzer, R. Weber, V. Schurig, *Angew. Chem. Int. Ed. Engl.* **1980**, *19*, 471.

[349] B. Koppenhoefer, K. Hintzer, R. Weber, V. Schurig, *Angew. Chem.* **1980**, *92*, 473.

[350] R. Weber, K. Hintzer, V. Schurig, *Naturwissenschaften* **1980**, 453.

[351] R. Weber, V. Schurig, *Naturwissenschaften* **1981**, *68*, 330.

[352] V. Schurig, W. Bürkle, *J. Am. Chem. Soc.* **1982**, *104*, 7573.

[353] V. Schurig, *J. Chromatogr. A* **1988**, *441*, 135.

[354] V. Schurig, J. Ossig, R. Link, *Angew. Chem. Int. Ed. Engl.* **1989**, *28*, 194.

[355] V. Schurig, J. Ossig, R. Link, *Angew. Chem.* **1989**, *101*, 197.

[356] S. Allenmark, V. Schurig, *J. Mater. Chem.* **1997**, *7*, 1955.

[357] V. Schurig, R. Weber, *J. Chromatogr.* **1984**, *289*, 321.

[358] V. Schurig, *Chirality* **1998**, *10*, 140.

[359] O. Trapp, V. Schurig, *Chem. Eur. J.* **2001**, *7*, 1495.

[360] P. J. Marriott, T. Massil, H. Huegel, *J. Sep. Sci.* **2004**, *27*, 1273.

[361] Z. Jiang, V. Schurig, *J. Chromatogr. A* **2008**, *1186*, 262.

[362] J. K. Haken, *J. Chromatogr.* **1984**, *300*, 1.

[363] I. F. J. Vankelecom, D. Tas, R. F. Parton, V. V. de Vyver, P. A. Jacobs, *Angew. Chem. Int. Ed.* **1996**, *35*, 1346.

[364] I. F. J. Vankelecom, D. Tas, R. F. Parton, V. Van De Vyver, P. A. Jacobs, *Angew. Chem.* **1996**, *108*, 1445.

[365] I. F. J. Vankelecom, *Chem. Rev.* **2002**, *102*, 3779.

[366] D. A. Armitage, *Comprehensive Organometallic Chemistry, Vol. 2*, Pergamon Press, Oxford, **1982**.

[367] P. M. Chevalier, I. A. MacKinnon, *J. Inorg. Organomet. Polym.* **1999**, *9*, 151.

[368] J. L. Speier, *Adv. Organomet. Chem.* **1979**, *17*, 407.

[369] B. D. Karstedt, **1973**, *US-A 3175452*.

[370] P. Strohriegl, *Makromol. Chem. Rapid Commun.* **1986**, *7*.

[371] M. Lux, P. Strohriegl, H. Höcker, *Makromol. Chem. Rapid Commun.* **1987**, *188*, 811.

[372] I. E. Markó, S. Stérin, O. Buisine, G. Mignani, P. Branlard, B. Tinant, J.-P. Declercq, *Science* **2002**, *298*, 204.

[373] B.-H. Han, P. Boudjouk, *Organometallics* **1983**, *2*, 769.

[374] L. A. van de Kuil, D. M. Grove, J. W. Zwikker, L. W. Jenneskens, W. Drenth, G. van Koten, *Chem. Mater.* **1994**, *6*, 1675.

[375] Y.-S. Fu, S. J. Yu, *Angew. Chem. Int. Ed.* **2001**, *40*, 437.

[376] Y.-S. Fu, J. S. Yu, *Angew. Chem.* **2001**, *113*, 451.

[377] M. D. Skowronska-Ptasinska, M. L. W. Vorstenbosch, R. A. van Santen, H. C. L. Abbenhuis, *Angew. Chem. Int. Ed.* **2002**, *41*, 637.

[378] M. Felder, G. Giffels, C. Wandrey, *Tetrahedron: Asymmetry* **1997**, *8*, 1975.

[379] A. Mandoli, M. Lessi, D. Pini, C. Evangelisti, P. Salvadoria, *Adv. Synth. Catal.* **2008**, *350, ,* 375.

[380] T. P. Yoon, E. N. Jacobsen, *Science* **2003**, *299*, 1691.

[381] M. J. Spallek, Master thesis, Ludwigs-Maximilians-Universität München (München), **2008**.

[382] S. K. Weber, O. Trapp, **2009**, *unpublished results*.

[383] P. D. Bartlett, L. H. Knox, in *Org. Synth. Coll. Vol., Vol. V*, WILEY-VCH Verlag GmbH & Co. KGaA, **1973**, pp. 194.

[384] G. Opitz, F. Schweinsberg, *Angew. Chem. Int. Ed. Engl.* **1965**, *4*, 786.

[385] G. Opitz, F. Schweinsberg, *Angew. Chem.* **1965**, *77*, 811.

[386] G. Opitz, *Angew. Chem. Int. Ed. Engl.* **1967**, *6*, 107.

[387] G. Opitz, *Angew. Chem.* **1967**, *79*, 161.

[388] B. O. Linn, C. R. Hauser, *J. Am. Chem. Soc.* **1956**, *78*, 6066.

[389] K. R. Kopecky, D. Nonhebel, G. Morris, G. S. Hammond, *J. Org. Chem.* **1962**, *27*, 1036.

[390] F. Fringuelli, A. Taticchi, *The Diels-Alder Reaction - Selected Practical Methods, Vol. 1*, Wiley & Sons, Weinheim, **2001**.

[391] K. Alder, *Nobel Lecture,* **1950**.

[392] O. Diels, *Nobel Lecture* **1950**.

[393] S. Danishefsky, J. F. Kerwin, S. Kobayashi, *J. Am. Chem. Soc.* **1982**, *104*, 358.

[394] W. R. Roush*, Vol. 5* (Eds.: B. M. Trost, I. Fleming, L. A. Paquette), Pergamon Press, Oxford, U.K., **1991**, p. 513.

[395] A. G. Fallis, *Acc. Chem. Res.* **1999**, *32*, 464.

[396] E. Marsault, A. Toró, P. Nowak, P. Deslongchamps, *Tetrahedron Lett.* **2001**, *57*, 4243.

[397] B. R. Bear, S. M. Sparks, K. J. Shea, *Angew. Chem. Int. Ed.* **2001**, *40*, 820.

[398] B. R. Bear, S. M. Sparks, K. J. Shea, *Angew. Chem.* **2001**, *113*, 864.

[399] K.-I. Takao, R. Munakata, K.-I. Tadano, *Chem. Rev.* **2005**, *105*, 4779.

[400] M. E. Jung, J. Gervay, *Tetrahedron Lett.* **1988**, *29*, 2429.

[401] M. E. Jung, J. Gervay, *J. Am. Chem. Soc.* **1989**, *111*, 5469.

[402] T. Butz, J. Sauer, *Tetrahedron: Asymmetry* **1997**, *8*, 703.

[403] J. S. Yadav, R. Renduchintala, L. Samala, *Tetrahedron Lett.* **1994**, *35*, 3617.

[404] V. Theurillat-Moritz, P. Vogel, *Tetrahedron: Asymmetry* **1996**, *7*, 3163.

[405] S. Akai, T. Naka, S. Omura, K. Tanimoto, M. Imanishi, Y. Takebe, M. Matsugi, Y. Kita, *Chem. Eur. J.* **2002**, *8*, 4255.

[406] Y. Kita, T. Naka, M. Imanishi, S. Akai, Y. Takebe, M. Matsugi, *Chem. Commun.* **1998**, 1183.

[407] F. Dallacker, I. Alroggen, H. Krings, B. Laurs, M. Lipp, *Ann.* **1961**, *647*, 23.

[408] D. Villemin, M. Hammandi, *Synth. Commun.* **1995**, *25*, 3141.

[409]   S. de la Moya Cerero, A. Garcia Martinez, E. Teso Vilar, A. Garcia Fraile, B. Lora Maroto, *J. Org. Chem.* **2003**, *68*, 1451.

[410]   A. W. Bishop, L. Claisen, W. Sinclair, *Ann.* **1894**, *281*.

[411]   M. O. Forster, *Proc. Chem. Soc., London* **1901**, *17*, 287.

[412]   S. M. Malmgren, *Ber.* **1903**, *36*, 2608.

[413]   G. M. Whitesides, D. W. Lewis, *J. Am. Chem. Soc.* **1970**, *92*, 6979.

[414]   E. M. McGarrigle, D. G. Gilheany, *Chem. Rev.* **2005**, *105*, 1563.

[415]   K. B. Hansen, J. L. Leighton, E. N. Jacobsen, *J. Am. Chem. Soc.* **1996**, *118*, 10924.

[416]   E. N. Jacobsen, *Acc. Chem. Res.* **2000**, *33*, 421.

[417]   C. Lauret, *Tetrahedron: Asymmetry* **2001**, *12*, 2359.

[418]   D. M. Bollag, P. A. McQueney, J. Zhu, O. Hensens, L. Koupal, J. Liesch, M. Goetz, E. Lazarides, C. M. Woods, *Cancer Res.* **1995**, *55*, 2325.

[419]   H. N. Itazaki, K.; Sugita, K.;, H. K. Yoshida, Y.; Yasuda, Y.; Matsumoto, K.; Ishii, K.; Uotani,, H. T. N.; Nakai, A.; Yoshimatsu, S., *J. Antibiot.* **1990**, *43*, 1524.

[420]   S. M. Kupchan, W. A. Court, R. G. Dailey, C. J. Gilmore, R. F. Bryan, *J. Am. Chem. Soc. Rev.* **1972**, *94*, 7194.

[421]   T. Katsuki, K. B. Sharpless, *J. Am. Chem. Soc.* **1980**, *102*, 5974.

[422]   K. B. Sharpless, *Angew. Chem.* **2002**, *114*, 2126.

[423]   R. A. Johnson, K. B. Sharpless, in *Catalytic Asymmetric Synthesis* (Ed.: I. Ojima), VCH Publishers, New York, **1993**, pp. 101.

[424]   W. Zhang, J. L. Loebach, S. R. Wilson, E. N. Jacobsen, *J. Am. Chem. Soc.* **1990**, *112*, 2801.

[425]   E. N. Jacobsen, in *Catalytic Asymmetric Synthesis* (Ed.: I. Ojima), VCH Publishers, New York, **1993**, pp. 159.

[426]   R. Irie, K. Noda, Y. Ito, N. Matsumoto, T. Katsuki, *Tetrahedron Lett.* **1990**, *31*, 7345.

[427]   D. A. Annis, Harvard University (Cambridge, Massachusetts), **1998**.

[428]   X. Zheng, C. W. Jones, M. Weck, *Chem. Eur. J.* **2006** *12*, 576.

[429]   F. Minutolo, D. Pini, P. Salvadori, *Tetrahedron: Asymmetry* **1996**, *7*, 2293.

[430]   B. B. De, B. B. Lohray, S. Sivaram, P. K. Dhal, *J. Polym. Sci., Polym. Chem. Ed* **1997**, *35*, 1809.

[431]   L. Canali, E. Cowan, H. Deleuze, C. L. Gibson, D. C. Sherrington, *Chem. Commun.* **1998**, 2561.

[432]   T. S. Reger, K. D. Janda, *J. Am. Chem. Soc.* **2000**, *122*, 6929.

[433]   C. E. Song, E. J. Roh, B. M. Yu, D. Y. Chi, S. C. Kim, K.-J. Lee, *Chem. Commun.* **2000**, 615.

[434]   H. Sellner, J. K. Karjalainen, D. Seebach, *Chem. Eur. J.* **2001**, *7*, 2873.

[435]   M. Kwon, G.-J. Kim, *Catal. Today* **2003**, *87*, 145.

[436]   M. Holbach, M. Weck, *J. Org. Chem.* **2006**, *71*, 1825.

[437]   L.-L. Lou, K. Yu, F. Ding, W. Zhou, X. Peng, S. Liu, *Tetrahedron Lett.* **2006**, *47*, 6513.

[438]   S. B. Ogunwumi, T. Bein, *Chem. Commun.* **1997**, 901.

[439]   L. Canali, D. C. Sherrington, *Chem. Soc. Rev.* **1999**, *28*, 85.

[440]   S. Laue, A. Liese, J. Wöltinger, C. Wandrey, *12th Int. Symposium on Homogeneous Catalysis* **2000**, Stockholm, Sweden.

[441]   M. Tokunaga, J. F. Larrow, F. Kakiuchi, E. N. Jacobsen, *Science* **1997**, *277*, 936.

[442] M. E. Furrow, S. E. Schaus, E. N. Jacobsen, *J. Org. Chem.* **1998**, *63*, 6776.

[443] S. E. Schaus, B. D. Brandes, J. F. Larrow, M. Tokunaga, K. B. Hansen, A. E. Gould, M. E. Furrow, E. N. Jacobsen, *J. Am. Chem. Soc.* **2002**, *124*, 1307.

[444] J. F. Larrow, K. E. Hemberger, S. Jasmin, H. Kabir, P. Morel, *Tetrahedron: Asymmetry* **2003**, *14*, 3589.

[445] L. P. C. Nielsen, C. P. Stevenson, D. G. Blackmond, E. N. Jacobsen, *J. Am. Chem. Soc.* **2004**, *126*, 1360.

[446] J. M. Ready, E. N. Jacobsen, *J. Am. Chem. Soc.* **2001**, *123*, 2687.

[447] J. M. Ready, E. N. Jacobsen, *Angew. Chem., Int. Ed.* **2002**, *41*, 1374.

[448] R. G. Konsler, J. Karl, E. N. Jacobsen, *J. Am. Chem. Soc.* **1998**, *120*, 10780.

[449] X. Zheng, C. W. Jones, M. Weck, *J AM CHEM SOC* **2007**, *129*, 1105.

[450] R. Breinbauer, E. N. Jacobsen, *Angew. Chem. Int. Ed.* **2000**, *39*, 3604.

[451] Y. Song, X. Yao, H. Chen, C. Bai, X. Hu, Z. Zheng, *Tetrahedron Lett.* **2002**, *43*, 6625.

[452] P. L. Osburn, D. E. Bergbreiter, *Prog. Polym. Sci.* **2001**, *26*, 2015.

[453] M.-a. Kwon, G.-J. Kim, *Catal. Today* **2003**, *87*, 145.

[454] W. Sodenko, G. Jas, U. Kunz, A. Kirschning, *Synthesis* **2007**, *4*, 583.

[455] G.-J. Kim, D.-W. Park, *Catal. Today* **2000**, *63*, 537.

[456] G.-J. Kim, J.-H. Shin, *Catal. Letters* **1999**, *63*, 205.

[457] M. Holbach, X. Zheng, C. Burd, C. W. Jones, M. Weck, *J. Org. Chem.* **2006**, *71*, 2903.

[458] D. H. Rich, J. H. Gardner, *Tetrahedron Lett.* **1983**, *24*, 5305.

[459] J. F. Larrow, E. N. Jacobsen, *J. Org. Chem.* **1994**, *59*, 1939.

[460] F. Bellezza, A. Cipiciani, G. Ricci, R. Ruzziconi, *Tetrahedron Lett.* **2005**, *61*, 8005.

[461] F. Swarts, *Recl. Trav. Chim. Pays-Bas* **1909**, *28*, 166.

[462] ChemOrganizer ChemOrganizer is an in-house softwaretool including an electronic laboratory notebook, a compound database and plotting tools. The program is running under Windows (2000, XP and Vista). For applications of the software please contact Prof. Dr. Oliver Trapp, http://www.trapp.uni-hd.de, 2009.

[463] O. Trapp, *J. Chromatogr. B* **2008**, *875*, 42.

[464] DCXplorer has been designed for the evaluation of elution profiles in dynamic chromatography (DGC, DHPLC, DSFC, DOTLC) and electrophoresis (DCE, DCEC, DMEKC, DOTCE) and is running under Windows (2000, XP and Vista). Experimental chromatograms can be easily evaluated by using the integrated data file explorer and zooming into the area of interest. All chromatograms in ascii file format can be accessed. The program is based on the Unified Equation, which is superior in precision and speed to any simulation process. For applications of the software please refer to the publications section on this homepage. http://www.trapp.uni-hd.de/download/DCXplorer.exe, 2009.

[465] RCXplorer is an in-house softwaretool to evaluate experimental chromatograms by using the integrated data file explorer. The program is running under Windows (2000, XP and Vista). All chromatograms in ascii file format can be accessed. For applications of the software please contact Prof. Dr. Oliver Trapp, http://www.trapp.uni-hd.de, 2009.

[466] F. Langer, L. Schwink, A. Devasagayaraj, P.-Y. Chavant, P. Knochel, *J. Org. Chem.* **1996**, *61*, 8229.

[467] W. M. Braje, J. Frackenpohl, O. Schrake, R. Wartchow, W. Beil, H. Martin, R. Hoffmann, *Helv. Chim. Acta* **2000**, *83*, 777.

11. Appendix

Erklärung

Die vorliegende Arbeit entstand unter Anleitung von Herrn Prof. Dr. Oliver Trapp am Organisch-Chemischen Institut der Ruprecht-Karls-Universität Heidelberg in der Zeit von Oktober 2008 bis Juni 2009 sowie in der Abteilung für Heterogene Katalyse des Max-Planck-Institutes für Kohlenforschung in Mülheim an der Ruhr in der Zeit von August 2006 bis September 2008.

Gemäß § 8 (3) b) und c) der Promotionsordnung der Ruprecht-Karls-Universität Heidelberg für die Naturwissenschaftlich-Mathematische Gesamtfakultät erkläre ich hiermit, dass ich die vorgelegte Dissertation selbst verfasst und mich keiner anderen als der von mir ausdrücklich bezeichneten Quellen bedient habe und dass ich an keiner anderen Stelle ein Prüfungsverfahren beantragt bzw. die Dissertation in dieser oder anderer Form bereits anderswertig als Prüfungsarbeit verwendet oder an einer anderen Fakultät als Dissertation vorgelegt habe.

Heidelberg, den 12.06.2009

....
Sven K. Weber

Academic Teachers

My academic teachers:

Prof. Dr. Hans-Josef Altenbach, Prof. Dr. Thorsten Benter, Prof. Dr. David Brauer, Prof. Dr. Hans Bürger, Prof. Dr. Klaus Burczyk, Prof. Dr. Reint Eujen, Prof. Dr. Siegmar Gäb, Prof. Dr. Per Jensen, Prof. Dr. Lukas J. Gooßen, Prof. Dr. Andrew B. Holmes, Prof. Dr. Jürg Hulliger, Prof. Dr. Wolfgang Piepersberg, Prof. Dr. Manfred T. Reetz, Prof. Dr. Walter Reineke, Prof. Dr. Ullrich Scherf, Prof. Dr. Jürgen Scherkenbeck, Prof. Dr. Ferdi Schüth, Prof. Dr. Walter Thiel, Prof. Dr. Oliver Trapp, Prof. Dr. Günter Vogel, Prof. Dr. Helge Willner.